




ALT`21

INTERNATIONAL CONFERENCE

Advanced Laser Technologies

BOOK OF ABSTRACTS



September 06-10, 2021

MOSCOW, RUSSIA

УДК 535.21; 535.23; 535.33; 535.37
ББК 22.343.4; 22.344; 22.345

Abstracts of the 28th International Conference on Advanced Laser
Technologies – 2021. – 214 с.

The book contains abstracts of ALT`21 conference reports devoted to fundamental and applied aspects of innovative laser technologies, laser-matter interaction, biophotonics, laser systems and materials, laser diagnostics, terahertz photonics and optoelectronics. The book contains abstracts of plenary, invited, oral and poster presentations. The official language of the conference is English.

ALT`21 Conference Book of Abstracts are on the conference website
<https://altconference.org/proceedings>

ISBN 978-5-6043721-9-7



9 785604 372197

© ООО "МЕКОЛ", 2021
© Prokhorov General Physics Institute
of Russian Academics of Sciences, 2021

BOOK OF ABSTRACTS

ALT`21

The 28th International Conference on Advanced Laser Technologies

September 06-10, 2021 / Moscow, Russia

Contents

Organizers and Sponsors	4
Program and Organizing Committees	5
Plenary Speakers	6
SECTION LM. Laser–Matter Interaction	11
SECTION B. Biophotonics	83
SECTION LS. Laser Systems and Materials	121
SECTION LD. Laser Diagnostics and Spectroscopy	143
SECTION THz. THz Photonics and Optoelectronics	173
SECTION Posters	194

Organizers and Sponsors



Prokhorov General Physics Institute
of the Russian Academic of Science
Russia



University of Bordeaux
France



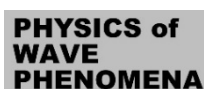
Lomonosov Moscow State University
Russia



National Research Nuclear University
MEPhI, Russia



FRC "Crystallography and Photonics"
of the Russian Academic of Science
Russia



Physics of Wave Phenomena journal
Russia



Special Issue "Laser-Generated
Periodic Nanostructures"
France

Conference Chairman

Ivan SHCHERBAKOV (Russia)

Program Committee Co-Chairs

Vitaly KONOV (Russia)
Guillaume DUCHATEAU (France)

International Program Committee

Nadezhda BULGAKOVA (Czech Republic)
Zhongping CHEN (USA)
Jean-Louis COUTAZ (France)
Aladar CZITROVSKY (Hungary)
Boris DENKER (Russia)
Dan DUMITRAS (Romania)
Thomas GRAF (Germany)
Sergey GARNOV (Russia)
Leonid GOLOVAN (Russia)
Tatiana ITINA (France)
Pavel KASHKAROV (Russia)
Sergey KLIMENTOV (Russia)
Yuri KULCHIN (Russia)
Yong Feng LU (USA)
Vladimir MAKAROV (Russia)
Xavier MATEOS FERRÉ (Spain)

Ion MIHAILESCU (Romania)
Tomas MOCEK (Czech Republic)
Tadao NAGATSUMA (Japan)
Attila NAGY (Hungary)
Beat NEUENSCHWANDER (Switzerland)
Kyung Hyun PARK (Korea)
Valentin PETROV (Germany)
Alexander PRIEZZHEV (Russia)
Philippe DELAPORTE (France)
Marc SENTIS (France)
Alexander SHKURINOV (Russia)
Valery TUCHIN (Russia)
Vadim VEIKO (Russia)
Haohai YU (China)
Irina ZAVESTOVSKAYA (Russia)
Jiyang WANG (China)

Organizing Committee Chair

Vladimir PUSTOVOY (Russia)

Plenary Speakers

P-I

SuperCam: a unique instrument for remote laser-based analyses on Mars

Bruno Bousquet¹, Elise Clavé¹, Sylvestre Maurice², Roger Wiens³ and the SuperCam team

¹ CELIA – CNRS : UMR5107, Université de Bordeaux, CEA – France

² IRAP – CNRS, université de Toulouse – France

³ Los Alamos National Laboratory – NASA – United States

In the frame of the NASA mission Mars 2020, the rover Perseverance landed on Mars on Feb, 18, 2021. Among the instruments onboard the rover, SuperCam [1,2] enables the remote analysis of rock and soil samples with three types of laser-based spectroscopy : laser-induced breakdown spectroscopy (LIBS), time-resolved Raman (TRR) and time-resolved luminescence (TRL).

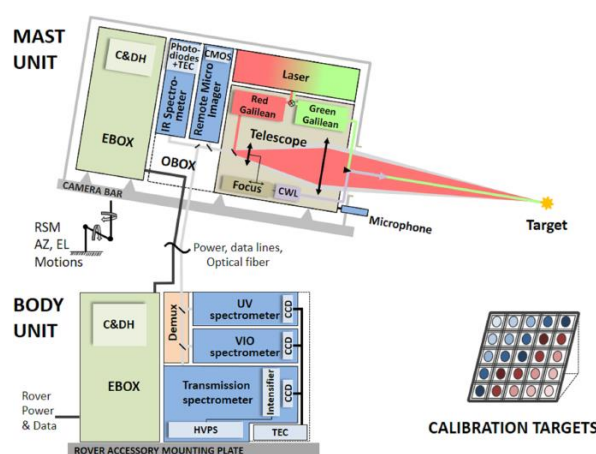


Fig.1. schematic diagram showing the major units and subcomponents of the SuperCam instrument suite is given in Figure 1.

The aim of this presentation is to give an overview of the Mars2020 mission and more precisely the SuperCam instrument schematically described in Figure 1. SuperCam is equipped with a diode pumped Q-switched Nd:YAG laser delivering nanosecond millijoule pulses at 1064 nm for LIBS and 532 nm for TRR and TRL, up to seven meter. It also records passive spectra in the visible and infrared, and high-resolution images and sounds.

After a brief update of the operations performed by Perseverance on Mars, we will present a selection of results including spectra, images and sounds to illustrate the role of the SuperCam instrument. We will also discuss the necessity of applying advanced data processing strategies to interpret the data.

Finally, we will present laboratory experiments of plasma-induced luminescence (PIL) [3] developed to support the SuperCam instrument and assess the potential of this type of spectroscopy as a complement to the techniques mentioned previously.

[1] Wiens, R.C., Maurice, S., Robinson, S.H. et al. The SuperCam Instrument Suite on the NASA Mars 2020 Rover: Body Unit and Combined System Tests. *Space Sci Rev* 217, 4 (2021). <https://doi.org/10.1007/s11214-020-00777-5>

[2] Maurice, S., Wiens, R.C., Bernardi, P. et al. The SuperCam Instrument Suite on the Mars 2020 Rover: Science Objectives and Mast-Unit Description. *Space Sci Rev* 217, 47 (2021). <https://doi.org/10.1007/s11214-021-00807-w>

[3] Clavé, E., Gaft, M., Motto-Ros, V. et al. Extending the potential of plasma-induced luminescence spectroscopy. *Spectrochim. Acta B At. Spectrosc.*, 177 (2021) 106111

10. Z.B. Wang et al.// *Scientific Reports* 9, 20293 (2019).

P-II**Raman spectroscopy and machine learning
for medical diagnostics and forensic purposes****Igor Lednev***Department of Chemistry, Department of Biological Sciences,
University at Albany, State University of New York (SUNY), USA*

Raman spectroscopy combined with advanced statistics is uniquely suitable for characterizing microheterogeneous samples. Understanding the structure and (bio)chemical composition of samples at the microscopic level is important for many practical applications including material science, pharmaceutical industry, etc. We have recently demonstrated a great potential of Raman hyperspectroscopy for disease diagnostics and forensic purposes. In this presentation, we will discuss the development of a new, noninvasive method for Alzheimer's disease (AD) diagnostics based on Raman spectroscopy of blood. Near infrared (NIR) Raman hyperspectroscopy coupled with advanced multivariate statistics was utilized for differentiating patients diagnosed with Alzheimer's disease, other types of dementia and healthy control subjects with more than 95% sensitivity and specificity. When fully developed, this fast, inexpensive noninvasive method could be used for screening at risk patient populations for AD development and progression.

Raman spectroscopy has already found numerous applications in forensic chemistry providing confirmatory identification of analytes. The technique is non-destructive, rapid and requires little or no sample preparation. Furthermore, portable Raman instruments are readily available allowing for crime scene accessibility. We have recently demonstrated that Raman microspectroscopy can be used for the identification of biological stains at a crime scene indicating the type of body fluid. In addition, peripheral and menstrual blood as well as human and animal blood can be differentiated. The time since deposition of bloodstain can be estimated up to two years. Most recently, we demonstrated the proof-of-concept for phenotype profiling based on Raman spectroscopy of dry traces of body fluids including the determination of sex, race and age group of the donor.

P-III

Optical Phenomena in Micrometer Dielectric Spheres

B.S. Lukiyanchuk

Faculty of Physics, Lomonosov Moscow State University

lukiyanchuk@nanolab.phys.msu.ru

In the Mie theory, representing the exact solution of Maxwell's equations for scattering plane wave on a homogeneous sphere, electromagnetic fields depend on the refractive index of the sphere, n , and the so-called size parameter, $q = 2\pi R / \lambda$, where R is the radius sphere, and λ is the radiation wavelength. The history of classical optics is associated with lenses, with a size of about one centimeter (Galileo's telescope, microscope, etc.). The corresponding size parameter in such optical systems is quite large, $q > 10^5$. The geometrical optics approximation is in good agreement with the Mie theory for $q > 10^2$. Research on the optics of nanostructures in plasmonics and nanophotonics refer to the systems where the size parameter is of the order of unity, $q \sim 1$. In this area, progress has been made in the study of optically resonant dielectric nanostructures with a high refractive index [1]. At the same time, structures with the size parameter of the ten, $q \sim 10$, are in the region between the wave and geometric optics turned out to be a "blank spot" on the map of optics due to the reason that lenses of the size of a few micrometers had no particular interest.

However, the studies on the optics of dielectric spheres micrometer sizes over the past twenty years, discover a number of unusual phenomena, including photonic nanojets [2], optical nanovortices [3], Fano resonances [4], magnetic light [5], the effects of overcoming the diffraction limit in the virtual image [6], effects associated with the excitation of anapole modes [7-9] and the excitation of giant magnetic fields [10]. The report gives an overview of these phenomena and discusses the physical mechanisms underlying these phenomena. The presence of a number of interesting applications indicates a new promising direction in optics.

This work was supported by the Ministry of Science and Higher Education Russian Federation (grant № 14.W03.31.0008) and also partially supported by the Russian Science Foundation (project № 20-12-00389) and by the Basic Russian Foundation (project № 20-02-00715).

References

1. A.I. Kuznetsov et al.// *Science* **354**, aag2472 (2016).
2. B. Luk`yanchuk et al.// *Optical Materials Express* **7**, 1820 (2017).
3. B. S. Luk`yanchuk et al.// *Journal of Optics* **15**, 073001 (2013).
4. B. Luk`yanchuk et al.// *Nature Materials* **9**, 707 (2010).
5. A.I. Kuznetsov et al.// *Scientific Reports* **2**, 492 (2012).
6. Z.B. Wang et al.// *Nature Communications* **2**, 218 (2011).
7. A.E. Miroshnichenko et al.// *Nature Communications* **6**, 8069 (2015).
8. B. Luk`yanchuk et al.// *Phil. Trans. Roy. Soc. A* **375**, 20160069 (2017).
9. B. Luk`yanchuk et al.// *Phys. Rev. A* **95**, 063820 (2017).
10. Z.B. Wang et al.// *Scientific Reports* **9**, 20293 (2019).

P-IV

Generation and detection of quantum-correlated pairs of optical and terahertz photons

G.Kh. Kitaeva

Lomonosov Moscow State University, Leninskie Gory 1-2, Moscow 119991 Russia

Generation of terahertz frequency (THz) fields with quantum properties and study of statistical parameters of THz radiation at the photonic level can provide a new understanding of the interaction of THz fields with matter and be useful for expanding optical quantum technologies, such as quantum field sensing [1], imaging [2], spectroscopy [3], photometry [4], for the THz range. Quantum-correlated pairs of photons of optical and terahertz ranges (“optical - terahertz biphotons”), generated under spontaneous parametric down-conversion (SPDC) in a strongly frequency non-degenerate regime [5,6], are first exciting examples of non-classical radiation matching the terahertz gap.

The prospects and challenges of generation and detection of optical-terahertz biphotons are analyzed theoretically, using the generalized Klyshko-Kirchhoff approach [6], and experimentally, by studying the SPDC fields generated under pulsed laser pumping of nonlinear Mg:LiNbO₃ crystal. Analysis of frequency-angular distributions of optical photons generated at the Stokes idler frequency shifts 0.2–5 THz at different crystal temperatures in the range from 300 K to 4.2 K enabled to predict the temperature behavior of the total number of THz idler photons, the temperature variation of the optical-terahertz biphoton function, and to study the contributions of classical thermal and pure quantum field fluctuations to parameters of biphotons [7]. It was shown that detecting only optical part of SPDC can provide information on THz properties of matter without direct detection of THz waves [8,9]. However, for a vast majority of attracting quantum applications such as ghost imaging without THz cameras, absolute calibration of quantum efficiency of THz detectors, and other tasks, the direct measurement of optical-terahertz correlation function $g^{(2)}$ is important. An experimental scheme for direct measuring of $g^{(2)}$ for the optical–THz biphotons has been designed and implemented recently. Terahertz radiation of type-0 SPDC in cooled down to 4.8 K Mg:LiNbO₃ was detected with a superconducting NbN bolometer operating in an analog detection mode [10–12]. A special procedure was proposed for evaluating $g^{(2)}$ in the absence of single-photon THz detectors and impossibility of using coincidence circuits. A quantum excess over the classical level of correlations between optical and terahertz fields was detected experimentally for the first time.

The work was financially supported by the Russian Science Foundation (Grant No. 17-12-01134).

- [1] A.S. Clark, M. Chekhova, J.C.F. Matthews, J.G. Rarity, R.F. Oulton, Special Topic: Quantum sensing with correlated light sources, *Applied Physics Letters*, vol.118, p.060401, (2021).
- [2] P.-A. Moreau, E. Toninelli, T. Gregory, M.J. Padgett, Ghost imaging using optical correlations, *Laser & Photonics Rev.*, vol. 12, p. 1700143, (2018).
- [3] D.A. Kalashnikov, A.V. Paterova, S.P. Kulik, L.A. Krivitsky, Infrared spectroscopy with visible light, *Nature Photonics*, vol.10, p.98 (2016).
- [4] S.V. Polyakov, A.L. Migdall, High accuracy verification of a correlated photon-based method for determining photoncounting detection efficiency, *Optics Express*, vol.15, pp. 1390-1407, (2007).
- [5] G.Kh. Kitaeva, V.V. Kornienko, A.A. Leontyev, A.V. Shepelev, Generation of optical signal and terahertz idler photons by spontaneous parametric down-conversion, *Physical Review A*, vol. 98, p. 063844, (2018).
- [6] G.Kh. Kitaeva, A.A. Leontyev, P.A. Prudkovskii, Quantum correlation between optical and terahertz photons generated under multimode spontaneous parametric down-conversion, *Physical Review A*, vol.101, p. 053810, (2020).
- [7] T.I. Novikova, K.A. Kuznetsov, A.A. Leontyev, G.Kh. Kitaeva, Study of SPDC spectra to reveal temperature dependences for optical-terahertz biphotons, *Applied Physics Letters*, vol.116, p. 264003, (2020).
- [8] K.A. Kuznetsov, E.I. Malkova, R.V. Zakharov, O.V. Tikhonova, G.Kh. Kitaeva, Nonlinear interference in strongly non-degenerate regime and Schmidt mode analysis, *Physical Review A*, vol. 101, p. 053843, (2020).
- [9] K.A. Kuznetsov, G.Kh. Kitaeva, S.P. Kovalev, S.A. Germansky, A.M. Buryakov, A.N. Tuchak, A.N. Penin, Complex extraordinary dielectric function of Mg-doped lithium niobate crystals at terahertz frequencies, *Applied Physics B*, vol.122, p.223, (2016).
- [10] G.Kh. Kitaeva, V.V. Kornienko, K.A. Kuznetsov, I.V. Pentin, K.V. Smirnov, Yu.B. Vakhtomin, Direct detection of the idler THz radiation generated by spontaneous parametric down-conversion, *Optics Letters*, vol. 44, pp. 1198-1201, (2019).
- [11] V.D. Sultanov, K.A. Kuznetsov, A.A. Leontyev, G.K. Kitaeva, Generation of optical–terahertz biphotons and detection of their terahertz component under frequency-nondegenerate parametric down-conversion, *JETP Letters*, vol. 112, pp. 269-273, (2020).
- [12] P. Prudkovskii, A. Leontyev, K. Kuznetsov, G. Kitaeva, Towards Measuring Terahertz Photon Statistics by a Superconducting Bolometer, *Sensors*, vol. 21, p. 4964 (2021).

LASER-MATTER INTERACTION

LMI-I-1

Ultrashort-pulse-laser excited dielectric materials: Unexpected transient optical properties

P. S. Sneftrup¹, S. H. Møller^{1,2}, T. Winkler¹, **P. Balling**¹

1- Dept. of Physics and Astronomy, Aarhus University, Ny Munkegade 120, DK-8000 Aarhus C, Denmark

2- Joint Attosecond Science Laboratory, University of Ottawa and National Research Council of Canada, 25 Templeton Street, Ottawa ON K1N 6N5, Canada

balling@phys.au.dk

It is well established that ultrashort laser pulses in the IR and visible parts of the electromagnetic spectrum can readily excite materials with a bandgap that vastly exceeds the photon energy. The excitation is initiated by strong-field excitation (e.g. multiphoton or tunnel excitation), and the carriers thus promoted from valence to conduction band give rise to major changes in the material. Many experiments, based on time-resolved (pump-probe) laser spectroscopy, have investigated the transient optical properties of different dielectric materials, and the behavior has often been attributed to the formation of an electron plasma described by a Drude model. For certain materials, predominately quartz, changes due to the formation of self-trapped excitons must also be included; see Ref. 1 for an overview.

In this presentation, we will focus on a few recent examples of experimental investigations of highly excited dielectric materials, which exhibit properties that are not explained by the current models. The first example reports on the ultrafast dynamics of fused silica, which has been investigated by measuring polarization-resolved reflectance of a wavelength-tunable probe pulse following a near-infrared pump pulse [2]. The data, which should, in principle, allow the determination of both real and imaginary parts of the time-dependent electric permittivity, turned out to become incompatible with an isotropic optical response ~ 200 fs after the excitation. This was reconciled with a uniaxial permittivity tensor, which predicts greatly enhanced absorption of p-polarized light, suggesting that an absorption channel is missing in the standard optical models for strongly excited dielectrics.

Another unexpected transient optical feature has been reported by investigating highly excited dielectric materials with slightly higher probe fluences than are normally used. By employing transmission pump-probe spectroscopy, it was demonstrated that both sapphire and quartz samples under appropriate conditions exhibit transient optical amplification of the probe pulses [3,4]. The gain is attributed to two-photon stimulated emission occurring due to an energetically localized population inversion between the bottom of the conduction band and the top of the valence band.

- [1] P. Balling and J. Schou, Femtosecond-laser ablation dynamics of dielectrics: basics and applications for thin films, *Rep. Prog. Phys.* **76**, 036502 (2013).
- [2] S. H. Møller, S. T. Andersen, and P. Balling, Transient optical properties of highly excited dielectric materials: Apparent birefringence and delayed reflectivity increase, *Phys. Rev. Research* **2**, 043010 (2020).
- [3] T. Winkler, L. Haahr-Lillevang, C. Sarpe, B. Zielinski, N. Götte, A. Senftleben, P. Balling, and T. Baumert, Laser amplification in excited dielectrics, *Nature Physics* **14**, 74-79 (2018).
- [4] T. Winkler, P. Balling, B. Zielinski, C. Sarpe, N. Jelzow, R. Ciobotea, A. Senftleben, T. Baumert, Unveiling nonlinear light-amplification regimes in fused silica with femtosecond imaging spectroscopy, *Physical Review Research* **2**, 023341 (2020).

LMI-I-2

Ultrafast oscillatory dynamics of free carriers in semiconductors driven by intense ultrashort laser pulses: a basis of novel technologies

Vitaly Gruzdev

*Department of Physics and Astronomy, University of New Mexico,
210 Yale Blvd. NE, Albuquerque, NM, 87106, USA*

E-mail: vgruzdev@unm.edu

A broad range of ultrafast laser interactions with semiconductors receive reasonable interpretation in terms of frequent electron-phonon collisions with characteristic collision time about 1 femtosecond. Those interpretations support a broad range of experimental data on laser-induced ablation, ultrafast melting, and characterization of transient optical response by pump-probe methods [1, 2]. However, reasonable interpretations of the recently reported generation of very high-order harmonics [3, 4] and electric charge [5, 6] in dielectrics and semiconductors assume minor perturbation of the laser-driven electron dynamics by electron-particle collisions. The latter means the electron-phonon collision time must be comparable to pulse width that is typically about 100 femtoseconds. The contradiction between the two assumptions is removed by considering energy dependence of electron-phonon collision time. Quasi-resonant promotion of valence-band electrons to the very bottom part of a conduction band results in the magnitudes of electron-particle collision time as large as hundreds of femtosecond. In this case, the laser-generated free electrons perform laser-driven oscillations with a minor perturbation from the low-rate collisions. This type of laser-driven free-carrier dynamics may serve as a fundamental mechanism of novel physical effects. Among them, we consider ultrafast conversion of multi-cycle laser pulses into femtosecond pulses of electric current and amplification of low-power probe laser pulses by the oscillating free-carrier plasma. In contrary to the pioneering results of Refs. [5, 6], the ultrafast light-to-current conversion by the laser-driven free-carrier oscillations is feasible for laser pulses carrying as many as 15 to 20 cycles, i. e., at pulse width of about 100 fs. We discuss parametric scaling of the photocurrent and its applications in sub-PHz optoelectronics, generation of ultrashort pulse of strong magnetic fields, and THz pulses. The oscillating free carriers may also experience induced inverse bremsstrahlung effect due to scattering by ions of a crystal lattice. Under some conditions specified by our theoretical calculations, that scattering results in domination of light amplification over absorption. This process may serve as a basis for novel approaches of parametric amplification of ultrashort laser pulses that may be especially efficient for mid-infrared spectrum range.

This work is supported by Research Technology & Laboratory Directorate / Basic Research Office of the US Department of Defense via Newton Award for Transformative Ideas during the COVID-19 Pandemic No. HQ00342010028 and the Air Force Office of Scientific Research under award number FA9550-15-1-0254.

LMI-I-3

Effects of Laser Energy Delocalization in the Regimes of Bulk Modification of Transparent Dielectrics

M. Zukerstein¹, V.P. Zhukov^{1,2,3}, N.M Bulgakova¹

1- HiLASE Centre, Institute of Physics ASCR, Za Radnicí 828, 25241 Dolní Břežany, Czech Republic

2- Federal Research Center for Information and Computational Technologies, 6 Lavrentyev Ave., 630090 Novosibirsk, Russia

3- Novosibirsk State Technical University, 20 Karl Marx Ave., 630073, Novosibirsk, Russia

bulgakova@fzu.cz

Femtosecond laser irradiation of dielectric materials enables deposition of laser energy in a highly localized region whose dimensions can be comparable with laser wavelength. This property of fs laser pulses is widely used for direct writing of multidimensional optical structures inside transparent materials for various photonic and optoelectronic applications [1] that requires gentle modifications of material properties without creation of cracks around the laser-affected zone. On the other hand, creation of extreme states of matter in the material bulk requires strongly localized absorption of laser energy at high energy density levels [2] that is hindered by the intensity clamping effect [3]. We have demonstrated numerically [4] that, using doughnut-shaped laser pulses can lead at certain irradiation conditions to overcoming the clamping effect and reaching very high densities of absorbed energy localized at nano-scales. Such localization is envisioned to result in generation of pressures up to hundreds of gigapascals, yielding in formation of unusual material polymorphs.

To verify the numerical data, experiments on laser modification of fused silica have been carried out using 35-fs, 800-nm laser (Astrella from Coherent). The experiments were performed with Gaussian and doughnut-shaped laser pulses in a wide range of beam energy with focusing inside fused silica bulk at NA = 0.25 as in [4]. At laser energies above 5 μ J, modification was not clearly observed at single laser pulses for both Gaussian and doughnut-shaped beams. Moreover, for multi-pulse irradiation, modification by the Gaussian beam was more pronounced than for doughnut-shaped pulses, contrary to the results presented to [4] for low beam energies. Numerical simulations performed for high-energy irradiation conditions revealed strong delocalization of the laser energy, similar to that reported for silicon in [5], with the maximum of the absorbed energy density insufficient for fused silica modification. Furthermore, the maximum of the absorbed energy density is higher for the Gaussian pulses, in agreement with the experimental data. At decreasing laser beam energy, situation is overturned: the maximum of the absorbed energy density becomes considerably higher for the doughnut-shaped pulses with achieving the conditions of material modification at single laser pulses. The physical processes responsible for the delocalization/localization effect and the dependence of the latter on the focusing conditions will be discussed.

[1] K. Sugioka, Progress in ultrafast laser processing and future prospects, Nanophotonics, vol. 6, pp. 393–413 (2017).

[2] V. Mizeikis, S. Kohara, Y. Onishi, N. Hirao, A. Saito, A. Vailionis, S. Juodkazis, Synthesis of high-pressure phases of silica by laser-induced optical breakdown, Appl Phys A, vol. 104, pp. 903–906 (2011).

[3] W. Liu, S. Petit, A. Becker, N. Aközbek, C. M. Bowden, S.L. Chin, Intensity clamping of a femtosecond laser pulse in condensed matter, Opt. Commun., vol. 202, pp. 189–197 (2002).

[4] V.P. Zhukov, A.M. Rubenchik, M.P. Fedoruk, N.M. Bulgakova, Interaction of doughnut-shaped laser pulses with glasses, J. Opt. Soc. Am. B, vol. 34, pp. 463–471 (2017).

[5] E.V. Zavedeev, V.V. Kononenko, V.M. Gololobov, V.I. Konov, Modeling the effect of fs light delocalization in Si bulk, Laser Phys. Lett., vol. 11, article 036002 (2014).

LMI-I-4

Solving Bloch equations to evaluate the energy deposition in silica induced by two-color femtosecond laser pulses

P. González de Alaiza Martínez¹, E. Smetanina², I. Thiele³, B. Chimier¹, G. Duchateau⁴

1- University of Bordeaux-CNRS-CEA, Centre Lasers Intenses et Applications, UMR5107, 351 Cours de la Libération, F-33405 Talence, France

2- Faculty of Physics, L. V. Lomonosov Moscow State University, Moscow, Russia

3- Department of Physics, Chalmers University of Technology, SE-412 96 Göteborg, Sweden

4- CEA, CESTA, 15 Avenue des Sablières, CS60001, 33116 Le Barp Cedex, France

Main author email address: guillaume.duchateau@cea.fr

The manufacturing industry widely uses micromachining (from the μm to mm scale) based on laser ablation in microelectronics and many other high-tech fields [1]. Regarding laser processing of dielectric materials, a large number of applications have emerged including surface processing such as patterning, texturing, and etching, and material removal such as cutting and drilling. In these applications, the laser pulse interacting with the dielectric target first drives electrons into excited states through photo- and impact ionization together with laser heating in the conduction band, and their subsequent relaxation towards the lattice through collisions leads to an effective energy deposition into the material [2]. If this deposited energy exceeds locally a given threshold of the material, then irreversible macroscopic material modifications take place a few picoseconds later.

To further optimize such laser processes by tailoring the electron dynamics and energy deposition, pulse-shaping techniques consisting of complex temporal envelopes, frequency chirps, or a mixture of colors are developed. The use of two-color laser pulses, i.e., two laser pulses with different colors, is of particular interest since specific processes of electron dynamics depend on the photon energy. A high-frequency pulse is efficient for seeding electrons through multiphoton ionization whereas a lower-frequency pulse is advantageous to heat these electrons and then cause material damage by an electron avalanche [3,32]. Since both wavelengths introduce opposite behaviors, by delaying in time the two laser pulses, one expects to find configurations that optimize the energy deposition into the material.

In this talk, the electron dynamics in dielectric materials induced by two-color femtosecond laser pulses is addressed by solving dedicated optical Bloch equations [3]. This model includes photo- and impact ionization, the laser heating of conduction electrons, their recombination to the valence band, and their collisions with phonons. The influence of photon energies, laser intensities, and pulse-to-pulse delay is analyzed. Depending on the interaction process, colors cooperate to excite electrons or drive them independently. For the given laser parameters, an optimal pulse-to-pulse delay is found which enhances significantly the energy deposition into the material, in agreement with experimental observations [4].

[1] K. Sugioka et al, Femtosecond laser 3D micromachining: a powerful tool for the fabrication of microfluidic, optofluidic, and electrofluidic devices based on glass, Lab on a Chip 14, 3447–3458 (2014).

[2] E. G. Gamaly, The physics of ultra-short laser interaction with solids at non-relativistic intensities, Phys. Reports 508, 91–243 (2011).

[3] E. Smetanina et al, Optical Bloch modeling of femtosecond-laser-induced electron dynamics in dielectrics, Phys. Rev. E 101, 063206 (2020)

[4] P. González de Alaiza Martínez et al, Modeling the time-dependent electron dynamics in dielectric materials induced by two-color femtosecond laser pulses: Applications to material modifications, Phys. Rev. A 103, 033107 (2021).

LMI-I-5

Ultrashort laser heating of Al and W metals: learning from self-reflectivity and ablation threshold measurements

Thibault Genieys¹, George Tsibidis², Marc Sentis¹, Olivier Utéza¹

1- Aix-Marseille University, CNRS, LP3 UMR 7341, F-13288 Marseille, France

2- Institute of Electronic Structure and Laser (IESL), Foundation for Research and Technology (FORTH) N. Plastira 100, Vassilika Vouton, 70013, Heraklion, Crete, Greece

Main author's email address: uteza@lp3.univ-mrs.fr

Laser energy coupling and redistribution in materials depends on their electronic structure and of the excitation characteristics (intensity, wavelength) [1]. For instance, excitation of nonthermal electron population has been observed or postulated with consequences on optical transient properties and on energy redistribution and relaxation [2-5]. In order to explore those fundamental mechanisms in the energetic regime of ablation and to progress into knowledge of laser excitation of metals, we use Gaussian ultrashort pulses of different pulse duration (15 – 100 fs @ 800 nm central wavelength) and incident energy (0.1 – 30 F_{th} , with F_{th} : ablation threshold fluence). This range of laser parameters gives a convenient tool for probing laser heating of metals in strong non-equilibrium conditions and under various situations of energy coupling and relaxation in the material. It also provides valuable experimental data for evaluating ablation characteristics and reliability of modeling approach, based on Drude-Lorentz and two-temperature approach, in a range of pulse duration little investigated yet. The study is applied to post-transition (Al) and transition (W) metals with diverse electronic structure, from free-electron gas Distribution of State (DOS) structure to more complex DOS distribution with possibility of excitation of bound d-band transitions. To provide quantitative details for further interpretation, we carefully measure the reflectivity integrated over the pump pulse below and above ablation threshold (see figure 1). Using post-mortem diagnostic (confocal microscopy) and classical diameter-regression technique, we also determine the ablation threshold fluence as a function of ultrashort pulse duration. The results obtained are detailed and discussed in view of bringing useful information for understanding laser energy deposition and transformation of metals in the ultrashort irradiation regime [6,7]. In particular, we retrieve the effective electron collision rate as a function of excitation which is an important marker to benchmark laser – matter interaction.

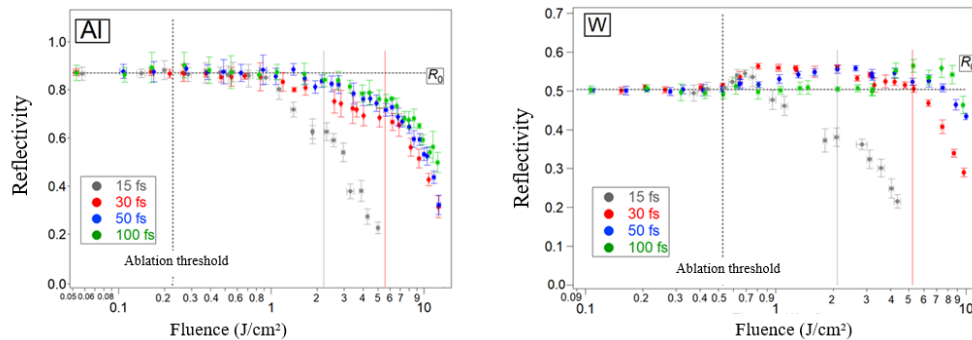


Fig. 1. Evolution of reflectivity as a function of incident fluence and for different pulse durations (15 – 100 fs) for two cases: Al (left) and W (right). R_0 indicates the value of unperturbed reflectivity ($F \ll F_{th}$). The red and grey lines indicate the energetic level above which nonlinear effects develop in our experiments. Note that F_{th} (dot line) was found identical for all pulse duration tested (15 – 100 fs).

- [1] E. Bévilion, R. Stoian, J.Ph. Colombier, Nonequilibrium optical properties of transition metals upon ultrafast electron heating, *J. Phys.: Condens. Matter* 30, 385401 (2018).
- [2] E. Carpene, Ultrafast laser irradiation of metals: Beyond the two-temperature model, *Phys. Rev. B* 74, 024301 (2006).
- [3] N. Del Fatti, C. Voisin, M. Achermann, S. Tzortzakis, D. Christofilos, and F. Vallée, Nonequilibrium electron dynamics in noble metals, *Phys. Rev. B* 61 (24), 16 956 (2000).
- [4] B.Y Mueller, B. Rethfeld, Relaxation dynamics in laser-excited metals under nonequilibrium conditions, *Phys. Rev. B* 87, 035139 (2013)
- [5] G.D. Tsibidis, Ultrafast dynamics of non-equilibrium electrons and strain generation under femtosecond laser irradiation of Nickel, *Appl. Phys. A* 124:311 (2018)
- [6] T. Genieys, M. Sentis, O. Utéza, Investigation of ultrashort laser excitation of aluminum and tungsten by reflectivity measurements, *Appl. Phys. A* 126, 263 (2020).
- [7] T. Genieys, M. Sentis, O. Utéza, Measurement of ultrashort laser ablation of four metals (Al, Cu, Ni, W) in single pulse regime, *Advanced Optical Technology* 9 (3), 131–143 (2020).

LMI-I-7

Influence of pulse duration and pulse separation on dynamics and efficiency of ultrafast laser ablation of metals

Jan Winter¹, Maximilian Spellauge¹, David Redka¹, Heinz P. Huber^{1*}

1- Munich University of Applied Sciences, Lasercenter, Lothstr. 34, 80335 Munich, Germany

**heinz.huber@hm.edu*

A surface irradiated with an ultrashort pulse passes through a sequence of physical processes, occurring on a temporal range spanning from femtoseconds to microseconds. Open questions remain as to why the pulse duration and temporal pulse separation influence the energy specific ablation volume.

Pump-probe ellipsometry (PPE) [1] reveals changes to the complex refractive index for the first tens of picoseconds, while pump-probe microscopy (PPM) [2] gives access to changes of the relative reflectivity from the initial pulse impact to the final state after about 1 μ s. Fig. 1 displays PPM experiments on Cu, Al and AISI304 in air, showing the transient evolution of the relative reflectivity change $\Delta R/R$ for probe pulse delay times ranging between -12.5 ps and 10 μ s.

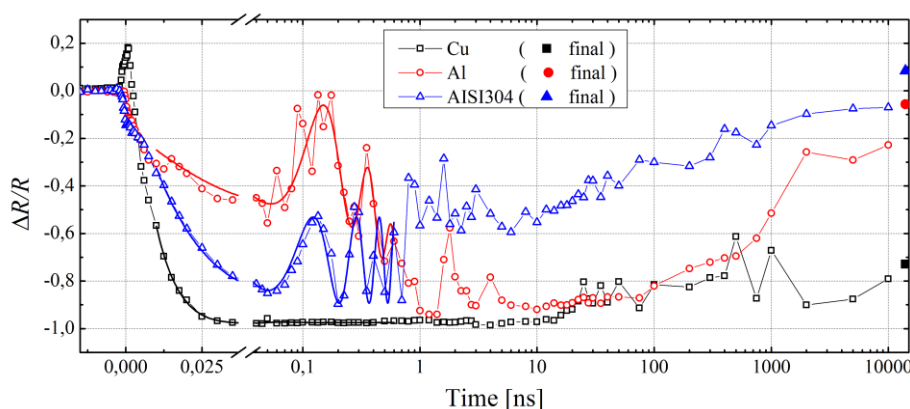


Fig. 1 Transient reflectivity change $\Delta R/R$ of Cu (black open squares), Al (red open circles) and AISI304 (blue open triangles)

The experiments indicate an ultrafast density decrease at the surface of 30% within the first 5 ps, which creates a surface expansion [3] as well as separation and propagation of a spallation layer from about 100 ps to 1 ns. Finally, the spallation layer disintegration and particle generation occurs from 1 ns to 100 ns [4].

Our measurements and simulations support the conclusion that the ablation process is efficient and precise when stress-confinement is fulfilled, which means, when initiated with pulse durations shorter than the mechanical relaxation time of about 5 ps and left un-interrupted until the final state is approached after about 10 to 100 ns [5]. MHz-burst processing leads to particle shielding, GHz-burst processing to re-deposition.

[1] S. Rapp, M. Kaiser, M. Schmidt, H.P. Huber, Ultrafast pump-probe ellipsometry setup for the measurement of transient optical properties during laser ablation, *Opt. Expr.* 24 (2016) 17572

[2] M. Domke, S. Rapp, M. Schmidt, and H. Huber, Ultrafast pump-probe microscopy with high temporal dynamic range, *Optics Express* 20 (2012) 10330

[3] J. Winter, S. Rapp, M. Schmidt and H.P. Huber, Ultrafast laser processing of copper: A comparative study of experimental and simulated transient optical properties, *Applied Surface Science* 417 (2017) 2

[4] J. Winter, S. Rapp, M. Spellauge, C. Eulenkamp, M. Schmidt, and H.P. Huber, Ultrafast pump-probe ellipsometry and microscopy reveal the surface dynamics of femtosecond laser ablation of aluminium and stainless steel, *Applied Surface Science* 511 (2020) 145514

[5] M. Spellauge, J. Winter, S. Rapp, C. McDonnell, F. Sotier, M. Schmidt, and H.P. Huber, Influence of stress confinement, particle shielding and re-deposition on the ultrashort pulse laser ablation of metals revealed by ultrafast time-resolved experiments, *Applied Surface Science* 545 (2021) 148930.

LM-I-8

Assessment of the time-dependent density functional theory for investigating femtosecond laser energy absorption by metals

T. J.-Y. Derrien¹, Y. Levy¹, N.M. Bulgakova¹

¹*Institute of Physics AS CR, HiLASE Centre, Za Radnici 828, 25241 Dolni Brezany, Czech Republic.*

derrien@fzu.cz

Measuring and predicting the absorption of laser energy by crystalline materials is of high interest for improving control in laser processing of solids [1]. Depending on the choice of laser parameters and of materials, a wide range of phenomena can affect the absorption dynamics of the intense light [1]. As a result, several kinds of theoretical descriptions are being developed to investigate this problem based on the Drude formalism, finite temperature DFT, combining DFT with two-temperature modeling, and time-dependent density functional theory (TDDFT) [2-5]. Among the listed approaches, only the TDDFT enables to get insight into non-equilibrium dynamics of laser-excited electron subsystems in solids, both in semiconductors [6-8] and metals [5,9]. Using this technique, the possibility to study high intensity regimes beyond the Kubo-Greenwood approximation was evidenced [9].

In this work, the TDDFT [10] was used to investigate the energy absorption of several metallic materials irradiated by ultrashort infrared and UV laser pulses. The energy absorbed and the electron current generated in the laser-irradiated metals were calculated as a function of time and for a wide range of laser intensities. The simulation results provide insights into the role of the fields induced by the oscillation of charges in the bulk of metals and allow to study the metal optical response at high intensities, beyond the usually employed approximations. A comparison of the obtained results with experimental data, which are available in literature, is provided.

[1] Shugaev, M. V. et al., *MRS Bulletin*, **2016**, *41*, 960-968.

[2] Shugaev, M. V. et al., in: *Advances in the Application of Lasers in Materials Science, Springer Series in Materials Science*, **2018**, *274*, 107-148.

[3] Bévillon, E. et al. *J. Phys. Cond. Mat.*, **2018**, *30*, 385401.

[4] Blumenstein, A. et al., *Phys. Rev. B*, **2020**, *101*, 165140.

[5] Volkov, M. et al. *Nat. Phys.*, **2019**, *15*, 1145-1149.

[6] Lucchini, M. et al. *Science*, **2016**, *353*, 916-919.

[7] Sommer, A. et al. *Nature*, **2016**, *534*, 86.

[8] Derrien, T. J.-Y. et al. *arXiv preprint arXiv:2104.0897*, 2021, Submitted.

[9] Andrade, X. et al. *Eur. Phys. J. B* **2018**, *91*, 229.

[10] Tancogne-Dejean, N. et al. *J. Chem. Phys.*, **2020**, *152*, 124119.

LM-I-9

Femtosecond Laser Induced Physicochemical Reactions

W. Kautek

University of Vienna, Department of Physical Chemistry, Vienna, Austria
wolfgang.kautek@univie.ac.at

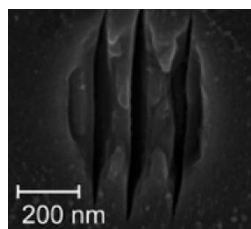


Fig. 1. LIPSS in the type I-b diamond ($N = 100$, $F = 0.5 \text{ J cm}^{-2}$. Polarization: horizontal).

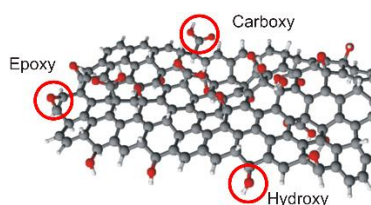


Fig. 2. Graphene oxide redox reactivity.

Investigations of pulse laser -induced chemical conversions and reactions in thin films and interfaces are reviewed. This includes femtosecond laser-induced phase transitions of diamond (Fig. 1) [1] and redox processes in graphene nanosheet synthesis [2] analogous to electrochemical control (Fig. 2) [3].

Hot electron electrochemistry shows the potential of ultrafast chemical processing [4-9]. The emission of hot electrons into an electrolyte containing electron scavengers allows the ultrafast monitoring of the electrochemistry of intermediates, and therefore provides the potential of insights in fast hot electron electrochemical kinetics, nanomedicine, and the laser-assisted generation of colloidal solutions (Fig. 3).

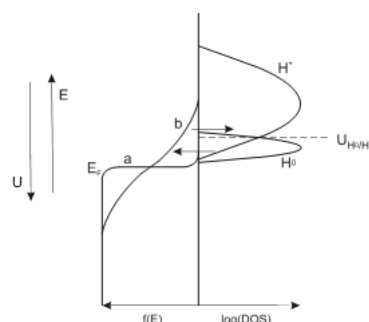


Fig. 3. Electronic Fermi-Dirac Distribution on the Metal and Density of States (DOS) of H_3O^+ and H_{ad} .

- [1] M. Forster, C. Huber, O. Armbruster, R. Kalish, W. Kautek, 50 nanometer femtosecond pulse laser induced periodic surface structures on nitrogen-doped diamond, *Diam. Rel. Mat.* 74 (2017) 114-118.
- [2] M. Pfaffeneder-Kmen, I. Falcon Casas, A. Naghilou, W. Kautek, Femtosecond laser assisted reduction of graphene oxide: effect of fluence and substrate on defects and electrochemical properties, 2021, in publication.
- [3] M. Pfaffeneder-Kmen, I. Falcon Casas, A. Naghilou, G. Trettenhahn, W. Kautek, A Multivariate Curve Resolution evaluation of an in-situ ATR-FTIR spectroscopy investigation of the electrochemical reduction of graphene oxide, *Electrochim. Acta* 255 (2017) 160-167.
- [4] A.G. Krivenko, J. Krüger, W. Kautek, and V.A. Benderskii, Subpicosecond-pulse-laser-induced thermoemission of hot electrons from metals into aqueous electrolytes: experiments at mercury and silver, *Ber. Bunsenges. Phys. Chem.* 99 (1995) 1489.
- [5] A.G. Krivenko, W. Kautek, J. Krüger, and V.A. Benderskii, Subpicosecond Emission from Mercury and Silver into Electrolyte Solution: An Experimental Study, *Russian J. Electrochem.* 33 (1997) 394.
- [6] A.G. Krivenko, V.A. Benderskii, J. Krüger, and W. Kautek, Gigantic hydrogen-ion discharge current initiated by a subpicosecond laser, *Russian J. Electrochem.* 33 (1998) 1068.
- [7] W. Kautek and O. Armbruster, *Non-Thermal Material Response to Laser Energy Deposition*, Springer Series in Materials Science 191 (2014) 43-66.
- [8] A. Naghilou, O. Armbruster, W. Kautek, Laser-Induced Non-thermal Processes, in "Handbook of Laser Micro- and Nano-Engineering", Ed. K. Sugioka, Springer Nature Switzerland AG 2020, pp 1-23.
- [9] O. Armbruster, H. Pöhl, W. Kautek, Femtosecond laser hot electron electrochemistry, 2021, in publication.

LM-I-10

Improvement of fabrication resolution in two-photon polymerization by using GHz burst mode

Koji Sugioka, Kotaro Obata, and Francesc Caballero-Lucas

RIKEN Center for Advanced Photonics, RIKEN, Wako, Saitama 351-0198, Japan

Main author email address: ksugioka@riken.jp

Two-photon polymerization (2PP) of photo-sensitive polymer materials using femtosecond (fs) lasers can create true three-dimensional micro- and nano structures with almost arbitrary shapes in an additive manner. One of the important features of 2PP is to achieve a high fabrication resolution far beyond the diffraction limit of the incident laser beam due to nonlinear absorption at the focal volume. Meanwhile, in order to explore more efficient process with higher quality, the ablation using a burst mode that oscillates groups of high-repetition rate pulse train with an extremely short time interval is currently widely investigated. The GHz bursts of fs laser enables to induce ablation before the residual thermal energy deposited by previous pulses diffuses away from the processed area, resulting in the reduction of the ablation threshold and enhancement of ablation efficiency [1]. In this study, we apply the fs laser beam operated with the GHz burst mode to 2PP of photo-sensitive polymers to investigate the effect of the burst on photochemical reactions.

2PP of a Zr-based organic-inorganic hybrid material mixed with photo-initiator has been performed using an fs laser system with a central wavelength of 1030 nm and a pulse duration of 220 fs. The number of pulses in the burst can be adjusted up to 25. Figure 1 shows dependence of polymerization threshold of the intra-pulse energy on the number of intra-pulses for the GHz burst mode. For comparison, the threshold for single pulse irradiation (single mode) is also shown. The polymerization threshold decreases as the number of intra-pulses increases, and 16 nJ of the threshold for 10 intra-pulses reduces by 55% compared to that for the single mode. However, it should be noted that the burst mode requires higher total power (dose) for the polymerization, indicating decrease of polymerization efficiency. More importantly, we have found that the GHz burst mode significantly improves the fabrication resolution, in particular the resolution along the beam axis, probably due to the reduced threshold associated with efficient heat accumulation by the burst mode.

[1] C. Kerse et al., "Ablation-cooled material removal with ultrafast bursts of pulses", *Nature* **537**, 84-88, (2016).

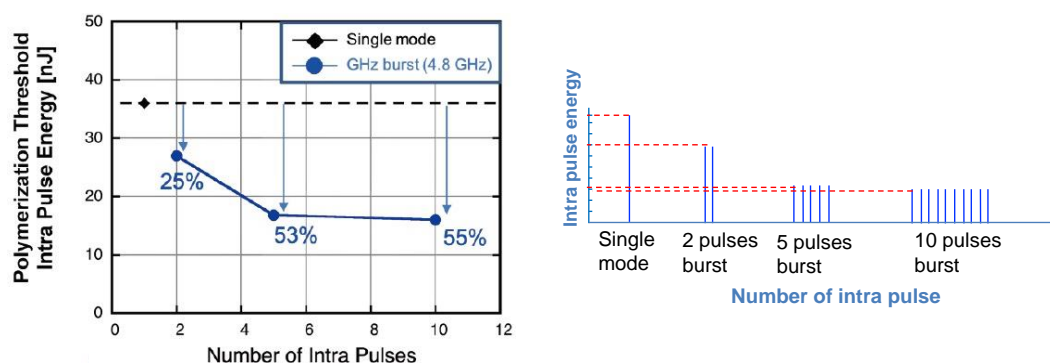


Fig. 1. Dependence of polymerization threshold of the intra-pulse energy on the number of intra-pulses at GHz burst mode. The threshold for the single mode is also shown for comparison.

LM-I-11

Laser-induced plasma in water as an origin of chemical reactions

V.V. Kononenko, V.M. Gololobov, K.H. Ashikkalieva, N.R. Arutyunyan and V.I. Konov

Prokhorov General Physics Institute of the Russian Academy of Sciences, Moscow, Russia

e-mail: vitali.kononenko@nsc.gpi.ru

The laser plasma in water is a problem of great interest in solution chemistry, biology, and medicine [1,2]. One of the most attracting technique based on the plasma-assisted processes is a photochemical reduction of metal salts. Recently, intense femtosecond laser radiation was demonstrated to effectively ionize solution and drive the formation of metal nanoparticles (NPs) in aqueous media [3]. This approach is "green", i.e. requires the minimum number of chemical reactants, and seems to provide precise control over the size and shape of synthesized nanoparticles. Here we present an experimental study of laser induced plasma in the gold aqueous solution ($\text{HAuCl}_4 \cdot 3\text{H}_2\text{O}$) and explore the correlation between its properties and a rate of the gold NPs synthesis.

Ionization of water was carried out in a strong optical field of the Ti:sapp femtosecond laser (pulse duration ~ 100 fs, wavelength 800 nm, intensity $> 10^{12}$ W/cm²). Both the refractive index and absorbance of the ionized zone were measured in the time window of ≈ 1.5 ns using a pump-probe interferometric technique which was developed for temporally and spatially resolved observation in solids. The measurements allowed quantifying the induced processes: ionization of water and solvation of excess electrons, geminate recombination and development of cavitation. Besides interferometric measurements the scattering of pump radiation on aqueous plasma was studied. The dependence of the intensity of the scattered light on the pulse energy allowed characterizing the plasma induced at high laser intensity ($> 10^{13}$ W/cm²) when the laser power exceeded remarkably the critical power and beam propagated in a quite nonlinear manner.

For the photochemical experiments the salt solutions were irradiated for times ≈ 10 minutes. The pulse energy was varied for each series. The kinetics of Au ions reduction and formation of Au NPs was measured monitoring (i) the absorption spectra of the solutions (a Perkin Elmer UV-vis-NIR double-beam spectrophotometer) and (ii) particle size distribution by a dynamic light scattering technique (an Zetasizer Nano analyzer). We discuss the relationship between the different regimes of water ionization and productivity of the metal ions reduction in laser-induced plasma. Presented data provide an experimental basis for theoretical models that describe the plasma-assisted processes in aqueous media.

This work was supported by the Russian Science Foundation (grant 19-12-00255).

[1] V. K. Meader, M. G. John, C. J. Rodrigues, K. M. Tibbetts, *The Journal of Physical Chemistry A*, 121~(36), 6742~(2017).

[2] A. Vogel, J. Noack, G. Huttman, G. Paltauf, *Applied Physics B*, 81~(8), 1015~(2005).

[3] C. Zhao, S. Qu, J. Qiu, C. Zhu, *J. Mater. Res.*, 18, 1710~(2003).

LM-I-12

Synthesis by laser ablation in liquid of alloy nanoparticles: controlling the structure and the composition for specific applications

V. Amendola¹

1- University of Padova, Department of Chemical Sciences 1, Via Marzolo 1-35131 Padova – ITALY

Main author email address: vincenzo.amendola@unipd.it

Laser ablation in liquid (LAL) emerged as a powerful technique for the production of nanoparticles (NPs) with peculiar surface chemistry and a large variety of compositions, included metastable phases and nanocomposites, all by the same self standing and simple set up.[1-2] Currently, several efforts are undergoing to improve the control on laser generated nanomaterials and to precisely understand the formation mechanism of NPs.[1,3,4] As part of these efforts, a whole catalogue of alloy NPs was accessible for fundamental studies about the structural motifs adopted by elements frozen at the nanoscale and the consequent set of physical-chemical properties. The insights on the structure-properties relation provided the basis for further optimization of the nanoalloys for specific applications. The cases of alloys designed to climb the volcano plot for specific electrocatalytic processes,[5,6] alloys where the coexistence of magnetic and plasmonic properties is engineered,[7,8] and noble metal alloys acting as 4-D multimodal contrast agents with enhanced clearance from the body[9] will be discussed. This is a general demonstration of the range of innovative results and functional optimization expected by the synergy between LAL synthesis, structural modelling, and experimental verification of functional properties in nonequilibrium nanoalloys.

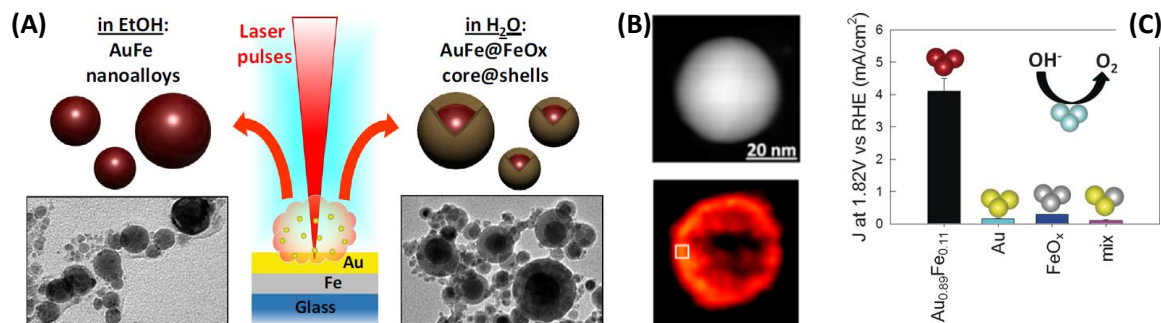


Figure 1. (A) Iron-rich Au-Fe nanoalloys are obtained in ethanol by nanosecond laser ablation of a bilayer Au/Fe film (left). When the same film is ablated in water, core-shell NPs of iron oxide-AuFe metal alloy (iron poor) are achieved.[3,4] These NPs possess interesting properties for photonics (B), exhibiting localized surface plasmons,[8] and for catalysis (C), with enhanced activity compared to single element analogues[5].

- [1] V. Amendola et al., Room-Temperature Laser Synthesis in Liquid of Oxide, Metal-Oxide Core-Shells, and Doped Oxide Nanoparticles, *Chem. Eur. J.*, 26, 9206 – 9242 (2020).
- [2] S. Crivellaro et al., A system for the synthesis of nanoparticles by laser ablation in liquid that is remotely controlled with PC or smartphone, *Rev. Sci. Instr.*, 90, 033902, (2019).
- [3] V. Amendola et al.; Formation of alloy nanoparticles by laser ablation of Au/Fe multilayer films in liquid environment, *J.Coll.Interf.Sci.*, 489, 18–27, (2017).
- [4] A. Tymoczko et al., One-step synthesis of Fe–Au core–shell magnetic-plasmonic nanoparticles driven by interface energy minimization, *Nanoscale Horiz.*, 4, 1326-1332, (2019).
- [5] I. Vassalini et al., Enhanced Electrocatalytic Oxygen Evolution in Au–Fe Nanoalloys, *Angew. Chem.*, 56, 6589–6593, (2017).
- [6] R. Brandiele et al., Climbing the oxygen reduction reaction volcano plot with laser ablation synthesis of Pt_xY nanoalloys, *Catal. Sci. Technol.*, 10, 4503–4508 (2020).
- [7] V. Amendola et al., Laser generation of iron-doped silver nanotruffles with magnetic and plasmonic properties, *Nano research* 8, 4007–4023, (2015).
- [8] D. Alexander et al., Electronic Structure-Dependent Surface Plasmon Resonance in Single Au–Fe Nanoalloys, *Nano Lett.*, 19, 5754–5761, (2019).
- [9] V. Torresan et al., 4D Multimodal Nanomedicines Made of Nonequilibrium Au–Fe Alloy Nanoparticles *ACS Nano* 14, 12840–12853 (2020).

LM-I-13

UV-laser induced contamination on space optics

F. R. Wagner¹, G. Gebrayel El Reaidy^{1,2}, D. Faye² and J.-Y. Natoli¹

1- Aix Marseille Univ, CNRS, Centrale Marseille, Institut Fresnel, Marseille, France

2- Centre National d'Etudes Spatiales, 18, Avenue E. Belin – 31401 Toulouse Cedex 9, France

frank.wagner@fresnel.fr

Laser Induced Contamination (LIC) is a phenomenon that takes place under multi-pulse laser irradiation and causes damage to optical surfaces. It was first mentioned in 1993 when working with a sealed Nd:YAG laser [1]. Today LIC is mostly a problem for high power photonics in vacuum, especially when working in the UV. In particular, LIC was identified as a major problem for operating lasers on satellites and just lately led to a strongly reduced lifetime of the 355nm laser of the ESA Aeolus mission (Aladin instrument) [2]. The development of the Aladin instrument triggered in fact an important research effort concerning LIC [3].

The physical and chemical processes behind LIC are the same as those exploited by Laser Induced Chemical Vapor Deposition (LI-CVD) of carbonaceous thin films on the optical elements: Polymers outgas volatile organic molecules that cover all surrounding surfaces including the optical elements. The laser radiation interacts directly or indirectly with the adsorbed molecules and cracks them. Some of the less volatile products bind strongly to the optical surface increasing its optical absorption coefficient. The enhanced optical absorption may lead to catastrophic laser induced damage of the optics (creating micro cracks) or simply decrease the performance of the optical system (especially in resonators).

Building on the former project oriented knowledge, we led some more fundamental investigations on the LIC process and characterized the LIC deposits.

A new setup was built, in which toluene vapor or the outgassing of 3M EC2216 epoxy glue were used as contaminants. An experimental protocol was established staying close to the one given by the DLR Stuttgart [4] and good reproducibility was demonstrated in terms of deposit morphology (measured by WLIM white light profilometer) and transmission loss of the 355 nm 13 ns laser pulses [5]. The optical properties of the LIC deposits were then analyzed using quantitative optical path difference microscopy combined with WLIM thickness data and it was shown that the deposit is not yet very absorbing in the first stage of the process [6]. When creating a LIC deposit on bare fused silica substrates, a slight anti-reflective coating effect can even be observed [5].

Laser induced fluorescence images easily allow to detect the deposit onset [3] and the transition from the first to the second stage of the process, *i.e.* the start of the crater formation in the initially bump shaped deposit. The average thickness growth rate during the first stage can thus be analyzed as a function of laser fluence and contamination conditions and the results be compared to CVD knowledge.

Finally, the lateral growth of the LIC deposit around the irradiated region shows that the process includes an important thermal component. Lateral crater growth is presumably driven by energy being absorbed in the center of the crater and subsequent heat conduction from the center towards the edges.

[1] F. E. Hovis, B. A. Shepherd, C. T. Radcliffe, A. L. Bailey, and W. T. Boswell, Optical damage at the part per million level: the role of trace contamination in laser-induced optical damage, in *Laser-Induced Damage in Optical Materials: 1993*, Proc SPIE, vol. 2114, pp. 145–153, (1994).

[2] https://www.esa.int/Our_Activities/Observing_the_Earth/Aeolus/Second_laser_boosts_Aeolus_power, Second laser boosts Aeolus power, last accessed on 2021-05-27, European Space Agency, (2019).

[3] H. Schröder, S. Borgmann, W. Riede, and D. Wernham, Investigation of laser induced deposit formation under space conditions, in *International Conference on Space Optics — ICSSO 2008*, Proc SPIE, vol. 10566, p. 105661K, (2017).

[4] W. Riede, H. Schroeder, G. Bataviciute, D. Wernham, A. Tighe, F. Pettazzi, and J. Alves, Laser-induced contamination on space optics, in *Laser-Induced Damage In Optical Materials: 2011*, Proc SPIE, vol. 8190, p. 81901E, (2011).

[5] G. G. El Reaidy, F. R. Wagner, D. Faye, and J.-Y. Natoli, Study of the first stages of laser-induced contamination, *Optical Engineering*, vol. 57, p. 121903, (2018).

[6] F. R. Wagner, G. Gebrayel El Reaidy, D. Faye, and J.-Y. Natoli, Laser induced deposits in contaminated vacuum environment: Optical properties and lateral growth, *Optics & Laser Technology*, vol. 122, p. 105889, (2020).

LM-I-14

Laser-induced periodic surface structures: when electromagnetics drives hydrodynamics

J. Bonse¹, M. Mezera¹, C. Florian^{1,2}, J. Krüger¹, S. Gräf³

1- Bundesanstalt für Materialforschung und -prüfung (BAM), Unter den Eichen 87, D-12205 Berlin, Germany

2- Princeton University, 70 Prospect Avenue, Princeton, NJ 08540, USA

3- Friedrich-Schiller-Universität Jena, Löbdergraben 32, D-07743 Jena, Germany

joern.bonse@bam.de

Laser-induced Periodic Surface Structures (LIPSS, ripples) are a universal phenomenon and can be generated in a contactless, single-step process on almost any material upon irradiation of solids with intense laser radiation [1,2]. Nowadays processing rates of up to m^2/min are enabling new industrial applications in medicine, optics, tribology, biology, etc. [3-6]. Depending on the specific type of LIPSS, their structural sizes typically range from several micrometers down to less than 100 nanometers – far beyond the optical diffraction limit – while their orientations exhibit a clear correlation with the local polarization direction of the laser radiation.

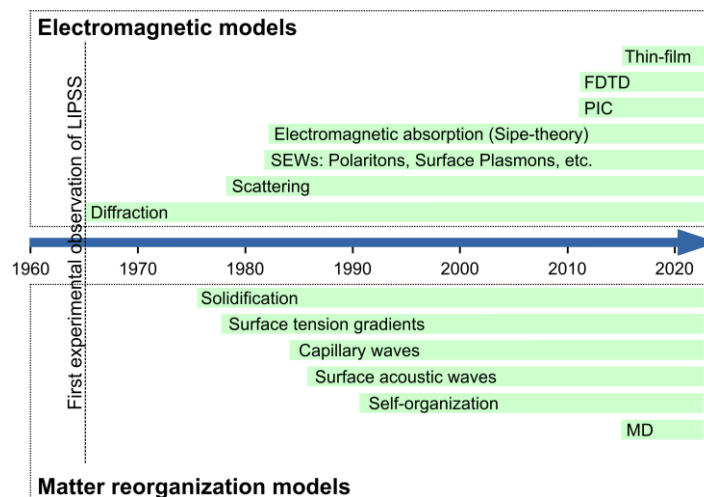


Fig. 1. Historic development of LIPSS theories based on electromagnetic models (top) or matter reorganization models (bottom).
Reproduced from [7]. (CC-BY 4.0 license)

From a theoretical point of view, however, a vivid, controversial, and long-lasting debate has emerged during the last two decades, whether LIPSS originate from electromagnetic effects (seeded already during the laser irradiation) – or whether they emerge from matter reorganization processes (distinctly after the laser irradiation), see Fig. 1. This presentation reviews the currently existent theories of LIPSS [7]. A focus is laid on the historic development of the fundamental ideas, their corresponding mathematical descriptions and numerical implementations, along with a comparison and critical assessment of the different approaches.

- [1] J. Bonse, J. Krüger, S. Höhm, A. Rosenfeld, Femtosecond laser-induced periodic surface structures, *Journal of Laser Applications*, 24, 042006, (2012). <https://doi.org/10.2351/1.4712658>
- [2] J. Bonse, S. Höhm, S.V. Kirner, A. Rosenfeld, J. Krüger, Laser-induced Periodic Surface Structures – A Scientific Evergreen, *IEEE Journal of Selected Topics in Quantum Electronics*, 23, 9000615, (2017). <https://doi.org/10.1109/JSTQE.2016.2614183>
- [3] C. Florian, S.V. Kirner, J. Krüger, J. Bonse, Surface functionalization by laser-induced periodic surface structures, *Journal of Laser Applications*, 32, 022063, (2020). <https://doi.org/10.2351/7.0000103>
- [4] S. Gräf, Formation of laser-induced periodic surface structures on different materials: fundamentals, properties and applications, *Advanced Optical Technologies*, 9, 11-39, (2020). <https://doi.org/10.1515/aot-2019-0062>
- [5] J. Bonse, Quo Vadis LIPSS? – Recent and Future Trends on Laser-Induced Periodic Surface Structures, *Nanomaterials*, 10, 1950, (2020). <https://doi.org/10.3390/nano10101950>
- [6] J. Bonse, S.V. Kirner, J. Krüger, Laser-Induced Periodic Surface Structures (LIPSS), *Handbook of Laser Micro- and Nano-Engineering* (K. Sugioka, Ed.), Springer, (2021). https://doi.org/10.1007/978-3-319-69537-2_17-2
- [7] J. Bonse, S. Gräf, Maxwell Meets Marangoni – A Review of Theories on Laser-Induced Periodic Surface Structures, *Laser & Photonics Reviews*, 14, 2000215, (2020). <https://doi.org/10.1002/lpor.202000215>

LM-I-15

Tailoring Sub-micrometer Periodic Surface Structures via Ultrashort Pulsed Direct Laser Interference Patterning

F. Fraggelakis ¹, G. D. Tsididis ¹ and E. Stratakis ^{1,2}

1. Institute of Electronic Structure and Laser (IESL), Foundation for Research and Technology (FORTH), N. Plastira 100, Vassilika Vouton, 70013, Heraklion, Crete, Greece

2. Department of Physics, University of Crete, 71003 Heraklion, Greece

Direct Laser Interference Patterning (DLIP) with ultrashort laser pulses (ULP) represents a precise and fast technique to produce tailored periodic sub-micrometer structures on various materials. In this work, an experimental and theoretical approach is presented to investigate the previously unexplored fundamental mechanisms for the formation of unprecedented laser-induced topographies on stainless steel following proper combinations of DLIP with ULP. The combined spatial and temporal shaping of the pulse increases the level of control over the structure features whilst it brings new insights in the structure formation process. DLIP is aimed to determine the initial conditions of the laser-matter interaction by defining an ablated region while double ULP are used to control the reorganisation of the self-assembled laser induced sub-micrometer sized structures by exploiting the interplay of different absorption and excitation levels coupled with the melt hydrodynamics induced by the first of the double pulses. A multiscale physical model has been developed to correlate the interference period, polarization orientation and number of incident pulses with the induced morphologies. Special emphasis is given to electron excitation, relaxation processes and hydrodynamical effects that are crucial to the production of complex morphologies. Results are expected to derive new knowledge of laser-matter interaction in combined DLIP and ULP conditions and enable enhanced fabrication capabilities of complex hierarchical sub-micrometer sized structures for a variety of applications.

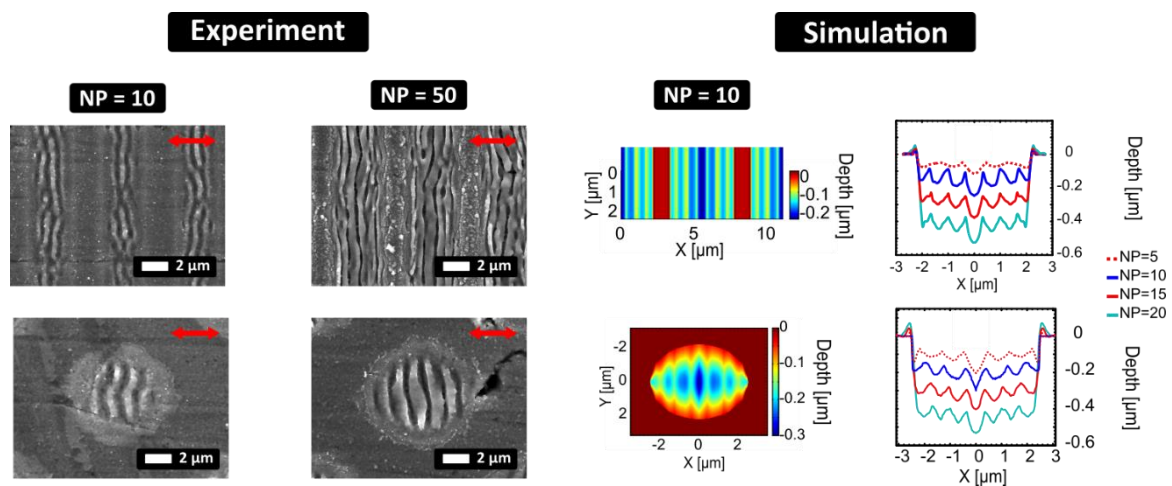


Fig.1. Experimental and theoretical data on stainless steel irradiation by spatially shaped double femtosecond laser pulses. Results are illustrated for two-DLIP (first row) and four DLIP (second row).

References

Fraggelakis F., Tsididis G.D., Stratakis E, *Phys. Rev. B* 103, 054105, 2021

LM-I-16

Laser-induced micro- and nano-structures for biomedical applications

Johannes Heitz*Institutes of Applied Physics, Johannes Kepler University Linz, Austria*

The generation of laser-induced micro- and nano-structures is a rapidly growing field to tailor special industrial, scientific, and biomedical applications. This is significantly driven by the exciting properties of micro- and nanopatterned materials found in natural biological species, including pronounced adhesive and anti-adhesive properties, wetting and directional fluid transport, and control of cell growth. The structuring techniques addressed here focus on developments in ultrafast laser processing. This includes direct writing techniques such as direct laser-writing and two-photon polymerization as well as the self-organized formation of micro- and nanopatterns at surfaces induced by exposure to laser radiation.

LM-I-17

Femtosecond Laser Induced Surface Crystalline-Amorphous Alternating Structure on a GST225 Thin Film for Optical Applications

S. Kozyukhin¹, T. Kunkel², M. Smayev³, Yu. Vorobyov⁴, P. Lazarenko⁵

1 – Kurnakov Institute of General and Inorganic Chemistry of RAS, 31, Leninsky pr., Moscow, 119991, Russia

2 - Moscow Institute of Physics and Technology, 9 Institutskiy Per., Dolgoprudny, 141701, Russia

3 - P.N. Lebedev Physical Institute of RAS, 53, Leninsky Pr., Moscow, 119333, Russia

4 - Ryazan State Radio Engineering University, Gagarin st. 59/1, Ryazan, 390005, Russia;

5 - National Research University of Electronic Technology, Shokin sq. 1, Zelenograd, 124498, Russia

sergkoz@igic.ras.ru

The fast switching time of Ge₂Sb₂Te₅ thin films between amorphous and crystalline states initiated by laser beam as well as significant change of their optical properties open wide perspectives for the application of these materials to fully optical devices, in particular, to reconfigurable metasurfaces. In this work, the formation of two-phase laser-induced periodic surface structures (LIPSS) on the surface of the initially amorphous Ge₂Sb₂Te₅ thin films under the illumination by fs-laser pulses has been studied [1,2]. The LIPSS appearance can be explained by the formation of surface plasmon-polariton and its subsequent interference with the incident beam resulting in spatial modulation of temperature on the film surface. The effect of parameters such as wavelength (from 515 nm to 1030 nm), frequency (1 kHz to 1 MHz), number of laser pulses (from 1 to 2²⁰), direction of the light field vector of the laser beam, thickness of Ge₂Sb₂Te₅ thin film (from 30 nm to 130 nm) and type of substrate material (dielectric and conductor) on LIPSS parameters was investigated. We have determined LIPSS parameters by several methods (optical microscopy, SEM, TEM, AFM, c-AFM) which correlate with each other. As the results indicate, the valleys consist of the crystalline phase, while the ridges remain amorphous, and their period depends on the wavelength of induced laser irradiation. The height difference between the valley and the ridge is several nanometers only, namely 2-3 nm, according to the AFM data in the case of $\lambda=1030$ nm. This value is more than the roughness of the as-deposited amorphous film, but significantly less than the height of the ripples observed in the similar film after the femtosecond laser irradiation with $\lambda = 515$ nm, where the 20 nm height ripples were observed. The formation of ripples has a trigger nature and begins with a certain threshold fluence at a constant number of laser pulses. It is shown that an increase in the pulse number leads to an exponential decrease in the threshold fluence, which is explained by the presence of positive feedback in the studied system. Additionally, we covered large areas with coherent LIPSS. The large area patterns created by scanning technique appear very regular, the effect of individual laser spots cannot be recognized and the ripples are all in phase with each other. This work was supported by RFBR (20-03-00379).

[1] S. Kozyukhin, P. Lazarenko, Yu. Vorobyov et al. Laser-induced modification and formation of periodic surface structures (ripples) of amorphous GST225 phase change materials. *Optics and Laser Technology*, 113, 87-94 (2019).

[2] S. Kozyukhin, M. Smayev, V. Sigaev et al. Specific features of formation of laser-induced periodic surface structures on GST225 amorphous thin films under illumination by femtosecond laser pulses. *Phys. Status Solidi B*, 1900617 (2020).

LM-I-18

Non-diffractive ultrafast beams; new opportunities for material processing

R. Stoian

Laboratoire Hubert Curien, CNRS UMR 5516, Université Jean Monnet, 42000 St Etienne, France

razvan.stoian@univ-st-etienne.fr

Material structuring represents today the base for rapidly growing application areas in emerging technologies. Ultrafast lasers contribute essentially to the development of micro/nanotechnologies, being able to structure materials with utmost precision [1]. Alongside efficiency, the question of resolution is crucial for further industrial insertion and the challenge lies now in pushing the capacity to reach the nanoscale, with resulting morphologies defining upgraded functions to be attached to the structured material. Optical processing being typically limited by diffraction to scales comparable to the wavelength, an alternative strategy to achieve extreme scales relies on harvesting material reactions to light, experiencing thus not an optical limit but a material organization limit which, for a large range of material phenomena, lies one order of magnitude below. We will discuss ultrafast laser irradiation concepts, combining beam engineering in space and time, capable of achieving structuring features with sub-wavelength characteristic sizes in direct irradiation modes as well as in periodic self-organization processes [2,3]. We will show the effects of far and near-field scattering and coherent superposition of wavelets in generating light patterns of various complexity, dynamically coupling electromagnetic and hydrodynamic evolution. We present advanced optical methods to resolve in-situ irradiation nanoscaled patterns and the growth of nanostructures beyond diffraction limit [4,5]. We indicate as well significant advantages of non-diffractive beams to structure materials with unprecedented resolution as well as with high efficiency. These advantages pertain to both transparent and non-transparent matter (Fig.1). A range of applications will be discussed.

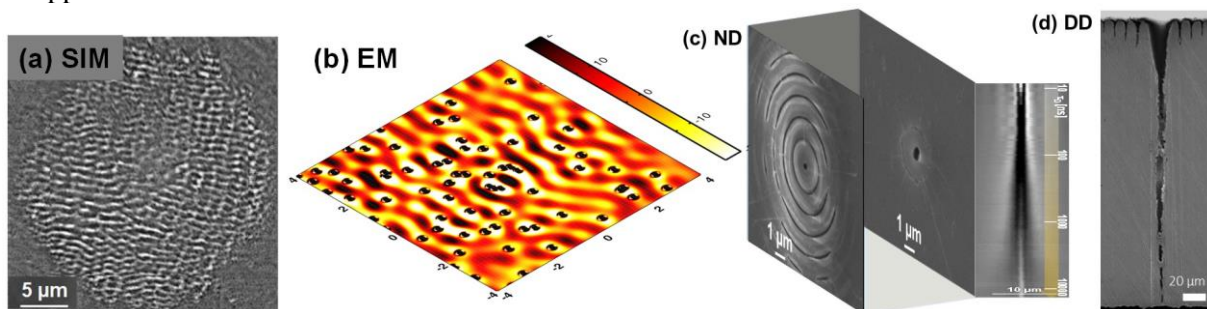


Fig 1. (a) Observing in-situ nanostructure on stainless steel using structured illumination microscopy [4]. (b) Regular patterns of light determining surface corrugation with periodic surface structures [3]. (c) Nanostructuring of transparent material (inset: process dynamics) with non-diffractive beams [2]. (d) Deep drilling in non-transparent materials with non-diffractive beams.

- [1] K. Sugioka and Y. Cheng, Ultrafast lasers-reliable tools for advanced materials processing, *Light: Sci. Appl.* 1, e149 (2014).
 [2] R. Stoian, M. K. Bhuyan, A. Rudenko, J.P. Colombier, and G. Cheng, High-resolution material structuring using ultrafast laser non-diffractive beams, *Adv. Phys.* X 4, 1659180 (2019)
 [3] A. Rudenko, C. Mauclair, F. Garrelie, R. Stoian, and J. P. Colombier, Self-organization of surfaces on the nanoscale by topography-mediated selection of quasi-cylindrical and plasmonic waves, *Nanophotonics*, <https://doi.org/10.1515/nanoph-2018-0206> (2019).
 [4] A. Aguilar, C. Mauclair, N. Faure, J. P. Colombier, and R. Stoian, In-situ high-resolution visualization of laser-induced periodic nanostructures driven by optical feedback, *Sci. Rep.* 7, 16509 (2017).
 [5] M. Somayaji, M. K. Bhuyan, F. Bourquard, P. K. Velpula, C. D'Amico, J. P. Colombier and R. Stoian, Multiscale electronic and thermo-mechanical dynamics in ultrafast nanoscale laser structuring of bulk fused silica” *Sci. Rep.* 10, 15152 (2020)

LM-I-19

Electron and Phonon Dynamics in Nonlinear Optics by Multiscale First-Principles Simulation

Atsushi Yamada¹

1-1-1 Tennodai, Tsukuba, Ibaraki Center for Computational Sciences, University of Tsukuba, Japan

Main author email address: ayamada@ccs.tsukuba.ac.jp

We have developed multi-scale simulation methods to describe coupled dynamics of light electromagnetic wave on macroscopic scale and electrons and optionally atoms (phonon) in microscopic scale. Our research interests are to investigate basic aspects of light-matter interaction from the atomistic level based on these methods, which are performed by our developed open-source computer software, SALMON [1,2]. In this talk, we give a presentation about (1) optical response change of some simple materials (α -quartz, silicon, and aluminum) using low to very high intensity short pulses, and (2) coherent phonon generation induced by impulsive stimulated Raman scattering (ISRS).

In the first topic (1), we show the changes of reflectivity and transmittance by increasing the pulse intensity as well as the electron dynamics under the nonlinear interaction by carrying out the multiscale coupled Maxwell's equation and time-dependent density functional theory (Maxwell + TDDFT method) based on the first-principles [3,4]. We then discuss the mechanisms of the change in the nonlinear optical responses.

In the second topic (2), the extended simulation with ionic motion, Maxwell + TDDFT + MD method is performed for pump-probe spectroscopy of diamond to study the generation process of coherent phonon and modulation of Raman signal. We also show the terahertz generation process of organic molecular crystal, 5,6-dichloro-2-methylbenzimidazole (DCMBI), induced by the ISRS by performing the force-field based classical molecular dynamics simulation coupled with the electromagnetic wave, namely Maxwell + polarizable MD method [5,6]. These calculations show the detailed behaviors of the interacting light fields and microscopic material systems in the spectroscopic processes.

References:

- [1] Web site of SALMON, <http://salmon-tddft.jp/>
- [2] M. Noda, S. A. Sato, Y. Hirokawa, M. Uemoto, T. Takeuchi, S. Yamada, A. Yamada, Y. Shinohara, M. Yamaguchi, K. Iida, I. Floss, T. Otake, K.-M. Lee, K. Ishimura, T. Boku, G. F. Bertsch, K. Nobusada, K. Yabana, "SALMON: Scalable Abinitio Light-Matter simulator for Optics and Nanoscience", *Comp. Phys. Comm.*, **235**, 356-365 (2019)
- [3] Atsushi Yamada and Kazuhiro Yabana, "Multiscale time-dependent density functional theory for a unified description of ultrafast dynamics: pulsed light, electrons, and lattice motions in crystalline solids", *Phys. Rev. B*, **99**, 245103 (2019)
- [4] Atsushi Yamada and Kazuhiro Yabana, "Modulation of probe signal in coherent phonon detection revisited: Analytical and first-principles computational analyses", *Phys. Rev. B*, **101**, 214313 (2020)
- [5] Atsushi Yamada, "Multiscale Coupled Maxwell's Equations and Polarizable Molecular Dynamics Simulation Based on Charge Response Kernel Model", *J. Chem. Phys.*, **152**, 094110 (2020).
- [6] Atsushi Yamada, "Multiscale simulation of terahertz radiation process in benzimidazole crystal by impulsive stimulated Raman scattering", *J. Chem. Phys.*, **153**, 244506 (2020)

LM-I-20

Scattering and self-healing of terahertz high-order Bessel beams transmitting through randomly inhomogeneous media and obstacles

B.A. Knyazev^{1,2}, V.S. Pavelyev¹, K.N. Tukmakov¹, A.S. Reshetnikov¹, V.V. Gerasimov², N.D. Osintseva²

¹ Samara National Research University, Moskovskoe Shosse 34, Samara, Russia, 443086

² Budker Institute of Nuclear Physics of SB RAS, Pr. Lavrentyeva 11, Novosibirsk, Russia, 630090

b.a.knyazev@inp.nsk.su

Bessel beams with orbital angular momentum are considered as one of the possibilities for creating multiplex communication lines in the atmosphere [1]. At the Novosibirsk free electron laser (NovoFEL) facility [2], experiments were being carried out in the terahertz range to study the propagation of Bessel beams (BB) of orders from zero to fourth through randomly inhomogeneous phase media and amplitude obstacles. The beams were created using binary silicon axicons with spiral zones, the period of which was 3.2 mm, and the height of the diffractive relief was calculated for a wavelength of 141 μm and was equal to 29.1 μm . A well-formed "diffraction-free" Bessel beam with such parameters existed at distances from 150 to 350 mm from the axicon [3].

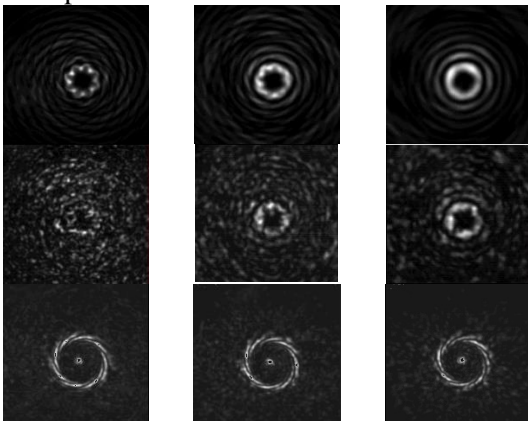


Fig. 1. Top row: images of the Bessel beam recorded at distances of 85, 141, and 197 mm from the axicon in the absence of obstacles. Middle row: images obtained after installing an 8 mm thick polyethylene foam sheet after the axicon. Bottom row: Image taken in the focal plane of a silicon lens with a focal length of 100 mm, mounted at the distances indicated above.

The laser generated monochromatic linearly polarized radiation with a pulse duration of 100 ps and a repetition rate of 5.6 MHz. The value of the mode radius of the Gaussian beam of the NovoFEL in the plane of the axicons was 12.1 mm. The intensity distribution was recorded by a Pyrocam IV pyroelectric detector with a matrix size of 25.6 \times 25.6 mm^2 . Obstacles were installed whether directly behind the axicon or at the beginning of the Bessel beam formation region at a distance of about 150 mm. The intensity distribution of the beam passing through the obstacle was recorded at different distances from the axicon up to the beam decay region (350 mm). To study the degree of conservation of the fraction of radiation containing the initial Bessel mode, we used the property of the BB to form a narrow ring at the focus of the lens, containing, in the case of non-disturbed BB, all the

energy of the initial beam. An example of the measurement results for a Bessel beam with a topological charge $\ell = 4$ is shown in Fig. 1. Knowing the properties exhibited by Bessel beams with orbital angular momentum when passing through the lens cascade, it can be argued that the results shown in Fig. 1 demonstrate a high content of the corresponding Bessel mode in the reconstructed beam.

This work was supported by the Russian Science Foundation, grant 19-72-20202. Experiments were carried out at the Novosibirsk free electron laser, which is a part of the Shared Research Facility "Siberian Synchrotron and Terahertz Radiation Center."

- [1] I.P. Lukin, E.Kh. Tanier. Formation of a Bessel beam with conical focusing in a turbulent atmosphere. Bulletin of the Tomsk Polytechnic University. v. 318, No. 2, 63-67 (2011).
 [2] G.N. Kulipanov, E.G. Bagryanskaya, E.N. Chesnokov, et al. Novosibirsk free electron laser—facility description and recent experiments. IEEE Trans. THz Sci. Techn, vol. 20, 798-809 (2015).
 [3] Y.Y. Choporova, B.A. Knyazev, G.N. Kulipanov, V.S. Pavelyev, M.A. Scheglov, N.A. Vinokurov, B.O. Volodkin, V.N. Zhabin. High-power Bessel beams with orbital angular momentum in the terahertz range. Phys. Rev. A. vol. 96, 023846 (2017).

LM-I-21

Optical Non-Linearity and Light Diffusion in Laser-Pumped Fluorescent Nanocomposites: From a Spontaneous Fluorescence Emission to a Random Lasing

Dmitry A. Zimnyakov^{1,2}, Sergey S. Volchkov¹, Leonid A. Kochkurov¹, Alexander F. Dorogov¹

1 – Yury Gagarin State Technical University of Saratov, 77 Polytechnicheskaya St., Saratov, 410054, Russia

2 – Institute for Problems of Precision Mechanics and Control, 24 Rabochaya St., Saratov, 410028, Russia

zimnykov@mail.ru

Fluorescence emission in multiple scattering random media under high-intensity pulse-periodic laser pumping is considered in terms of the localization of “hot” pumped zones in the laser-treated medium. This localization is caused by the granular structure (speckle patterning) of the pumping laser field due to a significant excess of the coherence length of laser radiation over the characteristic scales of radiation propagation in the medium. From this point of view, each laser speckle in the pumped volume is associated with a local low-finesse optical cavity with a characteristic size of the order of the pump wavelength. Speckle-caused confinement of the pumping in combination with the absence of optical feedback between statistically independent laser speckles is a natural limiter of the spectral quality of the fluorescence response even at pump intensities significantly exceeding the threshold of random lasing in pumped fluorescent random media. This feature is observed in numerous experiments on the excitation of random lasing in multiple scattering random media with a high fluorescence yield and can be described in terms of the ratio of the stimulated emission component to the spontaneous component of the fluorescence output.

Modeling of the rise/fall kinetics of fluorescence in random fluorescent media under speckle-patterned laser pumping [1] has shown that the crucial influence on the ratio of the stimulated to the spontaneous component fluorescence at high pump intensities is exerted by the depletion of the ground state of the fluorophore and radiation losses in speckle-associated local microcavities. It was found that the extreme value of the effective cross-section of radiation losses in local microcavities in the absence of radiative transfer between neighboring cavities is inversely proportional to the characteristic size of cavities and the fluorophore concentration in the medium. The real value of the effective cross-section of radiation losses turns out to be significantly (at least one and a half to two decades) less than the extreme value due to the significant effect of radiation exchange between the speckle-associated microcavities.

The discussed concept was verified in experiments on pulse-periodic laser pumping of layers of close-packed titania and silica nanoparticles doped with aqueous solutions of Rhodamine 6G [1,2]. The experimentally obtained dependences of the ratio of the stimulated to the spontaneous fluorescence component on the pump parameters and the characteristics of the pumped samples are in good agreement with the simulation results within the framework of the concept.

The results obtained may be of interest from the point of view of further development of fluorescence diagnostics of media with a complex structure.

[1] D.A. Zimnyakov, S.S. Volchkov, L.A. Kochkurov, V.I. Kochubey, A.G. Mel'nikov, G.V. Mel'nikov, Speckle patterning of a pumping laser light as a limiting factor for stimulated fluorescence emission in dense random media, *Optics Express*, 29, pp. 2309-2331, (2021).

[2] D.A. Zimnyakov, S.S. Volchkov, L.A. Kochkurov, A.F. Dorogov, Specific features of fluorescence transfer in multiply scattering randomly inhomogeneous layers under intense laser pumping, *Quantum Electronics*, 50, pp. 1007-1014, (2020).

LM-I-22

Laser dielectric interactions: new insight from double pulse experiments

Stéphane Guizard¹, Allan Bildé², Sergey Klimentov³, Alexandros Mouskeftaras⁴

1. *Laboratoire Interactions, Dynamiques et Lasers, UMR 9222 CEA, CNRS, Université Paris-Saclay, CEA Saclay, F-91191 Gif-sur-Yvette, France.*

2. *Laboratoire des Solides Irradiés, CEA/CNRS, Université Paris-Saclay, Ecole Polytechnique, 91128 Palaiseau, France,*

3. *General Physics Institute of the Russian Academy of Sciences, Vavilova St 38, 11991 Moscow, Russia.*
4 *Laboratoire LP3, Aix-Marseille University, CNRS, UMR 7341, 13009 Marseille, France.*

Corresponding author: stephane.guizard@cea.fr

Abstract : Ultrafast lasers are powerful tools to study the dynamics of the relaxation processes occurring in matter, and this domain of time resolved science has known a broad development since the spreading of femtosecond lasers. The temporal resolution currently accessible – typically 30 fs - is however not always sufficient to directly resolve and provide a clear picture of the different physical mechanisms involved. This is for instance the case when an intense pulse impinges on wide band-gap dielectrics. In that case, several processes are already competing during the laser pulse itself. First, obviously the different excitation channels: usually a non linear photo-excitation, via multiphoton or tunneling ionization from the valence band to the conduction band, followed by further laser heating of carrier in the conduction band by multiphoton or sequence of single photon absorption. Then the first relaxation events begin before the end of the pulse: carrier-carrier collisions like impact ionization, electron-phonon coupling, exciton formation, etc. The repeated combination of laser heating-impact ionization, leads to an increase of the excited carrier population, eventually giving rise to laser induced avalanche. Whatever the pulse duration, it is thus not possible to resolve these different processes. To encompass this intrinsic difficulty, we have carried out experiments with a double exciting pulse scheme. Under appropriate conditions, we can control independently the two key parameters: plasma density and temperature. Then, using time resolved interferometry as a probe, we could directly observe for the first time an electronic avalanche induced by a laser pulse in a solid, namely crystalline SiO₂ [1]. A complete modeling, using multiple rate equation and taking into account the laser propagation, allows to fully describe the experimental results. In materials where exciton self-trapping does not occur, no evidence of electronic avalanche is found, and the lifetime of excited carrier is much longer [2]. Our investigations on a large set of different materials (NaCl, KBr, CaF₂, etc) provide a strong indication that a link exists between two apparently opposite relaxation mechanisms, exciton self-trapping and laser induced impact ionization and avalanche.

[1] S. Guizard, A. Bildé, S. Klimentov, A. Mouskeftaras, under press.

[2] A. Bildé *et al.*, to be published in J. Phys: Condens Matter, 2021.

LM-I-23

Fundamentals of ultrafast intra-center and interband photoexcitations in bulk diamond for micromarking and tracing applications

S. Kudryashov¹, P. Danilov¹, N. Smirnov¹, N. Stsepuro¹, G. Krasin¹, O. Kovalchuk^{1,2},
E. Oleynichuk¹, A. Levchenko¹, M. Kovalev¹, A. Ionin¹, N. Melnik¹ and R. Khmelniitskiy¹

¹Lebedev Physical Institute, Moscow, Russia;

²Geo-Scientific Research Enterprise Public Joint Stock Company ALROSA, Mirny, Russia;

e-mail: kudryashovsi@lebedev.ru

This work presents an overview of basic fundamental processes, underlying ultrafast optical and electronic dynamics during femtosecond-laser photoexcitations in natural diamonds (Fig.1a) for micromarking and tracing applications. A number of consequent process – non-linear laser propagation of femtosecond-laser pulses [1], spectrally- and intensity-dependent non-linear interband and intra-center (Fig.1b) photoexcitation mechanisms [2], Auger recombination and ambipolar diffusion of dense electron-hole plasma, generation of Frenkel “interstitial-vacancy” pair, atomistic processes of laser-induced modification of the present optical centers in diamond are overviewed, using our recent original results.

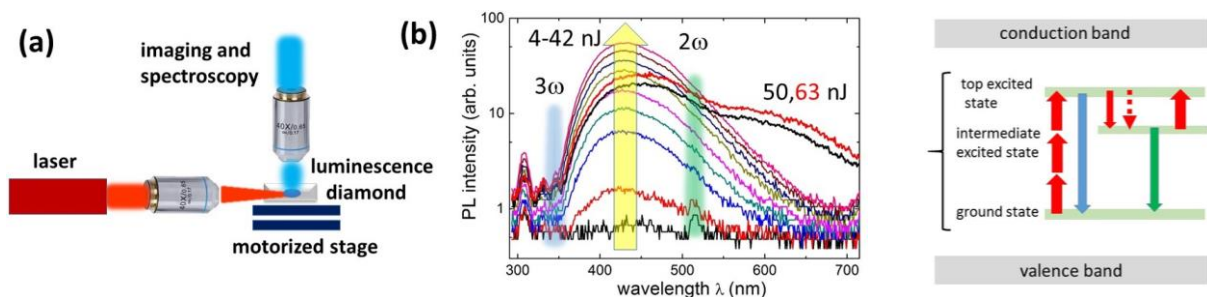


Fig.1. (a) Schematic of 1030-nm high-NA femtosecond-laser photoexcitation in diamond. (b) 3-photon blue-range A-band intra-center photoluminescence dynamically switching to 2-photon green-range photoluminescence from the intermediate process due to upper-level saturation, and the related three-level energy diagram.

This study is funded by the grant of Russian Science Foundation (project no. 21-79-30063).

[1] S.I. Kudryashov, A.O. Levchenko, P.A. Danilov, N.A. Smirnov, and A.A. Ionin, IR femtosecond laser micro-filaments in diamond visualized by inter-band UV-photoluminescence, *Optics Letters*, 45 (7), 2026-2029, (2020).

[2] S. Kudryashov, P. Danilov, N. Smirnov, A. Levchenko, O. Kovalchuk, R. Khmelniitskiy, M. Uspenskaya, and M. Kovalev, Broadband and fine-structured luminescence in diamond facilitated by femtosecond laser driven electron impact and injection of “vacancy-interstitial” pairs, *Optics Letters*, 46 (6), 1438-1441, (2021).

LM-I-24

Confinement of laser-matter interaction with shaped femtosecond pulses in dielectrics

Francois Courvoisier¹, M. Hassan¹, K Ardaneh¹, B. Morel¹,

J. Hoyo¹, R. Meyer¹, L. Furfaro¹, C. Billet¹, L. Froehly¹, R. Giust¹, C. Xie^{1,2}

¹ FEMTO-ST Institute, Univ. Bourgogne Franche-Comté, CNRS, 15B Avenue des Montboucons, 25030, Besançon Cedex, France

Ultrafast Laser Laboratory,

² Key Laboratory of Opto-electronic Information Technology of Ministry of Education,

School of Precision Instruments and Opto-electronics Engineering,

Tianjin University, 300072 Tianjin, China

francois.courvoisier@femto-st.fr

Ultrashort infrared laser pulses are enabling tools to process transparent materials in the three dimensions. The laser-matter interaction inside the bulk of condensed matter has opened new frontiers in the physics and technology of material treatment at micro or nanoscale. At the intensities of 10^{13} to 10^{14} W/cm², plasmas can be generated which lead to refractive index change, nanograting formation, or, depending on the conditions, to the formation of voids inside the bulk. Promising routes have been shown when femtosecond laser-induced microexplosions reach extreme conditions where new material phases can be generated.

Void formation with single shot Bessel beams has been demonstrated using both femtosecond and picosecond pulse durations [1]. In the femtosecond case, voids could be formed even with pulses down to typ ~50 fs, where avalanche would be expected to be quite inefficient [2]. The physics of energy deposition by ultrashort pulses shaped as Bessel beams is therefore questionable.

In this presentation, we will report on several experimental and numerical results of femtosecond pulse interaction with Bessel beams. Our simulations will provide insights into the dynamics of plasma generation. We report that high energy density is achieved inside the bulk of dielectrics using Bessel beams. We demonstrate, using double pulse illumination and the analysis of absorption dynamics, that warm dense matter can be created in the bulk of dielectrics. We will report on the specificity of Bessel beams in comparison with Gaussian ones to reach energy densities in the order of 10 MJ/kg [3].

Our results open up new opportunities for technological applications in terms of laser processing of glass and other dielectrics such as sapphire or diamond. New opportunities become also possible for nano-plasma physics and high-energy density physics inside materials with relatively low pulse energies, over volumes that are, for the first time, non-negligible since high energy density channels can be generated up to 1 cm length [4].

This research has received funding from H2020 European Research Council (ERC) under grant agreement 682032-PULSAR. This work was granted access to HPC resources PRACE (PULSARPIC PRA19 4980 and RA5614), TGCC(A0070511001 and A0090511001), and Mesocentre de Calcul de Franche-Comte.

References

- [1] M. K. Bhuyan et al, Appl. Phys. Lett, 97, 081102 (2010).
- [2] M.K. Bhuyan et al, Optica 4, 951 (2017)
- [3] J. Hoyo et al, Nanophotonics, 10, 1089-1097 (2021).
- [4] R. Meyer, et al, Appl. Phys. Lett., 114, 201105 (2019).

LM-I-25

Dual wavelength double fs-pulse laser irradiation for fused silica processing

J. Lopez¹, K. Gaudfrin^{1,2}, K. Mishchik³, M. Delaigue³, C. Hoenninger³, E. Audouard³, L. Gemini², R. Kling², G. Duchateau¹

1- Univ.Bordeaux, CNRS, CEA, CELIA UMR 5107, 33405 Talence, France

2- Alphanov, 33405 Talence, France

3- Amplitude Systemes, 33600 Pessac, France

john.lopez@u-bordeaux.fr

Ultrafast laser glass processing is a subject of high interest for many industrial applications in optics, medical device, or micro electronics industries. Indeed, ultrafast laser technology has the unique capacity to produce a high-quality surface or bulk modification in dielectric transparent materials thanks to nonlinear absorption. However, the throughput achieved with ultrafast lasers is still low compared to other laser technologies, laser-assisted chemical etching or mechanical processing. Temporal or spatial beam shaping is a smart and flexible technique to overcome this limitation and to meet industry requirements.

In the present work, we investigate the benefits and the drawbacks in using on dual-wavelength double fs-pulse laser irradiation for fused silica processing. Our purpose of this pump-pump experiment is to tune the electron dynamics in order to optimize energy deposition and then to improve ablated volume. We use green wavelength (515 nm) for the first pulse to enhance photo-ionization and near-infrared (1030 nm) for the second pulse to maximize electron heating and impact ionization. The investigated parameters are pulse-to-pulse delay (up to 20 ps), second pulse duration (1 and 10 ps) and total fluence (up to 20 J/cm²). The results will be discussed in terms of ablated volume and optical transmission. We demonstrate that (i) there is an optimum delay and (ii) the ablation behavior is intermediate between green and near-infrared single pulse irradiation. Our results are supported by a numerical model taking into account electron dynamics and absorbed energy density.

LM-I-26

Development of logic system elements based on new physical principles using quantum nanophotonics approaches for low-dimensional laser-induced surface topological structures

S. Arakelian, A. Kucherik, D. Bukharov, T. Khudaiberganov

Stoletovs Vladimir State University, Vladimir, Russia

arak@vlsu.ru

1. The 4D-laser technology fabrication of new structures and materials is considered. Nanostructures and thin films with controllable topology vs time (when thermodiffusion, gas-dynamic evaporation in pore-like structures with bubbles, ablation products, ballistic movement of the particles in liquid, being depended on the laser pulses duration) are under study. The interaction effects of solid targets with laser pulses of different durations for obtaining various nanocluster structures can be viewed as the possibility of synthesizing the 4D-objects, when the result depends not only on the stationary topological/geometric parameters of the system, but also on the dynamic interactions in the system leading to different final stable structures of different topology. This is due to the fact that for different durations of laser pulses the specific mechanisms of nanostructuring are activated. Therefore, time plays the role of a control parameter responsible for phase transitions, as well as the spatial parameters do when nanostructures of various dimensions arise – from quantum dots (0D) to 3D nanostructures. In addition, for short laser pulses we have non-equilibrium/transient phase transitions over the steady-state pressure-temperature phase-diagram according to the laser trajectory of heating. Although the conventionality of this consideration is obvious (the equilibrium phase diagram cannot be used for non-stationary processes), but it allows to discuss the current trends and clarifying the basic physical picture.

2. The topology peculiarities of the granulated metallic film deposited on dielectric substrates – due to clustered metallic structures in frame of the topology photonics – result in several principal items being observed in our experiment:

(1) In electroconductivity

- the tunneling delocalized effect depends on the size of nanoparticles, distance between them and shape of tunnel barriers as well as vs variation of the thickness of the films with transition from amorphous to crystalline structure
- the thermally activated hopping regime of the electronic transport between localized centers in 2D-array
- the topology superconducting cluster trend and tendency similar to topological insulator and coupling of charged particles by dimensional parameters;

(2) In optical characteristics

- the broadening of electronic levels
- optical metasurfaces characteristics
- strong optical response
- variation of the e-state density (on Fermi-surface).

3. The principal problem is under our discussion how to determine specific numerical values of the topology control parameters of a nanocluster system relying on these general relations for the achievement of the desired final result in the experiment. This requires a detailed research (in both theory and experiment) of the influence of nanocluster topological parameters on the functional properties of the substances used. Modelling of fundamental physical phenomena, e.g. a Mott-like long range quasi-particles, anomalous Hall-effect due to topology – transverse symmetry breaking and arising of the particle quantum size effects (Landau stair dependence) require to do the exact detail analysis. Nevertheless, the discussed phenomena give us an opportunity to establish the basis of new physical principles to create the functional elements for topological photonics in hybrid set-up (optics + electrophysics) being controlled by quantum coupled states and nonlinear dynamic processes with possible tendency and trends to superconductivity in selected by chemical composition of nanostructures.

LM-I-27

Atomistic view of laser ablation and nanoparticle fragmentation in liquids

Leonid V. Zhigilei

University of Virginia, Department of Materials Science and Engineering, Charlottesville, Virginia, USA

E-mail: lz2n@virginia.edu

The generation of colloidal solutions of chemically clean nanoparticles through pulsed laser ablation in liquids (PLAL) has evolved into a thriving research field that impacts industrial applications. Large-scale atomistic simulations have yielded important insights into the fundamental mechanisms of ultrashort (femtoseconds to tens of picoseconds) PLAL [1-5] and provided a plausible explanation of the origin of the experimentally observed bimodal nanoparticle size distributions. Recently, the atomistic simulations were extended to longer (hundreds of picoseconds to nanoseconds) laser pulses, enabling a detailed analysis of the effect of the pulse duration on the mechanisms responsible for the generation of nanoparticles [6]. In these simulations, three distinct nanoparticle generation mechanisms operating at different stages of the ablation process and in different parts of the emerging cavitation bubble were identified. The coexistence of the three distinct mechanisms of the nanoparticle formation at the initial stage of the ablation process can be related to the broad nanoparticle size distributions commonly observed in nanosecond PLAL experiments.

The generation of broad size distributions presents an obstacle for direct use of the colloids in advanced photonic, catalytic, and biomedical applications. To alleviate this limitation of PLAL, a complementary technique for laser processing of colloidal solutions of nanoparticles, the laser fragmentation in liquid (LFL) has been developed. In this technique larger nanoparticles are fragmented to produce a population of smaller nanoparticles with a narrow size distribution. First atomistic simulations of LFL of Au nanoparticles reveal the mechanisms that control the sizes, shapes and structure of the fragmentation products [7], as well as an important role the formation of a nanobubble around the irradiated nanoparticle plays in the fragmentation process.

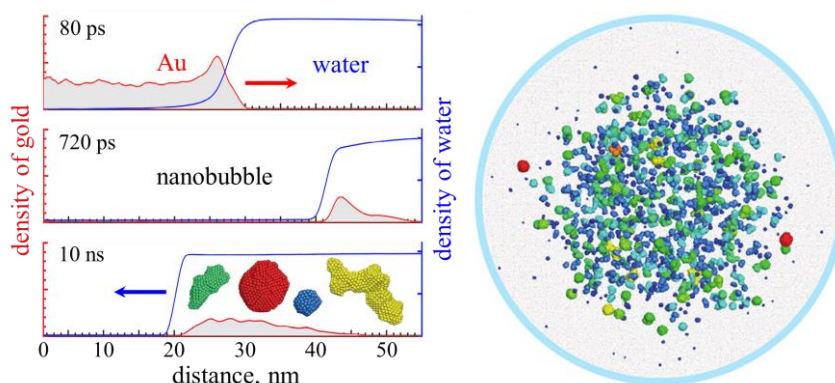


Figure 1. Density profiles and a snapshot of fragmentation products colored by nanoparticle size predicted in a simulation of LFL of a 20 nm Au particle irradiated by a 10 ps laser pulse in water [7].

- [1] C.-Y. Shih, C. Wu, M. V. Shugaev, and L. V. Zhigilei, Atomistic modeling of nanoparticle generation in short pulse laser ablation of thin metal films in water, *J. Colloid Interface Sci.* **489**, 3, 2017.
- [2] C.-Y. Shih, M. V. Shugaev, C. Wu, L. V. Zhigilei, Generation of subsurface voids, incubation effect, and formation of nanoparticles in short pulse laser interactions with bulk metal targets in liquid: Molecular dynamics study, *J. Phys. Chem. C* **121**, 16549, 2017.
- [3] C.-Y. Shih, R. Streubel, J. Heberle, A. Letzel, M. V. Shugaev, C. Wu, M. Schmidt, B. Gökce, S. Barcikowski, and L. V. Zhigilei, Two mechanisms of nanoparticle generation in picosecond laser ablation in liquids: the origin of the bimodal size distribution, *Nanoscale* **10**, 6900, 2018.
- [4] C.-Y. Shih, I. Gnilitzky, M. V. Shugaev, E. Skoulas, E. Stratakis, and L. V. Zhigilei, Effect of liquid environment on single-pulse generation of laser induced periodic surface structures and nanoparticles, *Nanoscale* **12**, 7674, 2020.
- [5] C.-Y. Shih, C. Chen, C. Rehbock, A. Tymoczko, U. Wiedwald, M. Kamp, U. Schuermann, L. Kienle, S. Barcikowski, and L. V. Zhigilei, Limited elemental mixing in nanoparticles generated by ultrashort pulse laser ablation of AgCu bilayer thin films in a liquid environment: Atomistic modeling and experiments, *J. Phys. Chem. C* **125**, 2132, 2021.
- [6] C.-Y. Shih, M. V. Shugaev, C. Wu, and L. V. Zhigilei, The effect of pulse duration on nanoparticle generation in pulsed laser ablation in liquids: Insights from large-scale atomistic simulations, *Phys. Chem. Chem. Phys.* **22**, 7077, 2020.
- [7] H. Huang and L. V. Zhigilei, Atomistic view of laser fragmentation of gold nanoparticles in liquid environment, *J. Phys. Chem. C*, in press, 2021, <https://doi.org/10.1021/acs.jpcc.1c03146>

LM-I-28

Studies of surface modifications with few-cycle laser pulses

Yingjie Chai¹, and M. J. Soileau¹

1- CREOL, the College of Optics and Photonics, University of Central Florida (UCF), Orlando,

Florida 32816, USA

**Email: yjchai@ucf.edu and mj@ucf.edu*

This paper reports progress in our studies of laser surface modifications with few-cycle laser pulses. High power laser-induced periodic surface structures are commonly generated and studied using many cycle lasers pulses. Few-cycle pulses offer a unique opportunity to study the initiation and growth of such structures. Models for the production of these structures invoke the interference of the field from subsequent cycles with surface polarization fields induced by previous cycles. For few-cycle pulses, one can study the onset and evolution of this process. Laser-induced damage experiment was conducted on ZnSe with (1) 170 fs 1030nm Yb: KGW laser, (2) 2-cycle, 11fs, and carrier-envelope-phase (CEP) stable infrared 1700nm centered laser source, and (3) 4-cycle, 13fs, and 1030nm centered near-infrared laser source. The poly-crystalline grain boundaries affect the beginning of surface damages morphologies, and the ripple evolved neatly as the laser shot accumulated. Single shot and multiple shots laserinduced damage test is demonstrated, and surface morphology evolution are carefully characterized according to ISO 21254. Electron dynamic calculations were employed according to Keldysh theory to demonstrate the electron density evolution in the ZnSe surface every shot. The experiment results demonstrated the very beginning of laser-induced ripples on the ZnSe surface by using the shortest infrared few-cycle laser pulse. Grain boundaries in polycrystalline material are regarded as the damage source at the very beginning of laser irradiation and eventually generate surface ripples which evolve to be orthogonal to the incident beam polarization (the geometry for most efficient coupling of incident fields with induced polarization fields). Different grain-sized polycrystalline ZnSe plates were precisely prepared and tooled to form optical windows or optical gain media and their damage threshold of different pulse numbers was carefully extracted. Laser-induced damage evolution along with the pulse number and grain boundary density are carefully characterized by SEM, AFM, and confocal Raman spectroscopy. Single crystal ZnSe was tested and characterized as well as a reference of a no-grain boundary. Experimental results will show the impact of grain boundary density on the laser-induced damage threshold of polycrystalline materials, which is of great value for future ultrashort laser pulse applications

Keywords: polycrystalline ZnSe, few-cycle laser, laser-ablation, laser-resistance.

LM-I-29

Relativistic plasma source optimization and applications

I.N.Tsymbalov^{1,2}, K.A.Ivanov^{1,3}, S.A.Shulyapov¹, D.A.Gorlova^{1,2}, A. B. Savel'ev^{1,3}

¹*Faculty of Physics, M.V. Lomonosov Moscow State University, Moscow, Russia;*

²*Institute for Nuclear Research of the Russian Academy of Sciences, Moscow, Russia;*

³*P.N. Lebedev Physical Institute of the Russian Academy of Sciences, Moscow, Russia*

e-mail: abst@physics.msu.ru

We present an overview of our recent activity on interaction of relativistic femtosecond laser pulses with dense plasma. Preplasma tailoring allows to achieve efficient generation of X-rays, gammas and well collimated electron beams with the tabletop terawatt femtosecond laser. We further consider possible application of the sources designed as well as feasibility of scaling to the larger laser facilities.

This study was supported in its different parts by the RFBR (grants №19-02-00104, №19-02-00740).

LM-I-30

Undesired X-ray emission during ultrashort pulse laser material processing

H. Legall¹, J. Bonse¹, J. Krüger¹

1- Bundesanstalt für Materialforschung und -prüfung (BAM), Unter den Eichen 87, D-12205 Berlin, Germany

joerg.krueger@bam.de

The use of ultrashort laser pulses for material processing in air has many advantages. Due to the progressive development in the laser sector, average powers in the kW range with pulse repetition rates exceeding the MHz-level are available [1]. The machining with high-intensity laser pulses can be accompanied by the generation of a near-surface electron plasma due to absorption and ionization of the material, a subsequent plasma heating by the laser pulse, and finally an interaction of “hot” plasma electrons with the workpiece leading to continuous and characteristic X-ray radiation (Fig. 1).

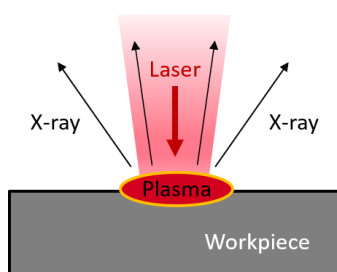


Fig. 1. Scheme of X-ray generation during ultrashort pulse laser material processing in air.

The amount of this unwanted X-ray radiation is determined by the laser parameters (pulse duration, intensity, wavelength, polarization), the workpiece (atomic number, surface preparation), and the laser process management (scanning or stationary regime, laser turning). The use of laser intensities above 10^{13} W/cm² in combination with laser pulse repetition rates in the few 100 kHz-range can lead to X-ray dose rates exceeding the permitted X-ray limits for members of the public. Especially the materials tungsten and steel show significant X-ray emission [2-7].

Recently, the current state of the art in the field of undesired generation of X-ray radiation during ultrashort pulse laser processing in air was reviewed [8]. In this presentation, important aspects of the measured X-ray doses, X-ray spectra, and practical issues of radiation protection are discussed.

- [1] C.J. Saraceno, D. Sutter, Th. Metzger, M.A. Ahmed, The amazing progress of high-power ultrafast thin-disk lasers, *Journal of the European Optical Society - Rapid Publications*, 15, 15 (2019). <https://doi.org/10.1186/s41476-019-0108-1>
- [2] H. Legall, C. Schwanke, S. Pentzien, G. Dittmar, J. Bonse, J. Krüger, X-ray emission as a potential hazard during ultrashort pulse laser material processing, *Applied Physics A* 124, 407 (2018). <https://doi.org/10.1007/s00339-018-1828-6>
- [3] R. Behrens, B. Pullner, M. Reginatto, X-ray emission from materials processing lasers, *Radiation Protection Dosimetry* 183, 361 (2019). <https://doi.org/10.1093/rpd/ncy126>
- [4] H. Legall, C. Schwanke, J. Bonse, J. Krüger, The influence of processing parameters on X-ray emission during ultra-short pulse laser machining, *Applied Physics A* 125, 570 (2019). <https://doi.org/10.1007/s00339-019-2827-y>
- [4] R. Weber, R. Giedl-Wagner, D.J. Förster, A. Pauli, T. Graf, J.E. Balmer, Expected X-ray dose rates resulting from industrial ultrafast laser applications, *Applied Physics A* 125, 635 (2019). <https://doi.org/10.1007/s00339-019-2885-1>
- [6] H. Legall, C. Schwanke, J. Bonse, J. Krüger, X-ray radiation protection aspects during ultrashort laser processing, *Journal of Laser Applications* 32, 022004 (2020). <https://doi.org/10.2351/1.5134778>
- [7] C. Freitag, R. Giedl-Wagner, X-ray protection in an industrial production environment, *PhotonicsViews* 17, 37 (2020). <https://doi.org/10.1002/phys.202000020>
- [8] H. Legall, J. Bonse, J. Krüger, Review of X-ray exposure and safety issues arising from ultra-short pulse laser material processing, *Journal of Radiological Protection* 41, R28 (2021). <https://doi.org/10.1088/1361-6498/abc116>

LM-I-31

Ultrafast laser-matter interactions in solids with tightly-focused mid-IR laser pulses

Fedor Potemkin¹

¹Faculty of Physics, M.V. Lomonosov Moscow State University, Leninskie Gory, bld.1/62, Moscow 119991, Russia
potemkin@physics.msu.ru

The development of high-power mid-IR laser applications requires a study on laser-induced damage threshold in the mid-IR. In this paper, we present a complex comparison of the effect of pulses of different durations (from 0.1-0.2 ps to 1.2 ps) of the near (1.24 μm) and middle (4.6 μm) infrared on transparent dielectrics (MgF_2) and semiconductors (Si) under tight ($\text{NA} = 0.85$) focusing of laser radiation into the bulk of the material. It was found that with such a change in the wavelength and the effect on the dielectric, the change in the ionization mechanisms is significant. While the rate of field ionization decreases smoothly with the wavelength, the mechanism of heating electrons in the conduction band goes from single-photon (direct and electron-photon-phonon absorption) to multiple photon inverse Bremsstrahlung absorption [1]. In practice, such a change in the heating mechanism leads to a weak dependence of the plasma formation threshold on the pulse duration in mid-IR (4.6 μm) and a significant impact in the case of the near-IR (1.24 μm) excitation. In the case of semiconductors, the ionization mechanism remains within the framework of the multiphoton approximation, but an increase in the photon order for excitation by mid-IR pulses leads to a decrease in delocalization processes and losses in the prefocal region.

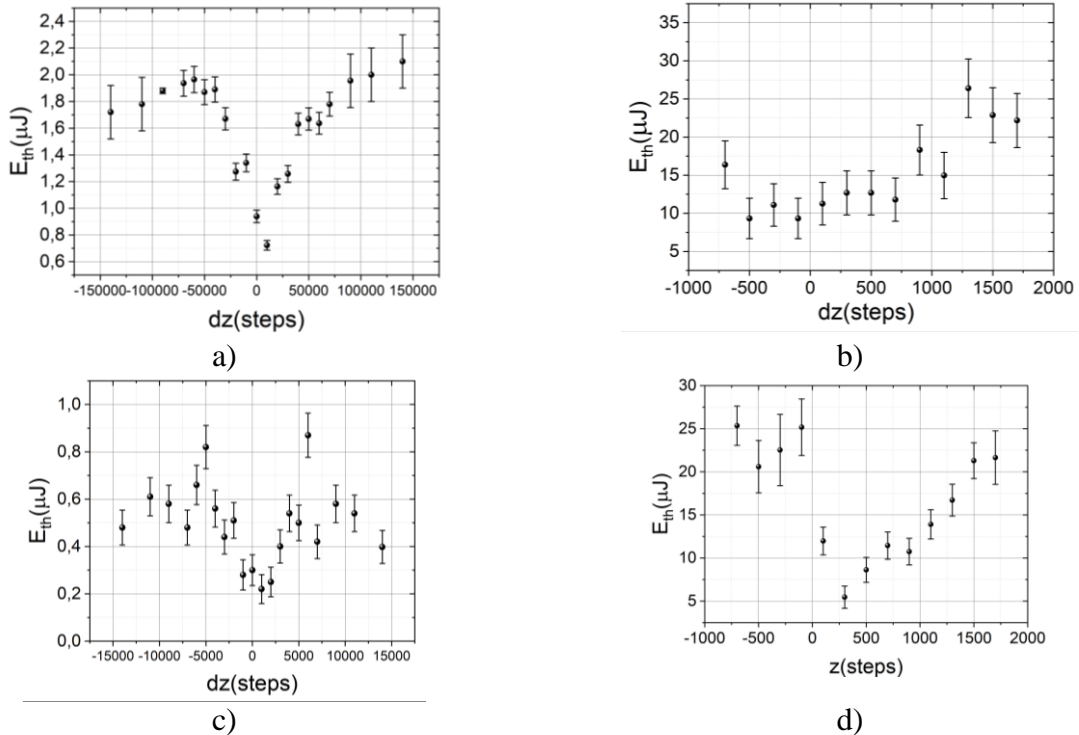


Fig.1. Plasma formation threshold as a function of the detuning length of the femtosecond compressor for different solids and pulse durations. a) MgF_2 1.24 μm , b) MgF_2 4.6 μm , c) Si 1.24 μm , d) Si 4.6 μm

In addition, it has been demonstrated that the maximum absorption $\sim 50\%$ (and hence the deposited energy density $\sim 6 \text{ kJ/cm}^3$) under the ultrafast laser excitation in dielectrics (for example, MgF_2) is achieved in the case of shortest pulses ($\sim 100 \text{ fs}$) with no matter to the excitation wavelength, while the deposited energy density higher for near-IR pulses. In semiconductors (for example, Si), greater absorption ($\sim 80\%$) is achieved for longer (sub-ps) laser pulses. These results will serve as the basis for the development of modern microprocessing technologies since the creation of modifications in the bulk of a semiconductor in this case does not require complex schemes of solid-state immersion or space-time chirping.

This work was supported by Russian Science Foundation (RSF) (Project No. 17-72-20130).

[1] E. Migal, E. Mareev, E. Smetanina, G. Duchateau, and F. Potemkin, Role of wavelength in photocarrier absorption and plasma formation threshold under excitation of dielectrics by high-intensity laser field tunable from visible to mid-IR, Scientific Reports, 10, Article number: 14007 (2020).

LM-I-32

Damage density measurements with small and large beams of optical components for high power lasers

L. Lamaignère, M. Veinhard, C. Bouyer, N. Roquin, R. Parreault

CEA-CESTA, 15 Avenue des Sablières, CS 60001, F33116 Le Barp Cedex, France

laurent.lamaignere@cea.fr

The determination of the laser damage resistance of optics in the nanosecond regime is based on statistical tests and approaches because the response of the components is related to the presence of defects randomly distributed in the optics and is therefore probabilistic in nature. The tests are mostly carried out with beams of small dimensions (few tens of μm) which make it possible to determine a damage probability from which a laser damage threshold is extracted. This threshold is however highly correlated with the size of the test beam. Some measurements are also made with beams of large dimensions (few mm) from which a damage density is determined. However, the relation between the damage probability and the damage density is not trivial. It is based on assumptions which are difficult to verify because the experimental validations are carried out on different laser installations. The coherence between these tests with small and large beams, as well as the link between damage probability and damage density are reported in this presentation. Tests were carried out on the same laser installation with a large beam and also with small beams shaped from phase objects specifically implemented to obtain several small beams from a single larger beam. The consistency of the laser damage results from both sets of measurements is here discussed. It validates the assumptions made and the specific mathematical treatments implemented to make the link between the two approaches. *In fine*, it also validates and reinforces the approach previously developed from the rasterscan procedure [1] used to measure damage densities from the scanning of optics with beams of small dimensions. The reported original work based on phase objects thus makes it possible to replicate small beams tests with a large beam facility. The comparison between the results from the small beams and the results from the large beam experiments definitely makes the link between damage probabilities and damage densities. This also shows that small beam tests are reasonably representative of tests carried out with large beams [2].

[1] L. Lamaignère, S. Bouillet, R. Courchinoux, T. Donval, M. Josse, J.-C. Poncetta, and H. Bercegol, An accurate, repeatable, and well characterized measurement of laser damage density of optical materials, *Rev. Sci. Instr.* **78**, 103105 (2007).

[2] L. Lamaignère, M. Veinhard, F. Tournemene, C. Bouyer, R. Parreault, R. Courchinoux, J. Y. Natoli, C. Rouyer, and S. Bouillet, A powerful tool for comparing different test procedures to measure the probability and density of laser induced damage on optical materials, *Rev. Sci. Instr.* **90**, 125102 (2019).

LM-I-33

Cutting of glass with an Airy Beam

D. Sohr^{1,2}, J. U. Thomas², S. Skupin¹

1- Institut Lumière Matière, UMR 5306 Université Lyon 1 - CNRS, Université de Lyon, 69622 Villeurbanne, France

2- SCHOTT AG, Hattenbergstrasse 10, 55122 Mainz, Germany

stefan.skupin@univ-lyon1.fr

When glass is cut to shape, ultra short pulse lasers used with beam profiles with an elongated focal volume (line focus) are increasingly replacing conventional cutting tools [1]. These straight line foci can be used to modify the workpiece throughout its entire depth with one single laser shot, effectively perforating it instantaneously, instead of having to dig into the material, as for example by ablation. At the same time, processed glass is often required to have a seamed or round edge. Currently this requires an extra grinding step to obtain for example the most common curved shape, the so called “c-cut”.

Here, we report on combining cutting and edge shaping of glass sheets in one laser process. To this end, we replace the commonly used Bessel-Gauss beam in the aforementioned line focus setup with an Airy-Gauss beam to directly achieve a curved edge as the result of the cutting process. The Airy beam is the most prominent non diffracting beam following a curved trajectory, that is to say its main lobe appears to be accelerated in the transverse plane during propagation [2]. Our results demonstrate curved modifications with lengths of up to 2 mm within borosilicate glass produced by single 1030 nm picosecond laser shots with an Airy beam profile. Plasma ignition in the side lobes of the beam as well as surface damage prove to be the crucial limitations for confined bulk energy deposition on a curved trajectory. A combined experimental and numerical analysis reveals optimum laser parameters for confined bulk energy deposition. This way we achieved single pass perforation of a 525 μm thick glass sheet and separation by a subsequent etching step [3], resulting in a well defined convex edge down to a radius of curvature of 774 μm .

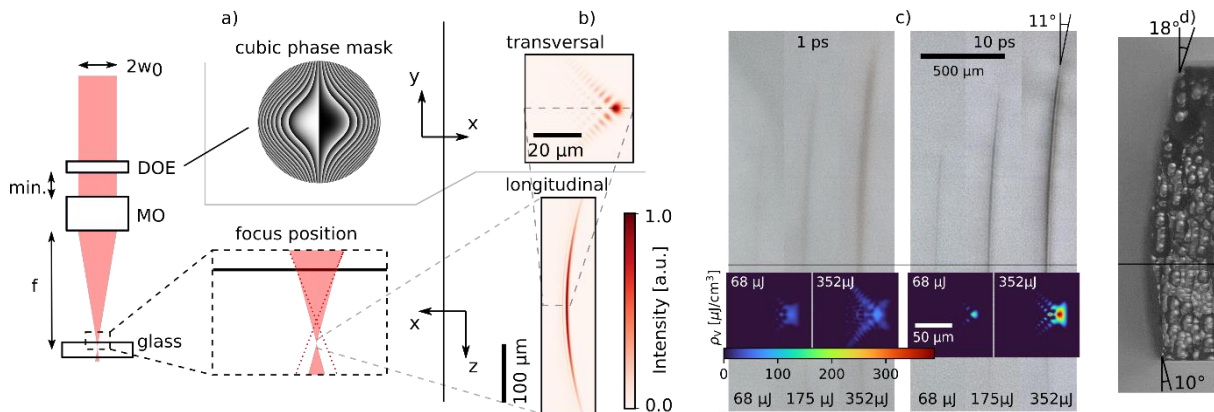


Figure 1 : Experimental 2f-setup (a) used for creating an Airy-Gauss beam and resulting intensity profiles (b) for a focal length of $f = 10$ mm. Light microscopy cross sections of permanent in-volume modifications in glass (c) also clearly follow the expected curved trajectory. Corresponding deposited energy densities in the focal plane (insets) obtained from numerical simulations confirm a higher confinement of deposited energy for long pulses. Result of cutting a 525 μm thick glass sheet by perforation with an Airy beam and subsequent etching is shown in (d). The cross section view parallel to the line of laser modifications shows the curved profile of the cut.

[1] M. Jenne et al., “Facilitated glass separation by asymmetric Bessel-like beams”, *Opt. Exp.* 28, 6552–6564 (2020)

[2] G. A. Siviloglou et al., “Observation of accelerating Airy beams”, *Phys. Rev. Lett.* 99 213901 (2007)

[3] J. Gottmann, “Microcutting and hollow 3d microstructures in glasses by in-volume selective laser-induced etching (isle)”, *J. Laser Micro/Nanoengineering* 8, 15–18 (2013)

LM-I-34

Fabrication of dense arrays of micro/nano-channels in fused silica by picosecond laser processing

N. Sanner¹, X. Liu^{1,2}, O. Utéza¹

*1- Aix Marseille Univ., CNRS, LP3 UMR 7341, 163 avenue de Luminy C.917, 13288 Marseille, France
2- State Key Laboratory of Transient Optics and Photonics, Xi'an Institute of Optics and Precision Mechanics of CAS, Xi'an 710119, China*

nicolas.sanner@univ-amu.fr

Ultrashort laser pulses have demonstrated their interests for ablation and structuration of transparent dielectric materials at the micrometric scale. Spatially shaping the intensity distribution of the laser irradiation therefore enables to broaden the range of patterns accessible with single-shot laser ablation. In this work, we report results on the fabrication of arrays of several-micrometres-deep microchannels by laser ablation at the surface of fused silica. To this aim, we develop a dedicated spatial beam shaping approach, which consists in generating a customized micro-Bessel beam with a reduced length.

Using a micro-Bessel beam generated with an axicon, we first demonstrate the realization of single microchannels at the front surface of fused silica. Blind channels of few tens of micrometres long and $\sim 1 \mu\text{m}$ diameter are obtained, with a good quality of the entrance of the channel, without rims or recast material [1]. Additional amplitude filtering with an annular aperture enables to provide a straightforward technique to offer length-tunability to the process. We obtain few-micrometres-long microchannels.

Then, in view of realization of micro-components based on arrays of microchannels, we investigate the possibility to process patterns composed of dense meshgrid of channels [2]. We address experimentally the crucial problem of crosstalk, i.e. the influence of the pre-existence of the previous channel on the propagation of the laser beam and, in turn, on the processing of the next one. We investigate how this can yield severe limitation to the process when the spatial pitch between adjacent channels approaches the micrometre range, despite the robustness of Bessel beam to obstacles. Finally, we identify a regime within which arrays of sub-micron-diameter channels with variable lengths can be processed one-by-one with single 1 ps pulses with a spatial periodicity down to $1.5 \mu\text{m}$.

This is a first step towards the realization of microscale integrated optical components by direct laser ablation, as an alternative to multistep technologies, offering a vacuum-free, non-chemical, flexible, programmable, fast and affordable technique.

[1] X. Liu, N. Sanner, M. Sentis, R. Stoian, W. Zhao, G. Cheng, O. Utéza, "Front-surface fabrication of moderate aspect ratio micro-channels in fused silica by single picosecond Gaussian-Bessel laser pulse", *Appl. Phys. A* 124, 206 (2018).

[2] X. Liu, Q. Li, A. Sikora, M. Sentis, O. Utéza, R. Stoian, W. Zhao, G. Cheng, and N. Sanner, "Truncated Gaussian-Bessel beams for short-pulse processing of small-aspect-ratio micro-channels in dielectrics," *Opt. Express* 27, 6996 (2019).

LM-I-35

Ultrafast-laser writing of birefringent nanogratings in alkali-containing glasses

S.V. Lotarev, S.S. Fedotov, A.I. Pomigueva, A.S. Lipatiev, V.N. Sigaev

Mendeleev University of Chemical Technology, 125047, Miusskaya sq. 9, Moscow, Russia

Main author email address: slotarev@muctr.ru

Birefringent periodical nanostructures inscribed by a series of ultrafast-laser pulses in the inside of glass which are known as nanogratings have become the first optically induced phenomena with regular period substantially smaller than the wavelength of light inducing it. First shown in fused silica [1], nanogratings drew strong attention due to their form birefringence and the possibility to control their orientation and optical retardance by the parameters of laser treatment. They have already been used in applications such as polarization converters, ultrastable data storage and microfluidics [2]. Most of the studies of this phenomenon were carried out in fused silica. Some years ago, the inscription of nanogratings was also demonstrated in several crystals and multicomponent glasses. The phenomenon of nanogratings occurred to be much more common than it was first considered to be. Due to presence of several types of elements with different diffusion properties, the formation of nanogratings in multicomponent glasses was shown to be a more complicated process relative to fused silica and could be accompanied by nanoperiodical elemental redistribution, partial crystallization [3,4], photodarkening [5] or could produce more than one nanostructure with different periods [6]. However, there are still only few studies of effect of glass composition and the content of various components on the possibility, conditions and mechanism of nanograting inscription.

In this study, we investigated formation and optical properties of nanogratings in binary alkali-containing glasses as a simple model system allowing for understanding of the role of the type and content of monovalent cations in this context. Glasses under study included a set of alkali silicate glasses $xR_2O-(100-x)SiO_2$ ($R = Li, Na, K$) and sodium germanate glasses with various Na_2O content. FEMTOLAB setup for laser processing based on PHAROS SP femtosecond laser (Light Conversion Ltd.) operating at 1030 nm wavelength was used in the performed experiments. Nanogratings could be inscribed in all glasses under study. The content of alkali oxide was shown not to be limiting factor for the possibility to form a nanograting in the studied range but had a drastic effect on the conditions of their inscriptions. In the case of sodium oxide, a number of ultrafast-laser pulses required to induce form birefringence manifested the exponential growth with its content. The existence of the upper limit of the peak intensity providing the formation of nanogratings was also revealed.

By the example of $22Na_2O \cdot 78GeO_2$ glass, an effect of the pulse repetition rate and laser-induced heat accumulation on the nanograting formation and unexpected behavior of their optical retardance are described. It is also shown that, depending on other parameters of the laser pulses, nanogratings and laser-induced crystallization can be realized simultaneously or in non-overlapping ranges of the pulse repetition rate.

This study was financially supported by the Russian Foundation for Basic Research (grant 21-53-12026).

- [1] Y. Shimotsuma, P.G. Kazansky, J. Qiu, K. Hirao, Self-organized nanogratings in glass irradiated by ultrashort light pulses, *Phys. Rev. Lett.*, vol. 91, p. 247405 (2003).
- [2] B. Zhang, X. Liu, J. Qiu, Single femtosecond laser beam induced nanogratings in transparent media - Mechanisms and applications, *J. Materiomics*, vol. 5, pp. 1-14 (2019).
- [3] S. Lotarev, S. Fedotov, A. Lipatiev, M. Presnyakov, P. Kazansky, V. Sigaev, Light-driven nanoperiodical modulation of alkaline cation distribution inside sodium silicate glass, *J. Non-Cryst. Solids*, vol. 479, pp. 49, (2018).
- [4] S.V. Lotarev, S.S. Fedotov, A.I. Kurina, A.S. Lipatiev, V.N. Sigaev, Ultrafast laser-induced nanogratings in sodium germanate glasses, *Opt. Lett.*, vol. 44, pp. 1564-1567, (2019).
- [5] S. Richter, D. Möncke, F. Zimmermann, E.I. Kamitsos, L. Wondraczek, A. Tünnermann, S. Nolte, Ultrashort pulse induced modifications in ULE - from nanograting formation to laser darkening, *Opt. Mater. Express*, vol. 5, pp. 1834-1850, (2015).
- [6] F. Zimmermann, A. Plech, S. Richter, A. Tünnermann, S. Nolte, Ultrashort laser pulse induced nanogratings in borosilicate glass, *Appl. Phys. Lett.*, vol. 104, p. 211107, (2014).

LM-I-36

Laser-Induced Changes in Surface Wettability: From Modeling to Applications

I. S. Omeje and T. E. Itina

1- Laboratoire Hubert Curien, UMR CNRS 5516, Université Jean Monnet, Saint-Etienne, France

Main author email address: tatiana.itina@univ-st-etienne.fr

One of the important advantages of femtosecond lasers resides in a possibility to form a set of hierarchical micro and nanostructures on solid surfaces thus allowing an efficient control over various surface properties. Among these properties, wettability is particularly affected and plays a crucial role in the development of numerous application not only in automobile or textile industry, but also in the biomedical field. Recently, several studies have already evidenced a pronounced effect of wettability, among other factors, on the behavior of cells, bacteria and even of viruses on laser-textured surfaces. In particular, changing surface relief and controlling wetting properties have a potential to better guide cell repulsion or attraction to the surfaces. For instance, these processes are known to play a role in both osseointegration and mechanotransduction, which are known to be key process in dental and orthopedic implant integration, as well as in a bioengineering in general.

Despite a large number of promising experimental results, it is still unclear how to predict and explain the wettability of laser textured surfaces. The classical models, such as the Wenzel and Cassie-Baxter, contain adjustable parameters and provide only rough explanations. The development of more realistic models remain challenging because of the lack of understanding of the effects of both surface and liquid properties on the behavior of a liquid droplet on the surface. In particular, the difficulty arises from the change in surface wettability with time after laser treatment, but also due to annealing, sterilization, ultra-sound or cold plasma treatment. The reasons for these changes are not yet well understood.

To better understand this process, we use a continuum-level modeling [1] to study the wetting dynamics of liquid droplet on plane and laser-textured Ti, Ti alloys, as well as on several other surfaces. The role of various surface reliefs and chemical composition are examined. The calculated evolutions of the contact angle with time for both structured and non-structured surfaces provide explanations of a set of experiments. In particular, the performed simulations confirm the role of surface energy, indicate how capillary forces change as a function of surface relief and composition, allow us to examine the role of liquid viscosity, of droplet shape, etc. Our results clearly demonstrate that such simulations are helpful and suitable for the better understanding of the process involved in the wettability changes of laser-textured materials

[1] S.F Kisler, Hydrodynamics of wetting,, JC Berg (Ed.) Wettability, New York, 1993.

LM-I-37

Ultrafast laser nanopatterning of metals below 100 nm

J.P. Colombier,¹ A. Nakhoul,^{1,2} A. Rudenko,³ C. Maurice,² F. Garrelie¹, F. Pigeon,¹

1- Univ Lyon, UJM-St-Etienne, CNRS, Institute of Optics Graduate School, Laboratoire Hubert Curien UMR 5516, F-42023 Saint-Etienne, France

2- Ecole Nationale Supérieure des Mines de Saint-Etienne, Laboratoire Georges Friedel, CNRS, UMR5307, 42023 St-Etienne, France

3- Arizona Center for Mathematical Sciences and College of Optical Sciences, University of Arizona, Tucson, AZ 85721, USA

jean.philippe.colombier@univ-st-etienne.fr

Ultrafast laser sources enable the structuring at the nanoscale driven by remarkable surface material response to photoexcitation involving extreme states of temperature and pressure far from equilibrium. During the lifetime of a transient laser-induced melting layer, we uncover that dissipative structures can emerge and continuously exchange energy and entropy with photonic flux to ensure relief growth and topographic organization upon solidification. Using a crossed-polarization irradiation strategy to prevent commonly oriented nanostripes formation, we report the formation of arranged laser-induced cavities and peaks well below the diffraction limit on metallic surfaces. Self-organized nanopatterns with various symmetries and aspect-ratios can be formed, demonstrating the potential of temporal beam shaping for the fabrication of advanced surfaces with a topography designed at the nanoscale [1-2].

Local field enhancement on local roughness fosters the energy absorption on the smallest dimensions much smaller than the light wavelength, resulting in extreme and inhomogeneous thermo-mechanical conditions. Fluctuations can be amplified upon positive feedback and trigger a convection instability at the nanoscale [3]. Destabilized forces arise from subtle contributions of Marangoni flows that follows transverse temperature gradients and longitudinal rarefaction shock wave relaxation. Distinct self-organization regimes can then result from this convection mechanism driven by light energy coupling on emerging surface patterns [4]. The surface and irradiation dose conditions required to switch from a self-organization regime to another one will be discussed based on experimental results interpreted by simulations coupling Maxwell solver to Navier-Stokes equations. Hydrodynamic instabilities, similar to the Rayleigh-Bénard-Marangoni flows, drives the matter towards self-organized convection nanocells and can induce thermocapillary waves oriented by nonradiative sub-diffraction near-field patterns.

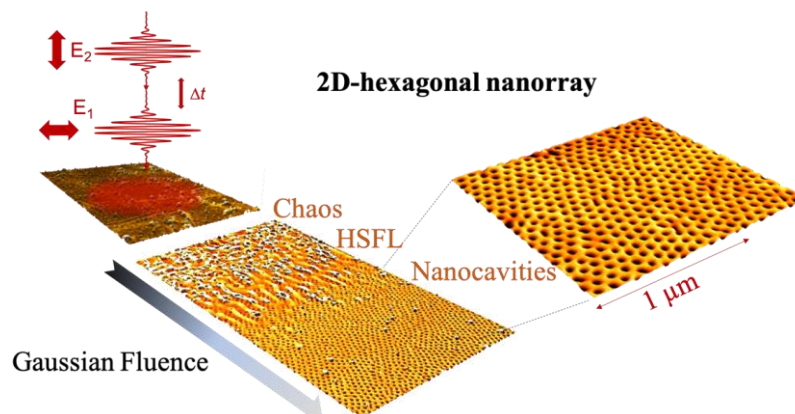


Figure 1: Crossed-polarized double pulse sequence for isotropic energy regulation. An hexagonal lattice of nanocavities of 20 nm in size and spaced by 60 nm has been performed on (100) Ni surface.

[1] A. Abou Saleh, A. Rudenko, S. Reynaud, F. Pigeon, F. Garrelie, & J.P. Colombier, “Sub-100 nm 2D nanopatterning on large scale by ultrafast laser energy regulation”, *Nanoscale* **12** (12), 6609 (2020).

[2] R. Stoian, & J.P. Colombier, “Advances in ultrafast laser structuring of materials at the nanoscale”, *Nanophotonics* **9** (16), 4665-4688 (2020).

[3] A. Rudenko, A. Abou-Saleh, F. Pigeon, C. Mauclair, F. Garrelie, R. Stoian, & J. P. Colombier “High-frequency periodic patterns driven by non-radiative fields coupled with Marangoni convection instabilities on laser-excited surfaces” *Acta Materiala* **194**, 93 (2020).

[4] A. Nakhoul, C. Maurice, M. Agoyan, A. Rudenko, F. Garrelie, F. Pigeon, & J.P. Colombier “Self-Organization Regimes Induced by Ultrafast Laser on Surfaces in the Tens of Nanometer Scales”. *Nanomaterials*, **11**(4), 1020 (2021).

LM-I-38

Three-Step Description of Single-Pulse Formation of Laser-Induced Periodic Surface Structures on Metals

Y. Levy¹, E. L. Gurevich², and N. M. Bulgakova¹

1- HiLASE Centre, Institute of Physics of the Czech Academy of Sciences, Dolní Břežany, Czech Republic

2- University of Applied Sciences Münster, Laser Center (LFM), Steinfurt, Germany

levy@fzu.cz

We presents a 3-step scenario of the formation of laser-induced periodic surface structures (LIPSS) on metals [1], upon irradiation by a single ultrashort laser pulse. In this model of LIPSS formation, the first step consists in the emergence of modulations in the electronic temperature at the surface due to the interference between the incident pulse and surface waves [2,3]. The second step corresponds to the thermal response of the system to that perturbation and the third step is the material relocation, that leads to the deformation of the target surface.

We focus mainly on the second step by studying the evolution of a temperature modulation on surfaces of different metals in the frame of the two-temperature model. We have used both a simplified analytical approach and 2D numerical simulations to that aim. The evolution of the amplitude of the temperature modulations and its growth rate are reported and the dynamics reveals that the spatial periods can be strongly suppressed depending, in particular, on the coupling factor and the in-depth heat diffusion. We compare the cases of 3 metals (Au, Al and Mo) with different thermophysical properties thus exhibiting different behaviors with respect to the spatial period.

[1] E. L. Gurevich, Y. Levy, N. M. Bulgakova, Three-Step Description of Single-Pulse Formation of Laser-Induced Periodic Surface Structures on Metals, *Nanomaterials*, 10, p. 1836 (2020).

[2] J. E. Sipe, J. F. Young, J. S. Preston, H. M. van Driel, Laser-induced periodic surface structure. I. Theory, *Physical Review B*, 27, pp. 1141-1154 (1983).

[3] P. Terekhin, O. Benhayoun, S. Weber, D. Ivanov, M. Garcia, B. Rethfeld, Influence of surface plasmon polaritons on laser energy absorption and structuring of surfaces, *Applied Surface Science* 512, p. 144420 (2020).

LM-I-39

Fs laser ablation of bone tissue for high resolution bone surgery**Laura Gemini¹, Samy Al Bourgol¹, Guillaume Machinet¹, Marc Fauçon¹, Rainer Kling¹***1- ALPhANOV, Rue François Mitterrand, 33400 Talence, France**laura.gemini@alphanov.com*

Thanks to the current readiness of the technology, lasers have become the tool of choice for surgeries where high precision and lack of unwanted tissue damage are essential [1]. Indeed several unique advantages with respect to conventional mechanical cutting can be found such as no direct contact with the tissue and the possibility to process any geometry with unique precision [2]. Nowadays CW/QCW Er:YAG lasers are mainly employed in bone surgery because of their optimized emission wavelengths of 2.94 μm . Nevertheless, strong thermal effects followed by high degrees of tissue carbonization are often associated to the use of these sources, preventing the process of tissue regeneration and a fast post-surgery healing. In this frame, the use of pulsed laser sources has shown to be an interesting option to obtain the minimization the thermal damage in the treated bone tissue and its surrounding [3,4]. It has been shown that an optimization of the ablation rate through an upscaling approach is possible by employing industrial femtosecond laser sources and parameters can be found to achieve an optimal quality of ablation without tissue carbonization [5]. Nevertheless, during the ablation process temperatures high enough to induce tissue denaturation can be reached also when no evident calcination is observable on the bone tissue. In this work, a comprehensive study of the thermal behavior of bone tissue during ultra-fast laser ablation is presented in order to define the best processing environment to avoid tissue denaturation. Three different processing environments were considered for the ablation of bone tissue: water, pressured-air flow and pressured-water flow. Temperatures were recorded during the laser interaction by two different methods to demonstrate the reliability of the measurements. A IR camera FLIR was employed to observe the temperature distribution; measurements at varying angles of view were also initially carried on a reference control sample to demonstrate the negligible dependance of the results from the angle of view between the camera and the sample. Temperature measurements by thermo-couple were also done to be able to compare the results from the two methods and obtain a more complete overview of the temperature behavior of bone tissue during ultra-fast laser processing. The best results were obtained in pressured-water flow where the temperature of the tissue stays always below the temperature for protein denaturation. The dynamics of heat dispersion shows that the maximum temperature in the tissue is reached after the laser processing ends, highlighting the need for efficient cooling of the tissue also after the process ends.

[1] K.-W. Baek, W. Deibe, D. Marinov, M. Griessen, M. Dard, A. Bruno, H.-F. Zeilhofer, P. Cattin and P. Juergens, A comparative investigation of bone surface after cutting with mechanical tools and Er:YAG laser, *Lasers Surg. Med.* 47(5), 426-32 (2015)

[2] U. Romeo, A. Del Vecchio, G. Palata, G. Tenore, P. Visca and C. Maggiore, Bone Damage Induced by Different Cutting Instruments: An in Vitro Study, *Braz. Dent. J.* 20, 162–168 (2009)

[3] L.T. Canguero, R. Vilar, A. M. Botelho do Rego and V.S.F. Muralha, Femtosecond Laser Ablation of Bovine Cortical Bone, *J. Biomed. Opt.* 17, 125005 (2012)

[4] F. Aljekhedab, W. Zhang, J. Favero, H. K. Haugen, G. R. Wohl and Q. Fang, Bovine Cortical Bone Ablation by Femtosecond Laser, *Proceedings of the Lasers in Dentistry XXIV*; Rechmann, P., Fried, D., Eds.; SPIE: San Francisco, United States, p. 14 (2018)

[5] L. Gemini, S. Al-Bourgol, G. Machinet, A. Bakkali, M. Faucon and R. Kling, Ablation of Bone Tissue by Femtosecond Laser: A Path to High-Resolution Bone Surgery, *Materials*, 14(9), 2429 (2021)

LM-I-40

Ultrafast time-resolved microscopy during femtosecond laser structuring

M. Garcia-Lechuga,^{1,*} D. Puerto,^{1,∞} J. Bonse,^{1,ϕ} Y. Fuentes-Edfuf,¹ J. Solis,¹ and J. Siegel,¹

¹ - Laser Processing Group, Instituto de Óptica, IO-CSIC, Serrano 121, Madrid, Spain

^{*} present address: Departamento de Física Aplicada, Universidad Autónoma, Madrid, Spain

[∞] present address: Polytechnic School of University, Alicante, Spain

^ϕ present address: Bundesanstalt für Materialforschung und -prüfung, Unter den Eichen 87, Berlin, Germany

j.siegel@io.cfmac.csic.es

Femtosecond laser processing of materials allows the fabrication of high-precision micro- and nano-structures for a wide field of applications. Yet, for an ultimate optimization of these structures, it is necessary to comprehend the complex transformation pathways of the material at the extreme excitation intensities used. Ultrafast time-resolved microscopy has proven to be a powerful technique for unraveling the mechanisms triggered by ultrashort laser pulses in dielectrics, semiconductors and metals [1]. The core technique is based on combining an optical pump-probe approach with optical microscopy, providing sub-ps temporal and μm spatial resolution, which can be extended by different imaging modalities. Applied to surface processing, femtosecond microscopy has the capability of resolving temporally and spatially numerous processes such as electron excitation, heating, melting, ablation, and solidification [2,3]. It also has the ability to estimate the density and temporal evolution of laser-induced free-electron plasmas in dielectrics, visualize the optical Kerr effect, identify the occurrence of uncommon ablation mechanisms based on the expansion of a transparent thin shell, as well as resolving the formation of a heat-affected layer [4,5]. A further extension of the technique, denominated “ultrafast moving-spot microscopy”, allows to study the formation dynamics of laser-induced periodic surface structures (LIPSS) [6]. We demonstrate in this talk that the visualization of the process dynamics obtained by time-resolved microscopy, covering fs to μs temporal ranges, is extremely useful for an understanding of the origin of the morphological features and properties of the obtained structures, paving the way for the optimization strategies and applications (see Fig. 1).

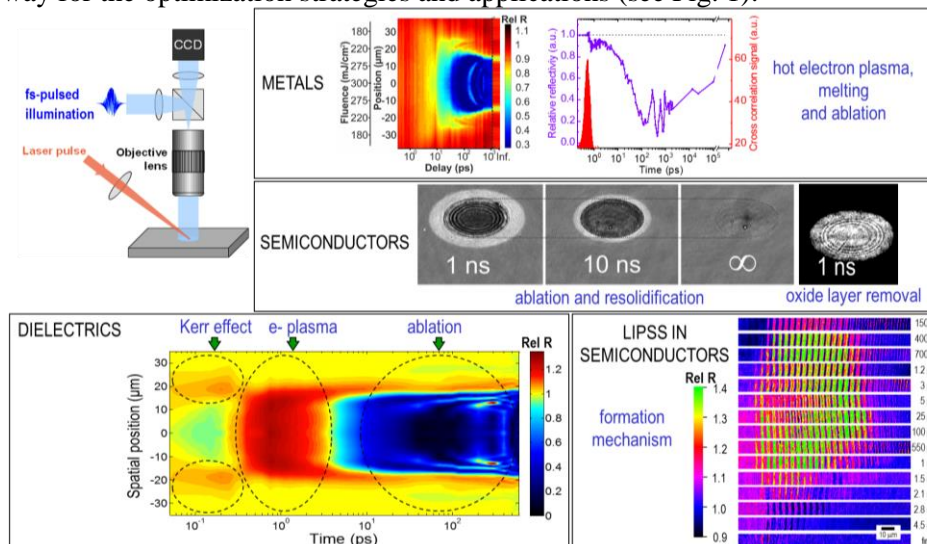


Fig. 1: Scheme of the basic fs microscopy technique (top left) and results obtained for different materials.

- [1] K. Sokolowski-Tinten, J. Bialkowski, A. Cavalleri, D. von der Linde, A. Oparin, J. Meyer-ter-Vehn, S. Anisimov, Transient States of Matter during Short Pulse Laser Ablation, *Phys. Rev. Lett.* 81, 224 (1998).
- [2] J. Bonse, G. Bachelier, J. Siegel, J. Solis, Time- and space-resolved dynamics of melting, ablation, and solidification phenomena induced by femtosecond laser pulses in germanium, *Phys. Rev. B* 74, 134106 (2006).
- [3] D. Puerto, J. Siegel, W. Gawelda, M. Galvan-Sosa, L. Ehrentraut, J. Bonse, J. Solis, Dynamics of plasma formation, relaxation, and topography modification induced by femtosecond laser pulses in crystalline and amorphous dielectrics, *J. Opt. Soc. Am. B* 27, 1065 (2010).
- [4] M. Garcia-Lechuga, J. Siegel, J. Hernandez-Rueda, J. Solis, Imaging the ultrafast Kerr effect, free carrier generation, relaxation and ablation dynamics of Lithium Niobate irradiated with femtosecond laser pulses, *J. Appl. Phys.* 116, 10 (2014).
- [5] M. Garcia-Lechuga, J. Solis, J. Siegel, Melt front propagation in dielectrics upon femtosecond laser irradiation: Formation dynamics of a heat-affected layer, *Appl. Phys. Lett.* 108, (2016).
- [6] M. Garcia-Lechuga, D. Puerto, Y. Fuentes-Edfuf, J. Solis, J. Siegel, Ultrafast Moving-Spot Microscopy: Birth and Growth of Laser-Induced Periodic Surface Structures, *ACS Photonics* 3, 1961 (2016).

LM-I-41

Functional surfaces for industrial applications due to direct laser texturing

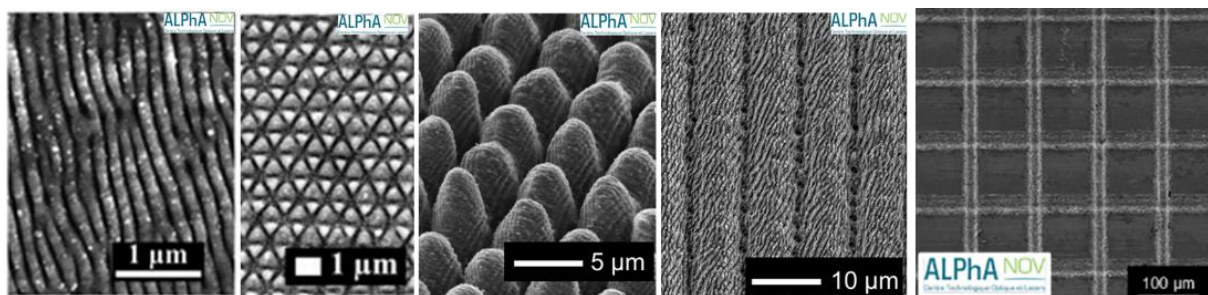
G. Mincuzzi¹, L. Gemini¹, A. Sikora¹, A. Bourtereau¹, S. Nourry¹, M. Faucon¹, R. Kling³

1- Alphanov Technology Center, Rue François Mitterrand, 33400 Talence, France

Main author email address: rainer.kling@alphanov.com

Materials processing with femtosecond lasers is often accompanied by a self-organization-effect creating regular patterns on the surface first discovered by Birnbaum in 1965 [1]. The effect has been intensively studied in the meantime to understand the fundamental mechanisms and to be able to control their shape. The nanoscale surface structures appear on most type of materials in particular metals, semiconductors and even crystalline dielectric materials. Due to their regular nature the patterns are called laser induced periodic surface structures - LIPSS. As the creation mechanism does not rely on conventional material ablation, their shape and height are not a direct mapping of the laser intensity profile but are moreover principally determined by the laser wavelength, polarization, fluence and the number of consecutive pulses. As the orientation of the nano textures is known to be influenced by the polarization of the laser pulse [2] we engage various polarization converters and double pulses with variable delay to manipulate the shape of the periodic structures. With different combinations of these influential parameters different topographies can be created to serve different applications with specific functions and surface properties, which are briefly introduced below.

Nano sized patterns on surfaces have a major influence on optical and mechanical surface properties. On metal surfaces grating structures diffract the light and can serve as colorization, decoration and anti-counterfeit. On reflective noble metals spike structures generate light trapping effects and therefore increase the absorptivity to more than 95% over a wide wavelength range [3]. For microfluidics the increase of surface energy leads to hydrophobicity exhibiting lotus effects [4]. To generate antimicrobial surfaces, nanopillars with a periodicity close to the size of the respective bacteria have been demonstrated to be most effective [5]. We believe our high-throughput approach will contribute to transfer laser functionalized surfaces into industrial applications.



All these texturations are typically generated by applying femtosecond laser pulses with fluencies near the ablation threshold. Scientific publications mostly rely on low power Ti:Sapphire lasers for LIPSS creation. In contrast to this we demonstrate high repetition rate processing (up to 15 MHz) based on femtosecond lasers with an average of up to 300W. Examples of different scales, different topologies and accordingly different surface functions are presented along with their application. The characterization of the surfaces is performed by means of optical microscopy, SEM images, absorptivity measurements, and contact angle measurements.

[1] M. Birnbaum J. Appl. Phys. 36,3688–3689 (1965)

[2] U. Klug, J. F. Düsing, T. Sato, K. Washio and R. Kling, Proc. SPIE 7590, (2010)

[3] A. Y. Vorobyev and C Guo, J. Appl. Phys. Vol. 110, 043102 (2011)

[4] X. Zhang, F. Shi, J. Niu, Y. Jiang and Z. Wang, J. Mater. Chem., 18, 624633. (2008)

[5] A. Lutey, L. Gemini, L. Romoli, G. Lazzini, F. Fuso, M. Faucon, and R. Kling. "Towards laser-textured antibacterial surfaces." Scientific reports 8, no.1, pp. 1-10 (2018)

LM-I-42

Laser nano- and microstructuring of halide perovskites

A.Y. Zhizhchenko^{1,2}, A.A. Kuchmizhak^{1,2}, S.V. Makarov³

1-Pacific Quantum Center, Far Eastern Federal University, 6 Sukhanova Str., Vladivostok, 690061 2-Russia Institute of Automation and Control Processes, Far Eastern Branch, Russian Academy of Science, Vladivostok, 690041 Russia 3-ITMO University, Saint Petersburg, Russian Federation

e-mail: s.makarov@metalab.ifmo.ru

Recently, halide perovskites have attracted enormous attention due to their exceptional optical and electrical properties being useful various optoelectronic devices. As a result, this family of materials can provide a prospective platform for modern nanophotonics and meta-optics, allowing us to overcome many obstacles associated with the use of conventional semiconductor materials. Namely, the perovskites provide simple and cheap wet-chemistry methods of nanofabrication, high quantum yield and pronounced excitonic properties at room temperature, broadband and reversible spectral tunability, high defect tolerance, high enough refractive index for light confinement at subwavelength scale, as well as flexibility regarding integration with various nanophotonics designs.

Here, we review the recent progress on laser ablation for application in halide perovskite nanophotonics starting from single-particle light-emitting nanoantennas [1,2] and nano/micro-lasers [3,4] to the large-scale designs working for surface coloration, anti-reflection, optical information encoding [4], and miro-optic elements fabrication [5].

The work was supported by the Russian Science Foundation (project № 19-73-30023).

REFERENCES:

- [1] Tiguntseva E.Y., Zograf G.P., Komissarenko F.E., Zuev D.A., Zakhidov A.A., Makarov S.V. and Kivshar Y.S. *Nano Letters* 18(2), pp.1185-1190 (2018)
- [2] Tiguntseva E.Y., Baranov D.G., Pushkarev A.P., Munkhbat B., Komissarenko F., Franckevicius M., Zakhidov A.A., Shegai T., Kivshar Y.S. and Makarov S.V. *Nano Letters*, 18(9), pp.5522-5529 (2018).
- [3] Zhizhchenko A., Syubaev S., Berestennikov A., Yulin A.V., Porfirev A., Pushkarev A., Shishkin I., Golokhvast K., Bogdanov A.A., Zakhidov A.A. and Kuchmizhak A.A. *ACS Nano*, 13(4), pp.4140-4147 (2019)
- [4] Zhizhchenko A.Y., Tonkaev P., Gets D., Larin A., Zuev D., Starikov S., Pustovalov E.V., Zakharenko A.M., Kulinich S.A., Juodkasis S. and Kuchmizhak A.A. *Small*, p.2000410 (2020)
- [5] AY Zhizhchenko, AB Cherepakhin, MA Masharin, AP Pushkarev, SA Kulinich, AP Porfirev, AA Kuchmizhak, SV Makarov *Laser & Photonics Reviews*, 2100094 (2021)

LM-I-43

Anisotropic resistivity surfaces produced in TCO-ITO films by fs-laser induced self-organization in the nanoscale

Carmen Lopez-Santos^{1,2}, Daniel Puerto³, Jan Siegel³, Manuel Macias-Montero³, Camilo Florian³, Jorge Gil-Rostra¹, Víctor López-Flores¹, Ana Borrás¹, Agustín R. González-Elipse¹, Javier Solís³

1- Nanotechnology on Surfaces Group, Institute of Material Science of Seville (US-CSIC), Américo Vespucio 49, Seville 41092, Spain

2- Departamento de Física Atómica, Molecular y Nuclear, Facultad de Física, University of Seville, Reina Mercedes, s/n, Seville 41012, Spain

3- Laser Processing Group, Institute of Optics (IO-CSIC), Serrano 121, Madrid 28006, Spain
j.solis@io.cfmac.csic.es

Transparent conducting oxides (TCOs) are materials with a comparably low optical absorption in the visible region of the spectrum which makes them particularly suitable for key applications in information technologies (organic light emitting diodes, flat panel displays, etc.) and energy harvesting (photovoltaics, low emissivity coatings, etc.). Among them, in spite of the scarcity of In, Indium Tin Oxide (ITO) still plays a very important role, especially in niche applications where the chemical stability in water solutions is a decisive factor (electrochemical sensors).

In this work we demonstrate the production of highly anisotropic resistivity surfaces by high repetition rate fs-laser irradiation of ITO films at 1030 nm [2]. Electrical anisotropy appears as a consequence of the formation of Laser Induced Periodic Structures (LIPSS) at the material surface. Still, the formation of LIPSS in this case involves a novel mechanism associated to the dynamical modification of the material composition at the laser exposed regions. LIPSS [3] have been coherently extended over large areas (cm-sized regions). We have identified two main optimized processing conditions (Fig.1). At the lower fluences, the material at the LIPSS ridges remains essentially unmodified while only partial ablation is observed at the valleys. In this case, the structures show a longitudinal conductivity twice the transverse one, and a resistivity similar to that of the pristine ITO film. At higher fluences, nearly complete ablation at the valleys of the LIPSS, and strong ablation at their ridges, accompanied by a preferential In-loss, lead to an insulating structure in the direction transverse to the LIPSS and conductive in the longitudinal one. The compositional changes induced as laser pulses accumulate, condition the LIPSS evolution and thus the result of the structuring process. Strategies to further improve the achieved anisotropic resistivity results are also provided.

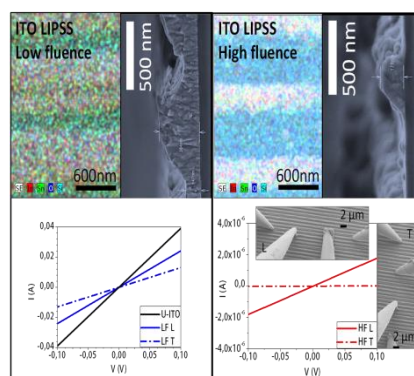


Fig.1 (Upper row) EDX maps and cross-sectional SEM images of LIPSS induced at low and high fluence in ITO films by fs-laser processing. (Lower row) Resistivity measurements in (left) macro- and (right) micro-scale configuration of the same structures.

[1] K. Ellmer, Nat. Photonics 2012, 6, 809

[2] C. Lopez-Santos, D. Puerto, J. Siegel, M. Macias-Montero, C. Florian, J. Gil-Rostra, V. López-Flores, A. Borrás, A. R. González-Elipse, J. Solís, Adv. Opt. Mater. 9, 2001086 (2020).

[3] J. Bonse, S. Hohm, S. V. Kirner, A. Rosenfeld, J. Kruger, IEEE J. Sel. Top. Quantum Electron. 2017, 23, 9000615

LM-I-44

Non-instantaneous third-order polarization at low intensities

Anton Husakou¹, Felipe Morales¹, Maria Richter¹, and Vladimir Olvo²

¹ Max Born Institute, Max Born Str. 2a, 12489 Berlin, Germany

² Department of Physics, Voronezh State University, Universitetskaya Ploshchad', 1, Voronezh, Russia, 394036

Third-order Kerr response of gases is at the core of contemporary nonlinear optics. Here we perform first-principle simulations of a hydrogen atom and demonstrate that, contrary to usual belief, the nonlinear polarization $P(t)$ cannot be described by $\varepsilon_0\chi^{(3)}E(t)^3$ even at low intensities and far from resonances.

A general expression for the third-order nonlinear polarization at a given time moment t is given by $P(t) = \varepsilon_0 \iiint \chi^{(3)}(\tau_1, \tau_2, \tau_3) E(t - \tau_1) E(t - \tau_1 - \tau_2) E(t - \tau_1 - \tau_2 - \tau_3) d\tau_1 d\tau_2 d\tau_3$, which can be also described in the frequency domain by $\chi^{(3)}(\omega_0; \omega_1, \omega_2, \omega_3)$, with $\omega_0 = \omega_1 + \omega_2 + \omega_3$. For pump frequencies far from resonances, instantaneous response $P(t) = \varepsilon_0\chi^{(3)}E(t)^3$ is commonly assumed, which is equivalent to ω -independent $\chi^{(3)}$ in the frequency domain. Surprisingly, we show that this is not the case even at modest intensities with near-IR sources: not only is $\chi^{(3)}$ strongly frequency-dependent, but also there are substantial delays in the response which correspond to losses.

We perform simulations of the polarization dynamics of a hydrogen atom by numerically solving the three-dimensional time-dependent Schrödinger equation for a range of intensities. We consider 8-fs input pulse with central wavelength 800 nm, far from any resonance of the atomic hydrogen. The predicted polarization is stripped of the linear part, and third-order response is separated into fundamental-frequency and third-harmonic parts, which are described by $\chi^{(3)}(\omega_0; \omega_0, \omega_0, -\omega_0)$, and $\chi^{(3)}(3\omega_0; \omega_0, \omega_0, \omega_0)$, correspondingly. We stress that both quantities would be equal if the third-order response of the atom were instantaneous.

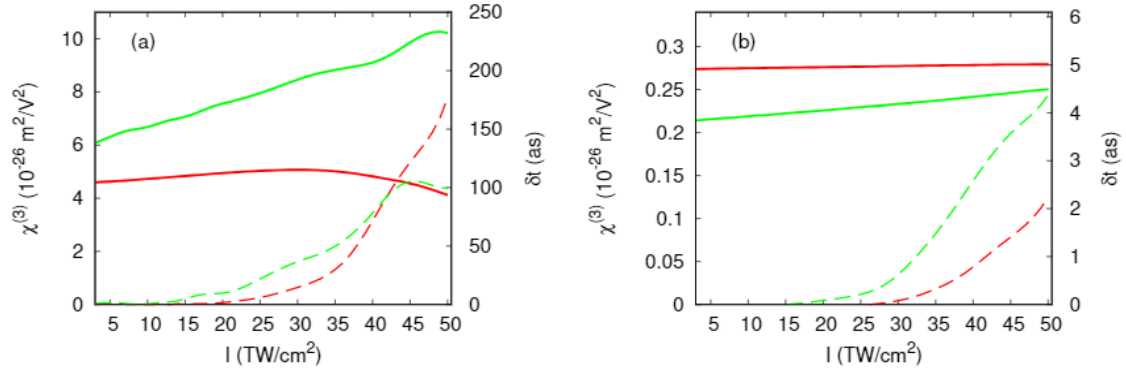


Fig. 1. Nonlinear refractive index (solid curves) and delay (dashed curves) for the fundamental-frequency response (red) and third-harmonic response (green). Hydrogen atom and Yukawa potential are considered in (a) and (b), correspondingly.

One can see that the nonlinear susceptibilities $\chi^{(3)}(\omega_0; \omega_0, \omega_0, -\omega_0)$ and $\chi^{(3)}(3\omega_0; \omega_0, \omega_0, \omega_0)$ [solid curves in Fig. 1(a)] are clearly different even for very low intensities around 5 TW/cm², where no higher-order effects can play a role. As the intensity grows the difference between the susceptibilities increases. We attribute this difference to the role of the excited states of the hydrogen atom and the interplay of the population in those states.

Additionally, one can see that at low intensities, the fundamental and third-order nonlinear responses are following carrier of the pump pulse without delay, as indicated by the dashed curves. We stress that zero delay does not mean that the response is instantaneous: the polarization carrier is not *shifted* from pump carrier, but its *shape* is still different from $\cos^3(\omega_0 t)$ since $\chi^{(3)}(\omega_0; \omega_0, \omega_0, -\omega_0) \neq \chi^{(3)}(3\omega_0; \omega_0, \omega_0, \omega_0)$. At high intensities delays become significant; they correspond to loss which constitutes up to 30% of the nonlinear response at around 50 TW/cm².

In order to elucidate the role of the excited states, we have repeated simulations for the Yukawa potential (with the same ionization potential), which is characterized by a significantly reduced influence of the excited states. One can see in Fig. 1(b) that the difference between $\chi^{(3)}(\omega_0; \omega_0, \omega_0, -\omega_0)$ and $\chi^{(3)}(3\omega_0; \omega_0, \omega_0, \omega_0)$ is smaller for this case, and the delays remain very close to zero.

In conclusion, we predict that the third-order response of hydrogen atoms is non-instantaneous even for low intensities and far from resonances. These findings are important both for design of the practical nonlinear optical setups and for fundamental understanding of the optical nonlinearities.

LM-I-45

Laser synthesis of copper oxides 2D structures with high thermo-sensitivity and high thermoelectric figure of merit

S.A. Mulenko¹, N. Stefan², E.G.Len¹, M.A.Skoryk¹, V.M.Popov³, O.Yo.Gudymenko⁴

1-G.V.Kurdyumov Institute for Metal Physics NAS of Ukraine, 36, Academician Vernadsky Blvd., UA-03142, Kyiv, Ukraine

2-National Institute for Lasers, Plasma and Radiation Physics, PO Box MG-54, RO-77125, Magurele, Romania

3-Institute for Microdevices NAS of Ukraine, 3, Severo-Syretskaya, UA-04136, Kyiv, Ukraine

4-V.F.Lashkaryov Institute of Semiconductor Physics, NAS of Ukraine, 41, Nauky Ave., UA-03028, Kyiv, Ukraine

Main author S.A. Mulenko e-mail: mulenko@ukr.net

A great interest is nowadays focused to thin films (2D structures) to find out the advantages of reduced thickness on the performances of electronic devices. Semiconductors are considered promising materials for thermo-sensors and thermo-converters. Before, for the first time, high thermo-sensitivity (S , Seebeck coefficient) and high thermoelectric figure of merit (ZT) were received with using non-toxic precursors, i.e. iron, chromium atoms, and oxygen molecules. Iron oxides in the form of 2D structures were deposited on $\langle 100 \rangle$ Si substrate by reactive pulsed laser deposition (RPLD) based on a KrF laser source ($\lambda = 248$ nm, $\tau_{FWHM} \leq 25$ ns). The S coefficient was high as (8.0-4.0) mV/K with $ZT \approx (1.0-12)$ in the range of (280-330) K [1]. In addition, high S coefficient was received on chromium oxides 2D structures deposited by RPLD on Si substrate too. The S coefficient was high as (3.0-8.0) mV/K in the range of (280-330) K with $ZT \approx (0.23-5.0)$ [2]. But unfortunately, in these cases, temperature dependencies of the S coefficient and ZT were not homogeneous owing to the existence of many iron and chromium oxides' crystalline phases, i.e. 8, 6, accordingly [1,2].

For the first time, the highest thermo-photosensitivity was achieved on 2D single-layered structure based on amorphous phases CuO, Cu₂O synthesized by RPLD using a KrF laser source ($\lambda = 248$ nm, $\tau_{FWHM} \leq 25$ ns) and deposited on Si substrate via the reaction of ablated Cu atoms with CH₄ molecules resulted in the highest S coefficient, i.e. 10.5 mV/K in the range of (290-340) K [3]. Here, for the first time, the photons generated by a KrF laser source were used for the synthesis of stable crystalline phases of copper oxides 2D single-layered semiconductor structures via the reaction of ablated copper atoms with oxygen molecules by RPLD. Obtained semiconductor 2D single-layered structures of (23-75) nm thickness were deposited on 293, 600 or 800 K $\langle 100 \rangle$ Si substrates in oxygen atmosphere at 1.0, 3.0 and 5.0 Pa. X-ray diffraction analysis evidenced polycrystalline structures of the deposits revealed only two crystalline semiconductor phases CuO(002) and CuO(111). Semiconductor temperature trend of 2D single-layered structures was detected with variable energy band gap (E_g) in the range of (0.10-1.5) eV depending on substrate temperature, oxygen pressure in the reactor and structure thickness. The optimum conditions were found out when the S coefficient was being homogeneously increased from 2.0 mV/K up to 10.5 mV/K and ZT from 0.035 up to 9.0 in the range of (290-340) K. The interpretation of behaviour for these 2D single-layered semiconductor structures of thermoelectric properties was provided. Obtained 2D single-layered structures based on copper oxides with such high S coefficient and high ZT are exceptionally strong candidates for a new effective thermo-sensors and thermo-converters operating at moderate temperature. Moreover, RPLD serves as an up-to-date method for the synthesis of 2D structures and 2D single-layered structures with such superior properties for thermo-sensors and thermo-converters.

[1] S.A.Mulenko, N.T. Gorbachuk, N. Stefan, Laser Synthesis of Nanometric Iron Oxide Films with High Seebeck Coefficient and High Thermoelectric Figure of Merit, Lasers Manuf. Mater. Process. vol. 1, pp. 21-35, (2014).

[2] S.A.Mulenko, N.T. Gorbachuk, N.Stefan, Laser synthesis of nanometric chromium oxide films with high Seebeck coefficient and high thermoelectric figure of merit, Int. Res. J. Nanosci. Nanotechnol., vol.1(2), pp.008-016, (2014).

[3] N.Stefan, S.A.Mulenko, M.A. Skoryk, V.M.Popov, O.Yo.Gudymenko, Laser synthesis of 2D structures for photo-thermo sensors with high sensitivity, Appl. Phys. B: Lasers and Optics, vol.126, pp.171-180, (2020).

LM-I-46

Femtosecond laser-generated shockwaves in transparent media: Experiments and Simulation

Alexandros Mouskeftaras¹, Olga Koritsoglou¹, Olivier Utéza¹, David Grojo¹, Nicolas Sanner¹ and Didier Loison²

1. Aix Marseille University, CNRS, LP3 UMR 7341, Campus de Luminy, Case 917,13288, Marseille cedex 9, France

2. Institut de Physique de Rennes, CNRS, Université Rennes 1, F-35042 Rennes, France

Interaction of intense femtosecond laser pulses with transparent materials has been a topic of growing interest in the past decades [1]. Among others, two features are particularly attractive. First, unprecedented material processing quality can be achieved as very small amount of energy is sufficient to induce the desired modification. Second, owing to localization of the laser peak intensity and the threshold-dependent nonlinear interaction, three-dimensional processing of transparent materials becomes possible. Although a growing number of applications exist [2], several limitations are present. As an example, there is an everlasting need to minimize the laser affected volume and thus avoid unwanted crack propagation or mechanical defect generation during in-bulk material processing.

In this paper, we study the thermomechanical coupling of laser energy in air. We use a 380-fs commercial laser system emitting at 1.03 μm to perform our experiments. Focusing down to a 1.5 μm spot diameter we achieve laser intensities up to 10^{15} W/cm² that are sufficiently high to transform almost any insulator into an absorber. Following the laser energy deposition, an important gradient of pressure and temperature builds up that results in a violent decompression through emission of a shockwave. A home-built time-resolved, high-resolution transmission microscope with visible light allows direct observation of both the plasma formation (Fig. 1-a) and the propagation of the shockwave in space (Fig. 1-b). Our technique allows measurement of the shockwave propagation speed at early delays with values reaching up to 6.5 km/s. Knowing the shockwave propagation speed, we use the conservation laws and the equation of state to theoretically estimate the pressure of the waves. To provide a larger picture of the interaction, we complement with measurement of the transmitted, excitation-pulse energy after the sample thus associating absorbed laser energy density to emitted shockwave characteristics. Our simulations suggest initial loading of up to 4.7GPa and emitted shockwaves carrying 440MPa at 7.2ps.

We will discuss the results and limitations of our approach but also possible implementation for measuring laser-driven dynamic stress fields in the case of transparent solids.

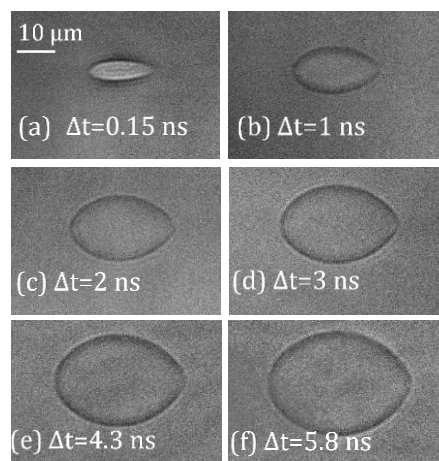


Fig. 1 Experimentally obtained transmission images in air depicting laser-generated shockwave following excitation by a single 6- μJ femtosecond pulse. Six delays after the arrival of the pulse are displayed.

References

- [1] R. R. Gattass and E. Mazur, "Femtosecond laser micromachining in transparent materials," *Nat. Photonics*, vol. 2, no. 6, pp. 378–379, 2008.
- [2] K. Sugioka and Y. Cheng, "Ultrafast lasers-reliable tools for advanced materials processing," *Light Sci. Appl.*, vol. 3, no. 390, pp. 1–12, 2014.

LM-I-47

Laser-matter interaction from ps to continuous regime: experiments and modeling

L.Videau^{1,2}, B.Bernecker¹, L. Berthe³, L .Lecherbourg^{1,2}, M.Scius-Bertrand^{1,2}

1- CEA ,DAM, DIF, F-91297 Arpajon cedex

2- Univ Paris Saclay, Lab Matiere Condit Extremes, CEA, F-91680 Bruyeres Le Chatel, France

3- Arts et Métiers Institute of Technology, CNRS, CNAM, PIMM, HESAM University, 75013 Paris, France

laurent.videau@cea.fr

Laser-matter interaction has been used for many years to study the matter under various conditions. Thanks to different laser sources available, it is a unique tool to study theoretical subjects such as nonequilibrium warm dense matter (fs to ps regime), behavior of material under shock loading conditions (ps to ns regime) or ablation processes (continuous regime). Thus, it has allowed the development of industrial applications like the Laser Shock Adhesion Test (LASAT) and the Laser Shock Peening (LSP) in ns regime, or welding and drilling laser processes. To have a better control and understanding of the laser-matter interaction in all these conditions, we have developed the numerical Lagrangian 1D Esther code [1].

First, we propose to briefly present the main Esther features which are needed for all applications (hydrodynamics, elastoplasticity, heat and radiative transfers, two temperature model) before describing the laser propagation and absorption models we have developed and implemented in the code. The first and most general method is based on the Helmholtz equation and it allows us to solve the majority of the problems in planar configurations. The second method is the raytracing method for which we have developed a specific and original resolution based on almost complete analytic formulations in the plane, cylindrical and spherical one-dimensional geometries. We compare and validate both numerical resolutions with theoretical Epstein profiles [2] we have adapted in transmission and reflection configurations.

We then present recent laser-matter experiments used to test and validate the Esther code in ps and ns regimes. In particular, we present a good comparison between pendulum and velocimetry measurements with numerical results, which allows us to establish empirical laws for the laser-induced ablation pressure in direct and confined interaction regime [3]. We finally present a laser ablation study in continuous regime and show how we have to adapt the hydrodynamics numerical scheme and use instead an isobaric model.

[1] S.Bardy, B.Aubert, T.Bergara, L.Berthe, P.Combis, D.Hebert, E.Lescoute, Y.Rouchausse and L.Videau. Development of a numerical code for laser-induced shock waves applications, *Optics and Laser Technology* 124 (2020)

[2] L.M. Brekhovskikh, R.T. Beyer, and Elsevier Science Technology (Firm). *Waves in Layered Media*. Applied mathematics and mechanics. Academic Press (1980).

[3] M.Scius-Bertrand, L.Videau, A.Rondepierre, E.Lescoute, Y.Rouchausse, J.Kaufman, D.Rostohar, J.Brajer, L.Berthe. Laser induced plasma characterization in direct and water confined regimes : new advances in experimental studies and numerical modelling, *J. Phys. D: Appl. Phys.* 54 (2021)

LM-I-48

Challenges of Direct Laser Writing of Single-crystal Waveguides in Oxide Glasses

Lipatiev A.S.¹, Lotarev S.V.¹, Okhrimchuk A.G.^{1,2}, Naumov A.S.¹, Lipateva T.O.¹, Fedotov S.S.¹, Sigaev V.N.¹

1 – Mendeleev University of Chemical Technology, Russia, Moscow, Miusskaya sq. 9

2 - Dianov Fiber Optics Research Center, Prokhorov General Physics Institute of Russian Academy of Sciences, Russia, Moscow, Vavilova str. 38

Main author email address: lipatievas@yandex.ru

Femtosecond laser-induced crystallization of glass paves the way to the direct laser writing of waveguides of Type I in which the core is presented by laser-precipitated crystal having a higher refractive index than the surrounding amorphous cladding. Fabrication of complex crystal-in-glass waveguides by the direct laser writing technique is a promising way to the creation of novel 3D integrated optical circuits, microlasers and photonics devices. Nevertheless, laser-induced growth of single crystals in glasses is generally a challenging task, which depends on many different factors such as the optical homogeneity and crystallization ability of glass host and laser exposure parameters. The possibility of the femtosecond laser-induced crystallization was demonstrated for many glasses with different crystallization ability [1-3], but the study on the direct laser writing of crystal-in-glass waveguides has been so far performed on the only example of lanthanum borogermanate glass [4,5].

In this work, we explore the possibility and the process of femtosecond laser-induced growth of a single-crystal channel waveguide in oxide glasses of the following molar compositions: 25La₂O₃•30B₂O₃•45GeO₂ (LBG), 33Li₂O•33Nb₂O₅•34SiO₂ (LNS) and 47.5BaO•5Al₂O₃•47.5B₂O₃ (BBO) and point out the challenges that must be overcome on the way to the high performance of laser-written crystal architectures. The FemtoLab setup based on PHAROS-SP laser emitting 180 fs pulses at 1030 nm wavelength was used for waveguide writing. The laser beam was focused into samples by Olympus LCPLN IR 20X objective lens (N.A.=0.45). The waveguides were inscribed in LBG glass at 520 nJ pulse energy by the two-pass method, including, first, laser scanning with a speed of 48 μm/s at which no glass crystallization occurred and, second, laser-induced crystal growth at a reduced scanning speed of 43 μm/s. The continuity and the absence of boundaries between crystalline grains in the crystal-in-glass waveguide are important for obtaining a waveguide effect, so we did not succeed in writing waveguides inside LNS glass where the crystallized structure is realized in the form of a nanograting [2], apparently due to large scattering losses during light propagation. On the other hand, direct laser writing of crystalline waveguides in BBO glass can be performed at ~3.5 times lower pulse energy and ~2 times higher laser beam scanning rate as compared with LBG glass. Thus, features in the laser writing of LaBGeO₅ and β-BaB₂O₄ crystalline waveguides are investigated and discussed.

This study was supported by the Russian Science Foundation (grant #17-73-20324).

[1] D. Tan, K. N. Sharafudeen, Y. Yue, J. Qiu, Femtosecond laser induced phenomena in transparent solid materials: Fundamentals and applications. *Progress in Materials Science*, 76, 154-228, 2016.

[2] J. Cao, M. Lancry, F. Brisset, L. Mazerolles, R. Saint-Martin, B. Poumellec. Femtosecond Laser-Induced Crystallization in Glasses: Growth Dynamics for Orientable Nanostructure and Nanocrystallization. *Crystal Growth & Design*, 19(4), 2189-2205, 2019.

[3] T. Komatsu, T. Honma, Laser patterning and growth mechanism of orientation designed crystals in oxide glasses: A review. *Journal of Solid State Chemistry*, 275, 210-222, 2019.

[4] A. Stone, H. Jain, V. Dierolf, M. Sakakura, Y. Shimotsuma, K. Miura, K. Hirao, J. Lapointe, R. Kashyap. Direct laser-writing of ferroelectric single-crystal waveguide architectures in glass for 3D integrated optics, *Sci. Rep.* 5, 10391, 2015

[5] A. S. Lipatiev, T. O. Lipateva, S. V. Lotarev, A. G. Okhrimchuk, A. S. Larkin, M. Y. Presnyakov, V. N. Sigaev. Direct laser writing of LaBGeO₅ crystal-in-glass waveguide enabling frequency conversion, *Crystal Growth & Design*, 17(9), 4670-4675, 2017

LM-O-1

Multiscale surface texturing of zirconium based thin film metallic glasses by femtosecond laser pulses

M. Prudent¹, F. Bourquard¹, A. Borroto², J.F. Pierson², F. Garrelie¹, J.P. Colombier¹

1- Univ Lyon, UJM-Saint-Etienne, CNRS, Institute of Optics Graduate School, Laboratoire Hubert Curien UMR CNRS 5516, F-42023 St-Etienne, France

2- Université de Lorraine, CNRS, IJL, F-54000 Nancy, France

jean.philippe.colombier@univ-st-etienne.fr

Metallic glasses are materials combining properties of crystalline metals and of glass materials. Thus, they possess unconventional characteristics, showing excellent wear and corrosion resistance and high elastic limits [1]. Their surface, which is particularly smooth, because free of usual crystalline defects, is ideal for ultra-short laser processing [2]. Typically, highly regular microstructures with few bifurcations can be generated [3], offering a wide range of possibilities for the surface functionalization of these materials.

The present work focuses on the surface texturing of zirconium-based metallic glass thin films. The chosen system (Zr-Cu) is particularly studied due to its simplicity of elaboration by physical vapour deposition (PVD), for its good glass forming ability as well as for its capacity to improve the mechanical properties of certain substrates [1]. The objective here was to functionalise a thin film metallic glass by creating a multi-scale surface structuring as well as local structural changes. A thin film of $Zr_{65}Cu_{35}$ fabricated by PVD was irradiated with a femtosecond laser by varying the fluence and the number of laser shots. The initial columnar microstructure of the films, due to the elaboration process, proved to be decisive for the overall results. Single pulses experiments revealed the creation of nanowells observed by Scanning and Transmission Electron Microscopy, while preserving the initial microstructure of the thin films. Time-dependent beam shaping (double pulses experiments) allowed the creation of a multi-scale structuring with the combination of nanowells and nanoripples. Fig. 1 presents the morphologies of the non-irradiated sample (Fig. 1a), the sample irradiated with single pulses experiments (Fig. 1b) and with double pulses experiments (Fig. 1c). The topographic changes induced under different irradiation atmospheres will also be discussed.

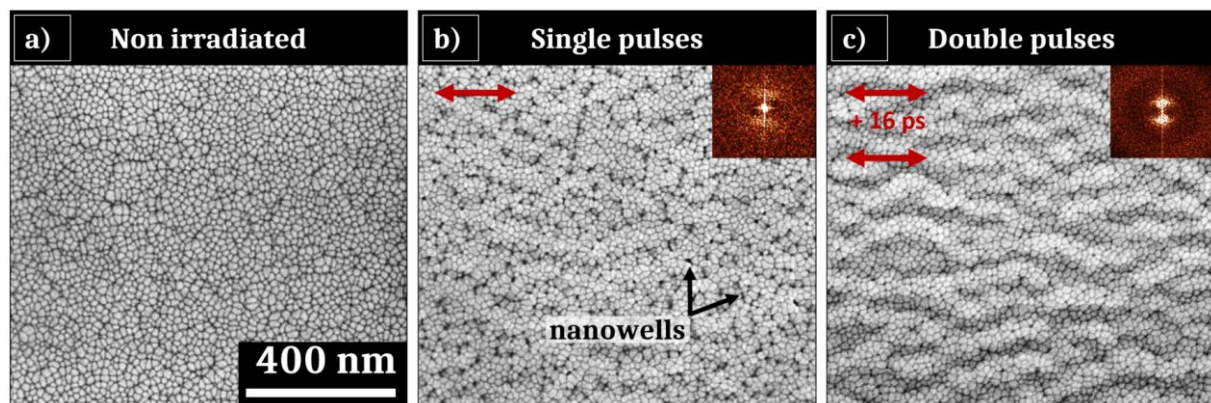


Figure 1. Scanning electron microscopy pictures of a $Zr_{65}Cu_{35}$ thin film metallic glass: (a) a non-irradiated area, (b) a zone irradiated with 50 pulses with a fluence of 0.06 J/cm^2 , (c) a zone irradiated with 50 double pulses with 16 ps of delay between the pulses and 0.06 J/cm^2 of total fluence. 2D-Fourier transforms shown as insets. The red arrows represent the electric field polarization.

- [1] M. Apreutesei, P. Steyer, A. Billard, L. Joly-Pottuz and C. Esnouf, « Microstructural, thermal and mechanical behavior of co-sputtered binary Zr–Cu thin film metallic glasses », *Thin Solid Films*, vol. 561, p. 53-59, juin 2014, doi: 10.1016/j.tsf.2013.05.177.
- [2] M. Prudent, F. Bourquard, A. Borroto, J.-F. Pierson, F. Garrelie, and J.-P. Colombier, « Initial Morphology and Feedback Effects on Laser-Induced Periodic Nanostructuring of Thin-Film Metallic Glasses », *Nanomaterials*, vol. 11, n° 5, p. 1076, mai 2021, doi: 10.3390/nano11051076.
- [3] C. Li, G. Cheng, X. Sedao, W. Zhang, H. Zhang, N. Faure, D. Jamon, J.P. Colombier and R. Stoian, « Scattering effects and high-spatial-frequency nanostructures on ultrafast laser irradiated surfaces of zirconium metallic alloys with nano-scaled topographies », *Optics Express*, vol. 24, n° 11, p. 11558, mai 2016, doi: 10.1364/OE.24.011558.

LM-O-2

Direct laser printing of continuous graphene patterns from a growth substrate

N. Kurochitsky¹, M. Komlenok¹, P. Pivovarov¹, M. Dezhkina¹, M. Rybin¹, S. Savin², A. Popovich¹, E. Obratsova¹, V. Konov¹

1 - Prokhorov General Physics Institute of the Russian Academy of Sciences, st. Vavilova 38, Moscow, 119991 Russia

*2 - MIREA - Russian Technological University, 78 Vernadsky Avenue, Moscow 119454 Russia
Main author email address: kuronick@mail.ru*

The technological process of transition from graphene synthesis to its use in microelectronics is often multi-step and is associated with high risks of contamination and damage of the initial carbon film structure [1, 2]. Modern trends in the transfer of carbon materials to the final carrier are associated with the use of laser printing methods [3, 4]. This significantly speeds up the transfer process and reduces costs, while maintaining the original characteristics of the material. As applied to low-dimensional carbon materials and especially to graphene films, different kinds of laser-induced transfer techniques have recently attracted great interest [5-7]. In this work, for the first time, we proposed to use the blister-based laser-induced forward transfer (BB-LIFT) for the direct printing of graphene patterns from a growth substrate to reduce the number of intermediate manipulation with graphene films. During the LIFT procedure, the laser pulse heats the absorbing layer covering the transparent donor substrate. Local heating leads to the partial evaporation of the absorbing layer and an increase in pressure, which results in the ejection of material from the site of the donor substrate facing the receiving sample–acceptor.

To minimize the number of manipulations with the carbon film it is necessary to solve a challenging task – to develop the synthesis of graphene on thin copper films used further for the absorbing of laser radiation. The standard technology for graphene synthesis is the method of chemical vapor deposition (CVD) on a copper foil surface at a high temperature from a mixture of argon, hydrogen, and methane under reduced pressure. The synthesis of graphene on thin copper films is a poorly studied topic, which is confirmed by only a few works [8-10]. We have improved the CVD technique for the synthesis of graphene on a copper film, recrystallized on a single crystal sapphire substrate. The regimes for the formation of a grain of a maximum-area copper crystal for further synthesis of single-layer graphene with the maximum grain size are studied. Selection of the optimal thickness of a copper film on a single-crystal sapphire substrate, preliminary cutting of the graphene film, and a decrease in the distance between the growth and receiving substrates during the BB-LIFT made it possible to achieve the transfer of continuous graphene fragments with sizes up to 50x50 μm . The report will present an analysis of the conditions of graphene synthesis and laser transfer, which critically affect the final characteristics of the transferred graphene patterns.

This research was funded by the Russian Science Foundation, grant number 18-72-10158.

1. M. Chen, R.C. Haddon, R. Yan, E. Bekyarova, Advances in transferring chemical vapour deposition graphene: a review, *Materials Horizons*, 4, 1054-1063 (2017).
2. B. Prevel, J.-M. Benoit, L. Bardotti, P. Melinon, A. Ouerghi, D. Lucot, E. Bourhis, and J. Gierak, Nanostructuring graphene on SiC by focused ion beam: Effect of the ion fluence, *Appl. Phys. Lett.*, 99, 083116–3 (2011).
3. S. Papazoglou, Y.S. Raptis, S. Chatzandroulis, I. Zergioti, A study on the pulsed laser printing of liquid-phase exfoliated graphene for organic electronics, *Appl Phys A*, 117, 301-306 (2014).
4. Arutyunyan N., Komlenok M., Kononenko T., Dezhkina M., Popovich A., Konov V., Printing of single-wall carbon nanotubes via blister-based laser-induced forward transfer, *Laser Physics*, 29, 2, 026001 (2019).
5. E.C.P. Smits, A. Walter, D.M.d. Leeuw, K. Asadi, Laser induced forward transfer of graphene, *Appl Phys Lett*, 111, 173101 (2017).
6. M. Komlenok, P. Pivovarov, M. Dezhkina, M. Rybin, S. Savin, E. Obratsova, V. Konov, Printing of Crumpled CVD Graphene via Blister-Based Laser-Induced Forward Transfer, *Nanomaterials*, 10, 6, 1103 (2020).
7. Praeger, M., Papazoglou, S., Pesquera, A., Zurutuza, A., Levi, A., Naveh, D., Zergioti, I., Eason, R., & Mills, B. Laser-induced backward transfer of monolayer graphene. *Applied Surface Science*, 533, 147488 (2020).
8. K.M. Reddy, A.D. Gledhill, C.-H. Chen, J.M. Drexler, N.P. Padture, High quality, transferrable graphene grown on single crystal Cu(111) thin films on basal-plane sapphire, *Appl Phys Lett*, 98, 113117 (2011).
9. P. Pavel, M. Jindřich, B. Dominik, L. Zuzana, D. Petr, V. Marek, S. Pauline, V. Anastasia, H. Dušan, P. Martin, K. Lukáš, B. Miroslav, E. Klaus, V. Peter, Č. Jan, Š. Tomáš, Ultrasoother metallic foils for growth of high quality graphene by chemical vapor deposition, *Nanotechnology*, 25, 185601 (2014).
10. T. Ma, H. Ariga, S. Takakusagi, K. Asakura, Smooth epitaxial copper film on sapphire surface suitable for high quality graphene growth, *Thin Solid Films*, 646, 12-16 (2018).

LM-O-3

Effect of alumina content on femtosecond laser processing of zirconia/alumina composites

Jide Han¹, Olivier Malek², Jozef Vleugels³, Annabel Braem³, Sylvie Castagne^{1,*}

¹ *KU Leuven, Department of Mechanical Engineering and Flanders Make@KU Leuven-MaPS, 3001 Leuven, Belgium*

² *Sirris Precision Manufacturing, 3590 Diepenbeek, Belgium*

³ *KU Leuven, Department of Materials Engineering, 3001 Leuven, Belgium*

* *sylvie.castagne@kuleuven.be*

Zirconia/alumina nanocomposites, which are composed of zirconia phase and alumina phase, are commonly used in biomedical applications, including dental implant and hip joint implant. These materials are often difficult to machine with conventional methods due to their exceptional mechanical strength and high brittle nature. Laser processing shows certain advantages over conventional methods when processing these ceramic materials. Since laser processing is the result of laser material interaction, the processing results are supposed to be influenced not only by laser parameters but also by material properties. In literature, there are many research studies that focused on the influence of experimental parameters on laser processing performance, while in this research we examined how changing the alumina content of zirconia/alumina composites will influence the processing outcome. To achieve this, six grades of zirconia/alumina composites with different alumina content were prepared and processed by femtosecond laser. The machining quality and material removal rate were examined under different experimental parameters. The results showed that the content of alumina of the composites had an obvious influence on machining performance. Therefore this research may serve as a useful reference for the material design when taking the machining performance into consideration.

LM-O-4

Laser micro-processing of graphite with pulsed ytterbium laser

T. Doualle^{1,*}, M. Reymond^{1,2}, Y. Pontillon¹, L. Gallais²

1 - CEA, DES, IRESNE, DEC, Cadarache F-13108 Saint-Paul-Lez-Durance, France

2 - Aix Marseille Univ, CNRS, Centrale Marseille, Institut Fresnel, Marseille, France

*email adress : thomas.doualle@cea.fr

Lasers are essential tools for macro and micro-processing for a whole range of materials in scientific research and industry. Processes involving lasers provide a unique solution with minimum mechanical and thermal influence on the processed part due to their selective energy control and deposition and allow generally high processing speeds.

In this work, we study laser micro-processing of graphite. This material is used in large number of scientific and industrial applications because of some of its peculiar properties: it is extremely resistant to heat, nearly inert in contact with almost any other material, has good thermal and electrical conductivity. Its refractory properties in combination with its mechanical properties make it a material of choice in very demanding applications in the nuclear or aerospace fields and lasers can be used in various ways to process it. The laser micro-processing of graphite employing an Ytterbium fibre laser delivering microsecond pulses at 1080 nm has been experimentally investigated, with the support of a numerical model to investigate and understand the laser ablation mechanisms processes.

High aspect ratio craters were obtained, with 400 μm depth and 50 μm diameter, and excellent crater quality with negligible heat affected zone (HAZ). We have applied micro-second laser pulse ablation approach for cutting graphite samples by identifying the best combination of scanning speed and repetition rate (beam overlap) to optimize the cut. We have shown that such laser cutting technique can produce parts with excellent quality (reduced affected area, no recast layer, no micro-cracks and no debris from ejected material) with high efficiency as shown in the Figure 1.

To go further in the investigation and understand the laser ablation mechanisms, simulations are conducted with the commercial software COMSOL which is based on the Finite Element Method. Heat transfer by conduction associated with deformed geometry and ray-tracing modules are employed for the analysis of the thermal effects, material evaporation and laser propagation on the fabricated structures.

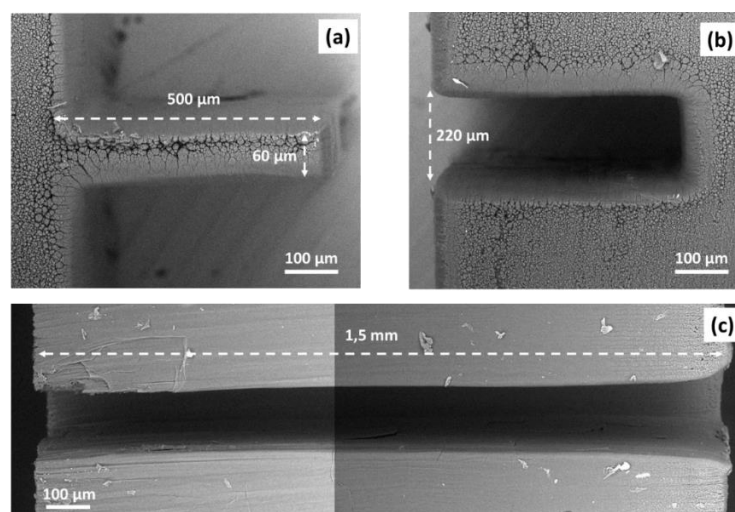


Figure 1 – SEM measurements of a pattern. (a) and (b) are top-views and (c) is the corresponding cross-section view of the part observed in (b).

LM-O-5

Laser ablation in liquid, structures, and shock peening

V. Zhakhovsky¹, Yu. Petrov^{2,3}, V. Khokhlov², V. Shepelev⁴, S. Fortova⁴, N. Inogamov^{1,2}

1- Center for Fundamental and Applied Research, Dukhov Research Institute of Automatics, Moscow, Russia

2- Landau Institute for Theoretical Physics of the Russian Academy of Sciences (RAS), Chernogolovka, Russia

3- Moscow Institute of Physics and Technology, Dolgoprudny, Moscow Region, Russia

4- Institute for Computer-Aided Design of the Russian Academy of Sciences, Moscow, Russia

nailinogamov@gmail.com

Lasers are used in many scientific and technological applications. We limit our report here to LSP (laser shock peening), LAL (laser ablation in liquid), and surface structuring. According to these applications this report is divided into three parts. (1) Formation of a shock wave under laser exposure. (2) Synthesis of colloidal solutions of nanoparticles by laser ablation in a liquid. (3) The appearance of surface structures. All three of these topics are closely related. The movement inside the target (topic 1) is inextricably linked with the movement outside the target (topic 2), i.e. internal motion is connected to a laser plume which is external motion. A laser plume ejected into a liquid is a source of nanoparticles. Movements inside and near the surface of the target ultimately leave an imprint on this surface (topic 3). This final imprint is the surface structures.

The radiation exposure scheme is as follows. There are two half-spaces contacting each other. One of them freely transmits laser radiation (vacuum, glass, water). The second half-space is filled with absorbent material. This half-space is the target. Laser radiation passes through a transparent medium and is absorbed in the target. The specific situation is determined by the type of transparent medium and the pulse duration. The energy of laser pulses for the described applications is fixed. Absorbed fluence is 0.1-10 J/cm² for ultrashort pulses and 1-100 J/cm² for nanosecond actions. We consider effects of non-one-dimensional geometry [1] in the propagation of shock waves in the interests of laser shock peening. One-dimensional evolution of ablation flow is well studied [1-4]. The report discusses how ablation proceeds in a liquid [1,5-9] (for applications connected to LAL) and describes the formation of various surface structures on films and bulk targets that accompanies these processes [10-14] (many applications with structuring).

[1] Inogamov et al., Picosecond-nanosecond laser flash, formation of powerful elastic waves in crystals, and shock peening. Proc. of the 32nd International Symposium on Shock Waves (ISSW32) (2019) doi:10.3850/978-981-11-2730-4_0506-cd.

[2] Demaske et al., Ablation and spallation of gold films irradiated by ultrashort laser pulses, Phys. Rev. B 82, 064113 (2010).

[3] Agranat et al., Strength properties of an aluminum melt at extremely high tension rates under the action of femtosecond laser pulses, JETP Lett. 91 (9), 471-477 (2010).

[4] Zhakhovskii, Inogamov, Elastic-plastic phenomena in ultrashort shock waves, JETP Lett. 92(8), 521-526 (2010).

[5] Inogamov et al., Laser ablation of metal into liquid: Near critical point phenomena and hydrodynamic instability, AIP Conference Proceedings 1979, 190001 (2018).

[6] Inogamov et al., Dynamics of Gold Ablation into Water, J. Experim. Theor. Phys. (JETP) 127(1), 79-106 (2018).

[7] Petrov et al., Hydrodynamic phenomena induced by laser ablation of metal into liquid, Applied Surface Science 492, 285-297 (2019).

[8] Petrov et al., Condensation of laser produced gold plasma during expansion and cooling in a water environment, Contrib. Plasma Phys. 59(6), e201800180 (2019).

[9] Inogamov et al., Hydrodynamic and molecular-dynamics modeling of laser ablation in liquid: from surface melting till bubble formation. Opt Quant Electron 52, 63 (2020).

[10] Wang, Kuchmizhak et al., Laser-Induced Translative Hydrodynamic Mass Snapshots: Noninvasive Characterization and Predictive Modeling via Mapping at Nanoscale, Phys. Rev. Applied 8(4), 044016 (2017).

[11] Inogamov et al., Solitary Nanostructures Produced by Ultrashort Laser Pulse, Nanoscale Research Letters 11, 177 (2016).

[12] Inogamov et al., Surface nanodeformations caused by ultrashort laser pulse, Engineering Failure Analysis 47, 328-337 (2015).

[13] Romashevskiy et al., Femtosecond Laser Irradiation of a Multilayer Metal–Metal Nanostructure, JETP Letters, Vol. 113, No. 5, pp. 308–316 (2021).

[14] Inogamov et al., Diffraction on a Microbubble and the Morphology of the Silicon Surface Irradiated through Glycerol by a Pair of Femtosecond Laser Pulses, JETP Letters, Vol. 113, No. 2, pp. 75–81 (2021).

LM-O-6

Ultrafast time-resolved experiments reveal the influence of a liquid confinement layer on the laser ablation dynamics of gold

Maximilian Spellauge^{1,2}, Carlos Doñate-Buendía^{2,3}, Stephan Barcikowski², Bilal Gökce^{2,3}, Heinz P. Huber¹

1- Department of Applied Sciences and Mechatronics, Munich University of Applied Sciences, 80335 Munich, Germany

2- Technical Chemistry I and Center for Nanointegration Duisburg-Essen (CENIDE), University of Duisburg-Essen, 45141 Essen, Germany

3- Materials Science and Additive Manufacturing, School of Mechanical Engineering and Safety Engineering, University of Wuppertal, 42119 Wuppertal, Germany

Main author email address: maximilian.spellauge@hm.edu

Laser ablation in liquid (LAL) is a versatile, environmentally friendly and scalable method to generate surfactant-free nanoparticles [1]. Compared to laser ablation in gaseous environments, the liquid layer present in LAL adds a layer of complexity as it represents an additional channel of energy loss, serves as a highly reactive environment, and confines the ablation products [2]. So far, experimental investigation of the ablation dynamics governing LAL has been mainly performed on timescales ranging from nanoseconds (ns) to microseconds (μ s). However, investigation of the sub-ns dynamics would significantly enhance the understanding of the LAL process, as the conditions under which nanoparticles are generated are established at this timescale [2], [3]. Furthermore, a detailed experimental analysis of the sub-ns LAL dynamics would allow experimental testing of recent computational predictions [4].

In order to investigate the influence of a water confinement layer on the ablation dynamics, ultrafast time-resolved experiments were performed on gold targets immersed in air and water. A pump-probe microscope (PPM) setup was used to analyze the transient reflectivity dynamics of the LAL process on timescales ranging from picoseconds to microseconds. Double-pulse ablation experiments with inter-pulse spacing ranging from 0 ps to 1 ns complemented the PPM measurements and allowed for the investigation of the ablation plume composition.

The detailed experimental investigation highlights the water confinement layers influence on the laser ablation process on the entire investigated timescale. This ranges from electron injection and the generation of a highly absorbing plasma within 1 ps after pulse impact to cavitation bubble development at approximately 1 ns. Furthermore, confinement of the ablation products and formation of primary particles is observed on timescales ranging from 20 ps to 200 ps and 200 ps to 1 ns, respectively.

The results enhance the understanding of the LAL process, confirm computational predictions and create the opportunity to further optimize the nanoparticle production in terms of size distribution and production-rate.

- [1] D. Zhang, B. Gökce, and S. Barcikowski, "Laser Synthesis and Processing of Colloids: Fundamentals and Applications," *Chem. Rev.*, vol. 117, no. 5, pp. 3990–4103, Mar. 2017.
- [2] A. Kanitz, M.-R. Kalus, E. L. Gurevich, A. Ostendorf, S. Barcikowski, and D. Amans, "Review on experimental and theoretical investigations of the early stage, femtoseconds to microseconds processes during laser ablation in liquid-phase for the synthesis of colloidal nanoparticles," *Plasma Sources Sci. Technol.*, vol. 28, no. 10, p. 103001, Oct. 2019.
- [3] A. Kanitz, D. J. Förster, J. S. Hoppius, R. Weber, A. Ostendorf, and E. L. Gurevich, "Pump-probe microscopy of femtosecond laser ablation in air and liquids," *Appl. Surf. Sci.*, vol. 475, no. September 2018, pp. 204–210, May 2019.
- [4] C.-Y. Shih, M. V. Shugaev, C. Wu, and L. V. Zhigilei, "Generation of Subsurface Voids, Incubation Effect, and Formation of Nanoparticles in Short Pulse Laser Interactions with Bulk Metal Targets in Liquid: Molecular Dynamics Study," *J. Phys. Chem. C*, vol. 121, no. 30, pp. 16549–16567, Aug. 2017.

LM-O-7

Generation of rarefaction and shock waves due to metal-nonmetal transition in laser ablation process

A.A. Samokhin, P.A. Pivovarov

*Prokhorov General Physics Institute of the Russian Academy of Sciences, 119991, Moscow, Vavilov str., 38
e-mail: asam40@mail.ru*

In [1] it was observed additional recoil pressure peak appearance during nanosecond laser ablation of liquid Hg. This effect as well as the whole pressure pulse displacement to earlier arrival times was supposed to be due to metal-nonmetal transition (MNT) in irradiated liquid. The arrival time decreasing was observed also in [2,3]. The pressure peak promotes shock wave generation which is responsible for the arrival time diminishing. Combined shock and rarefaction wave structure is analyzed in [4] for quasi-steady-state regime on the basis of conservation laws for mass and momentum fluxes at shock wave front (1) and rarefaction wave front (2) where MNT occurs.

$$\rho_0 D = \rho_1 (D - V_1), P_0 + \rho_0 D^2 = P_1 + \rho_1 (D - V_1)^2 \quad (1)$$

$$\rho_1 (d - V_1) = \rho_2 (d - V_2), P_1 + \rho_1 (d - V_1)^2 = P_2 + \rho_2 (d - V_2)^2 \quad (2)$$

The shock and rarefaction waves are propagating with constant velocities, respectively, $D > d > 0$ in the liquid which was initially at rest in the half-space $z \geq 0$ with pressure P_0 , density ρ_0 and velocity $V_0 = 0$ with pressure P_0 , density ρ_0 and velocity $V_0 = 0$. Between the fronts one has: $V_1 > 0$, $P_1 > P_0$ and $\rho_1 > \rho_0$ while after rarefaction wave front $V_2 < 0$, $P_2 > P_0$, and $\rho_c < \rho \leq \rho_2$, where ρ_c means critical density for liquid-vapor phase transition and P_2 at the irradiated surface depends on the metal ablation regime conditions. From (1), (2) for $m = d/D$ it follows

$$m = 1 - B_{01} + B_{01}^{\frac{1}{2}} [(P_2 - P_0) (\rho_0 D^2)^{-1} + B_{01} - 1]^{\frac{1}{2}} (1 - B_{12})^{-\frac{1}{2}} \quad (3)$$

Fig.1 shows m (B_{01}) dependence at fixed values of B_{12} and B_{01M} . It means that shock wave can appear at rather small subsonic d values. Its absolute value can be determined from energy flux conservation law where absorption of laser light should be taken into account. In general case one has to consider time-dependent problem of laser-metal ablation with strong decreasing of laser light absorption coefficient due to MNT. Such theoretical and experimental investigations are necessary for obtaining new information about metal critical parameters manifestations in non-equilibrium conditions of laser ablation [1,5].

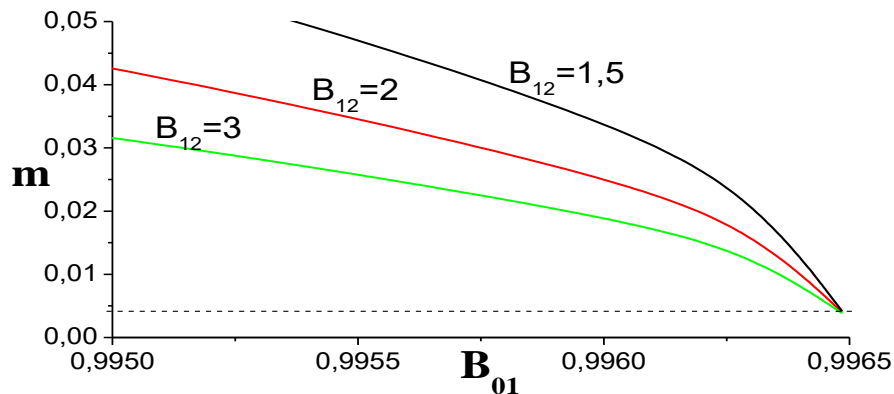


Fig.1 Dependencies of the value m on the ratio $B_{01} = \rho_0/\rho_1$ for three fixed ratio $B_{12} = \rho_1/\rho_2$ and one fixed ratio $(P_2 - P_0)/\rho_0 D^2 = 1 - B_{01M} = 3.5 \cdot 10^{-1}$

1. A.A. Samokhin, P.A. Pivovarov, E.V. Shashkov, I.A. Stuchebrukhov, Metal-nonmetal transition in nanosecond laser ablation, *Phys. of Wave Phenom.* 29(3) (2021)
2. A.A. Samokhin, E.V. Shashkov, N.S. Vorobiev, A.E. Zubko, On acoustical registration of irradiated surface displacement during nanosecond laser-metal interaction and metal-nonmetal transition effect, *Appl. Surf. Sci.*, 502, 144261 (2020).
3. S.I. Kudryashov, S. Paul, K. Lyon, S.D. Allen, Dynamics of laser-induced surface phase explosion in silicon, *Appl. Phys. Lett.* 98 25410 (2011)
4. A.A. Samokhin, P.A. Pivovarov, On the mathematical model of combined rarefaction and compression waves in condensed matter, *Mathematica Montisnigri*, 50, 104-107 (2021)
5. I. Iosilevskiy, V. Gryaznov, Uranium critical point location problem, *Zababakhin Scientific Talks (International Conference)* March 18–22 95 (2019).

LM-O-8

Applying Density Functional Tight Binding approach to study X-ray-induced phase transitions in solids

Vladimir Lipp^{1,2}, Victor Tkachenko^{3,1,2}, Michal Stransky^{3,4}, Bálint Aradi⁵, Thomas Frauenheim^{5,6,7}, and Beata Ziaja^{2,1}

¹Institute of Nuclear Physics, Polish Academy of Sciences, 31-342 Krakow, Poland

²Center for Free-Electron Laser Science CFEL, DESY, 22607 Hamburg, Germany

³European XFEL, 22869 Schenefeld, Germany

⁴Institute of Physics of the Czech Academy of Sciences, 182 21 Prague, Czech Republic

⁵Bremen Center for Computational Materials Science, Universitaet Bremen, 28359 Bremen, Germany

⁶Shenzhen JL Computational Science and Applied Research Institute, Shenzhen 518110, China

⁷Beijing Computational Science Research Center, Beijing 100193, China

Computer simulations of structural transitions in solids are essential for material processing applications. Here, we present a dedicated simulation tool developed to study X-ray- and XUV-induced phase transitions in a broad range of solid materials. This is possible due to the modular structure of the tool and utilization of the well-known density functional tight binding code, DFTB+, to follow band structure evolution of the irradiated targets. The computational scheme allows to simulate NVE thermodynamic ensemble for both atomic and electronic subsystems, which should make it relevant for laser material processing. The outstanding performance of the implementation is demonstrated with a comparative study of the XUV induced graphitization in diamond.

LM-O-9

On the sliding of steel surfaces subjected to ultra-short laser pulses on different kinds of snow

E. Maggiore¹, I. Mirza², D. Dellasega³, M. Tommasini¹, P.M. Ossi³

1- Dipartimento di Chimica, Materiali, Ingegneria Chimica “G. Natta”, Politecnico di Milano, P.za L. da Vinci, 32, 20133 Milano, Italy

2- HiLASE Centre, Institute of Physics of the Czech Academy of Sciences, Za Radnicí 828, 25241 Dolní Brezany, Czech Republic

3- Dipartimento di Energia, Politecnico di Milano, Via Ponzio, 34/3, 20133 Milano, Italy

Corresponding: paolo.ossi@polimi.it

Traditional ski bases for alpine skis manufactured in ultra-high molecular weight Polyethylene (UHMWPE) show an excellent sliding behaviour on natural snow. However, they undergo severe abrasion and wear against strongly aggressive (such as highly compacted, natural and artificial, even icy, barred) snow. In turn, ski edges, that are presently made in a low carbon steel (C60) rapidly deteriorate when sliding on slopes prepared with compacted snow. At high speed, ski edges warm up and cause a localized temperature increase of the surrounding UHMWPE regions with a permanent damage of the base, particularly severe in competition skis. A radical solution to the combined base and edge problem is to turn to hard, wear and oxidation resistant metallic materials such as stainless steels, notably AISI 301. In this study, we use a home-made snow tribometer to measure the friction coefficient (μ) of AISI 301 samples (5x5 cm² thickness 0.5 mm) sliding on tracks prepared with compact snow representative of realistic environment conditions. We performed different surface treatments obtaining Laser Induced Periodic Surface Structures (LIPSS) on cold rolled chemically cleaned AISI 301, with ultrashort laser pulses (wavelength 1030 nm, fluence 0.532 Jcm⁻², 75% overlapping of spot diameter both along X and Y) of duration 247 fs, 7 ps and 3 ps. We characterized the morphology of the LIPSS with SEM. The laser-treated AISI 301 surfaces display a marked increase in the contact angle value, measured with water droplets, with respect to an untreated AISI 301 surface. In the sliding tests on the tribometer, we used a normal load that reproduces the pressure exerted by an average weight skier. For different ranges of ski speed, we compared the measured friction coefficient values of AISI 301 and LIPSS treated AISI 301 to those of UHMWPE bases (prepared and waxed state of the art). On the slider speed range 5-25 kmh⁻¹ at temperatures not higher than -5°C, the μ value for LIPSS treated AISI 301-snow is comparable to that for UHMWPE-snow. Around 0°C we observed a deterioration of μ values for steel samples, more severe for the untreated material. We observed that, independent of the temperature, μ values increase with increasing sliding speed for untreated AISI 301, while they remain nearly constant for LIPSS treated AISI 301.

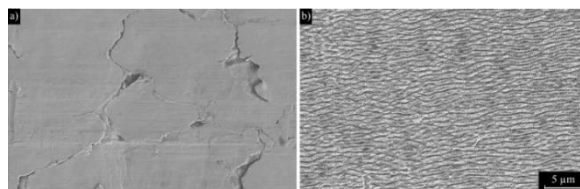


Fig. 1. SEM images of the untreated (a) and LIPSS treated (b) AISI 301 surface.

LM-O-10

Numerical Modeling of Thermal Response of Molybdenum Thin Film on Different Substrates Irradiated by Short Laser Pulse

K. Hlinomaz^{1,2}, Y. Levy¹, T. J. Y. Derrien¹ and N. M. Bulgakova¹

1- HiLASE Centre, Institute of Physics of the Czech Academy of Sciences, Za Radnicí 828, 25241 Dolní Břežany, Czech Republic

2- Czech Technical University in Prague, Faculty of Nuclear Sciences and Physical Engineering, Břehová 7, 115 19 Praha 1, Czech Republic

hlinomazk@fzu.cz

Heterostructures consisting of a thin metallic film deposited on a dielectric or semiconducting substrate are employed in a number of applications in the field of optoelectronics [1], photovoltaics [2], nanoparticle production [3] and in laser-induced forward transfer (LIFT) [4]. These thin films are often processed using ultra-short laser pulses. However, the type of substrate where they are deposited may affect the temperature evolution upon the laser exposure and the resulting structure.

In this work, numerical simulations based on two-temperature model (TTM) have been performed to study the effect of substrate on the thermal response of thin Mo film irradiated by a single laser pulse (wavelength 400 nm, pulse duration 200 fs at FWHM). The effect of three different dielectric substrates (fused silica, silicon, and soda-lime glass) was investigated in terms of temperature distribution and energy relaxation. For the same irradiation conditions, the results reveal different maximal temperatures achieved at the Mo-substrate interface for different substrates. In the case of fused silica substrate, the temperature at the interface can exceed its softening point with fluence even lower than the Mo thin film melting threshold. The softened state of fused silica can lead to the damage of the system at the Mo-substrate interface. A possible softening and corresponding compaction of fused silica was studied by systematically varying thickness of the film irradiated by laser pulses at the thickness-dependent melting threshold fluence. The time duration for which the substrate remains in its softened state has been calculated.

The numerical model, which includes temperature-dependent properties of substrate materials and molybdenum, was validated by controlling the energy conservation [5] and by comparing with the experimental melting threshold fluences of Mo films [4] for film thicknesses from 5 to 200 nm.

[1] A. D. Rakić, A. B. Djurišić, J. M. Elazar, M. L. Majewski, Optical properties of metallic films for vertical-cavity optoelectronic devices, *Applied Optics*, 37, 22 5271-5283, (1998).

[2] S. Zoppel, H. Huber, G.A. Reider, Selective ablation of thin Mo and TCO films with femtosecond laser pulses for structuring thin film solar cells, *Applied Physics A*, 89, 1 161-163, (2007).

[3] S. J. Henley, J. D. Carey, S. R. P.Silva, Metal nanoparticle production by pulsed laser nanostructuring of thin metal films, *Applied Surface Science*, 253, 19 8080-8085, (2007).

[4] M. Domke, S. Rapp, M. Schmidt, H. P. Huber, Ultra-fast movies of thin-film laser ablation, *Applied Physics A*, 109, 2 409-420 (2012).

[5] K. Hlinomaz, Y. Levy, T. J.-Y. Derrien, N. M. Bulgakova, Modeling the melting threshold of Mo films upon ultrashort laser irradiation, *Modern Machinery (MM) Science Journal*, Dec. 2019, 3585-3593 (2019).

LM-O-11

Ultrashort laser pulse ablation of bilayer Ti-Al thin films – effects of the thicknesses and layer position on the surface morphology

B. Gaković¹, S.I. Kudryashov², P.A. Danilov², D. Milovanović³, P. Panjan⁴, A.A. Ionin²

¹*Vinca Institute of Nuclear Sciences - National Institute of the Republic of Serbia, BU, 11000, Belgrade, Serbia*

²*Lebedev Physical Institute (FIAN, LPI), 119991 Moscow, Russia*

³*Institute of General and Physical Chemistry, 11000 Belgrade, Serbia*

⁴*Jožef Stefan Institute, 1000 Ljubljana, Slovenia*

biljagak@vin.bg.ac.rs

Laser processing of materials is a unique method, which allows their morphological and composition modifications. In the case of usage of ultrashort laser pulses (ULPs), pulse duration less than 10 ps, laser processing is extremely precise. Irradiation of materials by femtosecond laser enables removal or alteration of their surface at nano-micro level without change of the outer area [1,2]. Nano-scale thin films are attractive composite materials due to their properties that cannot be achieved in the case of the same bulk constituents [3]. Among them, bilayer metallic thin films (BMTFs) draw special attention [3,4]. Selective ablation of a layer from the BMTF, or the whole thin film with little or no damage of the layer or the substrate beneath, is significant for applications [4,5]. The effects of the ULPs on Ti-Al bilayers were investigated. The experimental samples were prepared by ion sputtering. The first layer composed of Al or Ti, was deposited on the Si substrate. It was 50 nm thick, while the second layers were 10 nm, 30 nm, 60 nm, and 100 nm. The fs laser ablations of the BMTFs were done with linearly polarized Gaussian laser beam- 515 nm wavelength, 300 fs pulse duration. The pulse energy ranged from 0.03 μJ to 1.2 μJ . Effects of laser-induced morphological and composition changes were monitored by scanning electron microscopy (SEM&EDX) and profilometry. The results are shown how the nano composition of BMTFs and pulse energy influence the ULP ablation (Fig.1). The damage threshold, defined as the fluence value at which apparent damage on BMTFs starts to generate, was determined too.

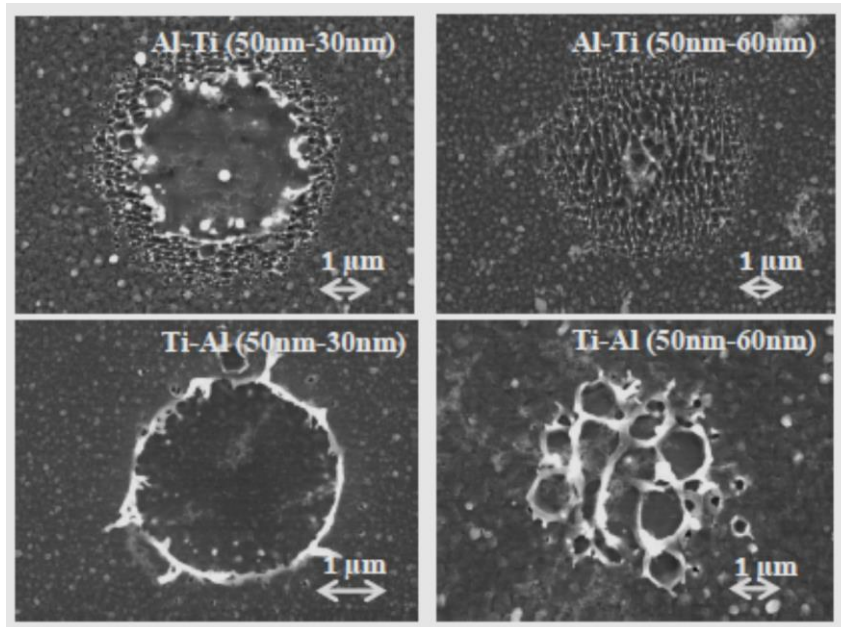


Fig. 1. Effects of 300 fs single pulse, energy of 0,06 mJ, on the BMTFs with Ti or Al on the surface (all thicknesses are written in the figures).

- 1 M.V. Shugaev , C. Wu , O. Armbruster, A. Naghilou, N. Brouwer, D.S. Ivanov, T.J.-Y. Derrien, N.M. Bulgakova, W. Kautek, B. Rethfeld, and L.V. Zhigilei, MRS Bulletin, 41, 960-968 (2016).
- 2 N.A. Inogamov, Y.V. Petrov, V.A. Khokhlov, V.V. Zhakhovsky, (Review), High Temperature, 58, 632–646 (2020).
- 3 S.I. Kudryashov, B. Gakovic, P.A. Danilov, S. Petrović, D. Milovanović, A.A. Rudenko, A.A. Ionin, App. Phys. Lett., 112, 023103 (2018).
- 4 S.A. Romashevskiy, et al. JETP Letters, 113, 311–319 (2021).

LM-O-12

Silicon surface amorphization and re-crystallization via single femtosecond laser pulses

C. Florian^{1,2,*}, **D. Fischer**¹, **K. Freiberg**³, **M. Duwe**⁴, **M. Sahre**¹, **S. Schneider**⁴,
A. Hertwig¹, **J. Krüger**¹, **M. Rettenmayr**³, **U. Beck**¹, **A. Undisz**⁵, **J. Bonse**^{1,†}

1- Bundesanstalt für Materialforschung und -prüfung (BAM), Unter den Eichen 87, D-12205 Berlin, Germany

2- Princeton University, 70 Prospect Avenue, NJ-08540, Princeton, USA

3- Friedrich-Schiller-Universität Jena, D-07743 Jena, Germany

4- Accurion GmbH, Stresemannstraße 30, D-37079 Göttingen, Germany

5- Technische Universität Chemnitz, Erfenschlager Straße 73, D-09125 Chemnitz, Germany

*camilo.florian@princeton.edu

†joern.bonse@bam.de

Silicon is the material responsible for most of the technological developments during the past century, making it one of the most studied materials along different disciplines. However, there are still unturned stones regarding its superficial re-solidification after femtosecond laser-induced local melting. In this presentation, we report irradiation experiments with single femtosecond pulses (790 nm, 30 fs) with a spatially Gaussian distribution on two different types of silicon with orientations $\langle 111 \rangle$ and $\langle 100 \rangle$. The surface modifications were studied in detail via different techniques, including optical microscopy, atomic force microscopy, spectroscopic imaging ellipsometry, energy dispersive X-ray spectroscopy and high-resolution transmission electron microscopy. We quantitatively estimate the resulting radial amorphous layer depth profiles with maximum thicknesses around some tenths of nanometers for fluences in between the melting and ablation thresholds [1].

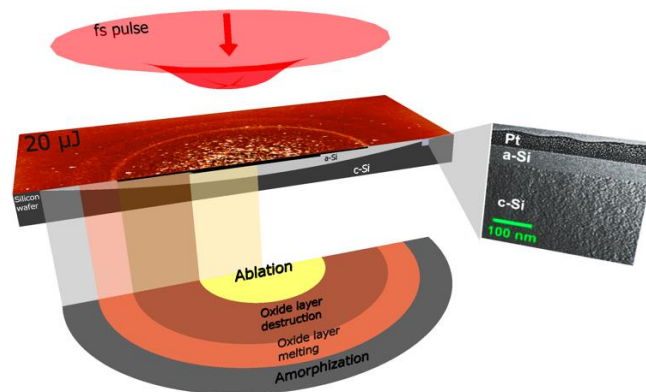


Fig. 1. General representation of a single fs laser pulse impinging a sample of crystalline silicon (c-Si) from the top. Data from the surface modifications gathered via AFM (among other techniques) allows the detection of different annular disks. Depending on the local laser fluence, different superficial modifications are produced as indicated by the colored semi-disks (bottom). A cross-sectional TEM characterization is included as an inset (right) to illustrate the thickness of the amorphous layer (a-Si) formed. Reproduced from [1]. (CC-BY 4.0 License).

In particular, spectroscopic imaging ellipsometry (SIE) allowed fast data acquisition using multiple wavelengths to provide experimental measurements for calculating the nanometric radial amorphous layer thickness profiles with micrometric lateral resolution based on a thin-film layer model. SIE proved to be capable of detecting and measuring nanometric structural and chemical modifications (oxidation) on the studied laser spots. The accuracy of the SIE-based calculations is verified experimentally by characterizing an in-depth material lamella via high-resolution transmission electron microscopy (HRTEM) and energy dispersive X-ray spectroscopy (STEM-EDX). For completeness, we present a mathematical modelling for the melt layer thickness considering different optical absorption processes including one photon absorption, two photon absorption and free-carrier absorption, highlighting the relevance of the latter one in the femtosecond laser-induced melting of silicon.

[1] C. Florian, D. Fischer, K. Freiberg, M. Duwe, M. Sahre, S. Schneider, A. Hertwig, J. Krüger, M. Rettenmayr, U. Beck, A. Undisz, J. Bonse, Single Femtosecond Laser-Pulse-Induced Superficial Amorphization and Re-Crystallization of Silicon, *Materials*, 14, 1651 (2021). <https://doi.org/10.3390/ma14071651>

LM-O-13

Formation of hollow microneedles on silicon surface by doughnut-shaped laser pulses using single- and multi-shot irradiation

J. Hrabovský^{1,2,*}, M. Zuckerstein¹, J. Sládek^{1,3}, I. Mirza¹, Y. Levy¹, and N. M. Bulgakova¹

¹HiLASE Centre, Institute of Physics of CAS, Dolni Brezany, Czechia

²Faculty of Mathematics and Physics, Charles University in Prague, Prague, Czechia

³Faculty of Nuclear Sciences and Physical Engineering, Czech Technical University, Prague, Czechia

Main author email adress: jan.hrabovsky@hilase.cz

Our work deals with the formation of tubular-like structures and hollow-core microneedles on the surface of monocrystalline silicon using ultrashort laser pulses. Highly deterministic surface processing is ensured by single-shot ablative modification of the sample surface as well as the multi-shot regime was used to study and modify the final structure shape. Both regimes were operated at laser fluences above the single-shot laser-induced damage threshold by a doughnut-shaped femtosecond laser pulses with duration of 35 fs (Astrella from Coherent, 800 nm wavelength). At laser fluences slightly above the ablation threshold, well reproducible tubular structures are formed whose height increases with fluence culminating with closing the structure on the top (fig. 1). Upon multi-pulsed irradiation, the height of the needle structures can be increased as compared to those produced by single pulses but, at certain number of pulses, ablation causes the entire structure to collapse. The origin of observed surface structures was discussed with respect to thermodynamics, hydrodynamics, and material stress theory.

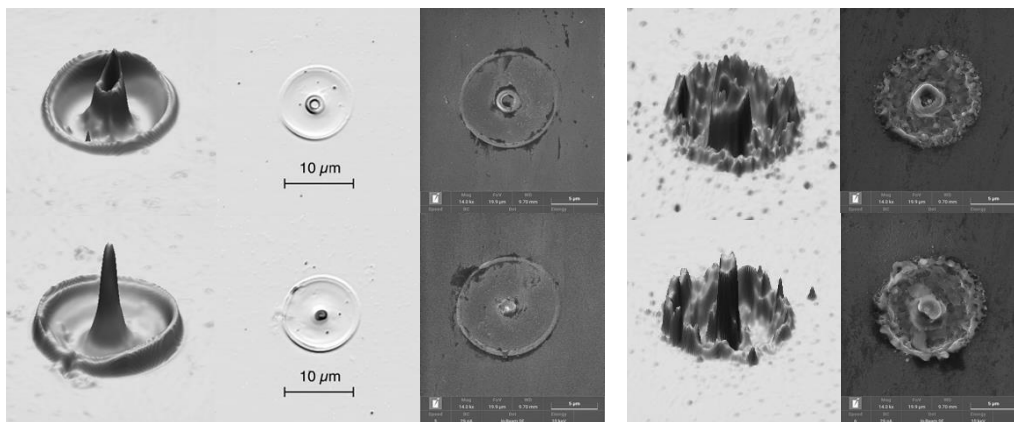


Fig.1 Created tubular-like structures (top line, 3D and top images) and hollow-core microneedle (bottom, 3D and top images) on the surface of monocrystalline silicon created by single (left) and multiple (right) doughnut-shaped femtosecond laser pulses studied using confocal microscopy and SEM.

Observations derived from our systematic study of hollow structures formation and their top closure offer new opportunities for applications in the fields of silicon photonics, silicon-based photovoltaic devices, and microstructures for optical field enhancement.

LM-O-14

Laser Synthesis of Chemically Pure Multielement Metal-Based Nanostructures

Miroslava Flimelova¹, Yury V. Ryabchikov^{1,2}

1– HiLASE Centre, Institute of Physics of the Czech Academy of Sciences, Scientific Laser Application Department, “Mid-IR and bioapplications” group, Za Radnici 828, 25241 Dolni Brežany, Czech Republic

2– P.N. Lebedev Physical Institute of the Russian Academy of Sciences, Department of Solid State Physics, Leninskii Prospekt 53, 19991 Moscow, Russian Federation

Corresponding author: yury.ryabchikov@hilase.cz

Multicomponent nanostructures consisting of several elements reveal a large research interest being served for various aspects in the field of biomedicine [1,2]. Combining different elements in a nanoparticle one can easily vary their physicochemical properties in a wide range adjusting their functionality. However, using chemical-based methods for synthesis can considerably obstruct their applications in biomedical fields due to their contamination by chemical residuals.

To overcome the aforementioned issues a versatile method of pulsed laser ablation in liquids is widely employed for the synthesis of pure one- and bi-metallic nanostructures widening their functional properties. As a result, they show wide prospects for applications in various fields of biomedicine, e.g. as contrast agents for magnetic resonance imaging [3,4]. However, manufacturing of composite metallic-based nanoparticles doped with semiconductor elements by means of pulsed laser ablation method is still challenging being at the early stage of its development. Nevertheless, laser-synthesized metallic-semiconductor nanocomposites have already shown promising perspectives for molecule detection using surface-enhanced Raman scattering (SERS) or infrared absorption techniques (SEIRA) having tracking features as Raman modality or paramagnetic defect labels at the same time [5,6].

In this work, gold-silicon nanocomposites with dual modalities were fabricated by direct femtosecond laser ablation in deionized water and characterized by structural and optical techniques. A method of chemical content variation is developed allowing fine-tuning of ratio between gold and silicon atom values. Successful employment of Au/Si nanocomposites for bacteria identification by SERS is demonstrated.

Acknowledgements:

This project has received funding from the European Union’s Horizon 2020 research and innovation programme under the Marie Skłodowska-Curie grant agreement No 897231 (LADENTHER). We are also thank the European Regional Development Fund and the state budget of the Czech Republic (Project BIATRI: CZ.02.1.01/0.0/0.0/15_003/0000445), the Ministry of Education, Youth and Sports (Programs NPU I-Project no. LO1602). Yu.R. also acknowledges Freie Universität Berlin for support within the Excellence Initiative of the German Research Foundation (0503121810) as well as personally Prof. J. Behrends.

References:

- [1] J.K. Lima, S.A. Majetich, Composite magnetic—plasmonic nanoparticles for biomedicine: Manipulation and imaging, *Nano Today*, vol. 8, pp. 98–113, (2013).
- [2] I. Monaco, F. Arena, S. Biffi, E. Locatelli, B. Bortot, L. Cava, G.M. Marini, G.M. Severini, E. Terreno, M.C. Franchini, Synthesis of Lipophilic Core–Shell Fe₃O₄@SiO₂@Au Nanoparticles and Polymeric Entrapment into Nanomicelles: A Novel Nanosystem for in Vivo Active Targeting and Magnetic Resonance–Photoacoustic Dual Imaging, *Bioconjugate Chemistry*, vol. 28, pp. 1382–1390, (2017).
- [3] V. Amendola, A. Guadagnini, S. Agnoli, D. Badocco, P. Pastore, G. Fracasso, M. Gerosa, F. Vurro, et al., Polymer-coated silver-iron nanoparticles as efficient and biodegradable MRI contrast agents, *Journal of Colloid and Interface*, vol. 596, pp. 332–341, (2021).
- [4] F. Waag, R. Streubel, B. Gökce, et al., Synthesis of gold, platinum, and gold-platinum alloy nanoparticle colloids with high-power megahertz-repetition-rate lasers: the importance of the beam guidance method, *Applied Nanoscience*, vol. 11, pp. 1303–1312, (2021).
- [5] M. Kögler, Yu.V. Ryabchikov, S. Uusitalo, A. Popov, A. Popov, G. Tselikov, A.–L. Välimaa, A. Al–Kattan, J. Hiltunen, R. Laitinen, P. Neubauer, I. Meglinski, A.V. Kabashin, Bare Laser–Synthesized Au–Based Nanoparticles as Non–Disturbing SERS Probes for Bacteria Identification, *Journal of Biophotonics*, vol. 11(7), pp. e201700225, (2018).
- [6] O. Bibikova, J. Haas, A.I. López–Lorente, A. Popov, M. Kinnunen, Yu. Ryabchikov et al., Surface enhanced infrared absorption spectroscopy based on gold nanostars and spherical nanoparticles, *Analytica Chimica Acta*, vol. 990, pp. 141–149, (2017).
- [7] Yu.V. Ryabchikov, Facile Laser Synthesis of Multimodal Composite Silicon/Gold Nanoparticles with Variable Chemical Composition, *Journal of Nanoparticle Research*, vol. 21(4), pp. 85, (2019).

LM-O-15

Polarization singularities of a plane electromagnetic wave scattered on a dielectric spherical nanoparticle

N. Y. Kuznetsov, K. S. Grigoriev, V. A. Makarov

Faculty of Physics, Moscow State University, Leninskie Gory 1, Moscow 119991, Russia

ny.kuznetsov@physics.msu.ru

Polarization singularities are the regions of the electromagnetic field, where the polarization ellipse of the electric field degenerates to a perfect circle (C^T -lines) or a line segment (L^T -lines). Distribution of the polarization ellipses around these lines is found to be topologically nontrivial, making the singularities persistent under changes of the field parameters [1]. We study the three-dimensional structure of the polarization singularities of a plane monochromatic electromagnetic wave with initially uniform elliptical polarization profile, scattered on a dielectric spherical particle of sub-wavelength radius [2]. For the various values of the incident radiation ellipticity degree we trace the C^T - and L^T -lines of polarization. We discuss existence and geometry of these lines in dependence of the incident radiation ellipticity and complex structures in the distribution of the polarization ellipses, found near their points. We also observe the strips, swept by the axes and normal vectors of the polarization ellipse being traced along a closed contour, which may form non-orientable surfaces, such as Möbius strips, around the singular lines and classify their behavior.

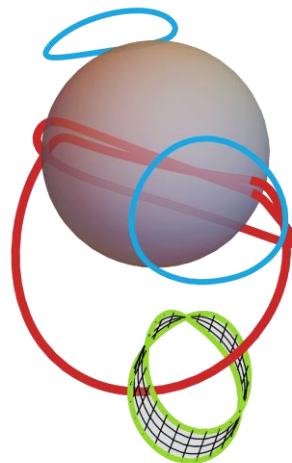


Fig. 1. A singular pattern and an optical Möbius strip.

We acknowledge financial support from Russian Foundation for Basic Research (19-02-00069 and 20-32-90123), Foundation for the Advancement of Theoretical Physics and Mathematics "Basis" and Nonprofit Foundation for the Advancement of Science and Education "Intellect".

[1] J. F. Nye and J. V. Hajnal, The wave structure of monochromatic electromagnetic radiation, Proc. R. Soc. A 409(1836)21–36 (1987).

[2] N. Y. Kuznetsov, K. S. Grigoriev, Y. V. Vladimirova, V. A. Makarov, Three-dimensional structure of polarization singularities of a light field near a dielectric spherical nanoparticle, Optics Express. — Vol. 28, no. 19. — P. 27293–27299 (2020).

LM-O-16

Peculiarities of Interaction of Radially and Azimuthally Polarized Laser Pulses with Transparent Dielectrics

V.P. Zhukov^{1,2}, N.M. Bulgakova¹, M.P. Fedoruk^{2,3}

1- HiLASE Centre, Institute of Physics of the Czech Academy of Sciences, Za Radnicí 828, 25241 Dolní Břežany, Czech Republic

2- Federal Research Center for Information and Computational Technologies, 6 Lavrentyev Ave., 630090 Novosibirsk, Russia

3- Novosibirsk State University, 2 Pirogova str., 630090, Novosibirsk, Russia

Email address: zukov@ict.nsc.ru

Spatially and/or temporally shaped laser pulses attract a high interest as a promising technique for improving efficiency, quality, and precision of material processing [1,2]. Recently by numerical modeling, we have demonstrated that application of radially -polarized doughnut-shape pulses for volumetric modification of fused silica can provide considerable differences in the strength and geometry of modification as compared with Gaussian pulses with the same irradiation parameters (beam energy, pulse duration, numerical aperture) [3]. In the case of a doughnut-shaped beam, the free-electron plasma generated in the focus region has a toroidal shape. Consequently, a part of laser radiation scattered by the plasma propagates to the axes of the laser-excited zone, contrary to Gaussian pulses where the laser light is mostly scattered to the periphery. As a result, the part of the beam scattered to the axis induces an enhanced ionization close to the axis where, according to simulations, the absorbed density of laser energy can be more than an order of magnitude higher as compared to the Gaussian laser pulse. On the stage of the elastoplastic relaxation of the laser -excited material, such a large absorbed energy will generate a huge mechanical stress comparable with the pressure levels in the Earth's mantle.

In this work, the action of the focused doughnut-shaped pulses with radial and azimuthal polarization on fused silica has been investigated numerically and the effects of polarization are studied for different numerical apertures. The model is based on nonlinear Maxwell's equations supplemented by the equations of hydrodynamic type for the description of the generation of the free electron plasma and its motion in the laser field [3]. The equations are solved by an original finite-difference scheme presented in Ref. [4].

[1] K. Fuse, Beam shaping for advanced laser materials processing, *Laser Tech. J.*, vol. 2, pp. 19-22 (2005).

[2] A. Möhl, S. Kaldun, C. Kunz, F. A. Müller, U. Fuchs, S. Gräf, Tailored focal beam shaping and its application in laser material processing *J. Laser Appl.*, vol. 31, article 042019 (2019).

[3] V. P. Zhukov, A.M. Rubenchik, M.P. Fedoruk, N. M. Bulgakova, Interaction of doughnut-shaped laser pulses with glasses, *J. Opt. Soc. Am. B*, vol. 34, No 2, pp. 463-471, (2017).

[4] V. P. Zhukov, M. P. Fedoruk, Numerically implemented impact of a femtosecond laser pulse on glass in the approximation of nonlinear Maxwell equations, *Math. Models Comput. Simul.*, vol. 12, No. 1, pp. 77–89, (2020).

LM-O-17

Ultrashort laser-induced damage and ablation of silicon in water and air environments

A. V. Bulgakov^{1,2}, M. Stehlik^{1,3}, I. Mirza¹, O. Gatsa¹, J. Hrabovský^{1,4}, N. M. Bulgakova^{1,2}

1- HiLASE Centre, Institute of Physics of the Czech Academy of Sciences, Za Radnici 828, 25241 Dolní Břežany, Czech Republic

2- S.S. Kutateladze Institute of Thermophysics SB RAS, Lavrentyev ave. 1, 630090 Novosibirsk, Russia

3- Aix Marseille Univ, CNRS, Centrale Marseille, Institut Fresnel, Marseille, France

4- Charles University, Faculty of Mathematics and Physics, Ke Karlovu 5, 121 16 Prague, Czech Republic

bulgakov@fzu.cz

Pulsed laser ablation in liquids (PLAL) is an efficient and flexible technique for nanoparticle production and surface nanostructuring. The technique is simple in realization but involves complicated physical and chemical processes which are not fully understood. As a result, controllable PLAL fabrication of both colloidal nanoparticles and surface structures is still a challenge. This study investigates systematically, both experimentally and theoretically, damage and ablation of silicon irradiated by ultrashort laser pulses in air and water. The fundamental output of a PHAROS laser at a 1030-nm wavelength and with tunable pulse duration from 260 fs to 10 ps was used for ablation. The morphology of the laser-produced craters and the ablation volumes are analyzed by microscopy methods as a function of laser fluence and the damage and ablation thresholds are measured. Comparisons of femtosecond and picosecond pulses, single-shot and multi-shot irradiation regimes, and water and air environments are performed.

All threshold fluences in water are found to be considerably lower than the corresponding values in air. The efficiency of ps-laser ablation is strongly enhanced in water with the ablation depth being several times higher than that in air (Fig. 1) while fs ablation is shown to be suppressed by non-linear effects (self-focusing, plasma scattering) during laser pulse propagation in water. A theoretical analysis of silicon heating and melting under the considered conditions is based on a two-temperature model and demonstrates that the observed deep craters under ps-laser ablation in water correspond to the silicon melting depth. Influences of the pulse duration, surface reflectivity, focusing conditions, cavitation vapor bubble, and accumulation effects under multi-shot irradiation on silicon damage and ablation on ultrashort laser damage and ablation in water are discussed.

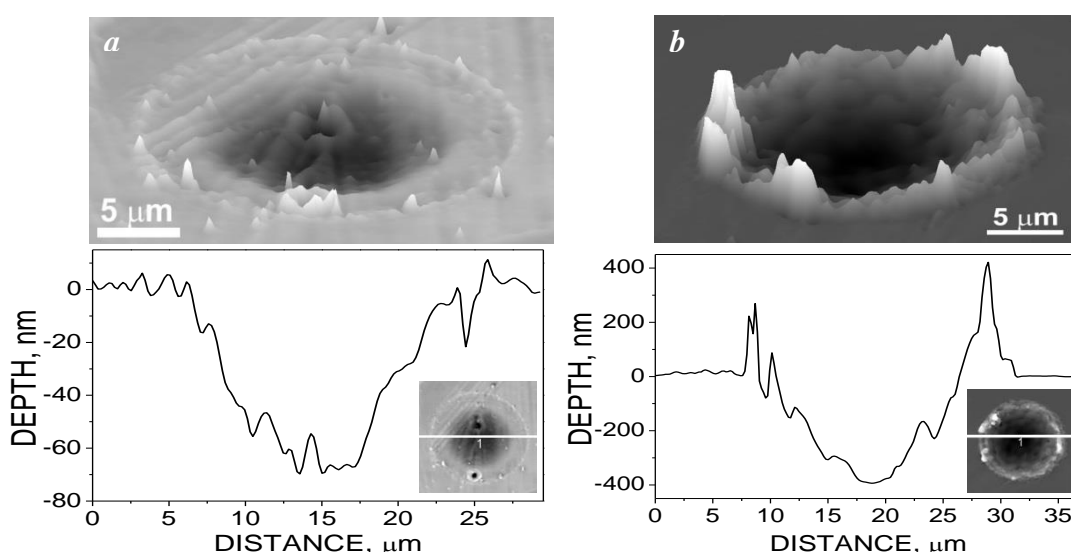


Fig. 1. Confocal 3D microscopy images of spots produced by individual picosecond laser pulses (7 ps pulse duration) at a peak fluence of 3.1 J/cm^2 in air (a) and water (b) and the corresponding cross section profiles. The insets in the profiles show the cross section line across the spots.

LM-O-18

Picosecond-laser-induced damage and ablation of gold in water: Effects of the water layer thickness

O. Gatsa¹, A. V. Bulgakov^{1,2}

1- HiLASE Centre, Institute of Physics of the Czech Academy of Sciences, Za Radnici 828, 25241 Dolní Břežany, Czech Republic

2- S.S. Kutateladze Institute of Thermophysics SB RAS, Lavrentyev ave. 1, 630090 Novosibirsk, Russia

oleksandr.gatsa@hilase.cz

Pulsed laser ablation in liquids (PLAL) is a very attractive technique for surface nanostructuring allowing fabrication of surface structures for various materials in a simple and controllable way at low laser fluences [1]. PLAL is also considered as an efficient promising alternative to the chemical method for synthesis of colloidal nanoparticles [2]. The PLAL process is very complicated and its understanding is a key step in optimization of applications of the technique. Laser-induced damage and ablation thresholds (DTs and ATs) are important parameters offering references for modeling. However, the threshold determination for PLAL conditions is not as straightforward as for the air environment and, e.g., for gold, the literature provides contradictory data for the thresholds, both higher and lower than the corresponding air values [3-5].

In this work, we have investigated damage and ablation of gold irradiated in water by picosecond pulses of a PHAROS laser (1030-nm wavelength, 6 ps pulse duration). The size and morphology of the irradiation spots produced under single-shot and multi-shot irradiation conditions are analyzed using microscopy methods and the DTs and ATs are determined. The main attention is paid to the effect of the thickness of the water layer (in the range 2-30 mm) and the results are compared with those obtained in air (Fig. 1). The DTs and ATs in water are found to be lower than the corresponding values in air (app. 1.2 and 1.9 J/cm², respectively) being weakly dependent on the water depth. It is demonstrated that self-focusing of the laser beam during its propagation in water plays an important role under the considered conditions even at low fluences, near the DT, and its contribution increases with the water layer thickness. It is also found that at a relatively high fluence, in the range of 6-10 J/cm² (depending on the water depth), there is an abrupt change in the ablation regime resulting in a strong decrease of the damage area and in a decrease of the ablation area as compared to the air behavior. This threshold-like transition to a different ablation regime is explained by manifestation of another non-linear effect, scattering of the laser beam by plasma produced due to the optical water breakdown. Influences of the surface reflectivity change of the target immersed in water and of the cavitation bubble on ps-laser-induced damage and ablation of gold in water are discussed.

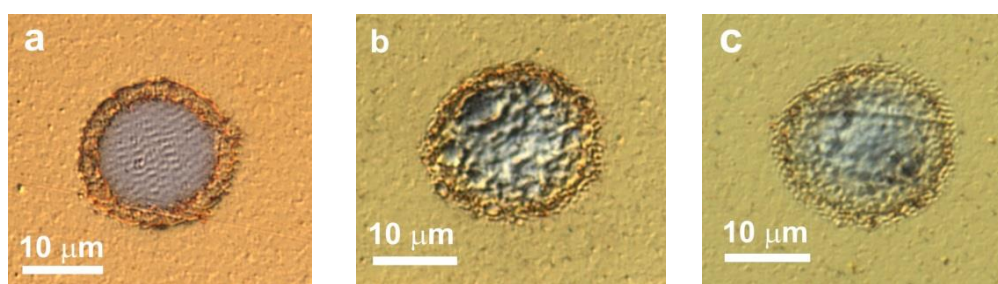


Fig. 1. Optical images of spots on the gold surface produced by single ps-laser pulses in air (a) and in water of the depth of 5 mm (b) and 20 mm (c) at a peak fluence at the surface of 3 J/cm². The damage (outer) and ablation (inner) regions are clearly seen.

[1] E. Stratakis, V. Zorba, M. Barberoglou, C. Fotakis, G.A. Shafeev, Laser writing of nanostructures on bulk Al via its ablation in air and liquids, *Nanotechnology* 20, 105303 (2009).

[2] D. Zhang, B. Gökce, S. Barcikowski, Laser synthesis and processing of colloids: Fundamentals and applications, *Chem. Rev.* 117, 3990-4103 (2017).

[3] J. Tomko, J.J. Naddeo, R. Jimenez, Y. Tan, M. Seiner, J.M. Fitz-Gerald, D.M. Bubb, S.M. Malley, Size and polydispersity trends found in gold nanoparticles synthesized by laser ablation in liquids, *Phys. Chem. Chem. Phys.* 17, 16327-16333 (2015).

[4] S.V. Starinskiy, Y.G. Shukhov, A.V. Bulgakov, Laser-induced damage thresholds of gold, silver and their alloys in air and water, *Appl. Surf. Sci.* 396, 1765-1774 (2017).

[5] S. Dittrich, R. Streubel, C. McDonnell, H.P. Huber, S. Barcikowski, B. Gökce, comparison of the productivity and ablation efficiency of different laser classes for laser ablation of gold in water and air, *Appl. Phys. A* 125, 432 (2019).

LM-O-19

Three-dimensional hybrid optoacoustic imaging of the laser-induced plasma and deposited energy density under femtosecond laser excitation of condensed medium

Rumiantsev B.V.¹, Mareev E.I.^{1,2}, Bychkov A.S.^{1,3}, Karabutov A.A.³, Makarov V.A.^{1,3}, Cherepetskaya E.B.^{1,3} and Potemkin F.V.¹

1 - Faculty of Physics, Lomonosov Moscow State University, Leninskie Gory bld.1/2, 119991 Moscow, Russia.

2 - Institute of Photonic Technologies FSRC "Crystallography and Photonics," RAS, Troitsk 108840, Russia.

3 - The National University of Science and Technology MISiS, Leninski Prospect 6, Moscow 119991, Russia.

runjancev.bv15@physics.msu.ru

Femtosecond laser processing at the present time is an area of the active scientific research and has a prospective for the transition into the field of technological applications in the near future. The subjects of special interest in this area is the femtosecond laser micromachining of the bulk waveguides [1] in the field of optoelectronics, femtosecond laser processing in the biophotonics and medicine [2] and ultrafast femtosecond processing of the bulk dielectrics [3]. Technological applications of the femtosecond laser processing requires use of the feedback allowing determination of the deposited energy density (DED, kJ/cm^3) distribution. The measurement of the plasma electron density distribution (cm^{-3}) can provide this feedback, since the plasma formation process directly precedes the energy transfer under plasma-mediated laser impact on the condensed medium bulk and therefore the measured electron density can be directly recalculated to the DED. In the present work the method of the three-dimensional optoacoustic imaging is developed and experimentally realized. The proposed method allows measurement of the three-dimensional distributions of the plasma electron density and DED under plasma-mediated laser impact on the condensed medium (Fig.1), that can't be achieved by any other modern techniques. As an experimental medium for the proof of method concept the distilled water was used. The proposed method is based on the shadowgraphy [4] and photoacoustic imaging techniques [5].

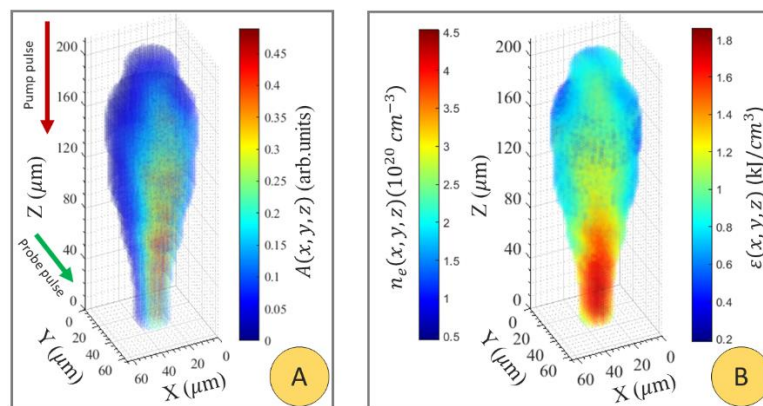


Fig.1. A) 3D distribution of the probe pulse absorption in the plasma volume. B) 3D distributions of the plasma electron density and DED.

The work was supported by the RSF grant no. 17-72-20130. Rumiantsev B.V. is the scholar of the foundation for the advancement of the theoretical physics and mathematics "BASIS".

[1] Chambonneau, M., et al. "Writing waveguides inside monolithic crystalline silicon with nanosecond laser pulses." *Optics letters* 41.21 (2016): 4875-4878.

[2] Gabel, Christopher V. "Femtosecond lasers in biology: nanoscale surgery with ultrafast optics." *Contemporary Physics* 49.6 (2008): 391-411.

[3] Butkus, Simas, et al. "Rapid cutting and drilling of transparent materials via femtosecond laser filamentation." *Journal of Laser Micro Nanoengineering* 9.3 (2014): 213.

[4] Rumiantsev, Boris, et al. "Photoacoustic and optical imaging of the femtosecond filament in water." *Nonlinear Optics and Applications XI*. Vol. 11026. International Society for Optics and Photonics, 2019.

[5] Potemkin, F. V., et al. "Two-dimensional photoacoustic imaging of femtosecond filament in water." *Laser Physics Letters* 15.7 (2018): 075403.

LM-O-20

Direct Laser Writing in Silica and K8 Glass in Athermal Regime

Vladislav Likhov, Andrey Okhrimchuk

*Prokhorov General Physics Institute of the Russian Academy of Sciences, Dianov Fiber Optics
Research Center, 38 Vavilov Str, Moscow 119333, Russia
Mendeleev University of Chemical Technology of Russia, 9 Miusskaya Sq, Moscow 125047, Russia*

vladislavlikhov@gmail.com

Direct Laser Writing (DLW) is a well-established micromachining technique used, in particular, in manufacturing optical waveguides in silica and BK7 glasses [1]. However, most works devoted to the subject are dealing with writing in thermal regime [2] where high pulse repetition rate ensures energy delivery is faster than heat diffusion [3]. However, laser structuring in thermal regime does not allow for a micrometer-scale refractive index modulation because the modified region considerably exceeds the laser exposed one. Meantime, submicrometer-scale precision is frequently needed in laser micromachining, and, in particular, in Bragg grating manufacturing.

Thus, we investigated refraction index change in these glasses in athermal inscription regime. We wrote and studied fs-laser inscribed tracks with different scan speeds and input pulse energies in the volume of silica and K8 glasses (a close analogue of Schott BK7® glass). We used an Yb:KGW femtosecond laser system with a pulse duration of 180 fs and pulse repetition rate of 5 kHz. The objective lens (NA = 0.65) was used for focusing and a 1 mm wide slit was placed before the objective lens in order to achieve a lenticular-shaped beam waist instead of a “standart” cigar-shaped beam waist. Tracks were inscribed at ~75 μm depth. The refractive index change (Δn) was estimated on the basis of measured phase difference ($\Delta\phi$) using a quantitative phase microscopy (QPm) technique.

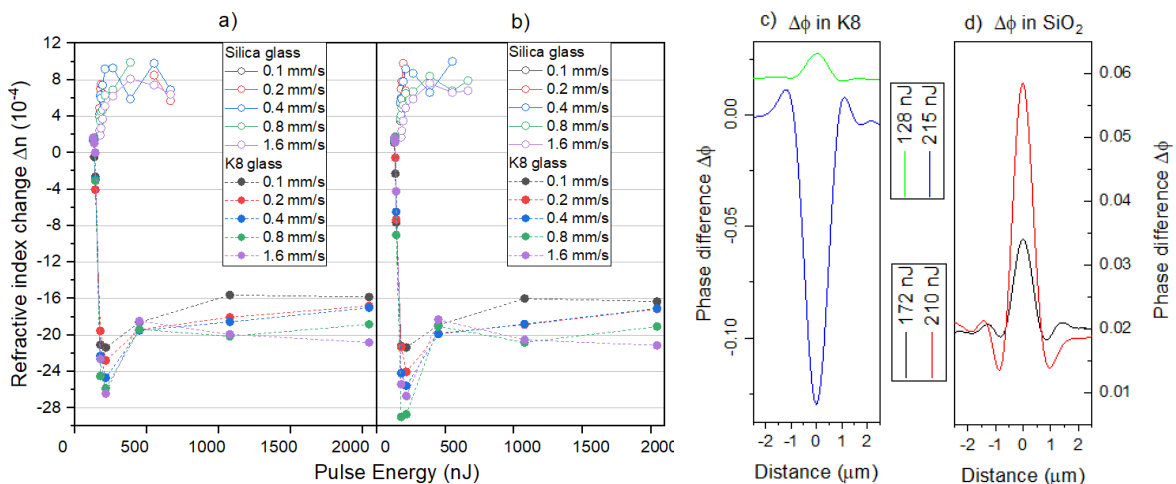


Fig. 1. Refractive index change in silica and K8 glasses versus input pulse energy for polarization of the writing beam perpendicular (a) and parallel (b) to scan direction; transverse profile of phase difference $\Delta\phi$ of tracks in K8 glass (c) and silica glass (d) for writing speed $V = 0.4$ mm/s and polarization of the writing beam perpendicular to scan direction.

As seen from Fig. 1, silica glass experiences only positive Δn under investigated energy range while in K8 glass Δn is positive for small input pulse energies (~130 nJ), and dramatically drops to negative values with energy increase. It is important to note that tracks written with high energy and low scanning speed in silica glass were disrupted similarly to “quill” writing described by Kazansky et al. [4]. These tracks are not presented on Fig. 1 due to impossibility of measuring their Δn .

The FWHM track widths are equal to 0.88 μm (128 nJ) and 0.98 μm (215 nJ) for K8, while for silica glass the values are 0.7 μm (172 nJ) and 0.75 μm (210 nJ). Maximum magnitude of the refractive index change is $3 \cdot 10^{-3}$ and $1 \cdot 10^{-3}$ for K8 and silica glass, correspondingly.

This prompts the conclusion that both investigated glasses are suited for submicrometer-scale micromachining; together, they can cover a wide range of applications due to different sign of the refractive index change.

- [1] Davis, K. Miura, et al. "Writing waveguides in glass with a femtosecond laser." *Optics letters* 21.21 (1996): 1729-1731.
 [2] Chen, George Y., et al. "Femtosecond-laser-written microstructured waveguides in BK7 glass." *Scientific reports* 8.1 (2018): 1-7.
 [3] Streltsov, Alexander M., and Nicholas F. Borrelli. "Study of femtosecond-laser-written waveguides in glasses." *JOSA B* 19.10 (2002): 2496-2504.
 [4] Kazansky, Peter G., et al. "“Quill” writing with ultrashort light pulses in transparent materials." *Applied physics letters* 90.15 (2007): 151120.

LM-O-21

Investigation of Laser-Induced Formation of Polychrome Marks on Glass

A. Ramos Velazquez¹, N.O. Gudz¹, R.A. Zakoldaev¹, V.P. Veiko¹

1- ITMO University, Kronverksky Pr. 49, bldg. A, St. Petersburg, 197101, Russia

Main author email address: alejandraramosv@itmo.ru

The development and improvement of laser-induced transfer technologies (e.g. LIFT [1]) is needed to support the trend of labeling glass products. First of all, such technologies are industrially attractive as they are implemented on industrial fiber laser systems and are easily integrated into the technological process. The core of the marking process is based on the fact that laser radiation passes through the optical workpiece and is absorbed on the target. Intense absorption causes the target ablation and target particles doping on the glass surface layer [2]. In this case the composition of the evaporated particles and ablation conditions directly affect the mark properties - color, adhesion, stress. Undoubtedly, the industry requires a wide color palette formed, which is important for a higher storage density, protection against counterfeiting, and for creating attractive labels. Currently, such technologies have entrenched the possibility of forming one color in connection with the use of one-component targets. Therefore, in this work, we decided to expand the color palette of applied amplitude marks to 3-4 colors and study the processes associated with the colors formation.

Here, we have demonstrated polychrome marks with high visibility shades on the glass by laser-induced transfer of brass target (Figure, a). Ytterbium fiber laser system ($\lambda=1064\text{nm}$, $\tau=2\text{-}200\text{ns}$, $f=2\text{-}1000\text{kHz}$) was employed for laser processing. The influence of laser parameters such as pulses overlapping, fluence, pulse duration on the mark properties were determined. As a result, yellow, red, green, brown and grey marks were obtained on the back side of the glass plate (Figure, b). Colorimetry properties were investigated in the visible range and corresponding SEM/EDX investigation were accomplished.

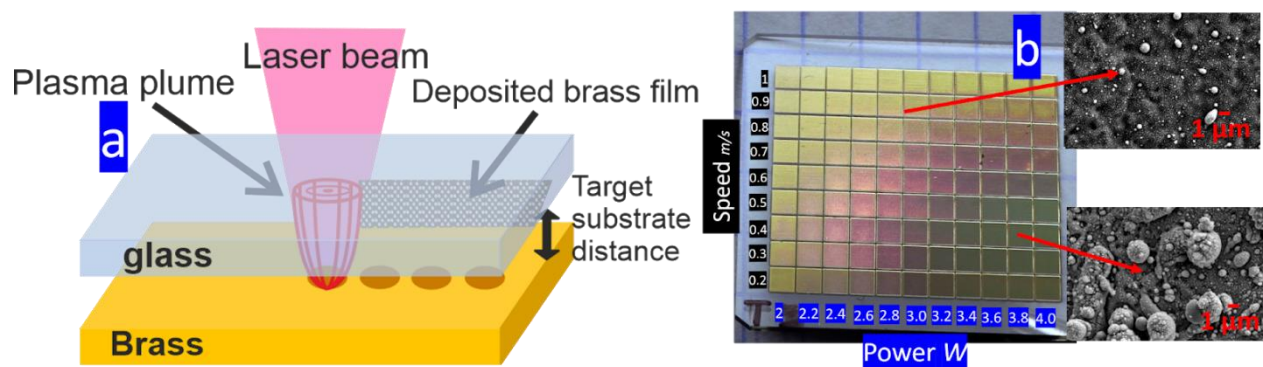


Figure 1. a) Schematic illustration of experimental procedure, b) investigation results - photo and SEM of the back-side.

Acknowledgment The reported study was financially supported by the Ministry of Science and Higher Education of the Russian Federation research agreement No. 075-11-2019-066 of 22.11.2019, project title "Development of high-tech production of equipment and technologies for laser coding of transported goods and their optical identification for the implementation in modern material flow management systems" (within the framework of decree of the Government of the Russian Federation No. 218 of 09/04/2010)

H Yamada, T Sano, T Nakayama, I Miyamoto, Optimization of laser-induced forward transfer process of metal thin films, *Applied Surface Science*, Vol. 197–198, pp 411–415 (2002)

James Macdonald, Henry de Fossard, Nadeem Gabbani, William O'Neill, Ronan Daly, Material ejection dynamics in direct-writing of low resistivity tracks by laser-induced reverse transfer, *Applied Surface Science*, Vol. 536, 2021,

LM-O-22

Laser-Induced Crystallization Kinetics of GeTe and Ge₂Sb₂Te₅ Thin Films

A.A. Burtsev, V.V. Ionin, A.V. Kiselev, N.N. Eliseev, V.A. Mikhalevsky, and A.A. Lotin

ILIT RAS — Branch of FSRC “Crystallography and Photonics” RAS, 140700, Shatura, Svyatoozerskaya Str., 1, Moscow Region, Russia

Main author email address: tonyiplit@gmail.com

Thin film chalcogenide materials based on germanium telluride (GeTe, Ge₂Sb₂Te₅) are widely used in photonic and optoelectronic devices [1]. These alloys have very high amorphization and crystallization rates in the order of nanoseconds which, combined with large cyclability and a pronounced property contrast between the crystalline and amorphous phases [2]. In this study researching of the crystallization process of chalcogenide (GeTe and Ge₂Sb₂Te₅) thin films (100 nm), deposited by vacuum thermal sputtering, is presented. The researching includes in situ optical parameters measurement and X-ray diffractometry (XRD). Phase transitions in films were induced by nanosecond pulsed laser radiation with «top hat» intensity distribution [3,4]. The threshold fluences to induce crystallization are determined for both materials. Structural information was characterized by XRD. The progress of the phase transition can be monitored using the increase in reflectance upon crystallization and analyzed using the Johnson–Mehl–Avrami–Kolmogorov model [5]. Results demonstrate different transition mechanism: one-step crystallization for GeTe [6] and two-step crystallization for Ge₂Sb₂Te₅ [7].

- [1] K.V. Sreekanth, M. ElKabbash, V. Caligiuri, R. Singh, A. De Luca, G. Strangi. *New Directions in Thin Film Nanophotonics*, ch. 3 (2019).
- [2] P. Guo, A. M. Sarangan and I. Agha. *A Review of Germanium-Antimony-Telluride Phase Change Materials for Non-Volatile Memories and Optical Modulators*. *Applied Sciences*, 9, 3, 530 (2019).
- [3] V. V. Ionin, A. V. Kiselev, N. N. Eliseev, V. A. Mikhalevsky, M. A. Pankov, A. A. Lotin, *Multi-level reversible laser-induced phase transitions in GeTe thin films*. *Applied Physics Letters*, 117, 011901 (2020).
- [4] N.N. Eliseev, A.V. Kiselev, V.V. Ionin, V.A. Mikhalevsky, A.A. Burtsev, M.A. Pankov, D.N. Karimov, A.A. Lotin. *Wide range optical and electrical contrast modulation by laser-induced phase transitions in GeTe thin films*. *Results in Physics*, 19, 10346 (2020).
- [5] V. Weidenhof, I. Friedrich, S. Ziegler, and M. Wuttig. *Laser induced crystallization of amorphous Ge₂Sb₂Te₅ films*. *Journal of Applied Physics*, 89, pp. 3168-3176 (2001).
- [6] Q. M. Lu, M. Libera. *Microstructural measurements of amorphous GeTe crystallization by hot-stage optical microscopy*. *Journal of Applied Physics*, 77, pp. 517-521 (1995).
- [7] I. Yang, K. Do, H.-J. Chang, D.-H. Ko, and H. Sohn. *Effect of Doped Nitrogen on the Crystallization Behaviors of Ge₂Sb₂Te₅*. *Journal of The Electrochemical Society*, 157, 4, H483-H486 (2010).

LM-O-23

Morphological and phase modifications of amorphous $\text{Ge}_2\text{Sb}_2\text{Te}_5$ thin films on dielectric substrate induced by femtosecond laser irradiation

A.V. Kolchin¹, S.V. Zaboltnov¹, D.V. Orlov¹, D.V. Shuleiko¹, L.A. Golovan¹, D.E. Presnov¹, T.P. Kamenskaya¹, P.I. Lazarenko², T.S. Kunkel³, S.A. Kozyukhin⁴, P.K. Kashkarov^{1,5}

1-M.V. Lomonosov Moscow State University, Moscow, Russia

2-National Research University of Electronic Technology Zelenograd, Russia

3-Moscow Institute of Physics and Technology, Dolgoprudny, Russia

4-N.S. Kurnakov Institute of General and Inorganic Chemistry, Moscow, Russia

5-National Research Center «Kurchatov Institute», Moscow, Russia

avkolchin@physics.msu.ru

Chalcogenide quasi-binary alloys such as $\text{Ge}_2\text{Sb}_2\text{Te}_5$ (GST225) are represented as a basic material for non-volatile and rewritable memory applications, as well as reconfigurable nanophotonical devices [1]. Femtosecond laser irradiation of amorphous GST225 thin films on conductive substrates possess both reversible phase switching and for mation of surface gratings with wavelength period [2]. However, similar investigations haven't been provided with such samples on dielectric substrates. It is necessary to demonstrate easy integration of formed ripples to all-dielectric nanophotonical devices.

Amorphous GST225 thin films with thicknesses 130 nm were deposited by magnetron sputtering on oxidized silicon substrate. The samples were subsequently treated by femtosecond laser pulses (1250 nm, 135 fs, 10 Hz, 0.1 J/cm²) at the scanning mode (laser pulses per spot N_s from 3 to 750).

Scanning electron (SEM) and atomic-force microscopies (AFM) techniques revealed formation of so-called laser-induced periodic surface structures (LIPSS) since $N_s=150$. The observed grain ridges are ordered with period 1200-1300 nm and directed orthogonally to the incident laser polarization. Such structural properties may emerge surface plasmon-polariton excitation during intensive photoinduction of free charge carriers [3]. Sipe-Drude theory simulations confirm this hypothesis [4]. In turn, wide broadband from 110 to 180 cm⁻¹ at the Raman spectra show amorphous structure of initial samples. The line 125 cm⁻¹ increases with the pulse number growth from $N_s=3$ to $N_s=15$. It indicates driven transition to metastable face-centered cubic (fcc) crystalline phase [5]. For the greater N_s (from 30 to 750) values the line 125 cm⁻¹ decreases. Such behavior may correspond to possible re-amorphization [2].

The research was supported by RFBR (grant № 20-32-90111).

[1] P. Guo, A.M. Sarangan, «A Review of Germanium-Antimony-Telluride Phase Change Materials for Non-Volatile Memories and Optical Modulators», Appl. Sci., vol. 9(3), pp. 530-556, 2019.

[2] S. Kozyukhin, M. Smayev, V. Sigaev, «Specific Features of Formation of Laser -Induced Periodic Surface Structures on $\text{Ge}_2\text{Sb}_2\text{Te}_5$ Amorphous Thin Films under Illumination by Femtosecond Laser Pulses», Phys. Stat. Sol. (B), vol. 257(11), pp. 1900617-1-7, 2020.

[3] V. Emel'yanov, E. Zemskov, V. Seminogov, «Theory of the formation of "normal" and "anomalous" gratings on the surfaces of absorbing condensed media exposed to laser radiation», Sov. J. Quantum Electron., vol. 14(11), pp. 1515-1521, 1984.

[4] J. Bonse, A. Rosenfeld, J. Krüger, «On the role of surface plasmon polaritons in the formation of laser-induced periodic surface structures upon irradiation of silicon by femtosecond-laser pulses», J. Appl. Phys., vol. 106(10), pp. 104910-1-5, 2009.

[5] P. Nemeč, V. Nazabal, A. Moreac, «Amorphous and crystallized $\text{Ge}_2\text{Sb}_2\text{Te}_5$ thin films deposited by pulsed laser: Local structure using Raman scattering spectroscopy», Mater. Chem. Phys., vol. 136, pp. 935-941, 2021.

BIOPHOTONICS

B-I-1

Surface-Enhanced Raman Scattering from Au Nanorods as a Function of their Aspect Ratio and Morphology: the Fourth-Power Law Revisited

N. G. Khlebtsov

*Institute of Biochemistry and Physiology of Plants and Microorganisms,
Russian Academy of Sciences, Saratov, Russia
E-mail: khlebtsov@ibppm.ru*

The on-resonance excitation of plasmonic nanoparticles is assumed to be necessary for increasing the Raman signal intensity of nearby molecules [1]. Still, there remain some gaps in the current understanding of the interplay between the near-field (SERS) and the far-field optical response. Indeed, the SERS EF scales like the fourth power of the local field [2]. However, the existing experimental data for Au nanorods (AuNRs) do not confirm such theoretical predictions. Most previous studies have used samples of AuNRs with different diameters, particle concentrations, amounts of impurities, and probably some variations in the nanorod shape. Here, we discuss a reexamination study [3] using a well-defined experimental model. We used the controllable etching method to prepare a set of AuNR samples of equal number concentrations by keeping the AuNR width and shape morphology. At the same time, the plasmon resonance was incrementally decreased from 925 to 650 nm through the finely tuned aspect ratio. The AuNRs were functionalized with 1,4-nitrobenzenethiol (NBT), and SERS spectra of the colloids were measured under 785-nm laser excitation. The nanorod concentration was quantified by atomic absorption spectroscopy and spectrophotometry combined with TEM statistical data and T-matrix simulations. The number of adsorbed NBT molecules per one nanorod ($\sim 10^4$) corresponded to the effective footprint ~ 0.55 nm² and was close to the monolayer packing density with the topological polar surface area of NBT 0.468 nm². SERS spectra of colloids and drop samples were measured under 785-nm laser excitation with a fiber-optic spectrometer and a Renishaw inVia Raman microscope. For PR wavelengths between 800 nm and 900 nm, both simulated and experimental EFs show minimal variations and are in reasonable agreement. However, for PR wavelengths between 650 nm and 785 nm, electromagnetic simulations still predict substantial variations in the SERS intensity within one order of magnitude, in stark contrast to the experimental EFs. By contrast to weak plasmonic dependence of SERS signals from the aspect ratio of AuNRs, minor variations in shape morphology lead to notable changes in SERS response. Specifically, when the initial AuNRs were further overgrown to have dumbbell morphology, their SERS intensity increased fivefold. Thus the rational design of the nanoparticle shape morphology is a more critical factor towards the highest SERS response compared to the tuning of the plasmonic peak for on-resonance excitation. This research was supported by the Russian Scientific Foundation (project no. 18-14-00016-II).

[1] N. Pazos-Perez, L. Guerrini, R. A. Alvarez-Puebla, Plasmon tunability of gold nanostars at the tip apices, ACS Omega, 3, 17173-17179 (2018).

[2] E. C. Le Ru, P. G. Etchegoin. Principles of Surface Enhanced Raman Spectroscopy and Related Plasmonic Effects, Elsevier (2009)

[3] B. Khlebtsov, V. Khanadeev, A. Burov, E. Le Ru, N. Khlebtsov, Reexamination of surface-enhanced Raman scattering from gold nanorods as a function of aspect ratio and shape, J. Phys. Chem. C. 124, 10647-10658 (2020).

B-I-2

Nanoparticles fabricated by laser ablation and fragmentation of nano- and microstructured silicon: perspectives in biophotonics applications

S.V. Zobotnov¹, L.A. Golovan¹, D.A. Kurakina², A.V. Khilov^{2,1}, E.A. Sergeeva^{2,1}, D.V. Shuleiko¹, O.I. Sokolovskaya¹, V.Yu. Nesterov¹, D. E. Presnov¹, P.K. Kashkarov¹, P.D. Agrba³, M.Yu. Kirillin²

1- Lomonosov Moscow State University, Faculty of Physics, 1/2 Leninskie Gory, Moscow, 119991, Russia

2- Institute of Applied Physics RAS, 46 Uljanov street, Nizhny Novgorod, 603950, Russia

3- Lobachevsky State University of Nizhny Novgorod, 23 Gagarin avenue, Nizhny Novgorod, 603950, Russia

Email: zobotnov@physics.msu.ru

Pulsed laser ablation in liquids (PLAL) is a convenient technique to fabricate nanoparticles with desirable size, physical and chemical properties [1,2]. Silicon nanoparticles (Si-NPs) produced employing this approach are promising in biophotonics [3–5] due to their biocompatibility and biodegradability. However, high-yield production of Si-NPs is quite time-consuming and requires employment of a high-power laser with significant pulse repetition rate. To enhance the efficiency of Si-NPs fabrication, we suggest using preliminary nano- or microstructured silicon instead of traditionally used crystalline silicon targets.

In our work we employed porous silicon films, silicon nanowires arrays and mechanically grinded silicon microparticles as targets for picosecond (1064 nm, 34 ps, 10Hz) and femtosecond (1250 nm, 160 fs, 10Hz) PLAL. Measurements of the ablation thresholds for the porous silicon and silicon nanowires targets in water and ethanol revealed that the thresholds to be several times smaller as compared to those for crystalline silicon and high-yield Si-NPs output is provided. Similar behavior was revealed for laser fragmentation of the silicon microparticles in these liquids.

Scanning electron microscopy and dynamic light scattering studies demonstrated that the mean Si-NPs sizes are in the range of 24–340 nm depending on the used target, buffer liquid, laser pulse duration and irradiation time. Raman spectroscopy data analysis revealed almost perfect crystallinity of the formed Si-NPs in the cases of silicon nanowires PLAL and laser fragmentation of the silicon microparticles.

The studied Si-NPs emit fluorescence in the range of 600–900 nm most likely caused by internal defects [4]. Fluorescence in this range indicates the prospects of the nanoparticles as fluorescence markers in optical bioimaging. Spectrophotometry measurements of the Si-NPs suspensions revealed their effective scattering in the spectral range of 400–1000 nm confirmed by Mie theory estimations. Optical coherence tomography imaging of the suspensions drops administered on agar gel surfaces indicated high efficiency of the Si-NPs as contrast agents providing the contrast up to 30 dB. Heating of tumor tissue with embedded nanoparticles using a laser beam was numerically modelled using real optical properties of nanoparticles suspensions in order to analyze Si-NPs efficiency for tumor hyperthermia [5]. The simulations indicate that embedding Si-NPs into a tumor results in increase of the heating maximum for up to 4°C in comparison with the same heating the tumor without nanoparticles.

Comparative analysis of the obtained results allowed to conclude on high potential of the Si-NPs fabricated via PLAL either in fluorescence and scattering bioimaging or in photohyperthermia.

This work was supported by the Russian Science Foundation (project № 19-12-00192).

[1] D. Zhang, B. Gökce and S. Barcikowski, *Chem. Rev.*, 117, 3990-4103, (2017).

[2] S. Besner, M. Meunier, *Laser precision microfabrication* (Springer), Laser synthesis of nanomaterials, (2010).

[3] A. Al-Kattan, Yu.V. Ryabchikov, T. Baati, et al., *J. Mater. Chem. B*, 4, 7852-7858 (2016).

[4] S.V. Zobotnov, A.V. Skobelkina, E.A. Sergeeva, et al., *Sensors*, 20, 4874 (2020).

[5] O.I. Sokolovskaya, S.V. Zobotnov, L.A. Golovan, et al., *Quantum Electron.*, 51(1), 64-72 (2021).

B-I-3

Laser-based techniques for verification of nanomaterials safety from microrheologic viewpoint

**A.E. Lugovtsov¹, A.I. Neznanov¹, A.A. Kapkov¹, I.M. Kadanova¹,
E.V. Perevedentseva², C.-L. Cheng², A.V. Priezzhev¹**

1 - Department of Physics, Lomonosov Moscow State University, Leninskiye Gory, 1-2, Moscow, 119991, Russia

2 - Department of Physics, National Dong Hwa University, Da Hsueh Rd., 1-2, Hualien, 974301, Taiwan

anlug@biomedphotonics.ru

Laser diffractometry, diffuse light scattering aggregometry, and fluorescence microscopy, as well as optical trapping were used to study various aspects of the interaction of nanoparticles (NP) perspective for medical applications, with rat and human red blood cells (RBC). In particular, we studied fullerenes, magnetic and non-magnetic nanodiamonds (ND), iron oxide Fe₂O₃, TiO₂, Si nanoparticles and others. Special attention was paid to the effect of NP on the mechanical and microrheological properties of RBC and on their safety for biomedical applications [1, 2]. It is expected that the results of the study of the interaction of the NP with RBC and other blood cells *in vitro* can provide a basis for determining their cytotoxicity without conducting experiments with animals *in vivo*. This test will significantly reduce the need for experiments with animals when studying the effect of NPs on the human organism. All experimental results were obtained by laser based techniques [3] on human and rat blood samples incubated with NP of different sizes and surface functionalization in different concentrations for *in vitro* and *in vivo* conditions.

It was shown that incubation of RBCs with NP at high concentrations of the latter does provoke decreasing of deformability of the cells, the effect being dependent on the particles concentration, size, and surface functionalization. The alterations in RBC ability to deform are more significant for higher NP concentrations and more pronounced for non-functionalized particles. The effect of nanomaterials on RBCs aggregation is ambiguous. Experiments conducted *in vitro* allow us to conclude that the iron oxide nanoparticles and fullerenes reduce the RBC aggregation, while the addition of ND enhance the aggregation of cells. These effects strongly depend on the concentration and slightly depend on surface functionalization with porphyrin and carboxylate groups of iron oxide NP and ND accordingly.

To further investigate the interaction between the NPs and RBCs, namely, to study sorption onto the membrane and cellular penetration, we performed experiments using the fluorescence laser confocal microscopy. Basing on our experimental results we can conclude that it is not possible to make a general conclusion about the effect of the nanoparticles on the rheological properties of RBC. However, under certain conditions, this effect can be very significant and it is necessary to check the hemocompatibility of each sample of nanoparticles *in vitro*. Also, we can conclude that the NP can be administered into the blood in ambient conditions at low concentrations (not higher than 30 µg/ml), without significant complications of the blood rheological properties.

The work was financially supported by the Russian Science Foundation grant No. 20-45-08004.

[1] Lin Y.C. et al., The influence of nanodiamond on the oxygenation states and micro rheological properties of human red blood cells *in vitro*, *Journal of Biomedical Optics*, 17(10), pp. 101512, (2012).

[2] Tsai L.-W. et al., Nanodiamonds for medical applications: Interaction with blood *in vitro* and *in vivo*, *International Journal of Molecular Sciences*, 17(7), pp. 111, (2016).

[3] Lugovtsov A. E. et al., Optical assessment of alterations of microrheologic and microcirculation parameters in cardiovascular diseases, *Biomedical Optics Express*, 10(8), pp. 3974–3986, (2019).

B-I-4

Tunable self-assembly in colloidal materials: Designing structures and properties with external fields

**Pavel A. Libet¹, Ivan V. Simkin¹, Sofia A. Korsakova¹, Kirill A. Komarov¹,
Egor V. Yakovlev¹, Nikita P. Kryuchkov¹, and Stanislav O. Yurchenko^{*1}**

¹*Bauman Moscow State Technical University, 2nd Baumanskaya str. 5,
105005 Moscow, Russia, *e-mail: st.yurchenko@mail.ru*

Tunable interactions in colloidal suspensions attract great interest because of their fundamental and practical significance. Self-assembly in suspensions of micro- and nanoparticles is a common phenomenon in nature, opening a way to create new materials for photonics, catalysis, and biomedical applications. Apart from practical interest, colloidal systems are of great importance for fundamental studies, since they mimic molecular behavior and can be used in particle-resolved studies of generic phenomena in condensed matter and active soft matter.

In this work, we present our results of theoretical and experimental studies of two-dimensional colloidal systems wherein the tunable interparticle interactions are induced and controlled by external rotating electric and magnetic fields [1-7]. By placing colloidal systems in rapidly rotating external electric or magnetic fields, we can effectively induce tunable interparticle many-body long-range interactions. Magnitude of the interactions is controlled by electric field and evolution of the system can be imaged using video-microscopy, that opens a way for detailed studies of such fundamental phenomena as self-assembly, condensation and evaporation, melting and crystallisation, spinodal decomposition, dislocation dynamics, nucleation and coalescence.

In this presentation, we consider briefly (i) experimental technology for particle-resolved studies of colloidal suspensions in rotating electric and magnetic fields [1-2]; (ii) results of interaction analysis [3, 6, 7]; (iii) phase diagram and pair correlations in crystals of monodisperse particles in external fields [4, 5]; (iv) tunable self-assembly in polydisperse systems; and (v) design of the interactions with internal structure of particles and spectral hodographs of external field rotation.

The results open fascinating prospects for engineering the structures with given properties using external electric and magnetic fields, spatial hodographs of their rotation, and composite internal structures. All these should be of interest in soft matter, physical chemistry, chemical physics, photonics, and materials science.

The results are supported by Russian Science Foundation Grant #17-19-01691.

[1] E.V. Yakovlev, K.A. Komarov, K.I. Zaytsev, N.P. Kryuchkov, K.I. Koshelev, A.K. Zotov, D.A. Shelestov, V.L. Tolstoguzov, V.N. Kurlov, A.V. Ivlev, S.O. Yurchenko, Tunable two-dimensional assembly of colloidal particles in rotating electric fields, *Scientific Reports*, 96, 043201 (2017).

[2] P.V. Ovcharov, N.P. Kryuchkov, K.I. Zaytsev, S.O. Yurchenko, Particle-resolved phase identification in two-dimensional condensable systems, *Journal of Physical Chemistry C*, 121, 26860-26868 (2017).

[3] K.A. Komarov, N.P. Kryuchkov, S.O. Yurchenko, Tunable interactions between particles in conically rotating electric fields, *Soft Matter*, 14, 9657-9674 (2018).

[4] N.P. Kryuchkov, F. Smalenburg, A.V. Ivlev, S.O. Yurchenko, H. Löwen, Phase diagram of two-dimensional colloids with Yukawa repulsion and dipolar attraction, *Journal of Chemical Physics*, 150 104903 (2019).

[5] E.V. Yakovlev, M. Chaudhuri, N.P. Kryuchkov, P.V. Ovcharov, A.V. Sapelkin, S.O. Yurchenko. Experimental validation of interpolation method for pair correlations in model crystals, *The Journal of Chemical Physics* 151, 114502 (2019).

[6] K.A. Komarov, A.V. Yarkov, S.O. Yurchenko. Diagrammatic method for tunable interactions in colloidal suspensions in rotating electric or magnetic fields, *The Journal of Chemical Physics*, 151, 244103 (2019).

[7] K.A. Komarov, S.O. Yurchenko. Colloids in rotating electric and magnetic fields: designing tunable interactions with spatial field hodographs, *Soft Matter*, 16, 8155-8168 (2020).

B-I-5

Direct in situ observation of nanoparticles in turbid colloidal solution

P.A. Demina^{1,2}, A. Kostyuk³, Y. Lu⁴, E.A. Sergeeva³, E.V. Khaydukov^{2,5}, A.V. Ivanov⁵, A.V. Zvyagin^{1,4,5}

¹ M.M. Shemyakin, Yu.A. Ovchinnikov Institute of Bioorganic Chemistry of the Russian Academy of Sciences

² Federal Scientific Research Center «Crystallography and Photonics» Russian Academy of Sciences

³ Institute of Applied Physics of the Russian Academy of Sciences, Nizhny Novgorod

⁴ Macquarie University, Sydney, Australia

⁵ Sechenov University, Moscow, Russia

Email: andrei.zvyagin@mq.edu.au

Direct observation of the composition and processes in biological fluids is often eclipsed by the fluid optical turbidity. Protein corona (PC) formation is an example of the process that requires *in situ* direct measurement of the particle-PC size distribution, aggregation state and kinetics. To address the need for direct *in situ* observation of photoluminescent particles in turbid colloidal solutions we developed an advanced fluorescence correlation spectroscopy technique with improved spatial and temporal resolutions termed short-interval correlation spectroscopy (SICS). The super-resolution in spatial domain was achieved by utilising the high-order nonlinear properties of core-shell upconversion nanoparticles of the composition NaYF₄:Yb³⁺@Tm³⁺/NaYF₄ heavily (8%) co-doped with thulium ions (8T-UCNP). The improved temporal resolution was achieved by sampling 8T-UCNP signals in short millisecond-scale intervals afforded by high brightness of 8T-UCNP photoluminescence. SICS appeared uniquely suitable for acquisition of the size distribution and kinetics of 8T-UCNP-PCs *in situ* in serum solutions. SICS enabled to unveil propensity of polymer-coated 8T-UCNP-PCs to heavily aggregate in solutions of serum proteins (human serum albumin, bovine serum albumin, transferrin, and foetal bovine serum) at the concentration of ~90 protein molecules per a 25-nm 8T-UCNP. These results were corroborated by super-resolution multiphoton microscopy and cryogenic transmission electron microscopy of 8T-UCNP-PC colloidal samples. We believe that the reported short-interval correlation spectroscopy provides new opportunities for direct observations in turbid media, including biological fluids and tissues.

This work was supported by the Ministry of Science and Higher Education of the Russian Federation, grant no. 075-15-2019-1927.

B-I-6

Macroscopic Time- and Spectrally Resolved Fluorescence Imaging

V. Shcheslavskiy^{1,2}, M. Shirmanova², J. Lagarto^{3,4}, D. Yuzhakova², A. Mozherov², F.S. Pavone^{3,4,5}, R. Cicchi^{3,4} and W. Becker¹

1-Becker&Hickl GmbH, Nunsdorfer Ring 7-9, 12277 Berlin, Germany

2-Privolzhskiy Research Medical University, Minin and Pozharsky Sq. 10/1, 603005 Nizhny Novgorod, Russia

3-1National Institute of Optics, National Research Council (INO-CNR), Via Nello Carrara 1, 50019, Sesto Fiorentino, Italy

4-European Laboratory for Non-linear Spectroscopy (LENS), Via Nello Carrara 1, 50019, Sesto Fiorentino, Italy

5-Department of Physics, University of Florence, Via G. Sansone 1, 50019, Sesto Fiorentino, Italy

vis@becker-hickl.de

Fluorescence lifetime imaging (FLIM) and optical spectroscopy techniques, such as fluorescence time-resolved spectroscopy and Raman spectroscopy are increasingly recognized as a valuable approach for its ability not only to assess structural information, but also to interrogate certain biochemical processes in living organisms and provide information on their functional characteristics [1,2]. In particular, multimodal approaches can enhance the specificity of optical measurements to deliver complimentary and multidimensional information from tissues, and, therefore, there has been much investigation in recent years focusing on increasing the practicality and versatility of multimodal instruments.

Usually FLIM is associated with Fluorescence Lifetime Imaging Microscopy. Consequently, it is often believed that FLIM can only be obtained from microscopic objects. In general, this is not true: FLIM can be combined with any optical technique that scans the sample with a focused beam of light. Centimeter sized objects can be scanned by placing them directly in the image plane of a confocal scan head. Here, we describe a macroscopic confocal laser scanning FLIM system applied for the whole tumor imaging. By placing a dispersive element between the macroscopic scanner and array of the detectors one can realize a macroscopic spectrally resolved FLIM. This arrangement provides an important opportunity not available in the conventional systems using bandpass filters: simultaneous observations of multiple fluorophores. We integrate a 16 channel spectral detector working in the single photon counting mode in the confocal macros scanner and demonstrate the capability of the system on the dispersed on the dish cells labelled with different fluorophores.

Finally, we report the development of a novel fiber-based system to realize co-registered simultaneous acquisition of fluorescence lifetime data and Raman spectra from the same area. Fluorescence lifetime measurements by means of time-correlated single photon counting are realized with periodic out-of-phase external illumination of the field of view, enabling acquisition of data under bright illumination of the specimen. Raman measurements in the near-infrared are realized asynchronously. We present a detailed characterization of this technique and validate its potential to report intrinsic contrast. Fiber-based fluorescence lifetime and Raman maps report complementary structural, compositional and molecular contrast in biological tissues with diverse compositional features.

The work related to spectral FLIM was supported by RSF, contract 20-65-46018.

[1] V.I. Shcheslavskiy, M.V. Shirmanova, A. Jelzow, and W. Becker, Multiparametric time-correlated single photon counting luminescence microscopy, *Biochemistry (Mosc)* 84, S51-S68 (2019).

[2] K. Suhling, L.M. Hirvonen, J. Levitt, P.-H. Chung, C. Tredigo, A. Marois et al, *Advanced Time-correlated single photon counting applications (Springer)*, Chapter 3 (2015).

B-I-7

Photophysics of fluorophores responsible for NIR fluorescence of biotissues

E. Shirshin, B. Yakimov

M.V. Lomonosov Moscow State University, 11991, Leninskie gory 1/62, Moscow, Russia

shirshin@lid.phys.msu.ru

Here we discuss the origin and photophysics of fluorophores responsible for NIR fluorescence in biotissues. Despite significant differences in molecular composition, the optical properties of these fluorophores are remarkably similar, and the reason for this remains largely unknown. We employed fluorescence spectroscopy with (sub)picosecond resolution to elucidate the role of electronic interactions within heterogeneous systems of fluorophores, which form as a result of oxidation processes in living organisms. We revealed an ultrafast decay component with characteristic decay lifetime of 0.5–1.5 ps and spectral diffusion originating from excitation energy transfer (EET) in the system. The rate of EET was positively correlated to the fraction of aromatic species and tightness of aromatic species packing. Diminishing the number of EET donor acceptor pairs resulted in a lower impact of the ultrafast component to fluorescence decay. Our results uncover the role of electronic coupling among fluorophores responsible for NIR optical properties formation in biosystems and provide a framework for studying photophysical processes in heterogeneous systems of natural fluorophores.

B-I-8

Multiparametric FLIM for cancer study using endogenous fluorescence and genetically encoded sensors

M. Shirmanova¹, A. Gavrina¹, A. Polozova¹, L. Shimolina¹, I. Druzhkova¹, N. Ignatova¹, V. Dudenkova¹, M. Lukina¹, V. Shcheslavskiy^{1,2}, K. Lukyanov³, V. Belousov⁴, E. Zagaynova^{1,5}

1-Privolzhsky Research Medical University, Nizhny Novgorod, Russia

2-Becker & Hickl GmbH, Berlin, Germany

3-Skolkovo Institute of Science and Technology, Moscow, Russia

4-Pirogov Russian National Research Medical University, Moscow, Russia

5-Lobachevsky State University of Nizhny Novgorod, Nizhny Novgorod, Russia

Shirmanovam@gmail.com

Nowadays, fluorescent proteins, the majority of which belong to the GFP family, represent an indispensable instrument for cancer research. A significant progress has been made in the development of genetically encoded fluorescence lifetime-based sensors that enable long-term, quantitative assessments of various parameters inside living cells using fluorescence lifetime imaging (FLIM) techniques. In addition, one of the most useful applications of FLIM is probing of cellular metabolism using endogenous fluorescence from the reduced nicotinamide adenine dinucleotide (phosphate) NAD(P)H and oxidized flavin adenine dinucleotide FAD. NAD(P)H and FAD act as electron carriers in a number of biochemical reactions and their fluorescence lifetimes are largely determined by protein binding. Unlike fluorescence intensity, fluorescence lifetime allows to overcome difficulties associated with an unknown and/or unstable fluorophore concentration, photobleaching, instrument configurations, absorption and scattering events [1].

In our work, we have developed methodologies for multiparametric imaging of cancer cells and tumors using simultaneous detection of endogenous fluorescence in the blue spectral range and far-red genetically encoded sensors.

To monitor non-invasively the cell cycle, genetically encoded indicator FUCCI-Red was used [2]. FUCCI-Red utilizes two red fluorescent proteins with different fluorescence lifetimes, mCherry and mKate2. These proteins carry cell cycle-dependent degradation motifs to resolve G1 and S/G2/M phases. The cell cycle was visualized in monolayer cell culture, tumor spheroids and animal tumors in vivo by FLIM-microscopy. To visualize apoptosis, the FRET (Förster Resonance Energy Transfer)-based sensor for caspase-3 activity, mKate2-DEVD-iRFP, was applied [3]. Caspase-3 activity was detected by measuring fluorescence lifetime of the donor protein mKate2. Due to the loss of energy transfer to the acceptor iRFP upon caspase-3 activation, fluorescence lifetime of the donor mKate2 increases. The execution of apoptosis was investigated in cultured cancer cells treated with different agents. Fluorescence lifetime-based mapping of cytosolic pH in cancer cells in vitro and tumor xenografts in vivo was performed using new SypHer-based genetically encoded sensor. Fluorescence lifetime of the sensor increases with increase of pH. pH measurements were done at the cellular level with FLIM-microscopy and at the level of a whole tumor with macroscopic FLIM.

The possibility of simultaneous imaging of the indicated parameters (cell cycle, apoptosis, pH) using the genetically encoded sensors and cellular metabolic state using fluorescence of metabolic cofactors was demonstrated in vitro and in vivo. In general, such multiparameter imaging improves our understanding of biological behavior of cancer cells.

The studies were supported by the Russian Science Foundation (project № 20-65-46018).

1. В. И. Щеславский, М. В. Ширманова, А. Ельцов и В. Беккер, Люминесцентная микроскопия на основе многопараметрического время-коррелированного счета фотонов, *Успехи биологической химии*, т. 59, с. 103–138 (2019).
2. Shirmanova, M.V., Gorbachev, D.A., Sarkisyan, K.S. et al. FUCCI-Red: a single-color cell cycle indicator for fluorescence lifetime imaging. *Cell. Mol. Life Sci.* (2021).
3. T.F. Sergeeva, M.V. Shirmanova, O.A. Zlobovskaya, et al., Relationship between intracellular pH, metabolic co-factors and caspase-3 activation in cancer cells during apoptosis. *BBA - Molecular Cell Research*, 1864(3): 604-611 (2017).

B-I-9

Complementary fluorescence and optoacoustic monitoring of treatment with novel photoactivatable agents for combined photodynamic and chemotherapy

**I. Turchin¹, M. Kirillin¹, A. Orlova¹, V. Perekatova¹, V. Plekhanov¹, E. Sergeeva¹, D. Kurakina¹,
A. Khilov¹, A. Kurnikov¹, P. Subochev¹, M. Shirmanova², A. Komarova², D. Yuzhakova²,
A. Gavrina², S. Bano³, S. Mallidi^{3,4}, T. Hasan³**

1 - Institute of Applied Physics RAS, 46 Uljanov Street, 603950, Nizhny Novgorod, Russia

2 - Privolzhsky Research Medical University, 10/1 Minin Square, 603005, Nizhny Novgorod, Russia

3 - Wellman Center for Photomedicine, Massachusetts General Hospital, Boston, MA 02114, USA

4 - Department of Biomedical Engineering, Tufts University, Medford, MA 02155, USA

Photodynamic therapy (PDT) is a therapeutic approach gaining wide recognition in clinical practice. It is based on irradiation of photoactive photosensitizers (PS) with light of a certain wavelength in the presence of oxygen in a tissue resulting in formation of cytotoxic reactive oxygen species [1]. Most of the modern studies aimed at improving the PDT efficiency are directed at development of novel photosensitizers, validation of new protocols of tumor irradiation, combination of PDT with other methods of anticancer treatment, and development of new methods of monitoring of tumor response to PDT. In this study we investigate the efficiency of complementary fluorescence (FL) and optoacoustic (OA) imaging monitoring approach to analyze *in vivo* both drug accumulation and its preservation in the blood flow and vascular response to treatment. The system for combined FL and OA imaging is described in general in [2]. It contains the raster-scan optoacoustic microscope at 532 nm wavelength with imaging depth up to 2 mm, axial/transverse resolution of 38/50 μm , and acquisition speed of 2000 A-scans per second. It enables to visualize the tumor vascular system development during natural growth, as well as under therapeutic effects. A newly developed approach has been applied to describe vasculature changes numerically by a specific vesselness index, associated with vessel density [3]. Wide-field FL imaging at 690 nm excitation wavelength was applied to control PS accumulation after drug administration, photobleaching during laser irradiation, and PS circulation after the procedure. For PDT combined cancer treatment we have engineered photoactivatable multi-inhibitor liposomes (PMILs) carrying a lipid-anchored derivative of the photosensitizer benzoporphyrin derivative (BPD) served as a PS in the bilayer (PALs) and topoisomerase I inhibitor (Irinotecan: IRI) served as a chemotherapy agent entrapped in the inner core of nanoliposomes L-[IRI]. This nanoconstructs are proposed for a cooperative enhancement of photodynamic and chemotherapeutic regimens. Our *in vivo* results on mice with CT26 tumor show that the PMILs demonstrate the best inhibitory effect on tumor growth compared to the treatment with monotherapies. When monitored by the complementary FL and OA imaging system, it appears that the largest increase in the vesselness index in tumors employing PMILs is in good agreement with the histological data. This shows that the strongest therapeutic effect manifested by the largest number of hemorrhage is in the PMILs treated mice as compared to PALs or L-[IRI] treated mice. We can conclude that the newly developed multimodal imaging system combining optoacoustic angiography and fluorescence emission of the photosensitizer allows for immediate response evaluation of post-treatment, suggesting that combined photodynamic and chemotherapy of tumors, employing PMILs is an efficient way to improve cancer therapeutic efficiency.

The study is supported by the RFBR project 17-54-33043 onko-a and the Center of Excellence «Center of Photonics» funded by The Ministry of Science and Higher Education of the Russian Federation, contract № 075-15-2020-906

[1] P. Agostinis, K. Berg, K. A. Cengel, T. H. Foster, A. W. Girotti, S. O. Gollnick, S. M. Hahn, M. R. Hamblin, A. Juzeniene, and D. Kessel, "Photodynamic therapy of cancer: an update," *CA: a cancer journal for clinicians* 61, 250-281 (2011).

[2] D. Kurakina, M. Kirillin, V. Perekatova, V. Plekhanov, A. Orlova, E. Sergeeva, A. Khilov, A. Nerush, P. Subochev, and S. Mallidi, "Towards Bimodal Optical Monitoring of Photodynamic Therapy with Targeted Nanoconstructs: A Phantom Study," *Applied Sciences* 9, 1918 (2019)

[3] V. Perekatova, M. Kirillin, P. Subochev, A. Kurnikov, A. Khilov, A. Orlova, D. Yuzhakova, and I. Turchin, "Quantification of microvasculature parameters based on optoacoustic angiography data," *Laser Physics Letters* (2021).

B-I-11

Applications of FLIM in regenerative medicine

A. Kashina¹, D. Kuznetsova^{1,2},
 A. Kashina¹, D. Kuznetsova^{1,2},
 A. Kashina¹, D. Kuznetsova^{1,2},
 V. Elagin^{1,7}, V. Dudenkova^{1,7}, S. Rodionova^{1,7}, N. Bobrov^{1,7}, A. Kashirina^{1,7}, E. Dashinimayev^{5,6,7}, E.
 V. Zagainov^{1,3}, V. Shcheslavskiy^{1,4}, N. Bobrov^{1,7}, A. Kashirina^{1,7}, E. Dashinimayev^{5,6,7},
 V. Zagainov^{1,3}, V. Shcheslavskiy^{1,4}, N. Bobrov^{1,7}, A. Kashirina^{1,7}, E. Dashinimayev^{5,6,7},
 V. Zagainov^{1,3}, V. Shcheslavskiy^{1,4}, E. Zagaynova^{1,2}

1-Privolzhsky Research Medical University, Nizhny Novgorod, Russia

2-Lobachevsky State University of Nizhny Novgorod, Russia

3-Privolzhsky Federal Medical Center, Nizhny Novgorod, Russia

4-Becker & Hickl GmbH, Berlin, Germany

5-Koltzov Institute of Developmental Biology, Russian Academy of Sciences, Moscow, Russia

6-Department of Regenerative Medicine, Research Institute of Translational Medicine, Pirogov Russian

National Research Medical University, Moscow, Russia

7-Department of Cell Biology and Histology, Faculty of Biology, Moscow State University, Moscow, Russia

Fluorescence lifetime imaging microscopy (FLIM), enabling live quantitative multiparametric analysis, is an emerging bioimaging approach in tissue engineering and regenerative medicine. FLIM in combination with the endogenous and exogenous fluorophores can monitor numerous processes in cells and tissues, including disease progression and drug efficacy. When combined with stem cell-derived 2D and 3D models, FLIM allows for tracing stem cells differentiation, stem cells niche, monitoring of the metabolic fluxes and plasma membrane viscosity changes, identifying disease phenotypes. FLIM-based on autofluorescence can be easily translated to in vivo monitoring in animal and human for effective clinical measurements of various pathologies and regeneration processes.

We used FLIM in combination with endogenous markers to study the metabolic status of 3D models based on cells differentiated from patient-specific induced pluripotent stem cells (iPSCs). We demonstrated that neurospheres with Down's syndrome (DS) are characterized by a more glycolytic phenotype than healthy ones. In addition, we report the use of viscosity-sensitive fluorophores based on a BODIPY core in combination with FLIM for monitoring of the plasma membrane viscosity changes in neurospheres. We revealed the increase of the membrane viscosity in neurospheres with DS relative to healthy neurospheres. Our results directly demonstrate that 3D models with DS have different viscosity properties of membranes, which reflect changes in the phenotype of pathological cells. The metabolic status and viscosity properties, assessed by FLIM, can be used as parameters for cells assessment in neurodegenerative diseases modeling.

There is a need for a rapid and safe method for the successful diagnosis of liver disease in order to plan surgery and to help avoid postoperative liver failure. We analyzed the structural and functional state of liver tissue in normal and pathological state and during regeneration by autofluorescence lifetime imaging in combination with the FLIM. The data can be used both to obtain new criteria for the identification of hepatic pathology and to develop a rapid technique for liver quality analysis in order to plan surgery and to help avoid postoperative liver failure in clinic. The problem of rapid assessment of the quality of pancreatic tissue and the number of viable and metabolically active islets without destroying the tissue structure and using exogenous dyes has not yet been resolved. In this study, based on FLIM and intracellular metabolite NAD(P)H was developed non-invasive and label-free method of the quality assessment of pancreatic islets in tissue and isolated islet cells.

Development of FLIM technologies, analysis, and applications will further advance biological research and clinical assessments.

The part of work on FLIM of iPSC-based 3D models has been financially supported by Russian Science Foundation (grant No. 14-17-01388). The part of work on FLIM analysis of liver was supported by Russian Science Foundation (grant No. 17-7520178). The part of work on FLIM analysis of liver was supported by Russian Science Foundation (grant No. 19-15-00263).

B-I-13

Probing Small Distances in Live Cell Microscopy

Herbert Schneckenburger¹, Verena Richter¹

1- Institute of Applied Research, Aalen University, Beethovenstr. 1, 73430 Aalen, Germany

E-Mail: herbert.schneckenburger@hs-aalen.de

Various methods of super-resolution microscopy for probing small distances in cells and tissues – including Single Molecule Localization Microscopy (SMLM), Stimulated Emission Depletion Microscopy (STED) and Structured Illumination Microscopy (SIM) – have been reported recently in the literature. However, several of these methods require high light exposure with a risk of phototoxicity to living cells and organisms. Therefore, we developed super-resolution methods, which are more tolerable to living cells, in particular SIM in combination with Total Internal reflection Fluorescence Microscopy (TIRFM) or SIM in combination with Axial Tomography. In addition, variable-angle TIRFM permitted measurements of cell membrane topology with nanometer resolution, e.g. for studies of cell growth or interaction with cytotoxic agents.

In addition, molecular parameters in the nanometer range can be deduced from spectral data, fluorescence lifetimes or non-radiative energy transfer (FRET) between a donor and an acceptor molecule. As an example, FRET between the epidermal growth factor receptor (EGFR) and the growth factor receptor-bound protein 2 (Grb2) is described. Since this interaction, as well as further processes of cellular signaling are sensitive to stimulation by pharmaceutical agents, methods (e.g. TIRFM) are transferred from a fluorescence microscope to a multi-well reader system for pharmacological tests and simultaneous detection of large cell populations.

Details and further information are reported in [1].

[1] V. Richter, P. Lanzerstorfer, J. Weghuber, H. Schneckenburger, Probing small distances in live cell imaging, *Photonics* 8(6), 176 (2021), <https://doi.org/10.3390/photonics8060176>.

B-I-14

The Fastest High-Resolution 3D Imaging of Sperm Cells during Free Swim

Natan T. Shaked

Department of Biomedical Engineering, Tel Aviv University, Israel.

Email: nshaked@tau.ac.il. Website: www.eng.tau.ac.il/~omni

I review our latest advances [1], presenting a new approach for dynamic three-dimensional (3D) sperm imaging without using cell staining. The selection of sperm cells possessing normal morphology and motility is crucial for intracytoplasmic sperm injection, a very common type of in vitro fertilization (IVF), in which a clinician chooses a single sperm cell using a micropipette and injects it into the female egg in a dish. Since stains cannot be used in human IVF, as they may damage sperm viability, clinicians examine sperm cells using imaging methods that only provide gross two-dimensional morphology, leading to a lack of consistency in sperm selection. Without staining, sperm cells are nearly transparent under bright-field microscopy. A contrast mechanism that can be used when imaging cells without staining is their refractive index, which can be recorded by tomographic phase microscopy in three dimensions. For tomography, the cell needs to be recorded from various angles. There are two approaches for obtaining these angular projections: rotating the entire sample and scanning the illumination. However, none of these approaches are fast enough for recording sperm cells during free swim. Even when using sperm staining in confocal fluorescence microscopy (which is not allowed in human IVF), it is very challenging to obtain the entire sperm head and tail 3D reconstruction during rapid free swim, due to the need to scan over time and the low amount of fluorescent emission in each temporal frame. In Ref. [1], we presented the first high-resolution tomographic phase microscopy method for acquisition of the entire sperm cell (head with organelles and tail) during free swim and without cell staining, in 2000 frames per second and spatial resolution of 0.5 micron. This method is based on the natural repetitive rotation of the sperm head during free swim, which gives access to its angular projections, and a novel set of reconstruction algorithms. By modeling the sperm head as an ellipsoid, we are able to predict the viewing angle based on the minor and major radii extracted from the segmented quantitative phase maps of the head. All off-axis holograms, experimentally acquired during the sperm free swim, are then processed into the complex-wavefront projections, which are positioned in the 3D Fourier spectrum, allowing reconstruction of the 3D refractive-index distribution of the sperm head through the optical diffraction tomography theory. The tail location in 3D is reconstructed from each frame, taking into consideration the fact that using off-axis holography we acquire the full complex wavefront, so that we can digitally refocus to various z planes for sparse objects like the sperm tail. See results in Fig. 1. The method has a great potential for revealing the mechanism that connects sperm movement, morphology and fertilization potential, thus increasing IVF success rates.

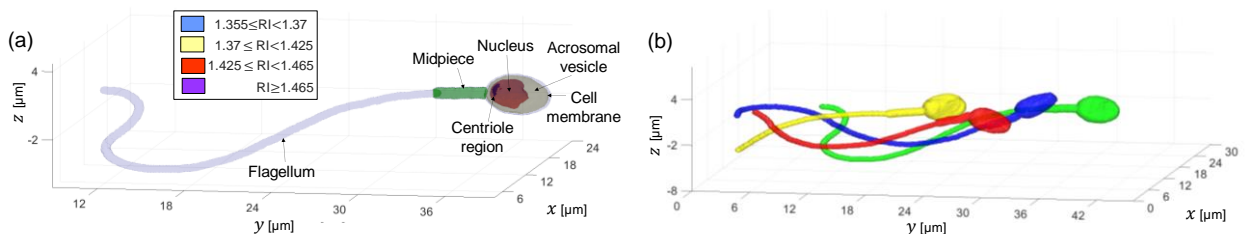


Fig. 1. High-resolution dynamic 3D imaging of a sperm cell swimming freely. (a) A single frame from the 3D motion in Movie S3 in Ref. [1], revealing the internal structure of the sperm cell. RI, Refractive index. (b) Overlay of four frames from the 3D motion in Movie S3 in Ref. [1].

- [1] G. Dardikman-Yoffe, S. K. Mirsky, I. Barnea, N. T. Shaked, High-resolution 4-D acquisition of freely swimming human sperm cells without staining, *Science Advances*, vol. 6, no. 15, eaay7619 (2020).

B-I-16

Highly sensitive optical methods for differential diagnosis of autoimmune diseases and identification of DNA molecules

**P.I. Nikitin¹, A.V. Orlov¹, V.A. Bragina¹, A.V. Pushkarev^{1,2}, E.N. Mochalova^{1,2},
M.P. Nikitin², B.G. Gorshkov¹**

1- Prokhorov General Physics Institute of the Russian Academy of Sciences, 38 Vavilov St., Moscow 119991, Russia

2- Moscow Institute of Physics and Technology, 9 Institutskii per., Dolgoprudny, 141700, Russia

Email: nikitin@kapella.gpi.ru

Highly sensitive optical methods are developed for differential diagnosis of autoimmune diseases based on the spectral-correlation interferometry [1] and image processing of a microarray glass sensor chip. The methods are based on real-time label-free measurements of changes in the thickness of bilayers formed by target and recognition molecules on the surface of a sensor chip.

The related biosensing system has been tested by measuring in human serum both critical characteristics of autoantibodies: concentration and native kinetic parameters that reflect autoantibody aggressiveness to the organism's tissues. Rapid (<25 min) and simultaneous characterization of several autoantibodies in the same serum sample has been demonstrated for anti-thyroglobulin (anti-TG) and anti-thyroid peroxidase (anti-TPO). The biosensor offers extremely high sensitivity: the limits of detection in serum are 1.7 and 6 IU/ml for anti-TPO and anti-TG, respectively. The dynamic range covers the whole range of clinically relevant concentrations.

New criteria in comprehensive diagnostics of autoimmune diseases has been proposed for the first time based not only on traditional measurements of concentration of autoantibodies, but also on quantitative evaluation of autoantibody aggressiveness.

The developed interferometric instruments have been also successfully used for biosensing based on glass sensor chips coated with a graphene layer functionalized with aptamers, which specifically bind low molecular weight compounds, e.g., Ochratoxin A [2].

Besides, the biosensor systems have been tested for counting magnetic nanobioconjugates, which were used simultaneously as carriers for magnetic separation of target molecules and as biospecific nanolabels that amplify the recorded optical signal.

A novel rapid method has been developed for accurate characterization of bioconjugates based on nanoparticles and determination of kinetic properties of their binding with target molecules. A mathematical model has been elaborated to describe analytically this binding process [3]. The method performance has been demonstrated by detection of protein enterotoxins (staphylococcal enterotoxin B) and biomarkers of cardiac diseases (cardiac troponin I).

Synthesized nanoparticles conjugated with biorecognition molecules have been also used for development of rapid formats of *in vitro* immuno- and DNA assays. In particular, a new ultrasensitive method is developed for direct (without amplification of reaction) measuring the concentration and identification of RNA / DNA molecules based on a combination of single-stranded RNA fragments and gold nanoparticles. The record sensitivity up to 30 fM is achieved for DNA concentration in an extremely small sample volume of 20 μ l with a rapid (15 min) and easy-to-perform immunochromatographic assay [4]. The achieved detection limit at such sample volume is on the level of a typical yield of target DNA from a biopsy sample (0.5 amol or 3×10^5 molecules). That is promising for development of new generation tools for diagnosing diseases.

[1] A.V. Orlov, A.V. Pushkarev, S.L. Znoyko, D.O. Novichikhin, V.A. Bragina, B.G. Gorshkov, P.I. Nikitin, Multiplex label-free biosensor for detection of autoantibodies in human serum: tool for new kinetics-based diagnostics of autoimmune diseases, *Biosensors & Bioelectronics*, vol. 159, p. 112187 (2020).

[2] N. Nekrasov, N. Yakunina, A. V. Pushkarev, A. V. Orlov, I. Gadjanski, A. Pesquera, A. Centeno, A. Zurutuza, P.I. Nikitin, Bobrinetskiy, Spectral-Phase Interferometry Detection of Ochratoxin A via Aptamer-Functionalized Graphene Coated Glass, *Nanomaterials*, vol. 11, p. 226 (2021).

[3] A.V. Pushkarev, A.V. Orlov, S.L. Znoyko, V.A. Bragina, P.I. Nikitin. Rapid and easy-to-use method for accurate characterization of target binding and kinetics of magnetic particle bioconjugates for biosensing. *Sensors*, vol. 21, p. 2802 (2021).

[4] V.R. Cherkasov, E.N. Mochalova, A.V. Babenyshev, A.V. Vasilyeva, P.I. Nikitin, M.P. Nikitin, Nanoparticle beacons: supersensitive smart materials with on/off switchable affinity to biomedical targets, *ACS Nano*, vol. 14, pp. 1792–1803 (2020).

B-I-17

The development of technologies for biomedical imaging of skin cancer

Elina A. Genina^{1,2}, Ekaterina N. Lazareva^{1,2*}, Vadim D. Genin^{1,2*}, Isabella A. Serebryakova^{1,2*}, Yury I. Surkov^{1,2*}, Alexey N. Bashkatov^{1,2}, Mohammad Ali Ansari³, Yana K. Kuzinova⁴, Olga M. Konopatskova⁴, Valery V. Tuchin^{1,2,5}

1 - Saratov State University, Astrakhanskaya str. 83, Saratov, 410012, Russia

2 - Tomsk State University, Lenin's av. 36, Tomsk, 634050, Russia

3 - Laser and Plasma Research Institute, Shahid Beheshti University, Tehran, Iran, 1983969411

4- Saratov State Medical University, Bolshaya Kazachia str., 112, Saratov, 410012, Russia

5 - Institute of Precision Mechanics and Control RAS, Rabochaya str. 24, Saratov, 410028, Russia

egenina@yandex.ru

The development of modern diagnostic and therapeutic methods and techniques is practically impossible without reliable quantitative optical models of tissues that take into account their multicomponent composition and morphology. Accordingly, the development of these models requires reliable data on optical parameters (refractive index, absorption coefficient, scattering coefficient, and scattering anisotropy factor) both healthy and pathologically altered biological tissues in a wide range of wavelengths. Knowledge of these parameters allows us to evaluate the content of the main chromophores. Multimodal approach in combined with optical clearing, based on the reduction of light scattering in tissues due to the partial replacement of the interstitial fluid with biologically compatible hyperosmotic immersion agents increases the effectiveness of methods of optical diagnostics of cancer.

In this study, a combination of high-resolution ultrasound examination and optical methods (Raman spectroscopy, optical coherence tomography (OCT), and backscattered diffuse reflectance spectroscopy) were used. OCT measurements were combined with the use of biocompatible optical clearing agents.

The study involved light-skinned volunteers with basal cell carcinoma and benign neoplasms and volunteers with high pigmented health skin. Differentiation of neoplasms was carried out using morphological research.

It was found that the skin scattering in the area of neoplasms is significantly reduced compared to healthy skin, there was an increased content of hemoglobin in the oxygenated form. For cancer, a characteristic feature was a low content of lipids and keratin. In the area of benign neoplasms, increased content of proteins, nucleic acids, lipids, and keratin was observed. The sizes of neoplasms were evaluated using ultrasound examination, and their internal structure was visualized using OCT.

The reported study was funded by the grant of RFBR (#20-52-56005) and INSF (#98029460), and the grant under the Decree of the Government of the Russian Federation No. 220 of 09 April 2010 (Agreement No. 075-15-2021-615 of 04 June 2021).

B-I-18

Cancer tissue detection with molecular IR and THz imaging and machine learning

Yury V. Kistenev^{1,2}, Alexey V. Borisov¹, Viktor V. Nikolaev¹, Denis A. Vrazhnov^{1,3},
Anastasya I. Knyazkova^{1,3}

¹Laboratory of Biophotonics, Tomsk State University, Tomsk, Russia,

²Siberian State Medical University, Tomsk, Russia,

³Institute of Atmospheric Optics of Siberian Branch of the RAS, Tomsk, Russia

Main author email address: yvk@mail.tsu.ru

A biopsy is a medical test involving extracting a cellular or tissue sample for examination to determine the disease's presence or extent. The term "optical biopsy" is commonly understood to represent using some form of optical measurements to non-invasively (or minimally invasively) perform diagnosis *in vivo* and in real-time. Tissue optical biopsy is based on laser molecular spectroscopy and imaging for morphological tissue structure and chemical content analysis.

Generally, similar data are strongly correlated because the feature space dimension exceeds the number of hidden independent variables by orders of magnitude. The high-dimension data demand special methods of analysis [1]. Machine learning is one of the most effective.

We plan to discuss the abilities of molecular IR and THz imaging combined with machine learning for cancer tissue detection and grading. The list of applications will include melanoma and lymphedema as an example of post-cancer complications.

The examples will demonstrate the peculiarities of informative feature selection/extraction, data clusterization, and predictive model construction to distinguish between two or more classes.

This work was supported by the Government of the Russian Federation (proposal no. №2020-220-08-2389 to support scientific research projects implemented under the supervision of leading scientists at Russian institutions of higher education).

[1] R. E. Bellman, Dynamic Programming, s.l.: Princeton University Press, (2003).

[2] Y.V. Kistenev, et al. Application of multiphoton imaging and machine learning to lymphedema tissue analysis //Biomed. Opt. Express. 2019. Vol. 10, № 7. P. 3353-3368.

B-I-19

Machine learning on diffuse reflectance spectra towards colorectal cancer diagnosis

Hélder P. Oliveira^{1,2}, Luís Fernandes^{3,4}, Sónia Carvalho^{5,6}, Isa Carneiro⁵, Rui Henrique^{5,7}, Valery V. Tuchin^{8,9,10}, Luís M. Oliveira^{3,4}

¹*Institute for Systems and Computer Engineering, Technology and Science, INESC TEC, 4200-465 Porto, Portugal*

²*Faculty of Science, University of Porto, FCUP, 4169-007 Porto, Portugal*

³*Center for Innovation in Engineering and Industrial Technology, Polytechnic of Porto – School of Engineering, 4249-015 Porto, Portugal*

⁴*Physics Department, Polytechnic of Porto – School of Engineering, 4249-015 Porto, Portugal*

⁵*Department of Pathology and Cancer Biology, and Epigenetics Group-Research Center, Portuguese Oncology Institute of Porto, 4200-072 Porto, Portugal*

⁶*Local Health Unit of Alto Minho, Viana do Castelo, Portugal*

⁷*Department of Pathology and Molecular Immunology, Institute of Biomedical Sciences Abel Salazar-University of Porto (ICBAS-UP), 4050-313 Porto, Portugal*

⁸*Research-Educational Institute of Optics and Biophotonics, Saratov State University, Saratov 410012, Russia*

⁹*Interdisciplinary Laboratory of Biophotonics, National Research Tomsk State University, Tomsk 634050, Russia*

¹⁰*Laboratory of Laser Diagnostics of Technical and Living Systems, Institute of Precision Mechanics and Control of the Russian Academy of Sciences, Saratov 410028, Russia*

The optical properties of biological tissues condition how a light beams propagate inside them and interact with their biological components. There are some optical properties that can be estimated for a biological material, but the most commonly used are the absorption coefficient (μ_a), the scattering coefficient (μ_s) and the anisotropy-factor (g). These fundamental properties quantify the number of photons that are absorbed and/or scattered per unit length and characterize the mean directionality of such scattering. The wavelength dependence of the optical properties of a tissue provides useful information for the optimization of current optical methods in clinical practice or for the development of new methods that operate at individual wavelengths within the electromagnetic spectrum.

Considering such recent discovery of UV-induced-windows to diagnose and treat pathologies, the current optical methods that work at visible and near infrared (NIR) wavelengths and the emerging THz techniques for clinical application, the need to map the optical properties of both normal and pathological tissues in a wide spectral range becomes urgent. The estimation or calculation of a set of optical properties for any tissue provides personal information, such as an identity card for that tissue, and consequently their evaluation might help in the discrimination between normal and pathological tissues. By knowing the optical properties of tissues, it is also possible to create individual light propagation models that can be used in the development of novel noninvasive optical diagnostic and treatment procedures. To develop such method, new approaches are necessary. A particular approach that can produce results with great precision relies on the use of Machine Learning (ML) models that can reproduce the optical properties of tissue samples from noninvasive optical measurements, such as diffuse reflectance (R_d).

In this work, we used ML techniques to reconstruct the wavelength dependence of the absorption coefficient of human normal and pathological colorectal mucosa tissues. Using only diffuse reflectance spectra from the mucosa tissues as input in the machine learning algorithms, different approaches were tried to estimate the absorption coefficient, using as ground truth the ones previously calculated for the mucosa tissues from experimental spectral measurements. Considering the optimized match for the results generated with the multilayer perceptron (MLP) regression method, we were able to identify differentiated accumulation of lipofuscin in the absorption coefficient spectra of both mucosa tissues, similarly with the corresponding results calculated directly from spectral measurements. In face of such accuracy and sensibility to the presence of hidden absorbers, with different accumulation between healthy and pathological tissues, this work, open good perspectives to develop noninvasive spectroscopy methods for early detection and monitoring of colorectal cancer.

Acknowledgements:

This work is financed by National Funds through the Portuguese funding agency, FCT - Fundação para a Ciência e a Tecnologia, within project UIDB/50014/2020.

B-I-20

Observation of osmotically induced strain in biological tissues with optical coherence elastography

Yu.M. Alexandrovskaya¹, O.I. Baum¹, A.A. Sovetsky², V.Yu. Zaitsev²

¹ *Institute of Photon Technologies, Federal Scientific Research Centre 'Crystallography and Photonics' of Russian Academy of Sciences, Troitsk, 108840 Moscow, Russia*

² *Institute of Applied Physics of the Russian Academy of Sciences, 603950 Nizhny Novgorod, Russia*

yu.alexandrovskaya@gmail.com

Application of non-isotonic solutions such as contrast and clearing agents for optical diagnostics of biological tissues produces strain gradients with an amplitude depending on the nature and concentration of the agent and permeability of a particular tissue [1,2]. Direct non-contact and real-time observation of the osmotically induced strains has been limited by the lack of instrumentation. Here, we present a new elastographic technique enabling 2D visualization of depth distribution of such strains and their dynamics during the agent diffusion. Additionally, thus monitored strain dynamics may provide information about the biological matrix hydration and permeability. The ability of the technique to reveal alterations in the tissue structure and integrity is demonstrated.

References

- [1] Yu. Alexandrovskaya, O. Baum, V. Zaitsev, A. Sovetsky, A. Matveyev, L. Matveev, K. Larin, E. Sobol, V. Tuchin, Optical and mechanical properties of the cartilage during optical clearing, In book *Tissue optical clearing: new prospects in optical imaging*, CRC Press (Dan Zhu, Elina Genina, and Valery Tuchin Eds.), 2021, Boca Raton, Florida, United States
- [2] Yu. M. Alexandrovskaya, O.I. Baum, A.A. Sovetsky, L.A. Matveev, A.L. Matveyev, and V.Yu. Zaitsev, Relaxation and osmotic-induced slow strain mapping in biological tissues by optical coherence elastography, Proc. SPIE 11845, Saratov Fall Meeting 2020: Optical and Nanotechnologies for Biology and Medicine, 1184503; <https://doi.org/10.1117/12.2590710>.

B-I-23

PDT-Duo: Dual-wavelength approaches in performance and monitoring of photodynamic therapy

**M. Kirillin¹, D. Kurakina¹, A. Khilov¹, A. Orlova¹, M. Shakhova^{1,2}, V. Perekatova¹,
N. Shishkova^{1,3}, A. Mironycheva², A. Malygina², I. Shlivko², S. Gamayuv^{1,4}, I. Turchin¹,
N. Orlynskaya², and E. Sergeeva¹**

¹*Institute of Applied Physics RAS, Nizhny Novgorod, Russia*

²*Privolzhsky Research Medical University, Nizhny Novgorod, Russia*

³*N.I. Lobachevsky State University of Nizhny Novgorod, Nizhny Novgorod, Russia*

⁴*Nizhny Novgorod Regional Clinical Oncology Center, Nizhny Novgorod, Russia*

Photodynamic therapy (PDT) is a modern treatment modality widely employed for both tumor and non-tumor pathologies. The treatment approach is based on photoactivation of a photosensitizer (PS) accumulated in the treated area prior to the procedure resulting in local production of reactive oxygen species, including singlet oxygen. Specific optical properties of different PSs usually exhibiting strong fluorescence excited in visible range together with high dispersion of biotissues optical properties in this range provide wide opportunities for both developing treatment protocols and fluorescence-based monitoring techniques. In this paper we report on development approaches for PDT performance and monitoring for chlorin-based PSs exhibiting absorption peaks in the blue and red regions (402 and 662 nm) of visible range. Owing to strong difference in biotissue absorption in the blue and red regions governed primarily by optical properties of blood, both procedure impact depth and fluorescence imaging probing depth can be controlled by the wavelength choice. Irradiation with blue or red light in the course of a PDT procedure allows to choose between superficial or deeper impact, while fluorescence excitation with blue or red light allows to analyze PS accumulation in superficial or deeper tissue layers. Moreover, complementary dual-wavelength probing in fluorescence imaging provides estimation of PS localization depth.

We present a comparative analysis of PDT performance with red and blue light irradiation for cancer treatment in animal studies. The difference in the treatment outcomes for different PS administration way (intravenous vs topical) and irradiation wavelength are revealed. The results of immediate noninvasive evaluation of procedure performance and tumor response (derived from dual-wavelength fluorescence imaging and optical coherence angiography) are compared with histology analysis taken in 7 days after the procedure.

Dual-wavelength fluorescence imaging approach is a highly promising technique in monitoring of PS accumulation and its redistribution as a result of a PDT procedure. An approach for estimation of typical PS localization depth is proposed both for PS topical administration and intravenous injection modes are proposed given that the optical properties of the biotissue are known. Good agreement of the numerical simulations with phantom studies are demonstrated. The developed approach is applied to interpret the results of dual-wavelength fluorescence monitoring of PDT procedures with chlorin-based PS delivered with red and blue light in laboratory animals and in patients.

The study is supported by Russian Science Foundation (project 17-15-01264).

B-I-24

Multimodal optical coherence tomography: biomedical achievements

M. Sirotkina¹, E. Gubarkova¹, E. Kiseleva¹, A. Plekhanov¹, K. Achkasova¹, D. Vorontsov², S. Kuznetsov³, A. Moiseev⁴, E. Zagaynova⁵, G. Gelikonov⁴, V. Zaitsev⁴, N. Gladkova¹

1- *Research Institute of Experimental Oncology and Biomedical Technologies, Privolzhsky Research Medical University, 603950 Nizhny Novgorod, Russia*

2- *Department of Oncology, Nizhny Novgorod Regional Oncologic Hospital, 603126 – Nizhny Novgorod/RU*

3- *Department of Pathology, Privolzhsky Research Medical University, 603950 – Nizhny Novgorod, Russia*

4- *Institute of Applied Physics of the Russian Academy of Sciences, 603950 – Nizhny Novgorod, Russia*

5- *Lobachevsky State University, 603105 Nizhny Novgorod, Russia*

Sirotkina_m@mail.ru

Multimodal optical coherence tomography (OCT) is the modern method of biological tissue visualization. OCT makes it possible to study the structure, functional state, mechanical and optical properties of biotissues. We believe that OCT technology can be applied in routine clinical practice in neurosurgery, oncology, abdominal surgery, gynecology and other fields of medicine. OCT is a non-invasive visualization that allows obtaining 3D images of subsurface tissues with a spatial resolution of 10-20 microns at a depth of 1-2 mm without any contrast agents in real time. Polarization-sensitive, elastographic (characterizing the elastic properties of tissues) and angiographic (blood and lymphatic vessels) images are obtained based on OCT. OCT angiography has shown high efficiency in assessing the early tumor response to photodynamic therapy (PDT) both in the experiment on the murine tumor model of colon cancer (CT26) and on the basal cell carcinoma. OCT angiography is sensitive to changes in perfusion and does not visualize vessels without blood flow. As a result of PDT, stasis and thrombosis occur in the tumor vessels, leading to a complete interruption of blood flow. Based on this phenomena, a predictor of PDT efficacy was formulated. Reduction of the tumor perfused vessels density up to <1.38% 24 hours after PDT predicts complete response with diagnostic accuracy of 93%. Reduction of the peri-tumor perfused vessels density up to < 1.4% predicts the formation of a hypertrophic scar after 12 months of observation with a diagnostic accuracy of 88% [1,2].

Compression optical coherent elastography (OCE) demonstrated a high sensitivity to changes in the microstructure of the tumor after chemotherapy and targeted therapy for murine colon cancer CT26 and murine breast cancer 4T1. OCT can detect perivascular edema, conglomerates of dystrophic cells, viable cells and necrosis areas with a resolution of 40-50 μm [3,4]. The OCE image permitting improvement in the contrast between non-tumorous and tumorous tissues for determining the breast cancer margin [5]. OCE imaging looks very promising for distinguishing of detection breast cancer with much higher contrast than it conventional and even polarization-sensitive structural OCT images.

Algorithms of CP OCT images processing, allowing numerically characterize density and direction of myelin fibers were developed [6].

The research was carried out with the financial support of the Russian Science Foundation, agreements No. 18-75-10068; 19-75-10096; 19-75-10084 and Russian Found of Basic Research, agreements No.18-29-01049

[1] Sirotkina M.A., *et al.* Accurate early prediction of tumour response to PDT using optical coherence angiography. *Scientific Reports*. 2019 9:6492

[2] Gubarkova E.V., *et al.* Optical coherence angiography for pre-treatment assessment and treatment monitoring following photodynamic therapy: a basal cell carcinoma patient study. *Scientific Reports*. 2019 9:18670

[3] Plekhanov A.A., *et al.* Histological validation of in vivo assessment of cancer tissue inhomogeneity and automated morphological segmentation enabled by Optical Coherence Elastography. *Scientific Reports*. 2020 10:11781

[4] Sirotkina M.A., *et al.* In vivo assessment of functional and morphological alterations in tumors under treatment using OCT-angiography combined with OCT-elastography. *Biomedical optics express* 2020 11, 1365-1382.

[5] Gubarkova EV, *et al.* OCT-elastography-based optical biopsy for breast cancer delineation and express assessment of morphological/molecular subtypes. *Biomed Opt Express*. 2019; 10(5):2244-2263.

B-I-25

Multimodal sapphire medical instruments for laser exposure, diagnosis and treatment of tissues

I.N. Dolganova^{1,2}, A.K. Zotov¹, I.A. Shikunova¹, D.A. Varvina³, P.A. Karalkin^{4,5}, K.I. Zaytsev^{2,6}, V.V. Tuchin⁷, and V.N. Kurlov¹

1- Institute of Solid State Physics of the Russian Academy of Sciences, Russia

2- Institute for Regenerative Medicine, Sechenov University, Russia

3- International School “Medicine of the Future”, Sechenov University, Russia

4- Institute for Cluster Oncology, Sechenov University, Russia

5- Hertsen Moscow Oncology Research Institute, National Medical Research Radiological Centre, Russia

6- Prokhorov General Physics Institute of the Russian Academy of Sciences, Russia

7- Science Medical Center, Saratov State University, Russia

in.dolganova@gmail.com

Sapphire possesses a combination of properties, which make it a favourable material platform for medical instruments [1,2]. Among them are biocompatibility, high chemical and thermal stability, transparency in visible and partly infrared (IR) ranges, and high hardness. Application of techniques of sapphire growth from melt, such as edge-defined film-fed growth (EFG), helps to fabricate sapphire crystals with complex shape without essential mechanical processing. EFG allows making capillary needles, fibers, waveguides, and ribbons with internal thin channels, which demonstrate high volume and surface quality with low concentration of defects [3]. Such sapphire shaped crystals can form a basis for multimodal medical instruments, since they can perform different functions. This is mainly due to the ability of accommodating optical fibers inside their capillary channels and the transparency of sapphire for visible and IR radiation. Capillary needles can be used for interstitial laser and photodynamic therapy, as well as for diagnosis of internal tissues, when the internal fiber is connected with a laser source or a spectrometer [4,5]. Having small outer diameter near 1 mm, they provide minimal invasiveness of medical treatment. Their tips can possess various forms, enabling different radiation patterns, from diffused to focused one. Sapphire scalpels with one, two, or three channels produced from thin ribbons by additional mechanical and chemical sharpening combine functions of tissue dissection, local diagnosis, and coagulation [1,7]. Diagnostic resolution of such scalpels can reach 2 mm, when the cutting-edge rounding can be as sharp as 100 nm. Sapphire neuroprobes can be used for intraoperative fluorescence diagnosis of brain tissues and aspiration, when having closed and open channels in its body. They also can be used for additional coagulation of tissues. Finally, sapphire cryoprobes can open novel abilities of cryosurgery, since they demonstrate promising feature of monitoring and controlling the freezing depth during application using optical methods, such as diffuse reflection or terahertz spectroscopy, or even optical coherence tomography [8]. In addition, such probes provide faster tissue freezing comparing to metal cryoapplicators. In this talk, we summarize the recent developments and studies of sapphire medical instruments, discuss their advantages and drawbacks, as well as further applications and clinical studies.

This work was supported by the Russian Science Foundation (RSF), research project # 19-79-10212.

[1] G.M. Katyba, et al., “Sapphire shaped crystals for waveguiding, sensing and exposure applications,” *Prog. Cryst. Growth Charact. Mater.* 64, 133–151 (2018).

[2] P.I. Antonov, V.N. Kurlov, “A review of developments in shaped crystal growth of sapphire by the Stepanov and related techniques,” *Prog. Cryst. Growth Charact. Mater.* 44, 63–122 (2002).

[3] V.N. Kurlov. Reference Module in Materials Science and Materials Engineering. Ed. by Saleem Hashmi. Oxford: Elsevier, 2016.

[4] V.N. Kurlov, S. N. Rossolenko, “Growth of shaped sapphire crystals using automated weight control,” *J. Crystal Growth* 173, 417–426 (1997).

[5] I.N. Dolganova, et al., “Optimization of sapphire capillary needles for interstitial and percutaneous laser medicine,” *J. Biomed. Opt.* 24(12), 128001 (2019).

[6] I.N. Dolganova, et al., “Microfocusing sapphire capillary needle for laser surgery and therapy: Fabrication and characterization,” *J. Biophoton.* 13(10), e202000164 (2020).

[7] I.A. Shikunova, et al., “Sapphire neurosurgical probe for aspiration of brain tumors with boundary demarcation by use of spectroscopy,” *Optics and Spectroscopy* 126, 545–553 (2019).

[8] V.N. Kurlov et al., “Sapphire smart scalpel,” *Bull. Rus. Acad. Sci.: Physics* 73, 1341–1344 (2009).

[9] A.K. Zotov, et al., “In situ terahertz monitoring of an ice ball formation during tissue cryosurgery: a feasibility test,” *J. Biomed. Opt.* 26(4), 043003 (2021).

B-I-26

Optothermal fiber converters and their medical applications

Andrey V. Belikov^{1,2}, Do Thanh Tung¹, Yulia V. Fyodorova¹

1-ITMO University, 49 Kronverksky, 197101 Saint-Petersburg, Russia

2-Pavlov First Saint Petersburg State Medical University, ul. L'va Tolstogo 6-8, 197022 St. Petersburg, Russia

avbelikov@gmail.com

Diode lasers with wavelengths of radiation in near IR wavelength range are actively used for excision and coagulation of soft biotissues. To increase the cutting efficiency of diode lasers in surgery optothermal fiber converters (OTFC) were used, the purpose of which is to effectively convert laser radiation into heat. Optothermal fiber converters are applied in general and vascular surgery, dentistry, urology, dermatology, etc. Optothermal fiber converters are currently evolving through the creation of new converters, improving their properties, and creating new medical applications. C-doped OTFC is most used. These converters can heat up to 1000°C, but a further increase in temperature or average power of the laser radiation falling on the converter leads to their destruction. Ti-doped converters are able to heat up to 2700°C without breaking up and have more than C-doped lifetime [1-3].

This study discusses the appearance, size and mechanical properties of C-doped and Ti-doped converters. C- and Ti-doped converters manufacturing technologies are considered. Optical and thermal models of C-doped and Ti-doped converters are presented. The variation in the optical properties of Ti-doped OTFC as its microstructure changes was determined.

Optical and thermal models describing the interaction of Ti-doped converter with vein wall during endovascular laser coagulation have been developed. The absorbance efficiency of laser radiation with 980nm and 1470nm wavelengths widely uses at endovascular laser coagulation for Ti-doped OTFC has been calculated. The optimal ranges of microstructure's parameters of Ti-doped OTFC for endovascular laser coagulation process with this converter were discussed. The relative between the power of the diode laser radiation, the temperature of Ti-doped OTFC and the traction speed of the converter inside the vein with the temperature at the inner vein wall surface is discussed. The results of the assessment of the size of the thermal damage zone of the vessel wall, based on the solution of the Arrhenius equation, are presented. A physical model of vein for investigation of visual, hydrodynamic, and thermal processes during vein endovascular laser coagulation have been presented and the results of research with this model are demonstrated. The results of a comparative study of *in vitro* exposure to C-doped and Ti-doped converters on soft biotissue in contact laser surgery using a diode laser are presented. The results of the study of *in-vivo* application of C-doped OTFC in dermatology when removing nevus are discussed. It is shown that in the process of laser removal the optimal temperature of the nevus excision depends on its type, excision technique and lies in the range of 700-1000°C.

[1] Zhigarkov V.S. et al., Hydrodynamic effects in laser cutting of biological tissue phantoms *Quantum Electron.*, 47 (10), 942, (2017)

[2] Belikov A.V., Skrypnik A.V., Soft tissue cutting efficiency by 980 nm laser with carbon-, erbium-, and titanium-doped optothermal fiber converters, *Laser. Surg. Med.*, 51 (2), 185-200, (2019)

[3] Romanos G.E., G.B. Altshuler, I.V. Yaroslavsky, EPIC Pro: Re Inventing Diode Laser Soft Tissue Therapy Using Science and Technology (Irvine, CA, USA: Biolase, Inc.), (2016).

B-I-27

Photonic regulation of secondary metabolite biosynthesis by binary spectral stress

Y.N. Kulchin¹, V.P. Bulgakov², E.P. Subbotin¹, D.O. Goltsova¹, A.S. Kholin¹, L.P. Lyakhova³, N.I. Subbotina¹, I.V. Gafitskaya², V.P. Grigorchuk², E.V. Burkovskaya², Yu.A. Khrolenko², I.Yu. Orlovskaya², O.V. Nakonechnaya²

¹ *Institute of Automation and Control Processes Far Eastern Branch of the Russian Academy of Sciences (IACP FEB RAS), Far Eastern Branch of the Russian Academy of Sciences, 5 Radio str., Vladivostok, 690041, Russia*

² *Federal Scientific Center of the East Asia Terrestrial Biodiversity (Institute of Biology and Soil Science), Far Eastern Branch of the Russian Academy of Sciences, 159 Stoletija str., Vladivostok, 690022, Russia*

³ *Far Eastern Federal University, 10 Ajax Bay, Russky Island*

Vladivostok 690922, Russia

Y.N. Kulchin: kulchin@iacp.dvo.ru

Secondary plant metabolites are unique sources for pharmaceuticals, food additives and industrially important biochemicals. The accumulation of these metabolites occurs in plants under stress. Here, we investigated the effect of abiotic stress caused by a binary change in the spectral composition of radiation generated by matrix LED light sources on the development and production of secondary metabolites using the example of *Eruca sativa* lettuce cultivated under fully controlled conditions. The dominant influence of the ratio of the intensities of the "blue" and "red" spectral ranges in binary switching light fluxes has been established. Regimes were found in which the accumulation of green biomass and the development of the root system of plants significantly exceed the control indicators. The presence of a compromise between the qualitative characteristics of the photon flux and abiotic stress, at which there is an increase in the wet weight of plants with a simultaneous increase in the synthesis of secondary metabolites, such as ascorbic acid and flavonoids, was revealed.

Thus, the results of the studies performed demonstrate the possibility of influencing the processes of primary and secondary plant metabolism by changing the quality of photon irradiation during plant development, which causes them to increase the accumulation of secondary metabolites.

B-I-28

THz pulsed spectroscopy and solid immersion microscopy of brain gliomas: A road toward intraoperative THz diagnosis

**K.I. Zaytsev^{1,2,3,*}, A.A. Gavdush^{1,2,3}, N.V. Chernomyrdin^{1,2,3}, I.N. Dolganova^{2,3,4},
P.V. Nikitin^{2,5}, G.A. Komandin¹, I.V. Reshetov⁶, and V.V. Tuchin^{7,8,9}**

1 – Prokhorov General Physics Institute of the Russian Academy of Sciences, Russia

2 – Institute for Regenerative Medicine, Sechenov University, Russia

3 – Bauman Moscow State Technical University, Russia

4 – Institute of Solid State Physics of the Russian Academy of Sciences, Russia

5 – Burdenko Neurosurgery Institute, Russia

6 – Institute for Cluster Oncology, Sechenov University, Russia

7- Science Medical Center, Saratov State University, Russia

8 – Institute of Precision Mechanics and Control of the Russian Academy of Sciences, Russia

9 – National Research Tomsk State University, Russia

*E-mail: kirzay@gmail.com

Terahertz (THz) technology offers novel opportunities in label-free diagnosis of malignant and benign neoplasms with different nosologies and localizations, relying on the strong sensitivity of THz waves to the content and state of tissues water [1–3]. Recently, a potential of THz spectroscopy and imaging in the intraoperative diagnosis of human brain gliomas with the different World Health Organization (WHO) grades was uncovered [4]. In our research, we focused on studies of the effective THz optical properties and THz microscopic images of the intact tissues and gliomas *ex vivo*, involving both the *ex vivo* tissues from human and those from rats. We were the first to demonstrate statistically-significant differences between the THz response of intact tissues and WHO Grades I–IV human brain gliomas [5]. Next, we described the picosecond relaxation dynamics of intact tissues and gliomas from humans using both the double-Debye and double-overdamped-oscillator models of a complex dielectric permittivity [6]. Relying on these models, an increased water content in a tumor was found to be the main origin of the observed contrast between intact tissues and a tumor in THz spectra and images. Finally, using the diffraction limited THz pulsed spectroscopy and the innovative 0.15λ -resolution THz solid immersion microscopy [7–8], we studied, for the first time, the THz response of monograft glioma model 101.8 from rats *ex vivo*, both in freshly-excised and paraffin-embedded forms [9]. The observed results justified a contrast between intact tissues and a tumor in the THz range. Moreover, it revealed heterogeneous character of brain tissues at the THz-wavelength scale, that agrees well with tissue measurements involving optical coherence tomography in the near-infrared range [10]. Heterogeneity of the intact tissues was attributed to the distinct response of white and gray matters, as well as to other neurovascular structures of the brain. In turn, that of a tumor mostly originates owing to the presence of necrotic debris and haemorrhages. Our findings demonstrated that THz technology hold strong potential in the intraoperative diagnosis of human brain tumors. However, a number of fundamental and applied problems should be solved before translation of THz instruments to a clinical practice.

This work was supported by the Russian Science Foundation, Project # 17-79-20346.

- [1] O.A. Smolyanskaya et al., *Progress in Quantum Electronics* 62, 1–77 (2018).
- [2] K.I. Zaytsev et al., *Journal of Optics* 22(1), 013001 (2020).
- [3] K.I. Zaytsev et al., *Journal of Biomedical Optics* 26(4), 043001 (2021).
- [4] G.R. Musina et al., *Journal of Biomedical Photonics & Engineering* 6(2), 020201 (2020).
- [5] A.A. Gavdush et al., *Journal of Biomedical Optics* 24(2), 027001 (2019).
- [6] A.A. Gavdush et al., *Biomedical Optics Express* 12(1), 69–83 (2021).
- [7] N.V. Chernomyrdin et al., *Applied Physics Letters* 113(11), 111102 (2018).
- [8] V.A. Zhelnov et al., *Optics Express* 29(3), 3553–3566 (2021).
- [9] A.S. Kucheryavenko et al., “Terahertz dielectric spectroscopy and solid immersion microscopy of *ex vivo* glioma model 101.8: Brain tissue heterogeneity,” *Biomedical Optics Express* (2021), under review.
- [10] I.N. Dolganova et al., *Biomedical Optics Express* 11(11), 6780–6798 (2020).

B-I-29

Towards Automated Digital Histopathology with Circularly Polarized Light

A. Bykov¹, M. Borovkova¹, V. Dremin², O. Sieryi¹, I. Meglinski^{1,2,3}

1- Optoelectronics and Measurement Techniques Unit, University of Oulu, Oulu, Finland

2- College of Engineering and Physical Sciences, Aston University, Birmingham, UK

3- Institute of Clinical Medicine, I.M. Sechenov First Moscow State Medical University, Moscow, Russia

alexander.bykov@oulu.fi

The gold standard of tissue analysis is currently represented by the microscopic, slide-based procedure. Conventionally, the tissue preparation protocol requires the specimen to be formalin-fixed, dehydrated and embedded in paraffin wax to enable slicing into thin layers. After that, the obtained slices are chemically stained to contrast tissue constituents for microscopic inspection. The described procedure, together with the subsequent analysis, can take up to several weeks. Moreover, the possible sampling limitations and the inability to observe tissue organelles in the native environment limit the efficiency of the method. Thus, there is a need for slide-free, stain-free, non-destructive automated digital histopathological imaging to address the mentioned issues.

Due to the high sensitivity of polarized light to the variations of structure in the analyzed sample, the spatially resolved polarized light spectroscopy has a great potential to be used for screening malformations in biological tissues. Our studies show that circularly polarized light scattered within the tissues is highly sensitive to the presence of cancer cells [1] as well as A β plaques [2] that allows identification of the cancerous lesions on early-stage or reliable Alzheimer's disease (AD) detection. For the measurements, the laboratory-built double-axis system containing both illumination and detection channels has been used. The illumination channel contains the supercontinuum fiber laser (Leukos Ltd., France). A high-speed acousto-optic tunable filter (Leukos Ltd., France) enables selecting the specific probing wavelength within the range of 400–650 nm. Circularly polarized light of the selected wavelength is then focused onto the sample at 55° angle. The light diffusely reflected from the sample is collected in the detection channel at 30° angle at a variable distance away from the point of incidence and analyzed by the Stokes polarimeter system (Thorlabs Ltd., USA). Spatial scanning of the samples is performed with the XY translation stage, providing a resolution of 5 μ m.

The multiple measurements have been performed on a formalin-fixed, paraffin-embedded blocks of early-stage breast cancer samples (ductal carcinoma *in situ*). We show that circularly polarized light scattered within the breast sample is sensitive to the presence of cancer cells and provides the information close to that obtained from the standard histological examination. The highest contrast between cancerous and healthy regions was observed for the wavelength of 450 nm. The degree of polarization (DoP) of the reflected light was found to be the most sensitive parameter indicating the malignant changes in the considered samples. Cluster analysis based on the k-means algorithm has been performed to implement the automated classification of the obtained data and delineate cancer zones of the specimens. A good correlation of the automatically recognized zones with the histopathological image obtained by a qualified pathologist with the conventional staining/slicing technique is observed.

The pilot results demonstrating the possibility of AD detection has been obtained in the mouse model. The comparison of the measured polarization parameters for the mice in the early stage of AD (group I, 11 animals, 50-75 days old) and for the well-developed disease (group II, 13 animals, 175-200 days old) is performed. The presence and the density of A β plaques were also confirmed with the conventional histopathologic analysis. The DoP for the samples of group I was remarkably higher than that of group II that can be explained by the higher scattering of the tissue from group II. The higher magnitude of birefringence was observed for group II and can be explained by the growing presence of A β plaques that exhibit significant birefringence. The proposed methodology demonstrates a great potential for developing a new diagnostic protocol for routine clinical practice.

The research was supported by the Academy of Finland (grants: 314369 and 325097) and EU H2020 ATTRACT project (777222). Authors acknowledge Northern Finland Biobank Borealis and Prof. Jens Pahnke, University of Oslo, Norway for the provided tissue samples.

[1] D. Ivanov et al., J. Biophoton. 13(8): e202000082 (2020).

[2] M. Borovkova et al., Biomed. Opt. Exp. 11(8), 4509-4519 (2020).

B-I-30

Diagnosis of glioma molecular markers in blood using spectroscopy and machine learning

O. Cherkasova^{1,2}, A. Mankova³, M. Konnikova^{2,3}, D. Vrazhnov⁴, Yu. Kistenev^{5,6}, Y.Peng⁷, A. Shkurinov^{2,3}

1-Institute of Laser Physics of SB RAS, 15B Lavrentyev Ave., 630090 Novosibirsk, Russia

2- Institute on Laser and Information Technologies - Branch of the Federal Scientific Research Centre "Crystallography and Photonics" of RAS, 1 Svyatoozerskaya st., 140700 Shatura, Moscow Region, Russia

3 - Lomonosov Moscow State University, 1 Leninskiye Gory, 119991 Moscow, Russia,

4 - Institute of Atmospheric Optics, Siberian Branch of the RAS, pr. Akademicheskii 1, 634055 Tomsk, Russia

5 - Tomsk State University, 36 Lenin Ave., 634050 Tomsk, Russia

6 - Siberian State Medical University, 2 Moskovsky trakt, 634050 Tomsk, Russia

7 - University of Shanghai for Science and Technology, 516 Jungong Rd., 200093 Shanghai, R. P. China

e-mail: o.p.cherkasova@gmail.com

Gliomas are brain tumors with high rates of recurrence and mortality. Early diagnosis of gliomas may be achieved by detecting the molecular biomarkers in body fluids [1]. It has been recently shown that one of specific markers for glioma differential diagnostics are enantiomers of 2-hydroxyglutarate (L-2HG and D-2HG), presented in brain tissues and blood. Blood constituents can be measured by THz, IR and Raman spectroscopy [2-4]. In this work, we use these methods, combined with machine learning, to study mouse blood plasma during glioblastoma development.

U87 human glioblastoma in the SCID line mice was created following the method described in [5]. Animals were excluded from the experiment at 7-th, 14-th, 21-st and 28-th day after tumor cells transplantation. Magnetic resonance spectroscopy has been used to identify glioma molecular markers at different stages of tumor growth [6]. A detailed description of the spectrometers was presented in our previous papers [2, 5]. The spectral data analysis was conducted by the Principal Component Analysis, and multidimensional scaling. The prognostic models were developed by the linear kernel Support vector machine, Random forests, and Gradient boosting methods [4, 7]. A novel approach based on the Raman and absorption spectroscopy for detection of glioma molecular markers in blood is discussed.

This work was supported by the Russian Foundation for Basic Research (grant # 19-52-55004), the Ministry of Science and Higher Education of the Russian Federation within the Agreement No. 075-15-2019-1950, within the State assignment FSRC "Crystallography and Photonics" RAS; by the Interdisciplinary Scientific and Educational School of Moscow University "Photonic and Quantum Technologies. Digital Medicine". This work was supported by the Government of the Russian Federation (proposal no. №2020-220-08-2389 to support scientific research projects implemented under the supervision of leading scientists at Russian institutions of higher education).

[1] O. Cherkasova, Y. Peng, M. Konnikova, et al., "Diagnosis of Glioma Molecular Markers by Terahertz Technologies", *Photonics*, vol. 8(1), pp. 22, (2021).

[2] M. M. Nazarov, O. P. Cherkasova, E. N. Lazareva, et al., "A Complex Study of the Peculiarities of Blood Serum Absorption of Rats with Experimental Liver Cancer", *Opt. Spectrosc.*, vol. 126, pp. 721-729, (2019).

[3] J. R. Hands, K. M. Dorling, P. Abel, et al., "Attenuated total reflection fourier transform infrared (ATR-FTIR) spectral discrimination of brain tumour severity from serum samples", *J Biophotonics*, vol. 7(3-4), pp. 189-199, (2014).

[4] A. A. Mankova, O. P. Cherkasova, E. N. Lazareva, et al., "Study of Blood Serum in Rats with Transplanted Cholangiocarcinoma Using Raman Spectroscopy", *Opt. Spectrosc.*, vol. 128(7), pp. 964-971, (2020)

[5] E. L. Zavjalov, I. A. Razumov, L. A. Gerlinskaya, A. V. Romashchenko, "In vivo MRI Visualization of U87 Glioblastoma Development Dynamics in the Model of Orthotopic Xenotransplantation to the SCID Mouse", *Russ. J. Genet. Appl. Res.*, vol. 6 (4), pp. 448-453, (2016).

[6] Shevelev O.B., Seryapina A.A., Zavjalov E.L. et al. // *Phytomedicine*. 2018. V. 41. P. 1.

[7] Kistenev Y.V., Borisov A.V., Kuzmin D.A. et al. *J. Biomed. Opt.* 22(1), 017002 (2017).

B-I-31**Laser Tweezers and Prospects for Live Cells Study****A. Priezzhev¹, A. Lugovtsov¹, A. Semenov², Kisung Lee³, P. Ermolinskiy¹, A. Kapkov¹***1- Physics Department, Lomonosov Moscow State University, Leninskie Gory, 1, Moscow, 119991, Russia**2- Biologic Department, Lomonosov Moscow State University, Leninskie Gory, 1, Moscow, 119991, Russia**3- Center for Soft and Living Matter, Institute for Basic Science, Ulsan 44919, Korea*avp@biomedphotonics.ru

With the advent of laser tweezers, for the invention of which Arthur Ashkin (USA) was awarded the 1986 Nobel Prize, optical trapping and manipulation of live cells without mechanical contact became practically feasible. The use of laser tweezers has opened new horizons for scientific and technological advances and developments, since it has provided new opportunities for studying the many phenomena in the molecular-cell interface that form the basis of living matter. However, the absence of mechanical contact does not always ensure the integrity of the living cell trapped by the laser beam, even though the laser wavelength is selected so as to be outside the absorption spectrum of the cell. This circumstance requires additional research.

The principle of operation of laser tweezers is based on the property of a sharply focused laser beam to exert an effect on dielectric microparticles located near the waist of this beam with a force that brings particles to an equilibrium position and holds them there. A change in the spatial position of the beam waist leads to a change in the position of the trapped particle. The removal of a particle captured by the laser tweezers from the equilibrium position by external forces can be calibrated so that these forces can be accurately measured in the range of 0.1-100 pN. This is the range of forces of elastic deformation of living cells and their interaction with each other. The ability to measure these forces without mechanical contact makes it possible to study the mechanisms of their interaction at the level of individual cells, which was previously impossible.

In this paper, we show the possibilities of studying with the help of laser tweezers various phenomena underlying the interaction of individual red blood cells (RBC) suspended in autologous plasma or solutions of different macromolecules, somehow affecting the properties of these cells [1-3]. We demonstrate the phenomenon of synergy discovered by us in the action of various components of blood plasma, which plays a significant role in the aggregation of RBC and significantly affects blood microcirculation. Also, we demonstrate that the microrheologic properties of RBC depend on their age, the duration of their presence in the microcirculation after they leave the blood marrow. This is caused, in particular, by the difference in adsorption of macromolecules by the membranes of RBC of different age and, also, by pathologic alterations [4-6]. We present our preliminary results in measuring the forces of interaction of RBC with endothelial cells *in vitro* ranging from 0 to 21 pN depending on the shape of RBC (discocytes or echinocytes), concentration of macromolecules (fibrinogen or dextran) in the suspending medium, and preactivation of the endothelial cells with the tumor necrosis factor TNF- α [7].

This work was supported by the Russian Foundation for Basic Research (grant No. 19-52-51015).

A.V. Priezzhev and K. Lee, Potentialities of laser trapping and manipulation of blood cells in hemorheologic research, *Clin. Hemorheol. Microcirc.* **64**, 587–592 (2016).

K. Lee, A.V. Danilina, M. Kinnunen, A.V. Priezzhev, and I. Meglinski, Probing the red blood cells aggregating force with optical tweezers, *IEEE J. Sel. Topics in Quant. Electron.* **22**(3), 7000106 (2016).

K. Lee, C. Wagner, and A.V. Priezzhev, Assessment of the “cross-bridge”-induced interaction of red blood cells by optical trapping combined with microfluidics, *J. Biomed. Opt.* **22**(9), 091516 (2017).

P.B. Ermolinskiy, A.E. Lugovtsov, A.I. Maslyanitsina, A.N. Semenov, L.I. Dyachuk, and A.V. Priezzhev, Interaction of erythrocytes in process of pair aggregation in blood samples from patients with arterial hypertension and healthy donors: measurements with laser tweezers, *JBPE* **4**(3), 030303 (2018).

K. Lee, E. Shirshin, N. Rovnyagina, F. Yaya, Z. Boujja, A. Priezzhev, and C. Wagner, Dextran adsorption onto red blood cells revisited: cell quantification by laser tweezers combined with microfluidics, *Biomed. Opt. Express* **9**(6), 2755-2764 (2018).

A.N. Semenov, E.A. Shirshin, A.V. Muravyov and A.V. Priezzhev, The effects of different signaling pathways in adenylyl cyclase activation on red blood cells deformability, *Frontiers in Physiology* **10**, №9236 1-10 (2019).

A.A. Kapkov, A.N. Semenov, P.B. Ermolinskiy, A.E. Lugovtsov, and A.V. Priezzhev, Forces of RBC interaction with single endothelial cells in stationary conditions: measurements with laser tweezers. Submitted to *JIOHS*.

B-I-32

Advances in tissue optical clearing for laser diagnostics and treatment

Valery V. Tuchin

Saratov State University, Saratov 410012, Russian Federation
National Research Tomsk State University, Tomsk 634050, Russian Federation
Institute of Precision Mechanics and Control of the Russian Academy of Sciences,
Saratov 410028, Russian Federation
tuchinvv@mail.ru

A description of the optical clearing (OC) technology based on controllable and reversible modification of tissue optical properties by their impregnation with a biocompatible optical clearing agent (OCA) will be done [1-3]. The major mechanisms of OC allowing one to enhance optical imaging and laser treatment facilities of living tissues will be presented. The hyperosmotic properties of OCAs will be discussed in the context of developing a provocative test to investigate the difference between the response of normal and pathological tissue to osmotic stress with the simultaneous optical detection of such a response.

The enhancement of probing/treatment depth and image contrast for a number of human and animal tissues investigated by using different optical modalities, including diffuse reflectance spectroscopy, collimated transmittance, OCT, fluorescence, and Raman microscopies will be discussed [4-8]. Experimental data on the diffusion and permeability coefficients of biocompatible FDA approved OCAs, such as glycerol, e-cigarettes vapes (glycerol/propylene glycol), CT contrast agents (Iohexol and Iodixanol), and MRI contrast agent (Gadobutrol) in skin and mucosal tissues will be presented.

Perspectives of immersion optical clearing/contrasting technique aiming to enhance imaging/treatment of skin and mucosal living tissues by using different imaging and laser treatment modalities will be discussed.

The research was carried out with the support of a grant under the Decree of the Government of the Russian Federation No. 220 of 09 April 2010 (Agreement No. 075-15-2021-615 of 04 June 2021).

References

- [1] E. A. Genina, et al., Optical clearing of biological tissues: prospects of application in medical diagnostics and phototherapy, *J. Biomed. Photonics & Eng.* **1**(1), 22–58 (2015).
- [2] A. N. Bashkatov et al., Measurement of tissue optical properties in the context of tissue optical clearing, *J. Biomed. Opt.* **23**(9), 091416 (2018).
- [3] L. Oliveira, V.V. Tuchin, *The optical clearing method: A new tool for Clinical Practice and Biomedical Engineering*, Basel: Springer Nature Switzerland AG, 2019.
- [4] D.K. Tuchina, I.G. Meerovich, O.A. Sindeeva, V.V. Zherdeva, A.P. Savitsky, A.A. Bogdanov Jr, V.V. Tuchin, Magnetic resonance contrast agents in optical clearing: Prospects for multimodal tissue imaging. *J. Biophotonics* **13**(11), e201960249 (2020).
- [5] Q. Lin, E.N. Lazareva, V.I. Kochubey, Y. Duan, V.V. Tuchin, Kinetics of optical clearing of human skin studied in vivo using portable Raman spectroscopy, *Laser Physics Letters* **17** (10), 105601(2020).
- [6] D.K. Tuchina, I.G. Meerovich, O.A. Sindeeva, V.V. Zherdeva, N.I. Kazachkina, I.D. Solov'ev, A.P. Savitsky, A.A. Bogdanov Jr, V.V. Tuchin, Prospects for multimodal visualization of biological tissues using fluorescence imaging, *Quantum Electronics* **51**(2), 104–117 (2021).
- [7] N.I. Kazachkina, V.V. Zherdeva, A.N. Saydasheva, I.G. Meerovich, V.V. Tuchin, Savitsky A.P., Bogdanov, A.A. Topical gadobutrol application causes fluorescence intensity change in RFP-expressing tumor-bearing mice, *Journal of Biomedical Photonics & Engineering* **7** 020301(2021).
- [8] I. Carneiro, S. Carvalho, R. Henrique, A. Selifonov, L. Oliveira, V.V. Tuchin, Enhanced ultraviolet spectroscopy by optical clearing for biomedical applications, *IEEE Journal of Selected Topics in Quantum Electronics* **27** (4), 1-8 (2021).

B-I-33

Combating bacterial biofilms and bacterial plankton for medicine and food industry via laser nanotechnology

**A.A. Ionin¹, S.A. Gonchukov^{1,2}, S.I. Kudryashov^{1,3}, A.A. Nastulyavichus^{1,3}, Yu.M. Romanova⁴,
I.N. Saraeva^{1,3}, A. A. Semenova³, N.A. Smirnov¹, E.R. Tolordava^{1,3,4}, Yu. K. Yushina³**

1 - P. N. Lebedev Physical Institute, 53 Leninsky prospect, 119991, Moscow, Russia

2 - National Research Nuclear University MEPhI, 31 Kashirskoe shosse, 115409, Moscow, Russia

3 - V.M. Gorbatov Federal Research Center for Food Systems, 26 Talalikhina Str., 109316, Moscow, Russia

*4 - N.F. Gamaleya Federal Research Center of Epidemiology and Microbiology,
25 Gamaleya Str., 123098, Moscow, Russia*

aion@sci.lebedev.ru

Solving the problem of pathogenic bacteria resistance is a key challenge of modern medicine and food industry. Nowadays, controlling pathogenic microorganisms is actually a global issue. Active and passive hybrid ways developed by us for controlling and suppressing biofilms and the planktonic form of pathogenic microorganisms based on different bactericidal nanomaterials obtained with modern laser technologies are discussed, which can find applications in medicine and food industry. An innovative mobile laser application of the complete suppression of biofilms in situ is described: namely, the procedure of laser-induced forward transfer (LIFT) for inactivation of pathogenic bacterial biofilms by metallic nanoparticles (NPs). The transparent substrate coated with the thin absorbing metal layer is irradiated from the back side with a laser that causes the NPs to be transferred due to light-matter interaction (Fig.1, left). Variable laser beam parameters and the spacing between donor and the glass substrate affect parameters of the transferred NPs as well as their quantity.

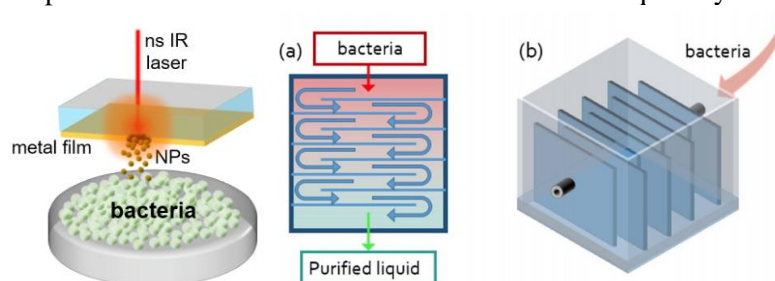


Fig.1. LIFT technology for transferring NPs onto a biofilm (left); schematic of the flow-along-nanostructures filter: (a) upper and (b) stereometric view (right)

The laser-ablative fabrication of antibacterial nanostructures, combining mechanical and chemo-toxic effects, by femto- and nanosecond laser ablation and their testing on *Staphylococcus aureus* and *Pseudomonas aeruginosa* are discussed. A titanium surface covered with nanospikes and periodical surface ripples provides a strong anti-biofilm effect, and the addition of cytotoxic NPs (Ag, Se) enhances the overall bactericidal activities. Application of a flow reactor including Ti nanospike-covered wafers as a through-flow sterilizer (Fig.1, right) resulted in reduction of the bacterial population by two orders of magnitude. Food pathogens (*Staphylococcus aureus*, *Listeria monocytogenes*, and *Pseudomonas aeruginosa*) in planktonic form were subjected to bactericidal treatment by colloidal nickel-oxide NPs. These colloidal NPs, as anti-biotic nanomaterial, were produced by laser ablation in deionized water and air, and comprehensively characterized by x-ray diffraction, scanning electron microscopy, etc. The opportunity of a time-resolved bacterial live/dead dynamics observation with the use of plasmonic nanospikes was demonstrated. Sharp nanospikes, fabricated on a 500-nm thick gold film by laser ablation with the use of 1030-nm femtosecond pulses, were tested as potential elements for antibacterial surfaces and plasmonic luminescence sensors.

B-O-1

Photothermal effect in skin tumor with embedded silicon nanoparticles: numerical simulation

O.I. Sokolovskaya¹, S.V. Zobotnov¹, L.A. Golovan¹, P.K. Kashkarov¹, A.V. Khilov^{2,1}, D.A. Kurakina², E.A. Sergeeva^{2,1}, M.Yu. Kirillin¹

1-Faculty of Physics, Lomonosov Moscow State University, Moscow, Russia

2-Institute of Applied Physics RAS, Nizhniy Novgorod, Russia

e-mail: oi.sokolovskaja@physics.msu.ru

Photothermotherapy (PTT) techniques are based on using inorganic nanomaterials as a thermal coupling agents for a biological sample [1]. Silicon is material of high biocompatibility, bioavailability, biodegradability and low toxicity [2]. In this study nodular basal cell carcinoma (BCC) laser heating in presence of silicon nanoparticles is simulated for temperatures corresponding to mild hyperthermia regimes (42-43 °C). The study was performed for nanoparticles obtained by picosecond laser ablation of silicon nanowires in water and ethanol. The optical properties of suspensions were obtained through Mie calculations based on the atomic force microscopy data on particles size distribution.

We used Monte Carlo simulation method to obtain volumetric density of absorbed energy distribution as a result of light absorption from continuous laser source. Then we solved time-dependent bioheat equation through COMSOL® Multiphysics package. Simulations revealed that irradiation by moderate laser powers of human skin containing carcinoma with size of several millimeters in presence of silicon nanoparticles formed by pulsed laser ablation of low-doped silicon nanowires in water in tumor tissue allows to reach the temperature of 42°C in all tumor volume, while without nanoparticles at the same irradiation conditions the full heating of considered carcinoma is not possible. The optimal laser powers were 100 mW for beam of 5.1 x 5.1 mm² and 170 mW for beam size of 10 mm², and the irradiation time was 600 sec. At these power values the maximal increase in heating efficiency of tumor tissue was 1.5°C and 1°C, respectively.

This work was supported by Russian Science Foundation (grant №19-12-00192)

[1] C. Hong, J. Lee et. al., Porous silicon nanoparticles for cancer photothermotherapy, *Nanoscale research letters*, vol.6, 321 (2011)

[2] Y. Park, J. Yoo, M. H.,Kang, W. Kwon, , & J. Joo, Photoluminescent and biodegradable porous silicon nanoparticles for biomedical imaging. *Journal of Materials Chemistry B*, vol. 7, 6271-6292. (2019).

B-O-2**Increasing the thermal effect efficiency of NIR laser radiation on biological tissue using Yb-containing dielectric nanoparticles****S.A. Khrushchalina, A.N. Belyaev, O.S. Bushukina, P.A. Ryabochkina, I.A. Yurlov**

National Research Ogarev Mordovia State University, 68 Bolshevistskaya Str., Saransk 430005, Russia

anabel-2005@yandex.ru

Near and middle infrared (IR) lasers are widely used in dermatology [1-6]. Optical fibers are usually used for radiation delivery to tissues, which makes it possible to realize contact and non-contact treatment modes [1-8]. The thermal effect on a biological tissue for contact treatment mode can be enhanced by the "blackening" of the fiber endface contacting directly with the tissue [4]. In this case, higher temperatures can be achieved in the contact zone (between the fiber endface and the biological tissue), and, as a consequence, the treatment efficiency can be increased [5]. In this paper, we propose another way for enhancing the thermal effect of NIR laser radiation on the biological tissue surface for non-contact treatment mode, which consists in preliminary deposition of Yb-containing nanosized dielectric particles on it. The heating of these nanoparticles upon 980 nm excitation to the Yb³⁺ ions absorption band has been studied and described previously [7].

White adult 180-220 g wistar rats were used as experimental animals. The rat was fixed in the prone position and a 6x4 cm section was shaved on its back. A stand with rat was fixed on a motorized translation stage (Zaber Technologies Inc.), which ensured its precise movement. The selected regions of bioobjects were covered with a Yb-contained crystalline powders. A semiconductor laser diode with wavelength of 980 nm and maximal output power of 1 W was used as radiation source for *in-vivo* experiments. The histological examination of samples was carried out using a method described in [8]. All *in-vivo* experiments were performed at room temperature and in accordance with the provisions of the European Convention for the Protection of Vertebrate Animals used for Experimental and Other Scientific Purposes (Strasbourg, 1986), in compliance with the Directive 2010/63/EU and Declaration of Helsinki.

We have demonstrated that preliminary coating of a biological tissue with Yb-containing nanoparticles provides more pronounced its thermal damage under the 980 nm laser exposure than without coating. The damage degree of the tissue depends on the laser radiation power and the exposure time. Experiments *in-vivo* also allowed to evaluate the dynamics of tissue healing.

This work is financially supported by a grant from the President of the Russian Federation (MK-5500.2021.1.2).

[1] A. Klein, W.B. Umler, M. Landthaler, P. Babilas, Laser thermal therapy of benign skin tumours: review and update, *Int. J. Hyperthermia*, vol. 27(8), pp. 762–770, (2011).

[2] B Azadgoli, RY Baker Laser applications in surgery, *Ann. Transl. Med.*, vol. 4(23), pp. 452 (1-7), (2016).

[3] <http://www.milon.ru/index.phtml?tid=124>

[4] A.V. Belikov, M.L. Gelfond, K.V. Shatilova, S.A. Sosenkova, A.A. Lazareva, 980 nm diode laser with automatic power control mode for dermatological applications, *Proc. of SPIE-OSA Biomedical Optics*, vol. 9542, p. 95420J (1-12), (2015).

[5] W.G. Stebbins, C.W. Hanke, J. Petersen, Novel method of minimally invasive removal of large lipoma after laser lipolysis with 980 nm diode laser, *Dermat. Ther.*, vol. 24, pp.125–130, (2011).

[6] U. Wollina, Three hundred patients treated with ultrapulsed 980 nm diode laser for skin disorders, *Indian J. Dermatol.*, vol. 61(5), pp. 540–544, (2016).

[7] P. A. Ryabochkina, S.A. Khrushchalina, V.M. Kyashkin, A.S. Vanetsev, O.M. Gaitko, N.Yu. Tabachkova, Features of the interaction of near-infrared laser radiation with Yb-doped dielectric nanoparticles, *JETP Letters*, vol. 103(12), pp. 743–751, (2016).

[8] A.N. Belyaev, A.N. Chabushkin, S.A. Khrushchalina, O.A. Kuznetsova, A.A. Lyapin, K.N. Romanov, P.A. Ryabochkina, Investigation of endovenous laser ablation of varicose veins *in vitro* using 1.885- μ m laser radiation, *Lasers Med. Sci.*, vol. 31(3), pp. 503–510, (2016).

B-O-4

Time-resolved analysis of upconversion nanoparticles and photosensitizers fluorescence to determine the type of cell metabolism

D.V. Pominova^{1,2}, I.D. Romanishkin¹, V.Y. Proydakova¹, E.Z. Sadykova², A.V. Ryabova^{1,2}

1 - Prokhorov General Physics Institute of the Russian Academy of Sciences, Moscow, 119991, Vavilova street, 38

2 - National research nuclear university MEPhI, Moscow, 115409, Kashirskoe highway, 31

Main author email address: pominovadv@gmail.com

According to the literature data, metabolic reprogramming occurs in the process of tumor initiation and progression, which leads to reorientation of immune cells to protect the tumor and promotes proliferation, invasion, metastasis, aggressiveness and resistance of tumors to treatment [1, 2]. In this regard, one of the promising approaches to treatment today is an indirect effect on the tumor due to the reverse metabolic reprogramming of immune cells to fight the tumor.

Within the framework of this work, we investigated the possibility of recognizing various populations of macrophage cells, including tumor-associated macrophages, using time-resolved fluorescence spectroscopy. The photosensitizer Chlorin E6 (“Radachlorin”, Rada-Pharma, Russia) and crystalline nanoparticles NaGdF₄ co-doped with Yb³⁺-Er³⁺ rare-earth ions were used as luminescent biomarkers. The nanoparticles were synthesized using solvothermal technique [3]. Particles of a pure hexagonal phase with averaged particle size of 20 nm were obtained. Populations of macrophage cells were obtained from culture of human monocytes THP-1. Differentiation of THP-1 monocytes into adhesive growing macrophages (M0) was achieved by adding 100 nM phorbol-12-myristate-13-acetate (PMA) to the culture for 24 hours. 48 hours after incubation with PMA, human recombinant interferon gamma (IFN- γ , 20 ng / ml, Sigma-Aldrich, USA) and lipopolysaccharide (LPS, 100 ng / ml, Sigma-Aldrich) were added to the medium for M1 polarization or with human recombinant interleukin-4 (IL-4, 20 ng / ml, Sigma-Aldrich, USA) and human recombinant interleukin-13 (IL-13, 20 ng / ml, Sigma-Aldrich, USA) for M2 polarization, respectively. Pro-inflammatory polarization of M1 has antimicrobial and antitumor activity, while M2 polarization, on the contrary, is anti-inflammatory and promotes tumor progression. After polarization, the cells were incubated with chlorin E6 or upconversion nanoparticles for 3, 6, and 24 hours. The cells were then washed with phosphate saline buffer and the accumulation of luminescent markers was analyzed by laser scanning microscopy (Carl Zeiss LSM 710 NLO, Carl Zeiss, Germany). After that, the cells were detached from petridish using trypsin, centrifuged, and the fluorescence lifetime from the cell sediment was measured using a streak camera (C9300-508 and C10627-13, Hamamatsu Photonics, Japan).

It was shown that the use of nanoparticles as luminescent markers provides better accumulation in macrophages due to the size of the nanoparticles. The change in the luminescence lifetime of the used markers inside the macrophages cells was registered. The possibility of determining the polarization of macrophages in vitro according to the data of time resolved fluorescence spectroscopy was demonstrated.

The study was funded by a grant from the Russian Foundation for Basic Research, project 20-02-00928.

[1] E. Persi, M. Duran-Frigola, M. Damaghi, W.R. Roush, P. Aloy, J.L. Cleveland, R.J. Gillies, E. Ruppin, Systems analysis of intracellular pH vulnerabilities for cancer therapy, *Nature Communications*, vol. 9, Article number: 2997, (2018).

[2] D. Chen, J. Xie, R. Fiskesund, W. Dong, X. Liang, J. Lv, X. Jin, J. Liu, S. Mo, T. Zhang, F. Cheng, Y. Zhou, H. Zhang, K. Tang, J. Ma, Y. Liu, B. Huang, Chloroquine modulates antitumor immune response by resetting tumor-associated macrophages toward M1 phenotype, *Nature Communications*, vol. 9, Article number: 873, (2018).

[3] J. Liu, G. Chen, S. Hao, C. Yang, Sub-6 nm monodisperse hexagonal core/shell NaGdF₄ nanocrystals with enhanced upconversion photoluminescence, *Nanoscale*, vol. 9, pp. 91-98 (2017).

B-O-5

Multiphoton microscopy and FLIM metabolic imaging of the hepatocytes during liver regeneration

S.A. Rodimova^{1,2}, D.S. Kuznetsova^{1,2}, N.V. Bobrov^{1,3}, A.A. Gulin^{4,5}, V.V. Elagin¹, M.M. Karabut¹, V.I. Shcheslavskiy^{1,6}, V.E. Zagainov^{1,3}, E.V. Zagaynova^{1,2}.

¹*Privolzhsky research medical university, Institute of Experimental Oncology and Biomedical Technologies, 10/1 Minin and Pozharsky sq., Nizhny Novgorod, Russia*

²*N.I. Lobachevsky Nizhny Novgorod National Research State University, 23 Gagarina ave., Nizhny Novgorod, Russia*

³*The Volga District Medical Centre of Federal Medical and Biological Agency, 14 Ilinskaya, Nizhny Novgorod, Russia*

⁴*Russian Academy of Sciences, N.N. Semenov Federal Research Center for Chemical Physics, 4 Kosygina, Moscow, Russia*

⁵*Lomonosov Moscow State University, Department of Chemistry, 1-3 Leninskiye Gory, Moscow, Russia*

⁶*Becker&Hickl GmbH, Nunsdorfer Ring 7-9, Berlin, Germany*

Surgical liver resection is still the most commonly used method for the treatment of hepatic tumors [1]. However, with a decrease in the regenerative potential of the liver, the risk of developing liver failure during resection increases [2]. Standard clinical methods are not informative enough do not predict the function of the remaining liver [3]. Using modern label-free methods of multiphoton microscopy in combination with FLIM (fluorescence lifetime imaging) and SHG (second harmonic generation) it is possible to assess the metabolic state of hepatocytes during regeneration [4]. In addition, Time-of-Flight Secondary Ion Mass Spectrometry (TOF-SIMS) provides information on the lipid and amino acid composition of liver tissue [8].

The experiments were performed on Wistar rats. Two models were chosen - 70% partial hepatectomy (PH) and 30% PH. Metabolic imaging was performed on 3rd and 7th days after surgery. We presented a separate analysis of NADH and NADPH to assess the contribution of various metabolic pathways as well as synthetic activity in hepatocytes. TOF-SIMS provides data on the lipid and amino acid composition of liver tissue.

As a result, an increase in the contribution of oxidative phosphorylation and biosynthetic processes in hepatocytes, which compensate for the energy consumption of hepatocytes during regeneration, has been shown. Using TOF-SIMS, we observed simultaneous increase in the signals representing triglycerides and cholesterol in the hepatocytes, combined with a decrease in the signals of amino acids peaks.

Thus, the approach used in this work allowed us also to identify the functional state of the liver tissue before and after resection and to determine the range of cellular metabolic heterogeneity for different stages of regeneration. The obtained data will be useful in determining the criteria for intraoperative express assessment of the regenerative potential of the liver after surgery.

The work was supported by the Grant from the Russian Science Foundation №19-15-00263 (metabolic imaging, analysis of FLIM data of liver tissue), and the Grant of the President of the Russian Federation MK-1649.2021.3 (morphological and morphometric study).

[1] Siegel, R. L., Miller, K. D., Jemal, A., Cancer statistics, CA Cancer J Clin, vol. 69, no. 1, pp. 7–34, (2019).

[2] Eshkenazy, R., Dreznik, Y., Lahat, E., Zakai, B. B., Zendel, A., Ariche A., Small for size liver remnant following resection: prevention and management, Hepatobiliary Surg Nutr, vol. 3, no. 5, p. 303, (2014).

[3] De Gasperi, A., Mazza, E., Prosperi, M., Indocyanine green kinetics to assess liver function: ready for a clinical dynamic assessment in major liver surgery? World J Hepatol, vol. 8, no. 7, p. 355, (2016).

[4] Roberts, M. S., Dancik, Y., Prow, T. W., Thorling, C. A., Lin, L. L., Grice, J. E., et al. Non-invasive imaging of skin physiology and percutaneous penetration using fluorescence spectral and lifetime imaging with multiphoton and confocal microscopy, Eur J Pharm Biopharm, vol. 77, no. 3, pp.469–488, (2011).

B-O-6

Visualization of viscous changes of membranes of tumor cell during chemotherapy

L. Shimolina^{1,2}, A. Hlynova¹, M. Lukina¹, N. Ignatova¹, M. Kuimova³, E. Zagaynova^{1,2}, M. Shirmanova¹

1 - Privolzhsky Research Medical University, 603005 Minin and Pozharsky Sq., 10/1, Nizhny Novgorod, Russia

2 - Nizhny Novgorod State University, 603950 Gagarin Av., 23, Nizhny Novgorod, Russia

3 - Imperial College London, Faculty of Natural Sciences, Department of Chemistry, SW7 2AZ, London, United Kingdom

shimolina.l@mai.ru

The microscopic viscosity is one of the key parameters that controls the diffusion rate of molecular species in living cells at the microscopic level. While methods to measure bulk (macroscopic) viscosity of tissues are well developed, imaging viscosity at the microscopic scale remains a challenge, especially *in vivo*. The microscopic viscosity of individual domains of live cells can be determined using fluorescence-based methods, including fluorescent molecular rotors. Molecular rotors are small synthetic viscosity-sensitive fluorophores in which fluorescence parameters, in particular fluorescence lifetime, are strongly correlated to the microviscosity of their immediate environment [1].

Although chemotherapy remains one of the main types of treatment for cancer, treatment failure is a frequent occurrence, emphasizing the need for new approaches to the early assessment of tumor response. Recent studies suggest that tumor response to chemotherapy is determined by not only interaction of the drug with the primary target (e.g. nuclear DNA or microtubules) but can include multiple physiological and physicochemical changes [2]. The study of the effects of chemotherapeutic drugs on the viscosity of living cells is important for better understanding the mechanisms of the drug action and evaluating the effectiveness of therapy.

The present work is aimed at the study of microviscosity of plasma membrane in cancer cells using the fluorescent molecular rotor BODIPY 2 and fluorescence lifetime imaging FLIM microscopy during chemotherapy.

The study was performed on cultured cancer cells CT26 (mouse colorectal cancer) and Hela Kyoto (human cervical cancer). Multiphoton tomograph MPTflex (JenLab, Germany) equipped with a TCSPC-based FLIM module (Becker&Hickl Inc., Germany) was used to detect the fluorescence lifetime of a molecular rotor. Viscosity was measured in the plasma membranes of individual cells using the fluorescent molecular rotor BODIPY2 (ex. 800 nm, em. 409–680 nm)

First, we developed protocol for imaging plasma membrane viscosity of cancer cells *in vitro* at the microscopic level. The developed protocols were applied to measure changes in membrane viscosity during chemotherapy *in vitro* in cell monolayers and 3D spheroids. We showed a significant increase in membrane viscosity in viable cells CT26 and Hela Kyoto in 24 h after cisplatin treatment up to 400 ± 27 cP. At earlier time-points (30-60 min) a tendency to decrease in membrane viscosity was displayed for both cancer cell lines.

The study of the action of drugs on the viscosity of living cells is important for a deep understanding of the mechanisms of their cytotoxicity. This work is supported by the Russian Science Foundation under grant No: 20-14-00111.

[1] Bull J. A. and Kuimova M. K., Chem. Commun., 2013.

[2] Rebillard A. et al. Canc. Res., 2007.

B-O-7

Scaffolds structural heterogeneity influence on the efficiency of stem cells osteogenic differentiation

**Shchechkin I.D.^{1,2}, Rodimova S.A.^{1,2}, Elagin V.V.¹, Karabut M.M.¹, Minaev N.V.³,
Shpichka A.I.³, Timashev P.S.³, Zagaynova E.V.^{1,2}, Kuznetsova D.S.^{1,2}**

1- *Research Institute of Experimental Oncology and Biomedical Technologies, Privolzhsky Research Medical University, Minin and Pozharsky Sq., 10/1, Nizhny Novgorod, Russia;*

2- *Nizhny Novgorod National Research State University N.I. Lobachevsky, Gagarin Ave., 23, Nizhny Novgorod, Russia;*

3- *Institute of Regenerative Medicine, Sechenov University, Trubetskaya st., Moscow, Russia.*

Ilihasa1992@gmail.com

One of the promising approaches for the restoration of damaged tissues is the implantation of mesenchymal stem cells (MSCs) in injuries. However, this approach does not provide complete defect recovery. In this regard, the use of 3D scaffolds is more effective, contributing to a better restoration of the integrity of the damaged tissue. The effectiveness of the recovery process depends on many factors; the effect of the structural heterogeneity of scaffolds on the behavior of cells and tissues at the site of damage has not been fully studied.

The aim of this work was to study the effect of the structure of scaffolds on the efficiency of osteogenic differentiation.

By the method of two-photon polymerization, scaffolds with a homogeneous (equal pore size) and heterogeneous (larger pore size of the central layer of scaffolds) structure were obtained. For each type, cultivation was carried out in a standard medium and medium for osteogenic induction for 28 days. The metabolic status of MSCs was analyzed by fluorescence lifetime imaging microscopy (FLIM) based on the data on the lifetimes of free and bound forms of NAD(P)H, as well as open and closed forms of FAD and their contributions. The efficiency of osteogenic differentiation was confirmed by staining with alizarin red C and fluorometric analysis for the content of secreted alkaline phosphatase (ALP).

Staining with alizarin red showed that MSCs cultured on homogeneous scaffolds in a standard medium do not proceed to spontaneous differentiation, while single differentiated cells were observed on heterogeneous scaffolds. When cultivated in an osteogenic medium, scaffolds of both types have the same red coloration, which indicates an effective induction of osteogenic differentiation. Analysis for ALP showed a significant increase on day 28 for MSCs on heterogeneous scaffolds, which indicates a greater efficiency of osteogenic differentiation. The FLIM method showed an increase in the contributions of the bound form of NAD(P)H and the closed form of FAD in the osteogenic medium, the efficiency of differentiation for heterogeneous scaffolds was higher. An increase in the contributions of the bound form of NAD(P)H and the closed form of FAD was also observed for heterogeneous scaffolds and in a standard medium, which indicates the induction of spontaneous differentiation. It is worth noting that the results of the analysis of standard methods and methods of fluorescence bioimaging agreed with each other.

Acknowledgments. This work was supported by the Russian Science Foundation, grant no. 19-75-10008.

B-O-8**Histological and in situ microscopic observation of femtosecond laser induced incisions in the crystalline lens****A. Talbi^{1,2}, O. Ben Moussa¹, G. Thuret¹, P. Gain¹, X. Sedao² and C. Mauclair²**

1. Laboratory "Biology, Engineering, and Imaging of Corneal Graft," BiiGC, Faculty of Medicine, University of Saint Etienne, France.

2. Laboratoire Hubert Curien, Université de Lyon, Université Jean Monnet, Saint Etienne, France.

Presbyopia is the gradual loss of the eye's ability to focus on nearby objects. It is caused by the degradation of accommodation capacity of the crystalline lens as part of human ageing process. There is no treatment for presbyopia but only solutions to compensate for the loss: wearing corrective eyeglasses or contact lenses, undergoing refractive surgery, or presbyopic clear lens exchange with a multifocal intra ocular lens. A new approach to restore the lens accommodation capacity is based on ultrafast laser treatment by generating microincisions, micro-cavitations, photo-chemical and/or photo-biological reactions [1-3]. This work is part of PresbInnov EAgLE project (Acronym for Eye Anterior segment Laser Engineering) and aims at investigating the femtosecond laser-lens interaction. More precisely, we aim at studying the lens behavior under laser irradiation in order to optimize the laser parameters allowing the generation of micro-bubbles/incisions, melting and/or ablation of lens tissue. To achieve this goal, we propose to carry out experiments based mainly on histological observations of laser induced-spots (ex vivo) and pump-probe experiments offering the possibility to visualize the laser-lens interaction in real time. Our results showed that lenses can have very different responses, depending on the laser energy, such as bubbles/cavitation generation and melting of lens fibers (fig .1). In the case of generated bubbles, a phenomenon of resorption over time was also noticed.

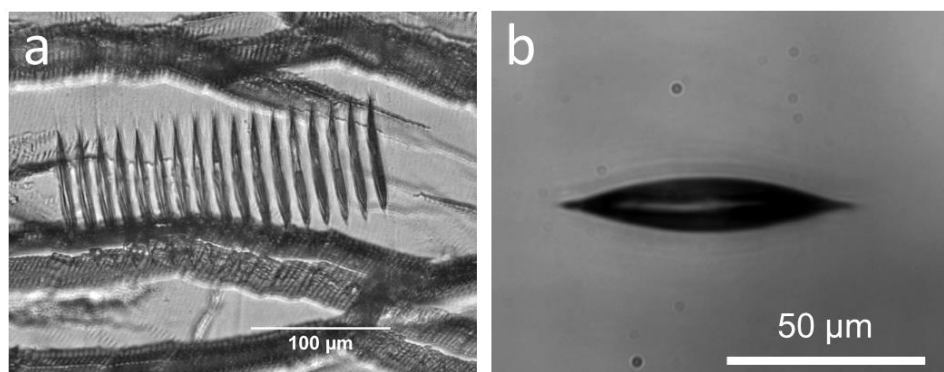


Fig. 1 a) Histological observation of fs laser induced spots on pig-lens and b) In situ microscopy image of laser induced bubble inside pig-lens.

References

- [1] T. Ripken, U. Oberheide, M. Fromm, S. Schumacher, G. Gerten, H. Lubatschowski, fs-Laser induced elasticity changes to improve presbyopic lens accommodation. *Graefe's Archive for Clinical and Experimental ophthalmology*, 246(6), 897–906, 2007.
- [2] O. Stachs, S. Schumacher, M. Hovakimyan, M. Fromm, A. Heisterkamp, H. Lubatschowski and R. Guthoff, Visualization of femtosecond laser pulse-induced microincisions inside crystalline lens tissue, *J Cataract Refract Surg*; 35:1979–1983, (2009).
- [3] S. Schumacher, U. Oberheide, M. Fromm, T. Ripken, W. Ertmer, G. Gerten and H. Lubatschowski, Femtosecond laser induced flexibility change of human donor lenses, *Vision Research*, 49(14), 1853–1859, (2009).

B-O-9

Raman characterization of aqueous solutions of diols

V.S. Novikov¹, K.A. Prokhorov¹, P.V. Ivchenko², E.A. Sagitova¹, V.V. Kuzmin¹,
L.Yu. Ustynyuk², G.Yu. Nikolaeva¹

1-Prokhorov General Physics Institute of the Russian Academy of Sciences, Vavilov Str. 38, 119991 Moscow, Russia

2-Department of Chemistry, M.V. Lomonosov Moscow State University, Leninskie Gory 1-3, 119991 Moscow, Russia

Aqueous solutions of ethylene glycol (EG, HO-CH₂-CH₂-OH) and 1,3-propylene glycol (1,3-PG, HO-CH₂-CH₂-CH₂-OH) are widely used as antifreezes in numerous applications. The relative contents of the diol and water determine the structure and physicochemical properties of the solutions, including the freezing point. Raman spectroscopy is an effective tool to evaluate the chemical composition and conformational order, and to characterize the intermolecular interactions of these polar molecules. The aims of this work were comparative Raman study of aqueous solutions of EG and 1,3-PG and the elaboration of Raman methods for their structural characterization.

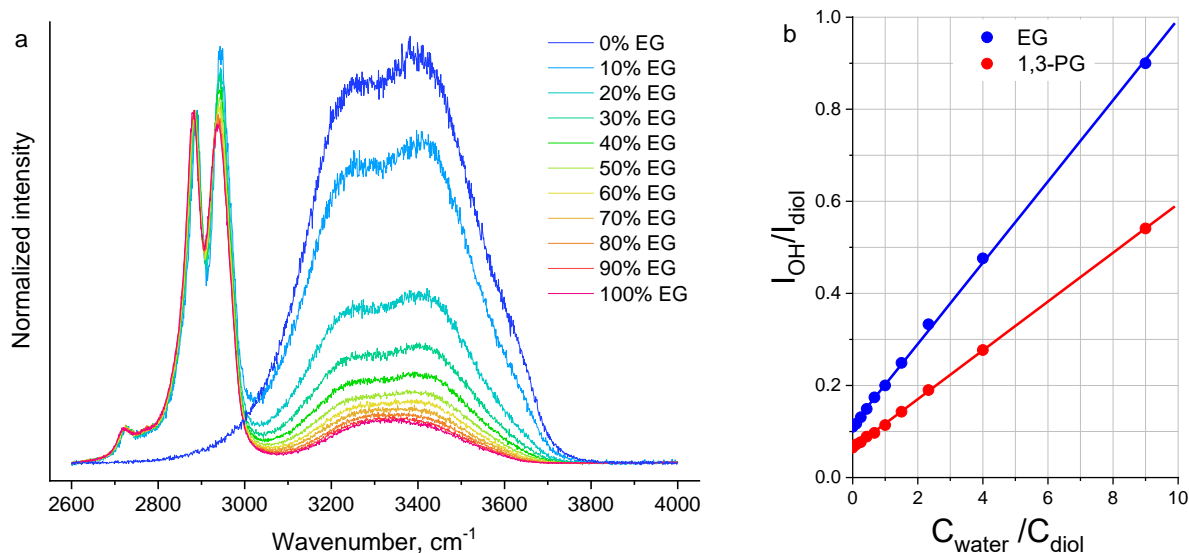


Figure 1. Raman spectra of aqueous solutions of EG with various EG mole contents (a) and ratios of the intensities of the OH stretching band and the selected diol reference bands (the EG band at 2880 cm⁻¹ or the 1,3-PG band at 2920 cm⁻¹) (b).

The Raman spectra of EG, 1,3-PG and water contain the O-H stretching band, extended from 2800 to 3800 cm⁻¹. Intensity of this band in the Raman spectra of aqueous solutions (Figure 1a) depends strongly on the diol content. We found out that the ratios of the intensities of the OH stretching band and the selected reference diol bands are the linear functions of the ratio of the contents of the solution components (Figure 1b) and, thus, can be used to evaluate the chemical compositions of these binary solutions.

Changes of the solution Raman spectra in the fingerprint region were insignificant in the full range of the diol concentrations. In particular, the diol bands at about 800 cm⁻¹, which are the markers of *gauche*-conformers in the O-C-C-O and O-C-C-C-O backbones of the diols [1], have similar intensities and peak positions independent on the diol concentration. Thus, there are no noticeable changes in the diol conformational compositions with dissolving in water.

This work was funded by the Russian Foundation for Basic Research (project No. 19-02-00931). We are grateful to the Joint Supercomputer Center of the RAS for the possibility of using their computational resources for our calculations.

[1] V.V. Kuzmin, V.S. Novikov, E.A. Sagitova, L.Y. Ustynyuk, K.A. Prokhorov, P.V. Ivchenko, G.Y. Nikolaeva, Correlations among the Raman spectra and the conformational compositions of ethylene glycol, 1,2- and 1,3-propylene glycols, J. Mol. Struct. (2021) 130847. <https://doi.org/10.1016/j.molstruc.2021.130847>.

B-O-10

Optical properties of functionalized microstructured fibers and their sensing capabilities

Timur Ermatov^{1,*}, Roman E. Noskov^{2,3}, Julia S. Skibina⁴, Valery V. Tuchin^{5,6,7}, Dmitry A. Gorin¹

1 - Skolkovo Institute of Science and Technology, 3 Nobelya str., Moscow 121205, Russia

2 - Department of Electrical Engineering and 3 - Light-Matter Interaction Centre, Tel Aviv University, Ramat Aviv, Tel Aviv 69978, Israel

4 - SPE LLC Nanostructured Glass Technology, 101 50 Let Oktjabrja, 410033 Saratov, Russia

5 - Saratov State University, 83 Astrakhanskaya str., Saratov 410012, Russia

6 - Tomsk State University, 36 Lenin's av., Tomsk 634050, Russia

7 - Institute of Precision Mechanics and Control of the Russian Academy of Sciences, 24 Rabochaya str., Saratov 410028, Russia

**The corresponding author, e-mail: timur.ermatov@skolkovotech.ru*

Microstructured optical fiber-based sensors (MOF) have been widely developed finding numerous applications in various fields of photonics, biotechnology, and medicine [1]. High sensitivity to the refractive index variation, arising from the strong interaction between a guided mode and an analyte in the test, makes MOF-based sensors ideal candidates for chemical and biochemical analysis of solutions with small volume and low concentration [2,3]. Functional nanocoatings of microstructured optical fibers have extended the domain of their applications to biosensing and photochemistry. Here, we review the modern techniques used for the modification of the fiber's structure, which leads to an enhanced detection sensitivity, as well as the surface functionalization processes used for selective adsorption of target molecules. Novel functionalized MOF-based devices possessing these unique properties, emphasize the potential applications for fiber optics in the field of modern biophotonics, such as remote sensing, thermography, refractometric measurements of biological liquids, detection of cancer proteins, and concentration analysis. In this work, we discuss the approaches used for the functionalization of MOFs, with a focus on potential applications of the produced structures.

[1] Ermatov, T., Skibina, J. S., Tuchin, V. V. & Gorin, D. A. Functionalized Microstructured Optical Fibers: Materials Methods Applications. *Materials* **13**, 921 (2020).

[2] Ermatov, T. *et al.* Multispectral sensing of biological liquids with hollow-core microstructured optical fibres. *Light: Science & Applications* **9**, 173 (2020).

[3] Perevoschikov, S. *et al.* Light guidance up to 6.5 μm in borosilicate soft glass hollow-core microstructured optical waveguides. *Optics Express* **28**, 27940–27950 (2020).

LASER SYSTEMS AND MATERIALS

LS-I-1

Upconversion pumping of continuous-wave tunable Tm³⁺-doped KY₃F₁₀ lasers near 2 and 2.3 μm

**Alphan Sennaroglu^{1,2}, Yağız Morova^{1,3}, Eylül Nihan Kamun^{1,3}, Mauro Tonelli⁴,
and Valentin Petrov⁵**

¹*Laser Research Laboratory, Departments of Physics and Electrical-Electronics Engineering, Koç University, Istanbul 34450, Turkey*

²*Koç University Surface Science and Technology Center (KUYTAM), Rumelifeneri, Istanbul 34450, Turkey*

³*Department of Physics, Istanbul Technical University, Istanbul 34469, Turkey*

⁴*Mega Materials srl and Dipartimento di Fisica dell' Università di Pisa, Largo B. Pontecorvo, 3, Pisa-.Italy*

⁵*Max Born Institute for Nonlinear Optics and Short Pulse Spectroscopy, Max-Born-St. 2a, 12489 Berlin, Germany*

Upconversion pumping can be employed to excite the 2-mm and 2.3-mm laser transitions of the Tm³⁺ ion. In this work, we report on the use of widely available 1064-nm Yb-fiber lasers for the upconversion pumping of the Tm³⁺-doped KY₃F₁₀ laser host. The presentation will focus on the design and operation of the Tm³⁺-doped KY₃F₁₀ laser upconversion pumped at 1064 nm, investigation of the nonlinear absorption characteristics of the gain medium, and measurement of the power efficiency as well as tunability near 2 mm and 2.3 mm.

LS-I-2

Rare earth doped selenide glasses as 5-6 μm laser materials

S.E.Sverchkov¹, B.I.Denker¹, B.I.Galagan¹, V.V.Koltashev³, V.G.Plotnichenko³, G.E.Snopatin², M.V.Sukhanov², A.P.Velmushov², M.P.Frolov⁴, P.Fjodorov^{4,5}, S.O.Leonov^{4,6}

1- Prokhorov General Physics Institute, Russian Academy of Sciences, Vavilova str.38, Moscow, Russia

2- Devyatikh Institute of Chemistry of High-Purity Substances, Russian Academy of Sciences, Tropinina 49, Nizhny Novgorod, Russia

3- Dianov Fiber Optics Research Center, Russian Academy of Sciences, Vavilova 38, Moscow, Russia

4- Lebedev Physical Institute, Russian Academy of Sciences, Leninsky prosp. 53, 19991, Russia

5- Institute for Combustion and Gas Dynamics – Reactive Fluids, University of Duisburg-Essen, Lotharstr. 1, 47057 Duisburg, Germany

6- Bauman Moscow State Technical University, 2nd Baumanskaya str. 5, 105005, Moscow, Russia

glasser@Lst.gpi.ru

Chalcogenide glasses for long attracted attention as potential hosts for mid-infrared lasers for their high infrared transparency and low multiphonon quenching rate of mid-infrared rare earth transitions. Nevertheless, the uncontrollable impurities in the glasses impeded the creation of such lasers. The latest achievements in fabrication of ultrapure rare earth doped chalcogenide glasses and fibers have made the creation of such lasers realistic. Samples of $\text{Ge}_{36}\text{Ga}_5\text{Se}_{59}$ glass activated by Ce^{3+} , Pr^{3+} or Tb^{3+} ions (up to 10^{20} cm^{-3}) were prepared. All these ions have 5-6 μm radiative transitions (Fig.1, Table 1) ending on the ground level with luminescence quantum yield in the investigated glass $>80\%$.

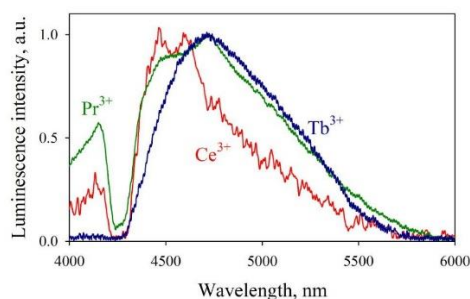


Fig.1. Mid-IR emission of Ce^{3+} , Pr^{3+} and Tb^{3+} ions

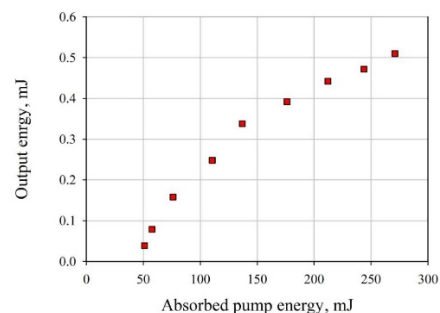


Fig.2. Mid-IR Ce^{3+} laser action in selenide glass

In the lasing experiments several pulsed solid-state lasers (Table 1) were used for bulk glass samples pumping. The Tb-doped fiber was pumped by CW holmium fiber laser. Fig. 2 shows an example of mid-infrared Ce^{3+} laser input-output characteristics.

Table 1. Pump and lasing wavelengths of Ce^{3+} , Pr^{3+} and Tb^{3+} in $\text{Ge}_{36}\text{Ga}_5\text{Se}_{59}$ glass.

Active ion and transition	Pump source (wavelength in μm)	Configuration	Lasing wavelengths, μm
Ce^{3+} , ${}^2\text{F}_{7/2} \rightarrow {}^2\text{F}_{5/2}$	Fe:ZnSe laser (4.08)	1-3 cm long bulk	5.1-5.52
Pr^{3+} , ${}^3\text{H}_5 \rightarrow {}^3\text{H}_4$	Er:glass laser (1.54)		5.5-5.9
	Cr:Tm:Ho YAG laser (2.08)		5.6-5.8
Tb^{3+} , ${}^7\text{F}_5 \rightarrow {}^7\text{F}_6$	Er:YAG laser (2.94)	20 cm long fiber	4.9-5.5
	Ho: fiber laser (1.98)		5.37-5.39

The investigations showed, that the attained purity level and optical quality of the doped selenide glasses enables to obtain laser action at 5-6 μm microns in all three investigated active ions.

Funding. Russian Foundation for Basic Research (18-29-20079); Russian Academy of Sciences (Program No. 5); Russian Science Foundation (20-79-00155).

LS-I-3

Waveguide Lasers Based on Fluoride Films Grown by Liquid Phase Epitaxy (Invited)

Pavel Loiko^{1,*}, Gurvan Brasse¹, Alain Braud¹, Jean-Louis Doualan¹, and Patrice Camy¹

1–Centre de Recherche sur les Ions, les Matériaux et la Photonique (CIMAP), UMR 6252 CEA-CNRS-ENSICAEN, Université de Caen Normandie, 6 Boulevard Maréchal Juin, 14050 Caen Cedex 4, France

*pavel.loiko@ensicaen.fr

Fluoride crystals are attractive for doping with rare-earth ions (RE^{3+}) for laser applications in the near- and mid-infrared spectral ranges. They combine good thermal properties, broadband transparency, low refractive index and low phonon energies with suitable spectroscopic properties of the RE^{3+} ions (in particular, long emission lifetimes and weak non-radiative path). RE^{3+} -doped fluoride materials represent a promising platform for waveguide (WG) lasers. Liquid Phase Epitaxy (LPE) is a well-known method for the growth of single-crystalline thin-films of high optical quality with a great potential for WG applications. In the present work, we review of recent results on WG lasers based on fluoride thin-films grown by LPE.

Single-crystalline thin films of LiYF_4 [1] and CaF_2 [2] doped with various RE^{3+} ions (Yb^{3+} , Tm^{3+} , $\text{Tm}^{3+}/\text{Ho}^{3+}$, Er^{3+} , etc.) were grown on bulk oriented undoped substrates by LPE using the following solvents: LiF (for LiYF_4) and CaCl_2 , LiF and NaF (for CaF_2). For LiYF_4 , the RE^{3+} doping level was up to 20 at.%, the thickness of the films was up to $\sim 200 \mu\text{m}$, the refractive index contrast was about 2×10^{-3} and the measured passive losses were down to 0.1 dB/cm. The orientation of the films and low lattice mismatch were confirmed by single-crystal XRD. The uniform distribution of RE^{3+} ions was confirmed by EDX element mapping.

Planar and channel WGs were fabricated. To produce the surface channel (ridge) WGs, the epitaxies were subjected to precision diamond saw dicing, Fig. 1(a). For $\text{Tm}:\text{LiYF}_4 / \text{LiYF}_4$ epitaxies, ridge WGs with a square cross-section of $\sim 30 \times 30 \mu\text{m}^2$ were fabricated in this way.

The laser operation was achieved both in the planar and channel WG geometry. The following emission ranges were studied: $\sim 1 \mu\text{m}$ ($\text{Yb}:\text{CaF}_2$), $\sim 1.9 \mu\text{m}$ ($\text{Tm}:\text{LiYF}_4$), $\sim 2.1 \mu\text{m}$ ($\text{Tm},\text{Ho}:\text{LiYF}_4$), $\sim 2.3 \mu\text{m}$ ($\text{Tm}:\text{LiYF}_4$), $\sim 2.8 \mu\text{m}$ ($\text{Er}:\text{LiYF}_4$). The results on an in-band pumped ridge $\text{Tm}:\text{LiYF}_4$ waveguide laser are shown in Fig. 1(b,c) for example. In the continuous-wave regime, this laser generated a maximum output power of 2.05 W at 1881 nm with a slope efficiency of 78.3%, a linearly polarized emission (π), a single-mode output and a laser threshold of only 12 mW. The results on passively Q-switched operation of Tm waveguide lasers will be also presented.

The developed family of low-loss fluoride waveguides is of practical importance for further design of integrated light sources generating ultrashort pulses at high repetition rates (GHz-range), as well as potential sensing applications.

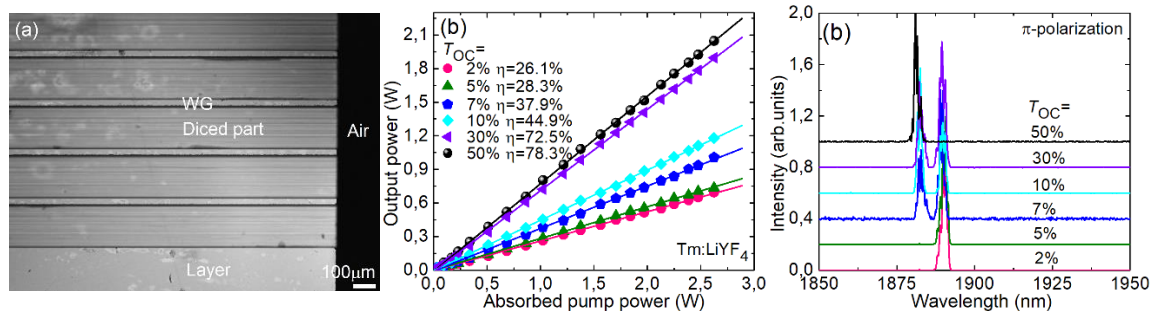


Fig. 1. Channel (ridge) waveguides based on $\text{Tm}:\text{LiYF}_4$ thin films grown by LPE and microstructured by diamond saw dicing: (a) confocal microscope image (top view); (b) input-output dependences, η – slope efficiency; (c) typical spectra of laser emission, the laser polarization is π . In-band pumping, $\lambda_p = 1679 \text{ nm}$.

[1] P. Loiko, R. Soulard, G. Brasse, J.-L. Doualan, B. Guichardaz, A. Braud, A. Tyazhev, A. Hideur, P. Camy, Watt-level $\text{Tm}:\text{LiYF}_4$ channel waveguide laser produced by diamond saw dicing, *Opt. Express*, vol. 26, pp. 24653-24662 (2018).

[2] P. Loiko, R. Soulard, E. Kifle, L. Guillemot, G. Brasse, A. Benayad, J.-L. Doualan, A. Braud, M. Aguiló, F. Díaz, X. Mateos, P. Camy, Ytterbium calcium fluoride waveguide laser, *Opt. Express*, vol. 27, pp. 12647-12658 (2019).

LS-I-4

Investigations on High Power Oscillators and Amplifiers Based on Birefringent Yb:LiLuF₄ Single Crystal Fibers Grown by the Micro Pulling Down

S. Pizzurro¹, M. Tonelli², A. Agnesi^{1,3}, **F. Pirzio**¹

1- Dip. di Ingegneria Industriale e dell'Informazione, University of Pavia, via Ferrata 5, IT-27100, Pavia, Italy

2- Mega Materials s.r.l and Dip. di Fisica, University of Pisa, Largo B. Pontecorvo 3, IT-56127 Pisa, Italy

3- Bright Solutions s.r.l., Via degli Artigiani 27, IT-27010 Cura Carpignano (PV), Italy

e-mail: federico.pirzio@unipv.it

Single crystal fibers (SCF) are a very attractive solution for power scaling of solid-state lasers owing to the convenient distribution of heat load along a relatively long, low-doped, thin crystal with a favorable surface-to-volume ratio. Micro pulling down (μ -PD) growing technique is particularly suited to the realization of SCFs. Indeed, in addition of been faster and cheaper than the traditional Czochralski method, it allows to directly obtain thin (down to ≤ 1 mm) and long (several cm) SCFs with no additional processing of the grown crystal. To now, μ -PD technique was exploited mainly for cubic crystals, especially YAG, with remarkable results in particular with Yb³⁺ doping [1, 2]. Recently, we demonstrated for the first time successful growth of a birefringent Yb:LiLuF₄ SCF (see Fig. 1 (a)) [3]. Birefringent Yb-doped fluoride SCFs, are particularly interesting for several reasons, e.g., they do not suffer of beam quality degradation at high thermal load due to depolarization, they benefit of the weaker thermal lens (and associated aberrations) of fluoride materials, and if pumped at 976 nm with commercial high-power laser diodes, they allow small quantum defect with laser emission at 1020 nm.

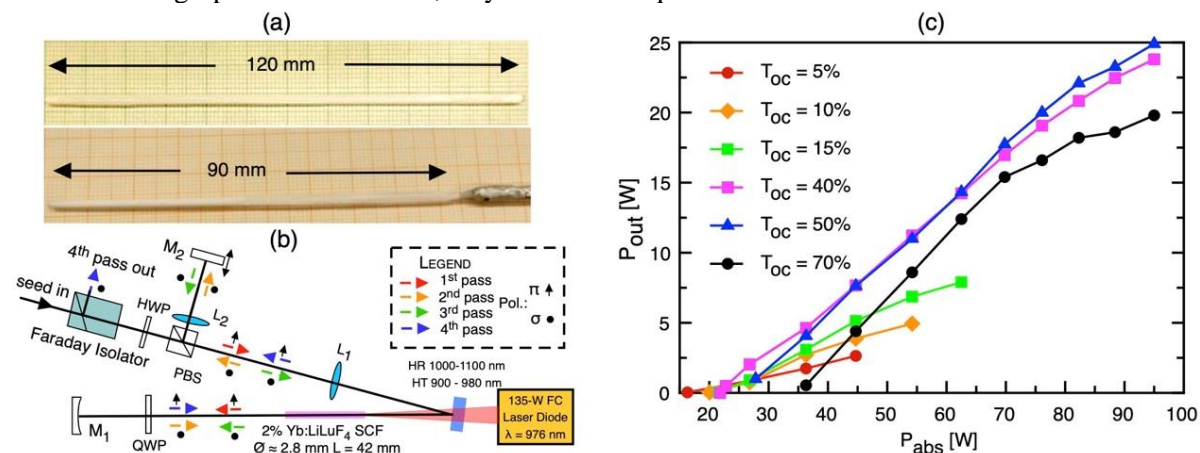


Fig. 1. (a) Examples of grown Yb:LLF SCFs; (b) Setup for multi-pass amplification experiments; (c) Laser oscillator best performance.

In this talk, we will present our latest results obtained both in multi-pass amplification (setup shown in Fig. 1 (b)) and laser oscillation, by pumping a 2%-doped, 42-mm long Yb:LiLuF₄ SCF with a 135-W laser diode at 976 nm. For the amplification experiments we employed either a 1-W cw seeder, or a 150- μ J, 100-ns PQS seeder at 5 kHz repetition rate. Four passes small signal gain $G_0 \sim 40$ was achieved at ~ 85 W of absorbed pump power with a maximum output power of 8 W in cw experiments and a 1-mJ amplified pulse energy, when seeding with the PQS laser. In both cases, diffraction limited beam quality was obtained at the maximum pump power. In laser oscillator experiment, we achieved up to 25 W (see Fig. 1(c)), with $M^2 \sim 2$ and $\sim 40\%$ slope efficiency in a simple confocal resonator layout.

[1] X. Délen, S. Piehler, J. Didierjean, A. Voss, M. Abdou Ahmed, T. Graf, F. Balembois, and P. Georges, "250 W single crystal fiber Yb:YAG laser," *Opt. Lett.* **37**, pp. 2898–2900, (2012).

[2] F. Lesparre, J. T. Gomes, X. Délen, I. Martial, J. Didierjean, W. Pallmann, B. Resan, M. Eckerle, T. Graf, M. A. Ahmed, F. Druon, F. Balembois, and P. Georges, "High-Power Yb:YAG Single-Crystal Fiber amplifiers for femtosecond lasers in cylindrical polarization," *Opt. Lett.* **40**, pp. 2517–2520, (2015).

[3] F. Pirzio, S. Jun, S. Tacchini, A. Di Lieto, G. Piccinno, M. Tonelli, and A. Agnesi, "Multi-watt amplification in a birefringent Yb:LiLuF₄ single crystal fiber grown by micro-pulling-down," *Opt. Lett.* **44**, pp. 4095–4098, (2019).

LS-I-5

High Efficiency In-Band Fiber-Laser Pumped 2- μm Lasers Based on Tm-doped Ceramics and Crystals and Mid-IR Conversion of Their Radiation

O.L. Antipov

*Institute of Applied Physics of the Russian Academy of Sciences, Nizhny Novgorod 603155, Russia
antipov@ipfran.ru*

Solid-state lasers based on Tm-doped materials and operating at wavelengths near 2.0 μm have a variety of applications in medicine, materials processing, environmental monitoring and pumping of lasers or mid-IR optical parametric oscillators (OPOs) [1]. Specifically, the high-power and high-energy 2- μm Q-switched lasers are promising pump sources for the mid-IR lasers based on Cr^{2+} ions and OPOs. The in-band pumping of a ${}^3\text{H}_6$ - ${}^3\text{F}_4$ Tm $^{3+}$ -ion transition enables the high-efficiency and high-power operation of Tm $^{3+}$ -doped lasers at 1900-2100 nm with a low quantum defect [2-4].

This report gives an overview of the recent studies of Tm-doped solid-state lasers based on Tm $^{3+}$:Lu $_2$ O $_3$ or Tm $^{3+}$:Y $_2$ O $_3$ ceramics and Tm $^{3+}$:YAP crystals in-band pumped by a fiber laser at 1670 nm and their frequency conversion to the mid-IR in Cr-doped crystals (Cr $^{2+}$:ZnSe or Cr $^{2+}$:CdSe) and mid-IR OPOs based on periodically poled structures (MgO:LiNbO $_3$ or KTA) or ZnGeP $_2$ crystals [5,6].

Two cavity configurations of the solid-state lasers based on Tm $^{3+}$:Lu $_2$ O $_3$ and Tm $^{3+}$:Y $_2$ O $_3$ ceramics or Tm $^{3+}$:YAP crystals were studied: a two-mirror linear configuration or a three-mirror L-shaped cavity configuration. The Raman-shifted Er-fiber laser at 1670 nm with the CW output of up to 50 W was used as an end-pumping source in both cavity configurations. The high efficiency and high average power lasing at 1890-2080 nm was achieved in the CW or Q-switched regimes. A repetitively-pulsed Q-switched operation was obtained by using the acousto-optical modulators in a linear cavity or by inserting the Cr $^{2+}$:ZnSe saturable absorbers into the output leg of an L-shaped cavity.

The Tm $^{3+}$:Lu $_2$ O $_3$ ceramic laser output was used to pump the Cr-doped single- or poly-crystals (Cr $^{2+}$:ZnSe or Cr $^{2+}$:CdSe). A high conversion efficiency to 2300-2600 nm was achieved in the Cr $^{2+}$:ZnSe laser both in the CW and repetitively-pulsed regimes, while a longer-wavelength 2600-2800 nm output was demonstrated in the single-crystalline Cr $^{2+}$:CdSe laser.

Finally, the mid-IR frequency conversion of Tm $^{3+}$:YAP was achieved in OPOs based on periodically poled MgO:LiNbO $_3$ or KTA. The Tm $^{3+}$:Lu $_2$ O $_3$ ceramic lasers were used as the pump sources for the mid-IR OPOs based on the ZnGeP $_2$ crystals or the periodically poled MgO:LiNbO $_3$ structures.

References:

- [1] K. Scholle, S. Lamrini, P. Koopmann, P. Fuhrberg in *Frontiers in Guided Wave Optics and Optoelectronics* (Croatia, InTech, 2010).
- [2] O. Antipov, A. Novikov, S. Larin, I. Obronov, "Highly efficient 2 μm CW and Q-switched Tm $^{3+}$: Lu $_2$ O $_3$ ceramics lasers in-band pumped by a Raman-shifted erbium fiber laser at 1670 nm," *Opt. Letters*, v. 41, 2298-301 (2016).
- [3] O.L. Antipov, Yu.A. Getmanovskiy, A.A. Dobrynin, H. T. Huang, D.Y. Shen, J. Wang, S.S. Balabanov, "High-efficiency CW and passively Q-switched operation of a 2050 nm L-shaped Tm $^{3+}$:Y $_2$ O $_3$ ceramic laser in-band fiber-laser pumped at 1670 nm," *Applied Physics B*, v. 127, 77(7) (2021)
- [4] O.L. Antipov, Yu.A. Getmanovskiy, A.A. Dobrynin, et al, "Low-Quantum-Defect CW and Q-Switched Operation of a Tm $^{3+}$:YAP Laser with the In-Band Fiber-Laser Pumping," in *Technical digest of CLEO'Europe 2021*, paper CA-P.17.
- [5] O.L. Antipov, I.D. Eranov, M.P. Frolov, et al, "2.92 μm Cr $^{2+}$:CdSe single crystal laser pumped by a repetitively pulsed Tm $^{3+}$: Lu $_2$ O $_3$ ceramics laser at 2.066 μm ," *Laser Physics Letters*, v. 12, N4, 045801 (2015).
- [6] D.B. Kolker, O.L. Antipov, S.V. Larin, L.I. Isaenko, V.N. Vedenyapin, A.R. Ahmatkhanov, V.Ya. Shur, "Mid-IR optical parametric oscillator based on periodically poled LiNbO $_3$ pumped by Tm $^{3+}$:Lu $_2$ O $_3$ ceramic laser," *Atmospheric and Oceanic Optics*, v. 32, N6, 724-729 (2019).

LS-I-6

NIR Fluorescence Concentration Self-Quenching and Quenching by OH⁻ Acceptors in Aqueous Colloids of Nd³⁺ Doped Fluoride Nanocrystals

Yu.V. Orlovskii^{1,2}, **A.V. Popov**¹, **E.O. Orlovskaya**¹, **A.S. Vanetsev**^{1,2}

1- Prokhorov General Physics Institute RAS, 38 Vavilov street, Moscow, Russia

2- Institute of Physics, University of Tartu, 1 Ostwald street, Tartu, Estonia

orlovski@lst.gpi.ru

Aqueous colloidal solutions of Nd³⁺: LaF₃ nanocrystals (NCs) synthesized using “green” hydrothermal - microwave treatment (HTMW) have established themselves as a promising fluorescent agent for near IR imaging in the first biological window (750 – 950 nm) [1,2], due to their higher temporal stability and lower fluorescence quenching in comparison with NCs synthesized by the traditional co-precipitation (CO) method [3]. Two processes control the fluorescence quenching in NCs synthesized by water-based methods: 1) Nd³⁺-Nd³⁺ self-quenching and 2) quenching caused by OH⁻ molecular groups located in their volume.

The main issue considered in the report is what are the main regularities and features of these processes in NCs, and why can we control the fluorescence quenching using a specific synthesis method and a specific crystal matrix for doping with Nd³⁺?

At first, when choosing a synthesis method, we connected fluorescence-quenching processes with defects in the crystal structure of nanoparticles. These defects are

- 1) Inhomogeneity of dopant distribution over the La³⁺ sites in the volume of the synthesized NCs, leading to the formation of closely spaced Nd³⁺ ions (pairs), which exhibit strong fluorescence self-quenching;
- 2) The arrangement of OH⁻ molecular groups in the volume of the NPs, which enhances the quenching of Nd³⁺ fluorescence and manifests itself in a decrease in the relative quantum yield and fluorescence brightness.

As a result, we found that a higher temperature of the reaction mixture for the HTMW synthesis method as compared to CO leads to a more uniform distribution of the Nd³⁺ dopant over La³⁺ sites and a lower concentration of OH⁻ acceptors in the NC volume, which leads to a higher brightness of NCs fluorescence in an aqueous colloid.

The effect of oven modification for HTMW treatment on fluorescence quenching will also be discussed.

In addition, we have established simple criteria for choosing a crystal matrix for doping with Nd³⁺ ions in the synthesis of aqueous colloidal solutions of fluoride nanocrystals using them as luminescent probes for obtaining images in the first biological window, which is most convenient for recording luminescence [4]. This is a large ratio of intensity parameters Ω_4/Ω_6 , used in the Judd-Ofelt theory to calculate the probability of radiative transitions, which increases the luminescence branching coefficient β at the ⁴F_{3/2} → ⁴I_{9/2} transition in the first biological window. A low value of the intensity parameter Ω_6 weakens the Nd-Nd luminescence self-quenching and the Nd-OH- quenching due to the weaker dipole-dipole ion-ion interaction. The hypothesis was tested on concentration series of aqueous colloidal solutions of Nd³⁺: LaF₃ and Nd³⁺: KY₃F₁₀ NCs, synthesized by HTMW treatment with PVP as a biocompatible surfactant. We found that due to the higher Ω_4/Ω_6 ratio and the lower value of Ω_6 in the Nd³⁺: LaF₃ compared to Nd³⁺: KY₃F₁₀ NCs, the fluorescence branching ratio at the ⁴F_{3/2} → ⁴I_{9/2} transition significantly increases for the former, while the fluorescence brightness increases four times. The latter is associated with a weaker donor-acceptor interaction, which depends on the specific crystal structure.

- [1] U. Rocha, J. Hu, E. M. Rodríguez, A.S. Vanetsev, M. Rähn, V. Sammelselg, Yu.V. Orlovskii, J. García Solé, D. Jaque, D.H. Ortgies, *Small*, 12, pp. 5394 – 5400 (2016).
- [2] D.H. Ortgies, F.J. Teran, U. Rocha, L. de la Cueva, G. Salas, D. Cabrera, A.S. Vanetsev, M. Rähn, V. Sammelselg, Yu.V. Orlovskii and D. Jaque, *Advanced Functional Materials*, 28(11) p. 1704434 (2018).
- [3] A. Vanetsev, K. Kaldvee, L. Puust, K. Keevend, A. Nefedova, S. Fedorenko, A. Baranchikov, I. Sildos, M. Rähn, V. Sammelselg, Yu. Orlovskii, *ChemistrySelect*, 2, pp. 4874 – 4881 (2017).
- [4] Yu.V. Orlovskii, A.V. Popov, E.O. Orlovskaya, A.S. Vanetsev, E.A. Vagapova, M. Rähn, V. Sammelselg, I. Sildos, A.E. Baranchikov, P.V. Grachev, V.B. Loschenov, A.V. Ryabova, *Journal of Alloys and Compounds*, 756, pp. 182 – 192 (2018).

LS-I-7

Yb:LuAP Laser Crystal for Mode-Locked Lasers and Chirped Pulse Regenerative Amplifiers

**V.E. Kisel¹, A.S. Rudenkov¹, A.S. Yasukevich¹,
K.L. Hovhannesian², A.G. Petrosyan², and N.V. Kuleshov¹**

1 - Center for Optical Materials and Technologies, Belarusian National Technical University, Minsk, Belarus

2 - Institute for Physical Research, National Academy of Sciences, Ashtarak-2, Armenia

E-mail: VEKisel@bntu.by

We report on recent results deal with spectroscopic properties and laser performance of novel laser media based on Yb-doped aluminum and lutetium perovskite crystals. Unique spectroscopic properties of trivalent ytterbium ions of these host media make these crystals good candidates for active elements of picosecond and femtosecond solid-state laser systems. The features of soliton and non-soliton mode-locking were studied using SESAMs as a saturable absorber. Maximum average output power of 7W with pulse duration of 130fs and 28.1% optical efficiency were obtained in soliton mode-locking regime. 90-fs pulses were generated with reduced to 2.9 W output power. Average output power up to 12W with 2ps pulse duration and 38% optical efficiency was obtained in non-soliton mode-locking regime with extremely low quantum defect between pump (980nm) and laser (999nm) wavelengths under longitudinal diode pumping. Chirped pulse regenerative amplifier based on Yb:LuAP crystal was investigated. Pulse duration as short as 165fs with average output power of 4.5W at 200 kHz pulse repetition frequency was demonstrated.

LS-I-8

Non-resonant PPLN optical parametric oscillator in the narrow-band regime

Li Wang,^{1,2,*} Weidong Chen,¹ and Valentin Petrov¹

1-Max Born Institute for Nonlinear Optics and Ultrafast Spectroscopy, Max-Born-Str. 2a, 12489 Berlin, Germany

2-Hefei Institutes of Physical Science, Chinese Academy of Sciences, Hefei, 230031, China

**Corresponding author: lwang@mbi-berlin.de*

In the absence of wavelength selective elements, the output spectrum of an optical parametric oscillator (OPO) is usually much broader than the pump spectrum due to the large parametric spectral gain bandwidth. This effect is more pronounced near degeneracy in type-I (ooe or eeo) or type-0 (eee) phase-matching due to the same polarization of signal and idler. This is the case in one of the most widely used nonlinear crystals, periodically-poled LiNbO₃ (PPLN). On the other hand, back conversion due to the high intracavity intensities reduces the efficiency and deteriorates the beam quality in conventional resonant OPOs including singly resonant (SRO) and doubly resonant (DRO) types [1]. These effects degrade the OPO performance and impede the applicability of such infrared coherent sources.

In this work we present a PPLN-based non-resonant OPO (NRO) equipped with a transversely chirped volume Bragg grating (TCVBG) for narrow-band operation and wavelength tuning and demonstrate power scaling with respect to our initial results [2]. In a NRO, one of the mirrors fully reflects the signal and fully transmits the idler while the other mirror fully reflects the idler and fully transmits the signal [3,4]. The NRO maintains the high parametric gain while alleviating the back conversion issue which occurs in conventional resonant OPOs. The experimental configuration is shown in Fig. 1(a), cf. [2] for more details. Tunable operation in a spectral range of 1.86-1.90 μm for the signal [see Fig. 1(b)] and 2.42-2.49 μm for the idler with spectral bandwidths less than 2 nm was achieved by using two TCVBGs with a chirp rate of 1 nm/mm. Average power scaling up to 8.63 W was obtained at a repetition rate of 35 kHz [see Fig. 1(c)].

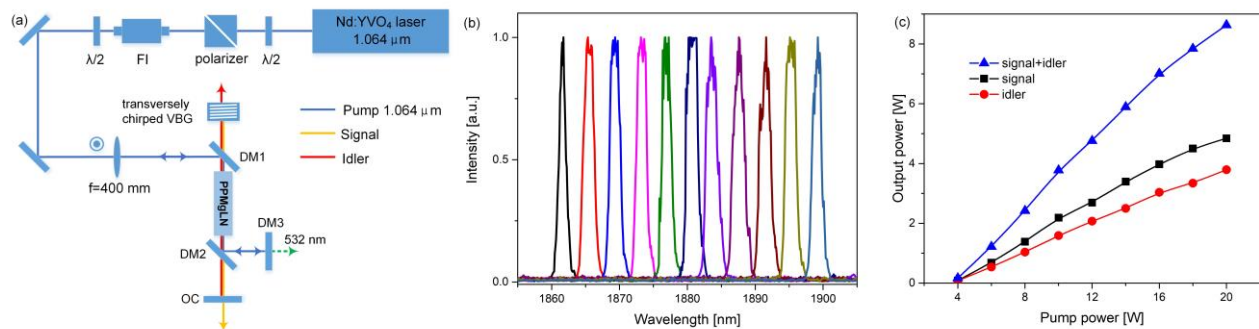


Fig. 1. (a) The experimental set-up of the tunable narrow-band PPLN-based NRO; (b) signal spectra; (c) input-output performance at 35 kHz.

[1] V. Petrov, "Frequency down-conversion of solid-state laser sources to the mid-infrared spectral range using non-oxide nonlinear crystals," *Prog. Quantum Electron.* **42**, 1-106 (2015).

[2] L. Wang, A. A. Boyko, A. Schirmacher, E. Büttner, W. Chen, N. Ye, and V. Petrov, "Narrow-band periodically poled lithium niobate nonresonant optical parametric oscillator," *Opt. Lett.* **44**, 5659-5662 (2019).

[3] M. M. Sushchik, V. M. Fortus, and G. I. Freidman, "A resonatorless parametric light oscillator," *Radiophysics and Quantum Electron.* **14**, 211-215 (1971) [transl. from *Izvestiya Vysshikh Uchebnykh Zavedenii, Radiofizika* **14**, 263-268 (1971)].

[4] A. I. Kovrigin and P. V. Nikles, "Resonatorless parametric light generator using an α -HIO₃ crystal," *JETP Lett.* **13**, 313-315 (1971) [transl. from *ZhETF Pis. Red.* **13**, 440-443 (1971)].

LS-I-9

Dual-comb mode-locked lasers based on intrinsic polarization-multiplexing

Maciej Kowalczyk^{1,*}, Łukasz Sterczewski¹, Xuzhao Zhang^{2,3}, Valentin Petrov⁴, Zhengping Wang², Jarosław Sotor¹

1- Laser & Fiber Electronics Group, Faculty of Electronics, Wrocław University of Science and Technology, Wybrzeże Wyspiańskiego 27, 50-370 Wrocław, Poland

2- State Key Laboratory of Crystal Materials, Shandong University, 250100 Jinan, China

3- Center of Nanoelectronics, School of Microelectronics, Shandong University, Jinan 250100, China

4- Max Born Institute for Nonlinear Optics and Ultrafast Spectroscopy, Max-Born-Str. 2a, 12489 Berlin, Germany

*m.kowalczyk@pwr.edu.pl

Recently, a great number of applications relying on dual-comb laser systems emerged. This primarily includes various spectroscopic techniques, but it also covers ranging, microscopy or communication. Standard realization of the dual-comb laser setup is based on a pair of mutually-coherent mode-locked lasers. However, it has been demonstrated that the experimental setup can be significantly simplified, if two individual pulse trains are simultaneously emitted from the single free-running laser [1].

In this paper we describe a novel, unprecedentedly simple technique for dual-comb generation from a single-cavity femtosecond solid-state laser [2]. Our concept relies on intrinsic polarization-multiplexing originating from double refraction inside a birefringent gain medium. In contrast to previous demonstrations, it does not require any additional components to be introduced to a standard laser resonator. Despite its simplicity, all the cavity components are common for both beams, supporting high relative coherence of the free-running combs.

We demonstrate the experimental implementation of this new scheme in a diode-pumped Yb:Ca₃NbGa₃Si₂O₁₄ (CNGS) mode-locked laser, with its setup schematically depicted in Fig. 1. The oscillator generates two orthogonally-polarized beams with a central emission wavelength around 1050 nm and the repetition rate difference of 4.73 kHz. The pulse durations of the combs amount to 88 and 93 fs, making this source the first sub-100 fs single-cavity dual-comb ytterbium-based laser source. Moreover, we also show that by changing the net cavity dispersion the laser can simultaneously operate in two distinct dispersion regimes with one beam following the conservative soliton pulse formation (pulse duration of 117 fs) and the other being strongly chirped (2360 fs).

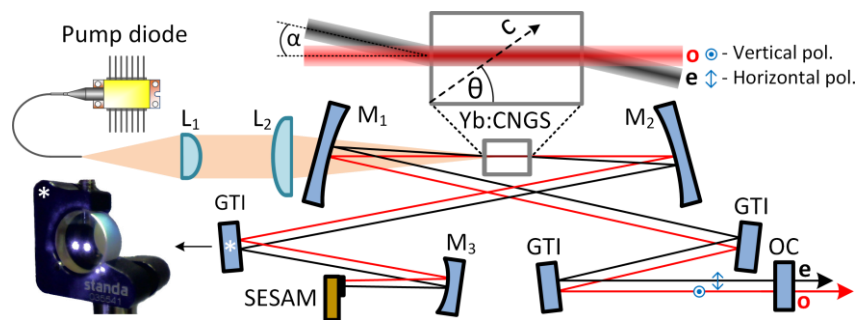


Fig. 1. Schematic of the dual-comb Yb:CNGS laser. Due to a double refraction inside the birefringent active crystal two orthogonally-polarized beams corresponding to extraordinary (e) and ordinary (o) rays are generated. The picture (*) presents a real image of the two beams incident on one of the cavity mirrors.

The phase stability of the generated soliton combs was carefully analysed indicating sub-kilohertz relative linewidth over 10 dual-comb beating periods, which, to the best of our knowledge, is the best noise performance ever demonstrated for a solid-state dual-comb laser. The excellent mutual coherence of the combs allowed us to perform free-running spectroscopic measurements of the fused silica etalon over second time scales with mode-resolved precision.

This work was supported by National Science Centre (NCN, Poland; 2015/18/E/ST7/00296).

[1] R. Liao, H. Tian, W. Liu, R. Li, Y. Song, and M. Hu, "Dual-comb generation from a single laser source: principles and spectroscopic applications towards mid-IR – A review," *J. Phys.: Photonics* 2, 042006 (2020).

[2] M. Kowalczyk, Ł. Sterczewski, X. Zhang, V. Petrov, Z. Wang, and J. Sotor, "Dual-comb femtosecond solid-state laser with inherent polarization-multiplexing," arXiv:2009.05454 (2020).

LS-I-10

Third Order Nonlinearity for Contrast Enhancement of High Power Femtosecond Lasers

Efim Khazanov

Institute of Applied Physics of the Russian Academy of Sciences, 46 Ulyanov St, Nizhny Novgorod, 603950 Russia

efimkhazanov@gmail.com

We have proposed a method for the simultaneous enhancement of the temporal contrast and power of powerful femtosecond laser pulses using a nonlinear polarization interferometer (NPI), see fig.1. For low-intensity radiation, the crystals in NPI induce a zero phase delay, so that the transmission through crossed polarizers is zero. Due to the nonlinear phase incursion π between orthogonal polarizations, thanks to which the transmission of the NPI approaches unity. The nonlinear phase incursion π can be provided both due to the anisotropy of the cubic nonlinearity (n_2 depends on the angle φ), and due to different wave intensities in orthogonal polarizations. For the first option, the KDP crystal has suitable properties and for the second option, any uniaxial crystal, see Fig.2. The NPI has an in-line geometry that does not require spatial beam separation and can be used at the output of any lasers with TW power and higher.

Moreover, the pulse that has passed through the NPI is self-phase modulated, which allows it to be compressed by reflection from the chirping mirrors (Fig.1): Compression after Compressor Approach (CafCA). Application of this idea, known since the 1960s, to lasers whose power is over 1 TW has been restrained until recently by a number of physical problems. The experimental results obtained over the past few years demonstrate the efficiency of the technique (compression by a factor of 5 at PW power level). CafCA features three undisputed merits: simplicity and low cost, negligible loss of pulse energy, and applicability to any high-power laser.

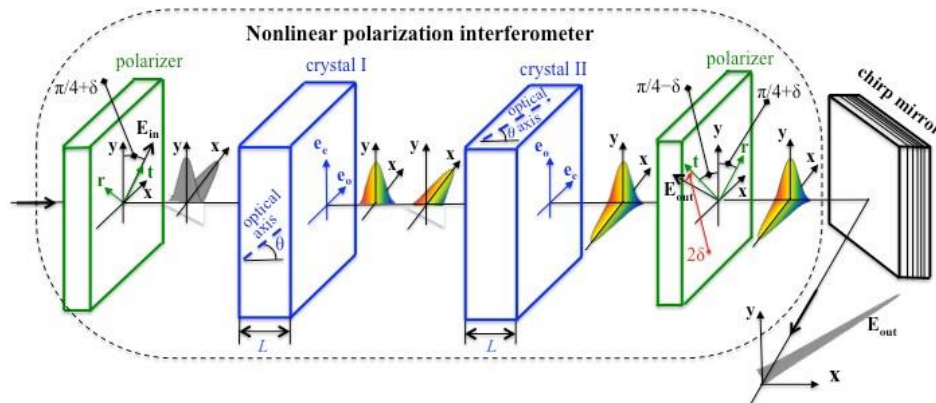


Fig. 1. Schematic of nonlinear polarization interferometer.

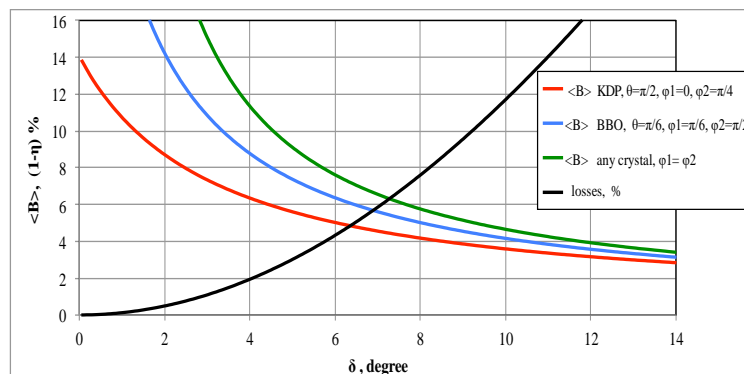


Fig. 2. Nonlinear phase of the output pulse of NPI $\langle B \rangle$ and losses $(1 - \eta)$ introduced by NPI.

LS-I-11

Advanced technologies for energetic lasers**D. Penninckx¹***1 – CEA DAM CESTA, F-33116 Le Barp, France**now with CEA DAM DIF, F-91297 Arpajon, France*Denis.Penninckx@cea.fr

There are less than two dozen high-power energetic (>kJ) laser facilities in the world. The most energetic ones, reaching the megajoule level, are the Laser Mégajoule (LMJ) in France [1], the National Ignition Facility in the USA [2] and the project Shen-Guan IV in China [3]. But these facilities may cost up to a few billion euros. Therefore, their design is the topic of a lot of research. Except a few ones based on iodine [4, 5] or excimer technologies [6], they are solid-state lasers.

One of the goals of the LEAP project, co-funded by the Région Nouvelle-Aquitaine and the European Union, is to develop new technologies for these lasers.

These solid-state lasers share all the same optics technologies:

- neodymium-doped laser glass for amplification (giving the operating wavelength: 1053nm),
- silica for windows and lenses,
- KDP crystals, which may be deuterated for polarization rotation and frequency conversion,
- various coatings for reflection management (either mirrors or anti-reflection coatings), for protection from the environment or for filtering,
- and various surface structuring technologies mainly for dispersion gratings.

Most of these technologies last from the late sixties but have been optimized during the last decades mainly to improve the resistance of the components to laser damage. Indeed the design of such energetic lasers is driven by Kerr effect and laser damage.

Because of its ideal features and its relatively low cost for wide aperture, Nd:glass remains today the best choice for kJ-class lasers. Up to 20kJ/beam may be reached. For higher energies, the number of beams has to be increased because of the physical barrier of amplified spontaneous emission. Thus, a significant increase in energy, i.e. > a few MJ, is today unlikely. The main trends are higher repetition rates (from few shots per day to one shot per min [7] or even higher for futuristic power supply facilities) and shorter pulses using Chirped-Pulse Amplification (CPA) [1] or even Optical Parametric Chirped-Pulse Amplification (OPCPA) in a KDP crystal pumped by an energetic laser [8]. Another trend is to split the large-aperture beams into sub-beams in order to use alternative technologies [9], even fibers [10]. But no such facility has been constructed yet.

Acknowledgement: This work was partly supported by the Conseil Régional de Nouvelle Aquitaine and the European Union through the LEAP project - Axes B et C (contracts CPER #16004205 and #DEE21-04-2019-5131820 and ERDF #2663710 and #3404410).

[1]: J-L. Miquel and E. Prene, "LMJ & PETAL status and program overview", Nucl. Fusion 59 032005 (2019)

[2]: M. L. Spaeth et al., "Description of the NIF Laser", Fusion and Science Technol., Vol. 69, pp. 25–145 (2016)

[3]: C. N. Danson et al., "Petawatt and exawatt class lasers worldwide", HPLSE, Vol. 7, (2019)

[4]: K. Jungwirth et al., "The Prague Asterix Laser System", Phys. of Plasmas, Vol. 8, No. 5 (2001)

[5]: S. P. Obenschain, "The Nike KrF laser facility: Performance and initial target experiments", Phys. of Plasmas 3 (1996)

[6]: I Annenkov et al., "New possibilities of the Iskra-5 facility", Quantum Electron. 36 (2006)

[7]: www.eli-beams.eu/facility/laser-4-aton-10-pw-2-kj/

[8]: J. Bromage et al., "Technology development for ultra-intense all-OPCPA systems", HPLSE, Vol. 7, (2019)

[9]: D. Eimerl et al., "A StarDriver-Class Laser Achieving 1 %Beam Uniformity in 1 ns", J Fusion Energ, 35 (2016)

[10]: L. Daniault et al., "XCAN – A coherent amplification network of femtosecond fiber chirped-pulse amplifiers", Eur. Phys. J. Special Topics, 224, (2015)

LS-I-12

HORIZON Laser: a new generation of kW-class ps amplifier

J. Lhermite*, C.Féral, D. Marion, A. Rohm, Ph. Balcou
D. Descamps, S. Petit, M.C. Nadeau, E. Mével

Université de Bordeaux-C.N.R.S.-C.E.A., Centre Lasers Intenses et Applications (CELIA), UMR 5107,
33405 Talence, France

*jerome.lhermite@u-bordeaux.fr

The LEAP project, with the Horizon laser, aims at the ambitious performance of 1 J at 1 kHz with a pulse duration of 1 ps, corresponding to an average power of 1 kW [1]. Many applications are on demand of high power levels and high repetition rate picosecond lasers such as secondary sources development (e.g. X-rays for medical applications) or space debris ranging to detect smaller and further objects. One of the main difficulties related to the generation of such power levels is the thermal management in the main amplifier. In our configuration, the laser gain medium is Yb:YAG to ensure amplification around 1030 nm. Contrary to other international projects aiming at kW/kHz operation using technologies such as thin disks [2] or cryogenically cooled amplifiers [3], we developed a new architecture of high power amplifiers, based on an original method of thermal management.

The strategy we are implementing combines three aspects intended to manage the thermal load. To distribute the heat, we use three cascaded 70 mm diameter Yb:YAG crystals with a thickness varying between 2 and 3 mm (Fig. 1). These disks are then immersed in a circulating fluid and rotated in order to spread the thermal load on a ring which limits the temperature rise of the disks below 50°C.

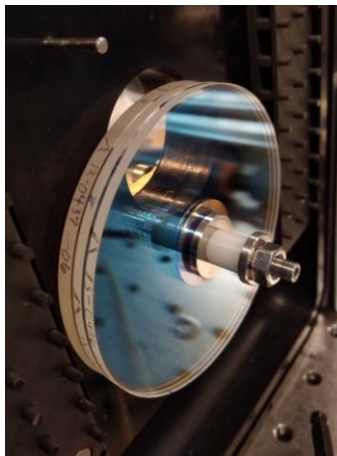


Fig 1 : The three Yb:YAG spinning disks

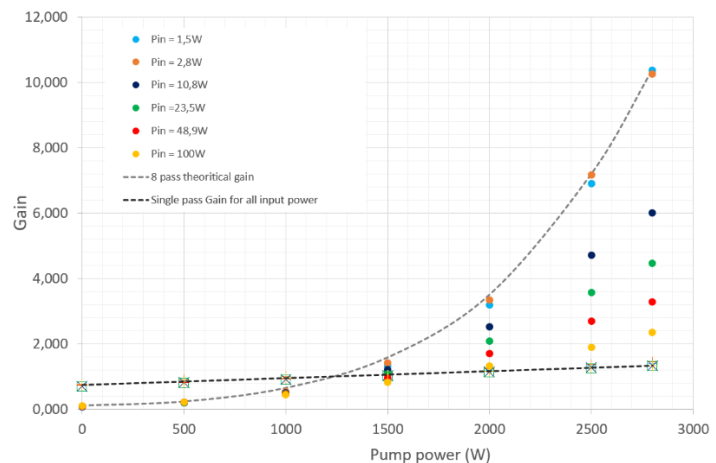


Fig 2: First gain measurements of the spinning head in CW regime for different input power levels

Due to the low single pass expected efficiency according to the simulations (around 1.4), the laser head is implemented in an 8-pass configuration. We recently measured the first gain values in continuous wave (CW) regime and with a pump level of 3 kW at 940 nm for a first step (Fig.2). The pump will be increased up to 13 kW in the second phase of our development coupled to a pulsed seeder delivering 100 mJ at 1 kHz.

Experimentally, the single pass gain reaches 1.35 which is in good agreement with the simulations. In 8-pass configuration, a small-signal gain of 10 has been measured. We observe a saturation of this gain at higher input power due to the small size of the spot signal and the mismatch with the pump spot size. These parameters are being optimized to allow the final objective of 1 J at 1 kHz.

[1] S. Petit, C. Feral, M.-C. Nadeau, P. Balcou, J. Brandam, D. Descamps, J. Lhermite, and D. Marion, "Towards a kW-class picosecond laser at 1 kHz," Conference on Lasers and Electro-Optics and European Quantum Electronics Conference (CLEO-EQEC), Munich, Germany, 2019, p. ca_8_6.

[2] C. Herkommer, P. Krötz, R. Jung, S. Klingebiel, C. Wandt, R. Bessing, P. Walch, T. Produit, K. Michel, D. Bauer, R. Kienberger, and T. Metzger, "Ultrafast thin-disk multipass amplifier with 720 mJ operating at kilohertz repetition rate for applications in atmospheric research," Opt. Exp., vol. 28, pp. 30164-30173, 2020

[3] Yong Wang, Han Chi, Cory Baumgarten, Kristian Dehne, Alexander R. Meadows, Aaron Davenport, Gabe Murray, Brendan A. Reagan, Carmen S. Menoni, and Jorge J. Rocca, "1.1 J Yb:YAG picosecond laser at 1 kHz repetition rate," Opt. Lett. **45**, 6615-6618 (2020)

LS-I-13

Periodically Poled Ferroelectric Crystals and Thin Films for Nonlinear Optical Conversions and Controlling of Coherent Light

**V. Shur¹, A. Akhmatkhanov¹, A. Esin¹, M. Chuvakova¹, B. Slautin¹,
V. Pavelyev², G. Sokolovskii³, D. Kolker⁴, A. Boyko⁴**

1- Institute of Natural Sciences and Mathematics, Ural Federal University, Ekaterinburg, Russia

2- Image Processing Systems Institute of the Russian Academy of Science, Samara, Russia

3- Ioffe Institute of the Russian Academy of Science, St. Petersburg, Russia

4- Novosibirsk State University, Novosibirsk, Russia

E-mail: vladimir.shur@urfu.ru

We present the achievements in application of the creation of the periodical domain structures in single crystals of lithium niobate (LN and LT) and potassium titanyl phosphate (KTP and KTA) families and LN thin films for realization of the second harmonic generation (SHG) and optical parametric oscillation (OPO) with record efficiency based on quasi-phase-matching. LN based tunable diffraction optical elements (DOE) will be discussed. The study of the domain structure evolution using complementary high-resolution domain imaging methods has been used for improvement of the poling techniques.

The wide range of wall velocities with orders of magnitude difference was observed for switching in a uniform electric field [1]. The kinetic maps were applied for distinguishing slow, fast, and superfast domain walls with different orientation in KTP and LN. The deep knowledge of the domain structure evolution in MgO:LN and MgO:LT allowed us to produce high-fidelity domain patterns.

The fan-out periodical domain structures created in 3-mm-thick MgO:LN wafers allowed creation of the widely tunable OPO generation with the signal wave from 2.5 to 4.5 μm using the 1.053 μm pump. The periodical domain structure with period of 40 μm was created in KTA single crystals for OPO generation at 2.4 μm using the 1.053 μm pump [2]. The abilities and perspectives of producing the elements with submicron periods has been discussed.

The opposite values of the linear electrooptic effect for neighboring ferroelectric domains allowed to demonstrate the electrical field controlled optical beam deflectors, diffusers, Fresnel zone plates and Shack-Hartmann sensors with continuous tuning of diffraction efficiency and response time less than 0.1 ms. The following tunable DOE have been created and tested by us: (1) hexagonal zone plate with focus distance 150 mm and aperture 1.7 mm, (2) 2D diffraction grating with 20- μm -period, (3) bidomain element for TEM00-TEM01 mode transformation [3]. The hexagonal zone plate has focused up to 25% of the laser light into a spot of 130 μm in diameter. The 2D diffraction grating allowed decreasing the diffraction maximum intensity by 80%.

The optimized periodical poling techniques have been used for creation of ridge waveguides in periodically poled MgOLN single crystals. The high-index contrast of obtained multi-mode waveguides allowed tuning of the SHG wavelength from 510 to 570 nm using the 1.064 μm pump [4].

The domain structure evolution has been studied in lithium-niobate-on-insulator (LNOI) wafers during local switching by the biased tip of the scanning probe microscope. The creation of the stable periodical domain structures with period down to 200 nm was demonstrated.

This work was supported by the Russian Foundation for Basic Research (Grant No. 18-29-20077-MK).

References

- [1] A. A. Esin, A. R. Akhmatkhanov, and V. Ya. Shur, Superfast domain wall motion in lithium niobate single crystals. Analogy with crystal growth, *Appl. Phys. Lett.* **114**, 192902 (2019).
- [2] O. Antipov, D. Kolker, D. Kal'yanov, S. Larin, V. Shur, and A. Akhmatkhanov, Near-infrared second-harmonic generation versus mid-infrared optical parametric oscillation in multigrating and fan-out PPMgO:LN structures pumped by a repetitively pulsed 2- μm Tm³⁺:Lu₂O₃-ceramics laser, *J. Opt. Soc. Am. B-Opt. Phys.*, **35**, 1674-1679 (2018).
- [3] A. A. Esin, A. R. Akhmatkhanov, V. S. Pavelyev, and V. Y. Shur, Tunable LiNbO₃-based diffraction optical element for the control of transverse modes of the laser beam. *Computer Optics*, **45**, 222-226 (2021).
- [4] V. V. Dudelev, A. R. Akhmatkhanov, E. D. Greshnyakov, S. Kh. Abdulrazak, V. E. Bugrov, E. A. Kognovitskaya, V. I. Kuchinskii, V. Ya. Shur, and G. S. Sokolovskii, Generation of the second harmonic in ridge waveguides formed in periodically poled lithium niobate, *Quantum Electronics*, **48**, 717-719 (2018).

LS-I-14

Destruction of Optical Fibers of Various Types under the Action of High-Power Laser Radiation

I. A. Bufetov

*Prokhorov General Physics Institute of the Russian Academy of Sciences,
Dianov Fiber Optics Research Center, Vavilov Str., 38, 119333, Moscow
iabuf@fo.gpi.ru*

Destruction wave propagation under the action of high-power laser radiation has been observed so far in various types of optical fibers: silica-based fibers with various core dopants, fluoride, chalcogenide, microstructured fibers, and hollow-core fibers [1-7]. This phenomenon is usually referred to as the fiber-fuse effect. Depending on the properties of the optical fibers and the parameters of the laser radiation, the physical characteristics of the wave destruction process of optical fibers vary over a wide range. E. g., the values of the threshold intensity of laser radiation required to maintain the process of destruction wave propagation determined experimentally in various investigations, vary in an interval covering eight orders of magnitude (Fig. 1).

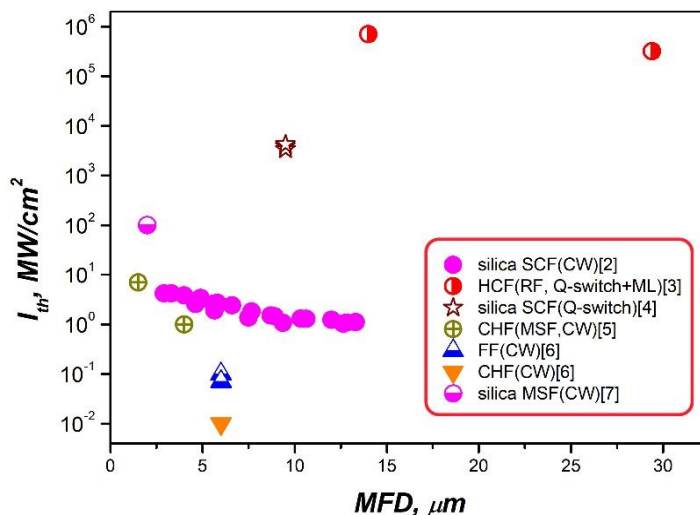


Fig. 1. Review of measured up to now values of threshold laser intensity for destruction wave propagation against mode field diameter for optical fibers of various structures, various core compositions and various laser radiation wavelengths. SCF – solid core fiber, HCF – hollow core fiber, RF – revolver hollow core fiber, CHF – chalcogenide fiber, MSF – microstructured fiber, FF – fluoride fiber, CW – destruction wave propagates under continuous wave laser radiation, Q-switch – pulse Q-switch laser driven destruction wave, Q-switch+ML – laser operates in a combined Q-switch and mode-lock regime.

A review of the main physical mechanisms responsible for the propagation of a destruction wave (in most cases, an optical discharge wave) through optical fibers will be given and the influence of the process of initiation of a destruction wave on wave parameters will be considered.

This work was supported by the Russian Science Foundation under Grant #19-12-00361.

- [1] R. Kashyap and K. J. Blow, "Spectacular demonstration of catastrophic failure in long lengths of optical fiber via self-propelled self-focusing," paper PD7, 8th National Quantum Electronics Conf., QE8, St. Andrews, Scotland, UK, (21–25 September 1987).
- [2] I. A. Bufetov and E. M. Dianov, "Optical discharge in optical fibers," *Phys. Uspekhi* **48**, 91–94 (2005).
- [3] I. A. Bufetov, A. N. Kolyadin, A. F. Kosolapov, V. P. Efremov, V. E. Fortov, *Opt. Express*, **27**, 18296 (2019).
- [4] A. A. Frolov, I. A. Bufetov, V. P. Efremov, M. Y. Schelev, V. I. Lozovoy, V. E. Fortov, and E. M. Dianov, "Optical discharge in silica-based fibers: high-speed propagation under kW-range laser radiation," *Proc. SPIE* **6193**, 61930W (2006).
- [5] S. Xing, S. Kharitonov, J. Hu, and C.-S. Brès, "Fiber fuse in chalcogenide photonic crystal fibers," *Opt. Lett.* **43**, 1443–1446 (2018).
- [6] E. M. Dianov, I. A. Bufetov, A. A. Frolov, V. G. Plotnichenko, V. M. Mashinsky, M. F. Churbanov, and G. E. Snopatin, "Catastrophic destruction of optical fibres of various composition caused by laser radiation," *Quantum Electron.* **32**, 476–478 (2002).
- [7] E. M. Dianov, A. A. Frolov, I. A. Bufetov, S. L. Semenov, Y. K. Chamorovsky, G. A. Ivanov, and I. L. Vorob'ev, "The fibre fuse effect in microstructured fibres," *Quantum Electron.* **34**, 59–61 (2004).

LS-I-15

Ultrashort pulses dynamics in 2 μm spectral range lasers and amplifiers

V.A. Kamynin, A.D. Zverev, S.A. Filatova, I.V. Zhluktova, N.R. Arutyunyan,

E.D. Obraztsova, and V.B. Tsvetkov

Prokhorov General Physics Institute of the Russian Academy of Sciences, 38, Vavilov str., 38, 119991 Moscow, Russia

Main author email address: kamyninva@gmail.com

All-fiber ultrashort pulses sources operating in the spectral range of 1900-2200 nm have numerous applications. Now, they are widely used in medicine, industry, and science [1, 2]. Ultrashort pulses in fiber lasers can be obtained in the passive mode-locking regime by using various artificial: nonlinear polarization evolution [3], nonlinear optical loop mirror [4], or real: SESAM semiconductor mirrors [5], films based on carbon nanotubes [6] of graphene [7], and topological insulators [8] saturable absorbers.

Fiber lasers operating in the 2 μm spectral range are often based on optical fibers doped with thulium, holmium, or thulium – holmium complexes. A broad luminescence spectrum of thulium and holmium ions allows one to obtain ultrashort pulses generation. Particularly, in thulium fiber lasers, pulses with durations from hundreds of femtoseconds to several picoseconds were realized [9-11]. Close pulses durations were obtained in holmium fiber lasers [12, 13]. Despite numerous works, investigation of influence cavity topologies, and saturable absorbers configuration on the mode-locking regimes is still in great demand.

In our work, we studied generation regimes of thulium and holmium fiber lasers with ring and dumbbell-shaped cavities. Mode-locking operation mode was realized by the implementation of a different number of SWCNT films into the cavity. Not only fundamental mode-locking with repetition rates from 5 to 20 MHz but pulse-burst with intrapulse interval less than 10 ns and harmonic mode-locking with repetition rates up to 110 MHz regimes were observed at the laser output. Then ultrashort pulse radiation from the master oscillators was amplified. We have investigated the time and spectral dynamics of different ultrashort pulses modes during the amplification by holmium- and thulium-doped fiber amplifiers.

- [1] Scholle K., Lamrini S, Koopmann P., and Fuhrberg P., Bishnu Pal, ed. (InTech, 2010), pp. 471-500.
- [2] Kerse C., Kalaycıoğlu H., Elahi P., Çetin B., Kesim D., Akçaalan Ö., Yavaş S., Aşık M.D., Öktem B., Hoogland H., Holzwarth R., Ilday F.Ö. *Nature*, 537 (7618), 84 (2016).
- [3] Matsas V.J., Newson T.P., Richardson D.J., Payne D.N. *Electron.Lett.*, 28 (15), 1391 (1992).
- [4] Duling I.N. *Opt. Lett.*, 16 (8), 539 (1991).
- [5] Kivistö S., Okhotnikov O.G. *IEEE Photonics Technol. Lett.*, 23 (8), 477 (2011).
- [6] Filatova S.A., Kamynin V.A., Zhluktova I.V., Trikshev A.I., Arutyunyan N.R., Rybin M.G., Obraztsova E.D., Batov D.T., Voropaev V.S., Tsvetkov V.B. *Quantum Electron.*, 49 (12), 1108 (2019)
- [7] Sotor J., Sobon G., Tarka J., Pasternak I., Krajewska A., Strupinski W., Abramski K.M. *Opt. Express*, 22 (5), 5536 (2014).
- [8] Yin K., Zhang B., Li L., Jiang T., Zhou X., Hou J. *Photonics Res.*, 3(3), 72 (2015).
- [9] Chernysheva M.A., Krylov A.A., Arutyunyan N.R., Pozharov A.S., Obraztsova E.D., Dianov E.M. *IEEE J. Sel. Top. Quantum Electron.*, 20 (5), 448 (2014).
- [10] Kieu K., Wise F.W. *IEEE Photonics Technol. Lett.*, 21 (3), 128(2009).
- [11] Sobon G., Duzynska A., Świniarski M., Judek J., Sotor J., Zdrojek M. *Sci. Rep.*, 7 (1), 1 (2017).
- [12] Chamorovskiy, A. Y., Marakulin, A. V., Kurkov, A. S., & Okhotnikov, O. G. *Laser Physics Letters*, 9(8), 602. (2012).
- [13] Filatova S.A., Kamynin V.A., Arutyunyan N.R., Pozharov A.S., Trikshev A.I., Zhluktova I.V., Zolotovskii I.O., Obraztsova E.D., Tsvetkov V.B., *JOSA B*, 35(12), 3122-3125 (2018).

LS-I-16

Multiband Supercontinuum Generation in the Mid-infrared Gas Fiber Raman Laser

A.V. Gladyshev^{*}, I.G. Pritulenko, Yu.P. Yatsenko, A.N. Kolyadin, I.A. Bufetov

Prokhorov General Physics Institute of the Russian Academy of Sciences, Dianov Fiber Optics Research Center, 38 Vavilov st., Moscow, Russia, 119333.

^{*}Corresponding author: alexglad@fo.gpi.ru

Mid-infrared (mid-IR) laser sources are required for many applications [1]. To reach the mid-IR, stimulated Raman scattering (SRS) of near-infrared radiation inside a gas-filled hollow-core fiber (HCF) can be used [2]. In this way, a sup-picosecond gas fiber Raman laser (GFRL) have been recently realized in the mid-IR via two-cascade SRS $1.03 \rightarrow 1.49 \rightarrow 2.68 \mu\text{m}$ in a D_2 -filled HCF [3].

Here, we study the influence of the pump pulse duration τ_{pump} on the spectral properties of the GFRL and generate a multiband supercontinuum (SC) with spectral coverage from 0.65 to $3.3 \mu\text{m}$.

Experimental setup and the HCF (Fig. 1a-b) were the same as published in [3]. The HCF was filled with D_2 at a pressure of 5 atm. The duration of initially transform-limited 250-fs-long pump pulses was varied by introducing various amount of positive frequency chirp to the pulses.

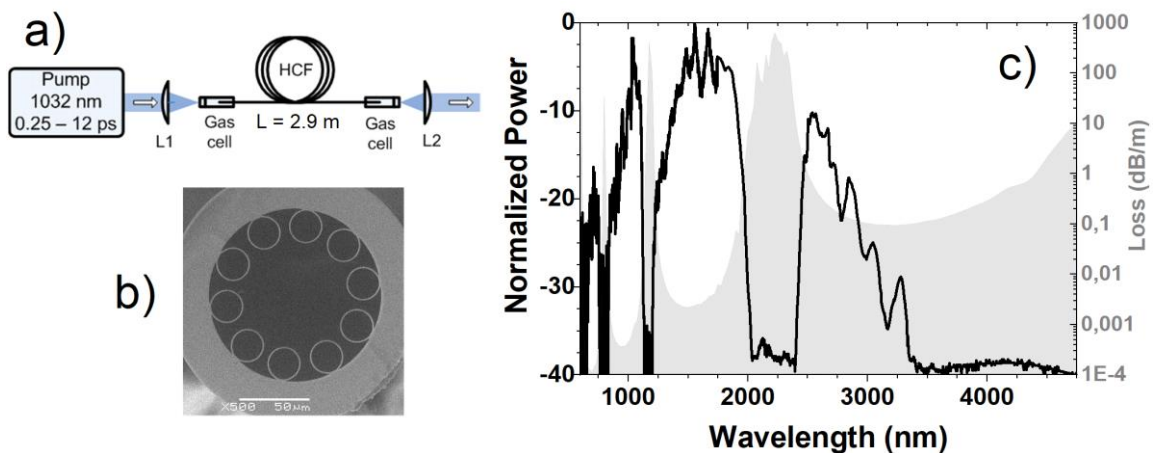


Fig. 1. (a) The scheme of the GFRL (See [3] for details). (b) Image of the HCF. (c) The output spectrum of the GFRL for $\tau_{\text{pump}} = 1 \text{ ps}$, $E_{\text{pump}} = 210 \mu\text{J}$, $P_{\text{D}_2} = 5 \text{ atm}$, $L_{\text{HCF}} = 2.9 \text{ m}$. Optical loss spectrum of the HCF is also shown (grey filled curve).

When sufficiently long pump pulses ($\tau_{\text{pump}} \approx 10 \text{ ps}$) were used, vibrational SRS is a dominant nonlinear effect. About 20 % of pump quanta is converted to the second Stokes wavelength of $2.68 \mu\text{m}$, and no spectral broadening is detected even for pump pulse energy as high as $210 \mu\text{J}$.

However, when τ_{pump} was shortened below $\sim 3 \text{ ps}$, a competition between SRS and other nonlinear effects, such as self-phase and cross-phase modulation, comes into play. The output spectrum of the GFRL experiences broadening with simultaneous reduction of SRS conversion efficiency. For τ_{pump} as short as 250 fs, the SRS conversion into mid-IR was not observed.

The most pronounced spectral broadening was observed for the case of $\tau_{\text{pump}} = 1 \text{ ps}$ and $E_{\text{pump}} = 210 \mu\text{J}$, where a multiband supercontinuum with spectral coverage from 0.65 to $3.3 \mu\text{m}$ was achieved (Fig. 1c), and about 6 % of pump quanta were converted to wavelengths above $2 \mu\text{m}$. Numerical modeling suggests that optimization of the SC width and efficiency is possible.

This work is supported by Russian Science Foundation (grant №19-12-00361).

- [1] K. L. Vodopyanov, *Laser-based Mid-infrared Sources and Applications* (John Wiley & Sons, Inc.) (2020)
- [2] M. Astapovich *et al.*, "Watt-Level Nanosecond 4.42- μm Raman Laser Based on Silica Fiber" *IEEE Photon. Technol. Lett.* **31**, 78 (2019)
- [3] A. Gladyshev *et al.*, "Mid-infrared 10- μJ -level sub-picosecond pulse generation via stimulated Raman scattering in a gas-filled revolver fiber," *Opt. Mater. Express* **10**, 3081-3089 (2020)

LS-O-1

Crystalline and electronic structure, spectroscopy and laser operation of Tm:KY(MoO₄)₂ crystal

Sami Slimi^{1,*}, Pavel Loiko², Anna Volokitina^{1,3}, Anatoly Pavlyuk⁴, Rosa Maria Solé¹, Josep Maria Serres¹, Uwe Griebner⁵, Valentin Petrov⁵, Magdalena Aguiló¹, Francesc Díaz¹, and Xavier Mateos^{1,#}

1-Universitat Rovira i Virgili, Física i Cristal·lografia de Materials i Nanomaterials, FiCMA-FiCNA, Marcel·li Domingo 1, 43007 Tarragona, Spain, #Serra Hünter Fellow

2-Centre de Recherche sur les Ions, les Matériaux et la Photonique (CIMAP), UMR 6252 CEA-CNRS-ENSICAEN, Université de Caen, 6 Boulevard du Maréchal Juin, 14050 Caen Cedex 4, France

3-ITMO University, 49 Kronverkskiy Pr., 197101 St. Petersburg, Russia

4-A. V. Nikolaev Institute of Inorganic Chemistry, Siberian Branch of Russian Academy of Sciences, 3 Lavrentyev Ave., 630090 Novosibirsk, Russia

5-Max Born Institute for Nonlinear Optics and Short Pulse Spectroscopy, Max-Born-Str. 2a, 12489 Berlin, Germany

*samislimi07@gmail.com

Among the laser host crystals for thulium (Tm³⁺) ions, double tungstates and molybdates with chemical formula ARE(XO₄)₂ (RE = Y, Gd, Lu and X = W, Mo) occupy a special position. They provide intense and broad spectral bands for dopant ions, high doping levels, weak concentration quenching and suitable thermo-optic properties. Efficient Tm lasers based on monoclinic potassium rare-earth double tungstates are known [1] but their double molybdate counterparts, e.g., KY(MoO₄)₂, are poorly studied. They feature a layered structure that enhances the polarization anisotropy of the spectroscopic properties and leads to a perfect natural cleavage which is attractive for microchip lasers. In the present work, we report on the structure refinement, spectroscopy and laser operation of Tm:KY(MoO₄)₂.

A single-crystal of 3 at.% Tm:KY(MoO₄)₂ was grown by the Low Temperature Gradient (LTG) Czochralski method [2]. Its crystal structure (orthorhombic, sp. gr. D¹⁴_{2h} – Pbnm) was refined by the Rietveld method, Fig. 1(a). The anions [Y(MoO₄)₂][−] form porous layers parallel to the *b*–*c* plane. The linkage of these layers along the *a*-axis is weak, which determines the perfect cleavage along the (100) plane, Fig. 1(b). The electronic structure of KY(MoO₄)₂ was calculated using the density functional theory (DFT). This crystal is an indirect band-gap material (the calculated bandgap is 3.47 eV). The theoretically obtained refractive index of KY(MoO₄)₂ is *n* = 2.09 at ~2 μm.

The polarized absorption and luminescence of Tm³⁺ ions were measured. The maximum SE cross-section for the ³F₄ → ³H₆ transition $\sigma_{SE} = 2.70 \times 10^{-20}$ cm² at 1856 nm (for *E* ∥ *b*) and its emission band is smooth and broad extending above 2 μm. The reabsorption-free lifetime of the ³F₄ state is 1.63 ms. The crystal-field splitting of the Tm³⁺ multiplets was determined, e.g. Δ*E* = 492 cm^{−1} for the ground state.

Continuous-wave diode-pumped lasing was achieved in a mechanically cleaved thin (70 μm) film yielding a maximum output power of 131 mW at 1972 nm with a slope efficiency of 45.2% and linearly polarized output (*E* ∥ *b*), Fig. 1(c). Tm:KY(MoO₄)₂ is promising for microchip lasers.

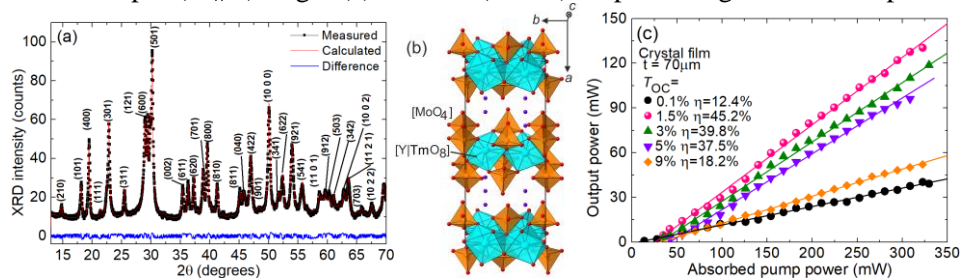


Fig. 1. Tm:KY(MoO₄)₂ crystal: (a) X-ray powder diffraction (XRD) pattern showing the result of the Rietveld refinement; (b) Projection of the crystal structure parallel to the *b*-*a* plane; (c) diode-pumped laser performance of (100)-oriented cleaved thin-film, η – slope efficiency.

[1] J. M. Serres, X. Mateos, P. Loiko, K. Yumashev, N. Kuleshov, V. Petrov, U. Griebner, M. Aguiló, F. Díaz, Diode-pumped microchip Tm:KLu(WO₄)₂ laser with more than 3 W of output power, Opt. Lett., vol. 39, pp. 4247–4250 (2014).

LS-O-2

Mid-Infrared Laser Operation of Er:KY₃F₁₀ Crystal at 2.80 μm

Liza Basyrova*, Pavel Loiko, Jean-Louis Doualan, Abdelmjid Benayad, Alain Braud, Christophe Labbé, and Patrice Camy

Centre de Recherche sur les Ions, les Matériaux et la Photonique (CIMAP) MR 6252 CEA-CNRS-ENSICAEN, Université de Caen Normandie, 6 Boulevard Maréchal Juin, 14050 Caen Cedex France

*liza.basyrova@ensicaen.fr

The development of erbium (Er) lasers emitting in the mid-infrared, at $\sim 2.8 \mu\text{m}$, is stimulated by their wide range of applications in medicine, sensing, IR countermeasures and pumping of mid-infrared OPOs. Among the known gain media for mid-IR Er lasers, fluoride crystals such as LiYF₄, BaY₂F₈ and CaF₂ have attracted a lot of attention [1]. Potassium yttrium pentafluoride (KY₃F₁₀) is less studied member of the fluoride crystal family. However, when doped with rare-earth ions, it is known for broadband emission properties [2]. In the present work, we aimed to demonstrate first laser operation of a highly Er³⁺-doped KY₃F₁₀ crystal at $\sim 2.8 \mu\text{m}$.

The crystal was grown by the Czochralski method using a composition of 22 mol% KF – 78 mol% (YF₃ + ErF₃). The nominal Er³⁺ doping level was 15 at.% (with respect to Y³⁺) and the actual ion concentration in the crystal N_{Er} was $22.7 \times 10^{20} \text{ cm}^{-3}$ according to a segregation coefficient of ~ 0.98 . Er:KY₃F₁₀ is cubic (sp. gr. O_h⁵) and optically isotropic.

Figure 1(a) shows the stimulated-emission (SE) cross-sections, σ_{SE} , for the ${}^4\text{I}_{1/2} \rightarrow {}^4\text{I}_{13/2}$ Er³⁺ transition, calculated by the Fuchtbauer–Ladenburg equation using a radiative lifetime τ_{rad} of 6.14 ms and a luminescence branching ratio β_{JJ} of 15.8%. The maximum σ_{SE} value is $1.77 \times 10^{-20} \text{ cm}^2$ at 2730 nm, corresponding to the zero-phonon line transition.

The quasi continuous-wave (qCW) laser operation of a 2.2-mm-thick sample was achieved under Ti:Sapphire laser pumping at two wavelengths, $\lambda_{\text{p}} = 970.6 \text{ nm}$ and 801.3 nm (pumping into the ${}^4\text{I}_{1/2}$ and ${}^4\text{I}_{9/2}$ states, respectively). A hemispherical cavity formed by a concave output coupler (transmission: $T_{\text{OC}} = 1.5\%$, radius of curvature: -75 mm) and a plane pump mirror was used. The pump was focused into the laser element using a 75 mm AR-coated achromatic lens. Under pumping into the ${}^4\text{I}_{1/2}$ state (the upper laser level), the Er:KY₃F₁₀ laser generated a maximum output peak power of 255 mW at 2800 nm with a slope efficiency η of 10.9% (versus the absorbed pump power) and a low laser threshold P_{th} of 58 mW (these results correspond to a duty cycle of 1:4), Fig. 1(b). When using the ${}^4\text{I}_{15/2} \rightarrow {}^4\text{I}_{9/2}$ pump transition, the output power was limited to 58 mW at the same wavelength with reduced $\eta = 18.9\%$ and slightly higher P_{th} of 71 mW . The spectra of unpolarized laser emission are shown in Fig. 1(c).

Er:KY₃F₁₀ crystals with optimized doping levels (between 5 – 15 at.%) are promising for mode-locked lasers at $\sim 2.8 \mu\text{m}$.

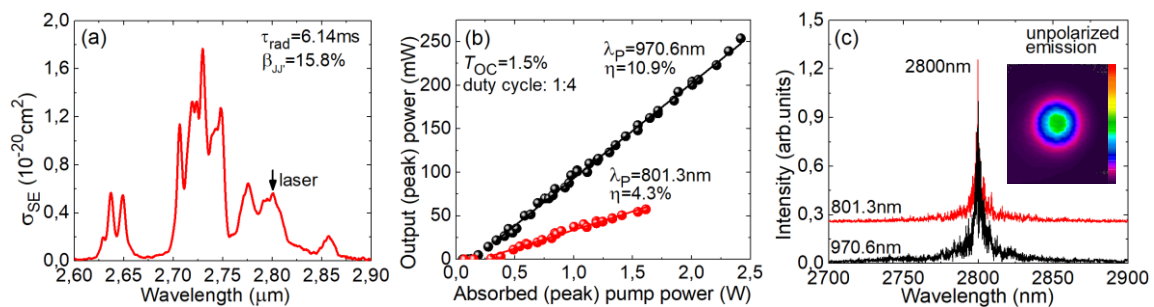


Fig. 1. 15 at.% Er:KY₃F₁₀ laser crystal: (a) stimulated-emission (SE) cross-sections, σ_{SE} , for the ${}^4\text{I}_{1/2} \rightarrow {}^4\text{I}_{13/2}$ Er³⁺ transition; (b,c) laser performance under Ti:Sapphire pumping: (b) input-output power dependences, η – slope efficiency; (c) typical spectra of output emission, inset – laser mode profile in the far-field.

[1] C. Labbé, J. L. Doualan, P. Camy, R. Moncorgé, M. Thuau, The $2.8 \mu\text{m}$ laser properties of Er³⁺ doped CaF₂ crystals, Opt. Commun., vol. 209, pp. 193-199 (2002).

[2] L. Guillemot, P. Loiko, R. Soulard, A. Braud, J. L. Doualan, A. Hideur, P. Camy, Close look on cubic Tm:KY₃F₁₀ crystal for highly efficient lasing on the ${}^3\text{H}_4 \rightarrow {}^3\text{H}_5$ transition, Opt. Express, vol. 28, pp. 3451-3463 (2020).

LS-O-3

Laser spectroscopy of a new $\text{CaSrBaF}_6:\text{Tm}^{3+}$ crystal

Alimov O.K., Doroshenko M.E., Konyushkin V.A., Kuznetsov S.V., Nakladov A.N.,
Nekhoroshikh A.V., Pierpoint K.A.

Prokhorov General Physics Institute of the Russian Academy of Sciences

e-mail: pierpoint@lst.gpi.ru

A new four-component $\text{CaSrBaF}_6:\text{Tm}^{3+}$ crystal has been grown by the Bridgman technique. The spectroscopic properties of Tm^{3+} ions in the crystal at two-micron transition were studied by the laser selective excitation technique. Previously synthesized CaSrBaF_6 single crystals demonstrated wide transparency spectral range [1]. The newly grown optical quality $\text{CaF}_2(39.5\%)\text{SrF}_2(40\%)\text{BaF}_2(20\%):\text{TmF}_3(0.5 \text{ mol. } \%)$ single crystal (see Fig.1) demonstrates that such compounds (CaSrBaF_6) are quite suitable for doping with rare-earth ions.

The X-ray phase analysis of the sample showed it is single-phase with face-centered cubic lattice with a lattice parameter $a = 5.747 \text{ \AA}$ being close to SrF_2 one – 5.800 \AA . The absorption spectra of $\text{CaF}_2:\text{Tm}^{3+}$, $\text{SrF}_2:\text{Tm}^{3+}$, $\text{BaF}_2:\text{Tm}^{3+}$, and $\text{CaSrBaF}_6:\text{Tm}^{3+}$ crystals measured at the ${}^3\text{H}_6 \rightarrow {}^3\text{H}_5$ magnetic dipole allowed transition at $T = 77 \text{ K}$ are presented in Fig.1. Certain Tm^{3+} ions absorption bands at this transition in CaF_2 , SrF_2 and BaF_2 crystals were attributed to the cubic (O_h), tetragonal (C_{4v}), and clustered centers in [2,3]. As can be seen from Fig. 1, the $\text{CaSrBaF}_6:\text{Tm}^{3+}(0.5 \text{ mol. } \%)$ crystal has a spectrum which reminds that of $\text{BaF}_2:\text{Tm}^{3+}$ crystal with relatively narrow intensive absorption lines in the region of cubic (1190 nm) and clustered Tm^{3+} centers absorption (1200–1220 nm) [3].

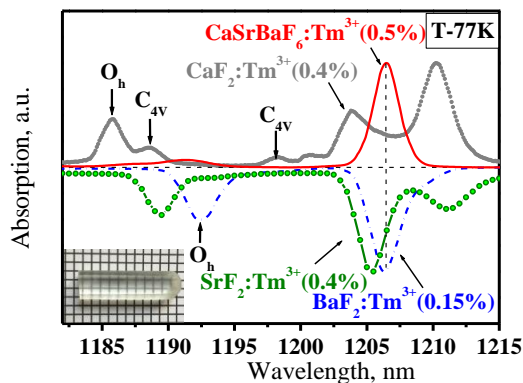


Fig. 1 - Absorption spectra of Tm^{3+} ions at the ${}^3\text{H}_6 \rightarrow {}^3\text{H}_5$ transition in CaF_2 , BaF_2 and CaSrBaF_6 crystals at $T = 77 \text{ K}$

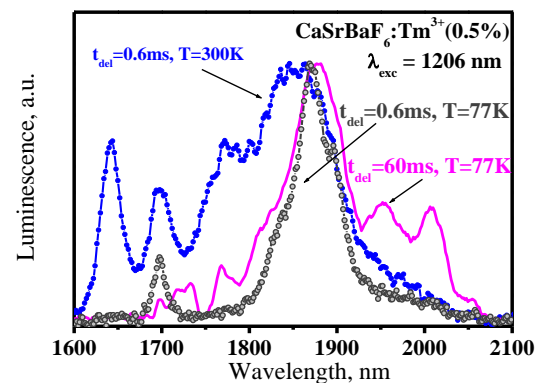


Fig. 2 - Time-resolved fluorescence spectra of Tm^{3+} ions at the ${}^3\text{F}_4 \rightarrow {}^3\text{H}_6$ transition in $\text{CaSrBaF}_6:\text{Tm}^{3+}(0.5 \text{ } \%)$ crystal at $T = 77$ and 300 K

The time-resolved Tm^{3+} ions fluorescence spectra at the ${}^3\text{F}_4 \rightarrow {}^3\text{H}_6$ transition measured under $\lambda_{\text{exc}} = 1206 \text{ nm}$ excitation into the clustered centers absorption band at $T = 300$ and 77 K are shown in Fig. 2. In a low-temperature spectrum for long delay time of $t_{\text{del}} = 60 \text{ ms}$ two lines at the long-wavelength spectrum edge were observed. The spectral positions of these lines correspond well with that of Tm^{3+} long-lifetime center in BaF_2 crystal [3].

The Tm^{3+} ions fluorescence decay curves of ${}^3\text{F}_4$ level at $T = 77$ and 300 K were measured at 1868 nm (the maximum of the fluorescence spectrum) under 1206 nm excitation. The Tm^{3+} ions lifetime measured at $T = 300 \text{ K}$ was $\approx 21.5 \text{ ms}$. Decay curve recorded at $T = 77 \text{ K}$ consisted of two exponents with lifetimes of ≈ 7.0 and $\approx 21.5 \text{ ms}$. Under excitation into the weak absorption band with a maximum of $\lambda = 1187.4 \text{ nm}$ ($\lambda_{\text{det}} = 1868 \text{ nm}$; $T = 300, 77 \text{ K}$) decay was a sum of two exponents with lifetimes of ≈ 12.5 and $\approx 67.0 \text{ ms}$. The short component decay time (12.5 ms) is in good agreement with the lifetime of clustered Tm^{3+} center in BaF_2 [3]. The long component lifetime was practically independent on temperature while its intensity was observed to increase from 300 to 77 K .

[1] S.N. Ushakov, M.A. Uslamina, A.A. Pynenkov, V.P. Mishkin, K.N. Nishchev, S.V. Kuznetsov, E.V. Chernova, P.P. Fedorov, Growth and physical properties of CaSrBaF_6 single crystals. *Condensed Matter and Interphases*, 23(1), 101-107. (2021).

[2] M. Bouffard, J.P. Jouart, M.-F. Joubert, Red-to-blue up-conversion spectroscopy of Tm^{3+} in SrF_2 , CaF_2 , BaF_2 and CdF_2 , *Optical Materials*, vol. 14(1), pp. 73–79, (2000).

[3] O.K. Alimov, M.E. Doroshenko, V.A. Konyushkin, A.N. Nakladov, A.G. Papashvili, V.V. Osiko, Spectroscopic properties of Tm^{3+} optical centers at the ${}^3\text{F}_4 \rightarrow {}^3\text{H}_6$ 2- μm laser transition in BaF_2 crystal. *Journal of Luminescence*, vol. 172, pp. 219–223, (2016).

LS-O-4

Structural and spectroscopic features of the rare-earth-doped bixbyite-type yttrium scandate

E. Dobretsova¹, O. Alimov¹, D. Guryev¹, S. Rusanov¹, V. Kashin¹, S. Kutovoi¹, V. Vlasov¹, V. Voronov¹, G. Kiriukhina^{2,3}, S. Simonov⁴, Olga Yakubovich², V. Tsvetkov¹

1 - Prokhorov General Physics Institute of the Russian Academy of Sciences, Moscow 119991, Russia

2- M. V. Lomonosov Moscow State University, Leninskiye Gory 1, Moscow 119991, Russia

3 - The Institute of Experimental Mineralogy, Russian Academy of Sciences, Chernogolovka 142432, Russia

4 - Institute of Solid State Physics, Russian Academy of Sciences, Chernogolovka 142432 Russia

elenadobretsova89@gmail.com, eadobr@kapella.gpi.ru

The yttrium scandate crystal fiber has been obtained through laser-heated pedestal growth (LHPG). Y_2O_3 and Sc_2O_3 powders of high purity were used as precursors.

The crystal structure has been characterized using X-ray diffraction on the powdered crystal fiber sample. The XRD pattern exhibits well-defined narrow peaks pointing to high crystallinity of the sample. According to X-ray powder diffraction data the yttrium scandate belongs to a bixbyite-type cubic structure with a space group $Ia\bar{3}$ and unit cell parameters $a = 10.228(1)$ Å.

A cubic $Ia\bar{3}$ crystal structure of $YScO_3$ has been refined using a single-crystal X-ray diffraction method. In the bixbyite-type structure, there are two symmetrically different positions for cations: $8b$ site (C_{3i} symmetry) and $24d$ site (C_2 symmetry). Two types of 6-vertex polyhedra ($M1O_6$ and $M2O_6$) statistically populated by Y^{3+} and Sc^{3+} cations in the almost equal ratio share corners and edges to form a chessboard packing, derived from the fluorite structure type [1, 2]. There are additional free cavities of octahedral shape in the structure that may serve as a reservoir for the insertion of rare-earth ions.

The spectral-kinetic characteristics of the rare-earth-doped $YScO_3$ crystal fibers were measured under selective laser excitation and luminescence determination. Luminescence excitation spectra of the rare-earth doped crystal fibers include two neighboring lines at low temperature ($T = 77$ K). However, the electric dipole – dipole transitions are forbidden for rare-earth ions placed in C_{3i} sites due to inversion symmetry, and the luminescence from these centers must be absent. Well-resolved fluorescence from two types of rare-earth local centers observed with comparable intensities might be responsible for decreasing of local symmetry due to the substitution of Y^{3+} and Sc^{3+} for rare-earth ions in the C_{3i} site, or inclusion of the rare-earth ions in the octahedral voids between the basic polyhedra.

[1] P. Moore and T. Araki, Braunitz; its structure and relationship to bixbyite, and some insights on the genealogy of fluorite derivative structures, *American Mineralogist*, vol. 61, pp. 1226-1240, (1976).

[2] O. Alimov, E. Dobretsova, D. Guryev et al., Growth and characterization of neodymium-doped yttrium scandate crystal fiber with a bixbyite-type crystal structure. *Crystal Growth & Design*, vol. 20, pp. 4593–4599, (2020).

LS-O-5

Silica Porous Glass Doped with Arsenic Trisulfide

J.A. Burunkova¹, G. Alkhalil¹, A.V. Veniaminov¹, I. Csarnovics², S. Kokenyesi²

1- ITMO University, Saint Petersburg, 197101, Russia,

2- University of Debrecen, Faculty of Science and Technology, Institute of Physics, Debrecen, 4032, Hungary

Gorg.kalel@yahoo.com

In this work we present the fabrication route and the optical properties of a new composite material based on silica porous glass doped with As₂S₃ nanoparticles. The fabrication method is based on chalcogenide nanoparticles dissolution in solvent and impregnation of the porous glass matrix followed by evaporation of the solvent. The presence of As₂S₃ inside the pores was confirmed by structural investigations and compositional analyses performed using SEM spectroscopy and Raman scattering measurements.

The optical and structural transformations which occur under active illumination and heat treatment in chalcogenide-containing composite were studied and compared with As₂S₃ thin films. In results, several light-induced changes in the optical properties were observed, such as the change in transmission spectra, the luminescence spectra, and the optical band gap.

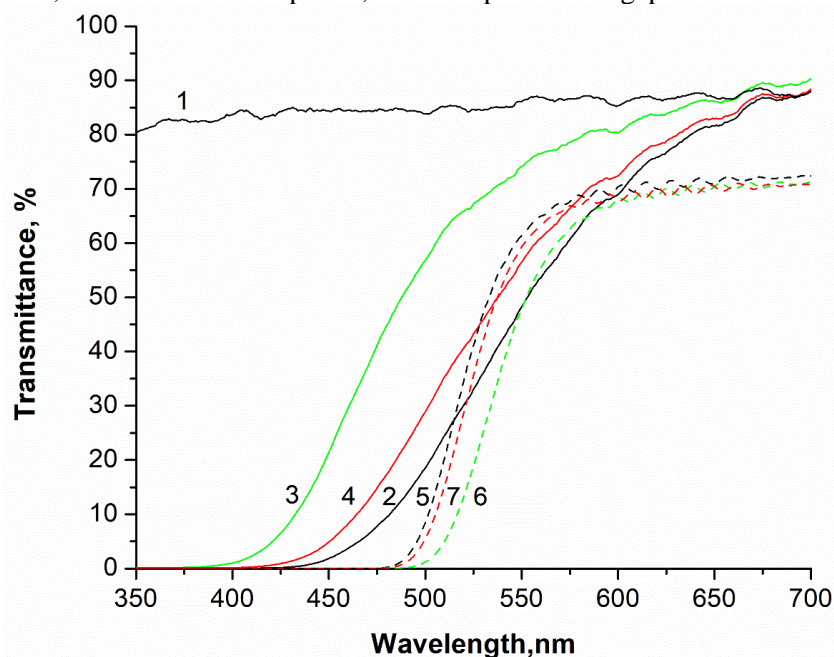


Fig. 1. Optical transmission spectra: pure porous glass (1), an initial sample of As₂S₃-PG composite (2), an illuminated sample of As₂S₃-PG composite (3), an illuminated-annealed sample of As₂S₃-PG composite (4), an initial sample of As₂S₃ thin layer (5), an illuminated sample of As₂S₃ thin layer (6), an illuminated-annealed sample of As₂S₃ thin layer (7).

The obtained composite exhibits a giant reversible photobleaching effect up to 50% of the optical transmission accompanied by an increase in the bandgap energy by 0.23 eV Fig.1. Photobleaching effect is the opposite behavior of As₂S₃ in thin films deposited by thermal evaporation in a vacuum (photo-darkening). It can be attributed to the confinement effect by nanosized pores of the porous glass. However, it is possible that among the photo-induced changes an oxidation process occurs during illumination and heat treatment, and plays role in changing the optical properties of the composite. These photo-induced changes were successfully employed for TEM model grid pattern recording using green light laser, and the obtained grid pattern was investigated by confocal microscopy.

Further developing and optimizing for the optical properties of the obtained As₂S₃-porous glass composites can be useful for creating 3D optical-structural patterns for different applications such as holographic data storage or functional optical elements for visible-infrared optics.

LASER DIAGNOSTICS AND SPECTROSCOPY

LD-I-1

Time-dependent density functional theory for extremely nonlinear optics

K. Yabana

Center for Computational Sciences, University of Tsukuba, Tsukuba 305-8577, Japan

yabana@nucl.ph.tsukuba.ac.jp

When we theoretically investigate interaction of an intense and ultrashort laser pulse with solids, there are two aspects that should be considered: the strong electric field of the light pulse induces extremely nonlinear electron dynamics in solids that cannot be described by perturbation theory. The nonlinear electron dynamics manifests as a nonlinear polarization in macroscopic scale that determines the propagation of the light pulse. Therefore, to describe the propagation of the intense light pulse, it is necessary to treat the coupled dynamics of the light electromagnetic fields and the electron dynamics. The scheme should also take into account the separation of the spatial scale of two dynamics. We have developed a theoretical and computational approach based on ab initio time-dependent density functional theory for interaction of strong and ultrashort laser pulse with solids and have applied the method to various phenomena. In my presentation, I will show our recent progresses of ab initio simulation in nano-optics.

For an interaction of intense light pulse with thin film materials, we solve a coupled equation, Maxwell equation for light pulse, time-dependent Kohn-Sham equation for electrons, and Newtonian equation for ions in Ehrenfest approximation [1,2]. For example, our method describes high harmonic generations (HHG) from thin films [3]. We can answer at which thickness the HHG becomes strongest and what is the difference between HHGs included in transmitted and reflected waves. When an intense light pulse irradiates on a meta-surfaces, 2D array of nano-particles, the optical response depends on size and density of the nano-particles. When the inter-particle distance becomes sub-nm region, tunneling current that flows between nano-particles is expected to affect much the optical response. We have developed a quantum mechanical approach for the problem [4].

Finally, we would like to mention that our computational code is made open to public as an open source software, SALMON (Scalable Ab-initio Light-Matter simulator for Optics and Nanoscience)[5], downloadable from our website, <https://salmon-tddft.jp>.

- [1] S. Yamada, M. Noda, K. Nobusada, K. Yabana, "Time-dependent density functional theory for interaction of ultrashort light pulse with thin materials", *Phys. Rev. B* **98**, 245147 (2018).
- [2] A. Yamada, K. Yabana, "Multiscale time-dependent density functional theory for a unified description of ultrafast dynamics: Pulsed light, electron, and lattice motions in crystalline solids", *Phys. Rev. B* **99**, 245103 (2019).
- [3] S. Yamada, K. Yabana, "Determining the optimum thickness for high harmonic generation from nanoscale thin films: An ab initio computational study", *Phys. Rev. B* **103**, 155426 (2021).
- [4] T. Takeuchi, K. Yabana, "Extremely large third-order nonlinear optical effects caused by electron transport in quantum plasmonic metasurfaces with subnanometer gaps", *Scientific Reports*, **10**, 21270 (2020).
- [5] M. Noda et.al, "SALMON:Scable Ab-initio Light-Matter simulator for Optics and Nanoscience", *Comp. Phys. Comm.* **235**, 356 (2019).

LD-I-2

Surface enhanced spectroscopy and sensing enabled by femtosecond-laser-printed plasmonic metasurfaces

Aleksandr Kuchmizhak^{1,2}

*1-Institute of Automation and Control Processes FEB RAS, 5 Radio Str., 690041 Vladivostok, Russia
2-Far Eastern Federal University, 6 Sukhanova Str., 690041 Vladivostok, Russia*

Ultrafast deposition of energy of a tightly focused femtosecond (fs) laser pulse into the thin substrate-supported noble metal films initiates a sequence of physical processes that start from a local solid-liquid transition following by surface morphology modification and resolidification. As a result of single-pulse fs-laser irradiation at below-threshold fluence, the unique 3D surface morphologies – nanobumps and nanojets – can be imprinted on the surface of the noble-metal films [1]. Within a certain range of laser processing parameters, formation of such 3D plasmonic nanostructures proceeds *without ablation* (i.e. ejection and redeposition of any material) resulting in extremely good printing reproducibility. This feature allows realization of novel practically relevant designs of plasmonic metasurfaces consisting of ordered arrays of nanobump and nanojets. Here, we highlight our recent results related to optical, nonlinear optical and sensing application of such laser-printed plasmonic metasurfaces, in particular, for tailoring spontaneous emission of IR-emitting HgTe quantum

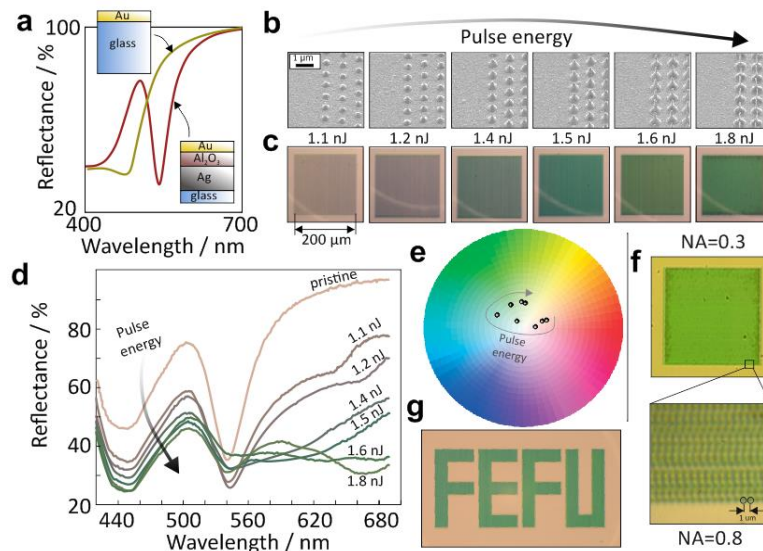


Figure 1. (a) Diffuse reflectance spectra of MIM sandwich (red curve) and bare 50-nm thick Au film on a glass substrate (yellow curve). (b) Series of side-view SEM images of the MIM surface textured at elevated pulse energy (from 1.1 to 1.8 nJ). (c) Corresponding bright-field optical image of the square-shape laser-patterned areas ($200 \times 200 \mu\text{m}^2$) processed at elevated pulse energies E as well as reflectance spectra (d) of these areas. (e) HCV color space with markers indicating the colors of the pristine MIM sandwich and the patterned areas from (c). (f) Bright-field optical image of the laser-patterned area ($E=1.8\text{nJ}$) visualized with microscope objective at $\text{NA}=0.3$ and 0.8 . (g) Bright-field optical image of the patterned area ($400 \times 80 \mu\text{m}^2$) arranged to form "FEFU" letters. The nanobumps were imprinted at pulse energy $E=1.8 \text{ nJ}$ and periodicity of $1 \mu\text{m}$.

dots [2], enhancement of second-harmonic generation [3], as well as for molecular and gas sensing based of surface-enhanced IR absorption [4]. Finally, we demonstrate that by patterning the top layer of a metal-insulator-metal (MIM) sandwich designed to support Fabry-Perot mode in the visible spectral range with the nanobumps and nanojets one can realize facile strategy for high-resolution color printing (Fig. 1a). We found that by changing the 3D shape of the nanobumps and nanojets through variation of the pulse energy and beam focusing conditions one can gradually tune the reflected color from reddish brown to pure green (Fig. 1b-f). Upscalable ablation-free laser fabrication method paves the way towards various applications ranging from large-scale structural color printing to optical sensors and security labeling at a lateral resolution of 25,000 dots per inch.

[1] F. Korte, et.al., Towards nanostructuring with femtosecond laser pulses, *Applied Physics A* 77 (2), 229-235 (2003).

[2] A.A. Sergeev, et.al., Tailoring spontaneous infrared emission of HgTe quantum dots with laser-printed plasmonic arrays, *Light: Science & Applications* 9 (1), 1-10 (2020).

[3] A.B. Cherepakhin, et.al., Laser-printed hollow nanostructures for nonlinear plasmonics, *Applied Physics Letters* 117 (4), 041108 (2020).

[4] D Pavlov, et.al., Coaxial hole array fabricated by ultrafast femtosecond-laser processing with spatially multiplexed vortex beams for surface enhanced infrared absorption, *Applied Surface Science* 541, 148602 (2021).

LD-I-3

Physical and chemical characterization of the nanoparticles formed during laser cladding with metal powder

A. Nagy¹, Sz. Kugler^{1,2}, J. Osán², L. Péter¹, V. Groma², A. Czitrovszky¹

¹*Wigner Research Centre for Physics, POB 49, H-1525 Budapest, Hungary*

²*Centre for Energy Research, POB 49, H-1525, Budapest, Hungary*

nagy.attila@wigner.hu

Laser based additive manufacturing is a rapidly developing industrial technology. 3D metal printers are widely used to produce parts for prototypes where special geometries or mechanical properties are required. In a laser 3D metal printer utilizing the directed energy deposition technique, an intense laser beam melts the metal powder, which is deposited onto the substrate through a special nozzle, building the part layer-by-layer. Nanoparticles formed during intense laser-metal interactions are known to be a major concern for occupational health. Besides their chemical composition, their physical properties also make them hazardous to the operators. These nanoparticles were characterized by means of particle mobility spectrometry and X-ray spectroscopic techniques. We studied the physical and chemical properties of the emitted particles during the 3D printing process using Ni and Fe based metal powders. The number and the mass concentrations were measured with a Scanning Mobility Particle Counter and Sizer. Size-fractionated samples were collected by a cascade impactor, and the elemental composition of the particles was determined by total reflection X-ray fluorescence analysis, Scanning Electron Microscopy, Energy Dispersive Spectroscopy, and microscopic X-ray fluorescence analysis in the different size fractions. The vast majority of the formed particles were found in the ultrafine region with a size below 100 nm. Our analysis showed that the ratios of the elements changed in the sampled particles compared to the original powder and the enrichment and oxidation of metals were correlated with each other. Our results confirmed that it is important to understand the processes that governs new particle formation and study its consequences on the performance of the operation and the operator's health as well.

This work was supported by the Hungarian National Research Development and Innovation Fund under grant no. 2017-1.3.1-VKE-2017-00039 and by European Structural and Investment Funds jointly financed by the European Commission and the Hungarian Government under grant no. VEKOP-2.3.2-16-2016-00011.

LD-I-5

Optical harmonics spectroscopy for the study of spin-induced nonlinearities

V. V. Pavlov

*Ioffe Institute, St. Petersburg, Russia**e-mail address: pavlov@mail.ioffe.ru*

In the vast area of nonlinear optics the processes of harmonics generation, sum and difference frequency generation play a particularly important role [1–3]. Nonlinear spectroscopy based on optical harmonics generation makes it possible to obtain fundamentally new information on solids as compared with studies using linear optical methods. This is due to the difference in the selection rules for single-photon and multi-photon processes. Among the various optical phenomena associated with frequency conversion of electromagnetic waves, the optical second harmonic generation (SHG) is the simplest nonlinear process of the second order. The next important third-order nonlinear optical process is the optical third harmonic generation (THG). Distinctive features of the SHG and THG processes are their high sensitivity to the symmetry of crystals, the local type of crystallographic environment, and the spin order in transition metal compounds [4, 5].

In this talk, nonlinear magneto-optical phenomena associated with SHG and THG in various classes of materials, such as magnetic dielectrics – garnet ferrites, hexagonal multiferroic manganites, and antiferromagnetic oxides will be considered. New nonlinear magneto-optical phenomena in magnetic, diluted magnetic and diamagnetic semiconductors ($A^{II}B^{IV}$ and $A^{III}B^V$) will be discussed. Various aspects of nonlinear optical spectroscopy such as polarization, temperature and field dependences will be analysed; crystallographic, ferroelectric, ferro- and antiferromagnetic contributions will be considered and identified. The possibility of visualization of antiferromagnetic domains indistinguishable by linear optics methods will be demonstrated. The possibilities of the SHG and THG methods for revealing new mechanisms for nonlinear optical interaction on exciton states in bulk semiconductors will be shown [6–9].

The Russian Foundation for Basic Research (project 19-52-12063-NNIO_a) and the Deutsche Forschungsgemeinschaft (ICRC TRR160, project C8) are acknowledged.

- [1] N. Bloembergen, *Nonlinear Optics, Lecture Notes* (W.A. Benjamin, New York, Amsterdam, 1965).
- [2] Y. R. Shen, *The Principles of Nonlinear Optics* (Wiley, New York, 1984).
- [3] R. W. Boyd, *Nonlinear Optics* (Academic, San Diego, 1993).
- [4] M. Fiebig, V. V. Pavlov, R. V. Pisarev, “Second-harmonic generation as a tool for studying electronic and magnetic structures of crystals: review”, *JOSA B* **22**, pp. 96-118 (2005).
- [5] R. V. Pisarev, “Second harmonic generation spectroscopy in magnetic and multiferroic materials”, *J. Luminescence* **133**, pp. 169-174 (2013).
- [6] R. V. Pisarev, B. Kaminski, M. Lafrentz, V. V. Pavlov, D. R. Yakovlev, M. Bayer, “Novel mechanisms of optical harmonics generation in semiconductors”, *Phys. Status Solidi B* **247**, pp. 1498–1504 (2010).
- [7] D. R. Yakovlev, W. Warkentin, D. Brunne, J. Mund, V. V. Pavlov, A. V. Rodina, R. V. Pisarev, M. Bayer, “Novel mechanisms of optical harmonic generation on excitons in semiconductors”, *Proc. of SPIE* **9503**, pp. 950302-1-8 (2015).
- [8] D. R. Yakovlev, V. V. Pavlov, A. V. Rodina, R. V. Pisarev, J. Mund, W. Warkentin, M. Bayer, “Exciton spectroscopy of semiconductors by the method of optical harmonics generation (review)”, *Physics of the Solid State* **60**, pp. 1471–1486, (2018).
- [9] V. V. Pavlov, “Magnetic field effects in optical harmonics generation by excitons” *Physics of the Solid State* **62**, pp. 1624-1632, (2020).

LD-I-6

Circular anisotropy of the third harmonic generated in tilted silicon nanowire array

A. S. Ustinov¹, L. A. Osminkina^{1,2}, D. E. Presnov^{1,3,4}, L. A. Golovan¹

1 – Faculty of Physics, M.V. Lomonosov Moscow State University, Moscow 119991, Russia

2 – Institute for Biological Instrumentation of Russian Academy of Sciences, Pushchino 142290, Russia

3 – Quantum Technology Centre, M.V. Lomonosov Moscow State University, Moscow 119991, Russia

4 – D.V. Skobeltsyn Institute of Nuclear Physics, M.V. Lomonosov Moscow State University, Moscow 119991, Russia

Photonic spin Hall effect, i.e., splitting of opposite spin photons perpendicular to the incident plane of impinging light beam, is of great interest for modern photonics with its potential applications in such devices as beam splitters, demultiplexers by photonic spin degree of freedom, chiral molecule sensors, etc. Here, we report on numerical simulation and experimental detection of this effect in an array of densely arranged tilted silicon nanowires (SiNWs) of about 100 nm in diameter. We compared scattering of fundamental near-infrared radiation and the third harmonic (TH) generated in the structures. The latter case approves high sensitivity of nonlinear optical process to local fields within the structure, thus allowing us to probe the sub-wavelength evolution of photons in it.

Numerical simulations of circularly polarized light scattering by a single SiNW and a group of 13 SiNWs used as a geometrical approximation of the real SiNW array indicate maintenance of helical modes in SiNWs for the light incident at an oblique angle to their axis. Helical guided-like mode structure in SiNWs evidences synthetic gauge field for photons resulting in its turn in asymmetric scattering diagram both for fundamental frequency and the TH.

SiNWs were formed by means of metal-assisted chemical etching of (110) crystalline silicon (c-Si). They were tilted to the c-Si substrate at an angle of 45°. The array demonstrated significant linear light scattering preventing it from exhibiting of circular anisotropy. Nevertheless, experiment on the TH generation pumped by femtosecond laser pulses at 1250 nm has demonstrated significant difference in the TH signals for cases of left- and right-handed circularly polarized fundamental radiation. The effect was detected for oblique (60°) light incidence on SiNWs, whereas for the laser radiation propagating along the SiNWs or perpendicularly to them TH signal did not depend on the pump radiation photon helicity sign.

Thus, we have demonstrated polarization-dependent routing of circularly polarized near-infrared radiation in a SiNW array, which is evidenced by different TH generation efficiencies in such structure in response to incident radiation with circular polarization of opposite signs.

[1] Y. Liu, Y. Ke, H. Luo et al., Photonic spin Hall effect in metasurfaces: a brief review, *Nanophotonics*, vol. 6, pp. 51–70, (2017).

[2] V. A. Sivakov, G. Bronstrup, B. Pecz et al., Realization of Vertical and Zigzag Single Crystalline Silicon Nanowire Architectures, *J. Phys. Chem. C*, vol. 114, pp. 3798–3803, (2010).

LD-I-7

Study of colloidal suspensions of carbon nanoparticles using fluorescence, Raman and CARS spectroscopy

S. Burikov¹, K. Laptinskiy², T. Dolenko¹

1- Department of Physics, Lomonosov Moscow State University, Leninskie Gory 1/2, 119991 Moscow, Russia

2- Skobeltsyn Institute of Nuclear Physics, Lomonosov Moscow State University, Leninsky Gory 1/2, 119991 Moscow, Russia

Carbon nanoparticles (CNP), primarily nanodiamonds (ND), carbon quantum dots, and complexes based on them, have a whole set of properties that make them very promising in terms of applications in biomedical applications [1]. They are non-toxic, biocompatible, have a developed multifunctional surface, and they have stable and intense luminescence. Therefore, CNP can be used as drug carriers, luminescent markers, and adsorbents.

One of the key issues related to the prospects of using CNP in biomedicine is the question of their interactions in suspensions with water molecules and biomacromolecules – proteins, DNA, etc. On the one hand, these interactions can affect certain properties of the CNP, on the other hand, the CNP itself can influence the components of the biological environment. It has been found that CNP significantly alter the hydrogen bonds between water molecules in suspensions. At the same time, the properties of the CNP themselves depend on the strength of the hydrogen bonds in the suspensions. Thus, Raman spectroscopy and luminescence spectroscopy were used to determine the dependences of the luminescent properties of the CNP on the strength of hydrogen bonds between water molecules in suspensions and the efficiency of interaction with biomacromolecules [2].

An important practical application of CNP is their use as luminescent markers. At the same time, a serious problem is the separation of the useful luminescence signal of the marker against the background of intense broadband luminescence of the biological environment (autoluminescence). In order to solve this problem, machine learning methods, in particular, artificial neural networks (ANN), are successfully used. ANN, due to such properties as resistance to noise and the ability to learn on patterns, have proved to be an indispensable tool for solving this problem [3].

Another approach to solving the problem of CNP visualization in the biological environment is the use of CARS (Coherent Anti-Stokes Raman scattering) spectroscopy. Due to the fact that the CARS signal is located in the anti-Stokes region of the spectrum, the problem of distinguishing the useful signal against the background of autoluminescence is eliminated. CARS spectroscopy has also been successfully used to study the interactions of ND with protein molecules.

At the current stage of development of researches in this field, it can be argued that the combination of various spectroscopy methods – fluorescence spectroscopy, Raman spectroscopy, and CARS spectroscopy - allows one to obtain information about the processes occurring in colloidal suspensions of CNP, about their interactions with environmental molecules, and about the properties of CNP in suspensions and biological media.

This study was supported by the Russian Science Foundation (Project no. 20-72-00144).

[1] J.M. Rosenholm, I.I. Vlasov, S.A. Burikov, T.A. Dolenko, O.A. Shenderova, Nanodiamond-Based Composite Structures for Biomedical Imaging and Drug Delivery, *Journal of Nanoscience and Nanotechnology* 15(2), 959–971 (2015)

[2] K.A. Laptinskiy, E.N. Vervalde, A.N. Bokarev, S.A. Burikov, M.D. Torelli, O.A. Shenderova, I.L. Plastun, T.A. Dolenko, Adsorption of DNA Nitrogenous Bases on Nanodiamond Particles: Theory and Experiment, *The Journal of Physical Chemistry C* 122(20), 11066–11075 (2018).

[3] O.E. Sarmanova, S.A. Burikov, S.A. Dolenko, I.V. Isaev, K.A. Laptinskiy, N. Prabhakar, D. Karaman, J.M. Rosenholm, O.A. Shenderova, T.A. Dolenko, A method for optical imaging and monitoring of the excretion of fluorescent nanocomposites from the body using artificial neural networks, *Nanomedicine: Nanotechnology, Biology and Medicine* 14(4), 1371–1380 (2018).

LD-I-8

Monodisperse formamidinium tin iodide nanocrystals

D. N. Dirin^{1,2}, A. Vivani^{1,3}, M. I. Bodnarchuk², M. Aebli¹, I. Cherniukh^{1,2}, A. Guagliardi^{3,4}, M. V. Kovalenko^{1,2*}

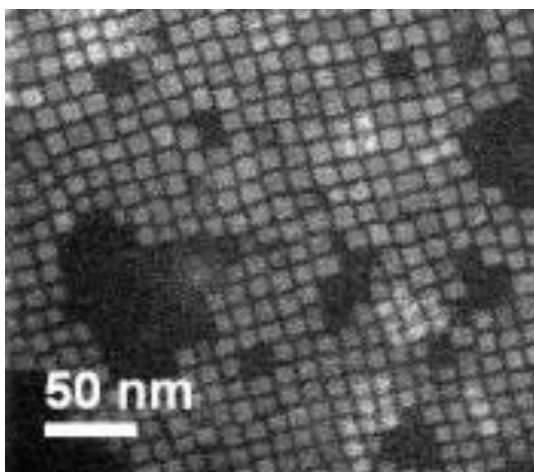
¹*Department of Chemistry and Applied Biosciences, ETH Zürich*

²*Laboratory for Thin Films and Photovoltaics, Empa*

³*University of Insubria, Department of Science and High Technolog*

⁴*Institute of Crystallography, Italy*

Over the last nine years, lead halide perovskites have been a subject of continuous interest due to a combination of several unique properties, particularly long diffusion length of carriers, optoelectronic tolerance to intrinsic defects, and highly dynamic crystal lattice. These materials have exhibited the well-recognized success towards application in solar cells, light-emitting devices, and high-energy radiation detectors. There was also significant progress in the understanding of the origin of their unique optoelectronic properties on both bulk- and nano-scale levels. This new understanding indicates that finding an alternative lead-free material with similar optoelectronic properties among other, non-group-14 metal halides can be very challenging if possible at all. On the other hand, recent advances in metal halide perovskite photovoltaics indicate that the closest analog to lead halide perovskites, namely formamidinium tin iodide, could exhibit similarly exciting performance if synthesized with a low number of trap states. The main challenge with this material relates to the easiness of trap states generation during the processing of this material, which is often ascribed to the oxidation of Sn(II) to Sn(IV). In this work we present a new synthesis of colloidal formamidinium tin iodide nanocrystals with a high degree of monodispersity and show that such oxidation is not the only pathway of formamidinium tin iodide degradation and low photoluminescence quantum yield.



LD-I-9

Fluctuating potentials in Cu(In,Ga)Se₂ solar cells: recombination channels and limiting effects on open circuit voltage

J. P. Leitão,¹ J. P. Teixeira^{1,2}, P. M. P. Salomé^{2,3}

1-Departamento de Física and i3N, Universidade de Aveiro, 3810-193 Aveiro, Portugal

2-International Iberian Nanotechnology Laboratory, 4715-330 Braga, Portugal

3-Departamento de Física, Universidade de Aveiro, 3810-193 Aveiro, Portugal

J. P. Leitão: joaquim.leitao@ua.pt

Cu(In,Ga)Se₂ (CIGS) based technology achieved the highest light to power conversion efficiency among chalcogenide solar cells. Two properties can be highlighted for these CIGS films: i) they are Cu poor which implies the presence of a high defect density on the network; ii) commonly, the $[Ga]/([Ga]+[In])$ ratio varies in-depth (see Fig.1 (a)). As a result, optical and electrical properties are strongly influenced by both potential fluctuations [1] in the material and the implemented Ga-profile [2]. In this work, we study two sets of samples in which the above properties are investigated. The first set consists in two cells with different Ga-profiles: notch and linear, as illustrated in the right panel of Fig. 1 (a). The dominant recombination channels in the two samples were investigated by the dependence of the photoluminescence (PL) on excitation power and temperature. In the notch Ga-profile, evidences were found for two tail-impurity radiative transitions ascribed to the CIGS/CdS interface and notch region, whereas for the linear Ga-profile, the dominant recombination transitions are of band-impurity type [2]. In the second set of samples, the average depth of potential fluctuations was intentionally varied in three cells through different $[Cu]/([Ga]+[In])$ ratios. PL, external quantum efficiency, and electrical measurements were performed and complemented with a theoretical study of the various types of fluctuations expected for CIGS, based on the analysis of extensions to the Shockley-Queisser model. The obtained results show that the cell performance is strongly affected by fluctuations, in particular, the loss observed in the open circuit voltage (V_{oc}) values. Among the various types of fluctuations (electrostatic, Urbach, and bandgap), the electrostatic ones have the dominant contribution to the V_{oc} losses [1]. Our results also show that potential fluctuations are important in the cell behavior at room temperature.

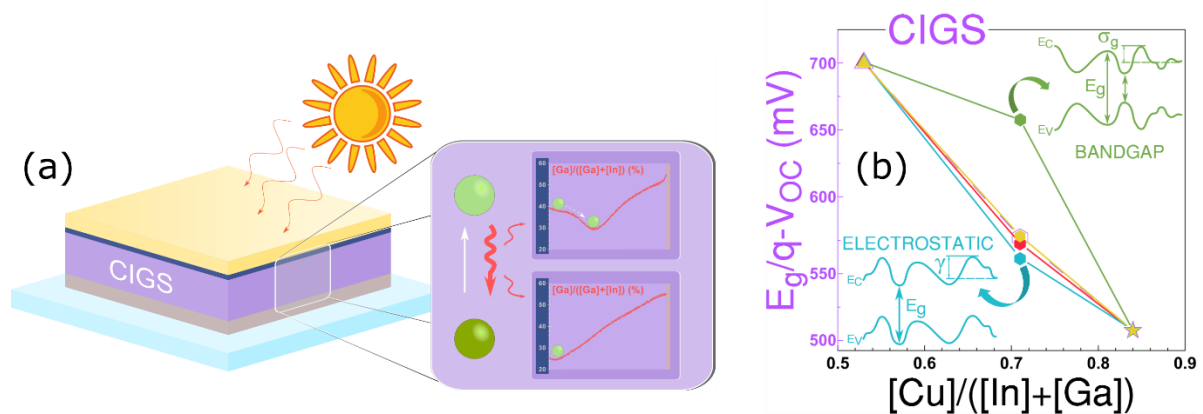


Fig. 1. (a) Basic structure of a CIGS solar cell (left panel) consisting in the soda lime glass (cyan), Mo (brown), CIGS absorber layer (purple), CdS (blue), ZnO (yellow), and schematic illustration of the Ga-profiles: notch (right panel, top); linear (right panel, bottom). (b) Experimental V_{oc} losses for samples with different $[Cu]/([In]+[Ga])$ values. Different types of fluctuating potentials were considered.

[1] J. P. Teixeira, P. M. P. Salomé, B. Alves, M. Edoff, J. P. Leitão, Evidence of limiting effects of fluctuating potentials on V_{oc} of Cu(In,Ga)Se₂ thin-film solar cells, *Phys. Rev. Appl.*, 11, 054013 (2019)

[2] J. P. Teixeira, R. B. L. Vieira, B. P. Falcão, M. Edoff, P. M. P. Salomé, J. P. Leitão, (2020). Recombination Channels in Cu(In,Ga)Se₂ Thin Films: Impact of the Ga-Profile, *J. Phys. Chem. C*, 124, 12295 (2020)

LD-I-10

Low noise GaInAsSb/GaAlAsSb Avalanche Photodiodes for Detecting Radiation of Solid-State Lasers

M.P. Mikhailova, A.P. Dmitriev, I.A. Andreev, E.V. Kunitsyna, E.V. Ivanov, Yu.P. Yakovlev

Ioffe Institute, 26 Politekhnicheskaya str., 194021 St. Petersburg, Russia

kunits@iropt9.ioffe.ru

Avalanche photodiodes for the detection of high-frequency laser radiation should meet a number of requirements including high avalanche gain, large ratio of the impact ionization coefficients for holes and electrons, fast response time and low excess noise factor.

The GaSb band structure combines two unique features: firstly, the heavy L-valley in the conduction band for the (111) direction that is situated 85 meV below Γ -minimum so as the considerable number of electrons are in the Γ -valley and besides, the band "resonance", i.e. $E_g \approx \Delta_0$, where Δ_0 is the spin-orbit splitting of the valence band. It is shown theoretically and experimentally [1] that in GaSb-related materials the maximum ratio of impact ionization coefficients for holes β and electrons α can be achieved due to monopolarity of multiplication by holes from the spin-orbit split off valence band, the threshold energy value for which is minimal and equal to $\varepsilon_{th} \approx \Delta_0$. This study has allowed us to suggest a new approach to developing the almost "noiseless" avalanche photodiodes.

The avalanche photodiodes with separate absorption and multiplication regions (SAM APD) have been developed based on GaInAsSb/GaAl(As)Sb heterostructures grown on the GaSb (111) substrates. The minimum detectable power level $\eta \langle P_{APD} \rangle$ for the optoelectronic receiver using SAM APD was determined under illumination by monochromatic radiation with wavelength of $\lambda = 2.1 \mu\text{m}$ and calculated [2] at the ratio of the ionization coefficients of $k = \beta/\alpha \approx 60$ and the multiplication factor of $M = 30\text{--}40$. It was accepted in our calculations, that the bit rate is $B = 500 \text{ Mbit/s}$, the bit error rate is $\text{BER} = 10^{-9}$, the diameter of the APD sensitive area is $200 \mu\text{m}$, and the value of the sensitivity at the maximum of the spectral characteristic ($\lambda = 2.1 \mu\text{m}$) is 1.1 A/W . The minimum excess noise factor $F(M) = 1.6$ was reached at $k = \beta/\alpha \approx 60$ and $M = 20\text{--}40$.

The optoelectronic receiver with the GaInAsSb/GaAl(As)Sb SAM APD was tested under illumination of the YLF:Ho ($\lambda = 2.06 \mu\text{m}$) and YAG-Cr,Tm:Ho ($\lambda = 2.09 \mu\text{m}$) solid-state lasers. A comparison of the minimum detectable power level for the GaInAsSb/GaAl(As)Sb SAM APD at $\lambda = 2.1 \mu\text{m}$ and for the Ge APD at $\lambda = 1.55 \mu\text{m}$ was made. The SAM APD receiver demonstrate $\eta \langle P_{APD} \rangle = -42.3 \text{ dBm}$ at $M = 34\text{--}39$, as well as the threshold value of the pulse energy of $6.2 \times 10^{-16} \text{ J}$. The receiver with the standard Ge APD has $\eta \langle P_{APD} \rangle = -41.8 \text{ dBm}$ at $M = 10$ ($\beta/\alpha = 2$) and the minimum detectable pulse energy of $6.2 \times 10^{-15} \text{ J}$.

These results show the potential for use of the GaInAsSb/GaAl(As)Sb SAM APDs in the systems for optical fiber communication including the detection of weak pulse signals of solid-state lasers in IR region of $2\text{--}3 \mu\text{m}$.

[1] M.P. Mikhailova and I.A. Andreev, Mid-infrared Semiconductor Optoelectronics, ed. by A. Krier (Springer-Verlag), Part III, 547 (2006).

[2] R.C. Smith and S.D. Personick, Semiconductor Devices for Optical Communications, ed. by H. Kressel (Springer-Verlag), Chapter 4, 89 (1982).

LD-I-11

Plasmon-enhanced optical spectroscopies of semiconductor nanostructures

**A.G. Milekhin^{1,2}, M. Rahaman³, T.A. Duda¹, E.E. Rodyakina^{1,2}, R.B. Vasiliev⁴, I.A. Milekhin³,
K.V. Anikin¹, S.A. Kuznetsov¹, V.G. Mansurov¹, A.V. Latyshev^{1,2}, D.R.T. Zahn³**

¹ A.V. Rzhanov Institute of Semiconductor Physics, 630090, Novosibirsk, Lavrentjev av. 13, Russia

² Novosibirsk State University, Novosibirsk, 630090, Pirogov str., 1, Russia

³ Semiconductor Physics, Chemnitz University of Technology, D-09107 Chemnitz, Germany

⁴ Department of Material Science, Moscow State University, Moscow, Russia

milekhin@isp.nsc.ru

The results of a Tip-Enhanced Raman Scattering (TERS) and Surface-Enhanced InfraRed Absorption (SEIRA) study of CdSe nanocrystals (NCs) and CdSe/CdS nanoplatelets (NPLs) on arrays of Au nanodisks and nanoantennas fabricated using nanolithography are discussed. In addition, the perspectives of nano-IR spectroscopy for hyperspectral infrared nanoimaging of AlN nanocolumns are also considered.

Monolayers (MLs) of CdSe NCs with a size of 5-6 nm and sub-MLs of CdSe/CdS NPLs consisting of 1.5 nm CdSe core and 0.6 nm CdS shell were deposited on plasmonic substrates using the Langmuir-Blodgett technology.

TERS by longitudinal optical (LO) and surface optical (SO) phonons in CdSe-based nanostructures placed in the gap between the TERS tip apex and Au nanodisks was observed. The TERS signal from MLs of CdSe NCs on Au nanodisk arrays forms a pattern of ordered rings with a diameter equal or below that of the Au nanodisks dependent on the excitation energy. A superposition of the TERS image on the corresponding AFM topography shows that the centers of the rings and Au nanodisks perfectly coincide. This indicates a strong dependency of TERS phonon mode intensity on the LSPR energy of the coupled system of the tip and the nanodisk and their relative position as well as evidences the electromagnetic mechanism of TERS.

TERS maps for CdSe/CdS NPLs reproducing the size and shape of the NPLs are consistent with AFM images and allowed the phonon spectrum of single NCs and NPL to be investigated.

SEIRA by optical phonons of MLs of CdSe-based nanostructures on Au nanoantennas with structural parameters allowing the coupling to the LSPR modes is discussed. The frequency positions of the absorption features evidence that the SO phonons of MLs of CdSe/CdS NPLs are active in the SEIRA spectra.

We also present the results of the hyperspectral infrared nanoimaging of AlN nanocolumns based on fourier transform infrared nanospectroscopy. AlN nanocolumns with a diameter and height of about 200 and 50 nm, respectively, were grown by molecular-beam epitaxy. IR nanospectroscopy allows the spatial localization of optical phonon modes with different symmetry in AlN to be studied.

Acknowledgements

The reported study was funded by Volkswagen Foundation and RFBR in the research projects 19-52-12041_NNIO and 18-29-20066_mk.

LD-I-12

Tuning of the optical properties of CdSe atomically thin nanosheets by spontaneous folding: effect of the length and type of ligands.

D.A. Kurtina¹, A.V. Knotko^{1,2}, A.V. Garshev^{1,2}, R.B. Vasiliev^{1,2}

1- Department of Chemistry, Lomonosov Moscow State University, 119991, Moscow, Russia

2- Department of Material Science, Lomonosov Moscow State University, 119991, Moscow, Russia

romvas@inorg.chem.msu.ru

Two-dimensional semiconductors have unique electronic and optical properties that are different from those of bulk materials. In this regard, atomically thin nanosheets of cadmium chalcogenides have recently attracted great interest due to the two-dimensional electronic properties and record-narrow bands of exciton transitions [1, 2]. In present work, we report an effect of spontaneous folding of atomically thin CdSe nanosheets and analyze its impact on a structure and optical properties. We studied the effect of carboxylates and thiolates ligands, including analyzed the effect of the length of the hydrocarbon chain of ligand.

Atomically thin CdSe nanosheets with precise thickness of 2.5 and 3.5 monolayers (0.6 and 0.9 nm) were grown by the colloid method [3]. Seed-mediated growth allows extending lateral sizes of nanosheets up to 700 nm. The native stabilizer – oleic acid was exchanged for various ligands, including different thiols and carboxylic acids with different chain length. Analysis of the crystal structure, morphology, and composition was carried out using HRTEM, HAADF-STEM, SAED, XRD and FTIR methods in dependence on ligand type.

We show that CdSe nanosheets are uniformly rolled up in multiwall scroll-like nanostructures folding along [110] direction due to spontaneous folding effect [4]. The systematic exchange of ligands for carboxylic acids with different chain lengths made it possible to change the inter-wall distance in rolled nanostructures, leading to compression or stretching of the nanostructures. Using small-angle diffraction, the dependence of the inter-wall distance on the ligand chain length was established, indicating the formation of a close-packed monolayer of ligands in the inter-wall space.

The optical properties of nanosheets were studied by absorption and photoluminescence spectroscopy. Well-resolved LH, HH, and SO exciton transitions was found and a pronounced exciton luminescence band were observed. The exchange of ligands to thiolates led to a spectral shift of all bands by a value of about 50 nm in the red region. A bathochromic shift in the spectral position of exciton luminescence bands with an increase in the chain length of carboxylic acids on the surface of rolled nanostructures was found. This effect makes it possible to fine tune the energy of the exciton bands. A model of spontaneous folding due to compression or tension deformations at the semiconductor/ligand interface caused by the mismatch of limiting areas the basal cation-rich plane (001) and the size of footprint of carboxylate and thiolate ligands is proposed.

This work was supported by the Russian Foundation for Basic Research (grant № 19-03-00481).

[1] A. Di Giacomo et al., Colloidal Synthesis of Laterally Confined Blue-Emitting 3.5 Monolayer CdSe Nanoplatelets, *Chem. Mater.*, 32, 9260-9267, (2020).

[2] R.B. Vasiliev et al., High-energy exciton transitions in quasi-two-dimensional cadmium chalcogenide nanoplatelets. *Phys. Rev. B*, 95, 165414, (2017).

[3] D.A. Kurtina et al., Atomically Thin Population of Colloidal CdSe Nanoplatelets: Growth of Rolled-up Nanosheets and Strong Circular Dichroism Induced by Ligand Exchange, *Chem. Mater.*, 31, 9652-9663, (2019).

[4] R.B. Vasiliev et al., Spontaneous Folding of CdTe Nanosheets Induced by Ligand Exchange, *Chem. Mater.*, 30, 1710-1717, (2018).

LD-I-13

Luminescence Solar Concentrators with Silicon Quantum Dots

Ilya Sychugov

*Department of Applied Physics, KTH – Royal Institute of Technology
Hannes Alfvéns väg 12, 114 19 Stockholm, Sweden*

Inorganic nanocrystals find applications as light converters in many areas, such as light-emitting diodes, bio-labels, and photovoltaics. In particular, silicon quantum dots (QDs) belong to the class of benign materials with high elemental abundance and low toxicity. In this presentation our recent results on synthesis and basic spectroscopic characteristics of such ultra-small (< 10 nm) particles will be summarized. Fabrication and performance of a particular photovoltaic device with Si QDs will be also presented.

We utilized both top-down and bottom-up approaches for Si nanocrystal fabrication. The former is realized by etching and oxidation of a very thin device layer of silicon-on-insulator wafers. As a result, Si QDs passivated with oxide are formed [1, 2]. They can be studied by single-dot spectroscopy technique thanks to spatial separation being larger than one micron. Spectroscopy characterization revealed narrow photoluminescence lines at low temperature with a peak position varying from 1.2 to 2.0 eV [2], ascribed to the quantum size effect. In addition, we found a high degree of linear polarization in Si QD emission, which can be attributed to dielectric confinement in elongated Si nanoparticles. Comparison of the emission and absorption spectroscopy with theoretical calculations allowed to elucidate evolution of the electronic structure for this technologically important material at the nanoscale [3].

For bottom-up chemical synthesis we relied on disproportionation reaction for the non-stoichiometric silica [4, 5]. This approach allows to obtain large quantities of Si QDs featuring a high quantum yield (50-60%), which is attractive for light-converting applications. Solid-state nanocomposite of Si QDs in the off-stoichiometry thiol-ene polymer with good nanoparticle dispersion were fabricated by selecting ligands with monomer-matching polarity. Ester functional groups appeared to be the most suitable [4, 5].

Finally, we applied these nanocomposites in photovoltaic application as luminescent solar concentrators. Such semi-transparent solar cells can be integrated to building facades, combining glazing and photovoltaic functions in the urban environment [6, 7]. Our 20x20 cm² prototypes with ~80% visible light transparency featured power conversion efficiency up to 1.7%, very low haze and good photostability [8].

- [1] J. Zhou, F. Pevere, H. Gatty, J. Linnros, I. Sychugov, Photoluminescence intensity enhancement of single silicon quantum dots on a metal membrane with a spacer, *Phys. Status Solidi A*, 217 (2020) 1900575.
- [2] J. Zhou, F. Pevere, H. Gatty, J. Linnros, I. Sychugov, Wafer-scale fabrication of isolated luminescent silicon quantum dots using standard CMOS technology, *Nanotechnology*, 31 (2020) 505204.
- [3] M.O. Nestoklon, I. Avdeev, A.V. Belolipetsky, I. Sychugov, F. Pevere, J. Linnros, I.N. Yassevich, Tight-binding calculations of optical properties of Si nanocrystals in SiO₂ matrix, *Faraday Discuss.*, 222 (2020) 258-273.
- [4] J. Huang, J. Zhou, T. Haraldsson, A. Clemments, M. Fujii, H. Sugimoto, B. Xu, I. Sychugov, Triplex Glass Laminates with Silicon Quantum Dots for Luminescent Solar Concentrators, *Solar RRL*, 4 (2020) 2000195.
- [5] J. Zhou, J. Huang, J. Linnros, A. Samanta, Z. Yang, I. Sychugov, Cost-effective Synthesis of Silicon Quantum Dots with Near-infrared Photoluminescence and Near-unity Internal Quantum Efficiency, submitted, (2021).
- [6] I. Sychugov, Analytical Description of a Luminescent Solar Concentrator, *Optica*, 6 (2019) 1046-1049.
- [7] I. Sychugov, Geometry effects on luminescence solar concentrator efficiency: analytical treatment, *Appl. Opt.*, 59 (2020) 5715-5722.
- [8] J. Huang, J. Zhou, J. Linnros, A. Samanta, E. Jungstedt, L. Berglund, I. Sychugov, Large-area Efficient Luminescent Solar Concentrator with Silicon Quantum Dots as Building Envelope Material, submitted, (2021).

LD-I-14

Probing with single quantum emitters: measuring at nano-scale and characterizing at micro- and macro level

A. V. Naumov

*Institute of Spectroscopy RAS, 5 Fizicheskaya Street, 108840 Troitsk, Moscow, Russia
Moscow State Pedagogical University, Malaya Pirogovskaya Ulitsa, 1/1, Moscow, 119435
Moscow, Russia*

Author's email address: a_v_naumov@mail.ru

It is shown how nanoscopy methods based on the registration of single fluorescent molecules and semiconductor quantum dots were used to characterize dielectric materials. In the described studies, single quantum emitters were used both as point light sources and as sensitive multiparameter local probes that detect interactions of light with matter at the nanoscale. Measuring a sufficient number of probes simultaneously makes it possible to map the dielectric parameters of some materials. The mapping procedure, if performed using a suitable mathematical model, can be accurate down to nanometers and give reliable averages at micro and macro scales.

LD-I-15

Re-scan Confocal Microscopy of ESCRT-mediated lysosome repair

**Stefan G. Stanciu¹, Iustin Floroiu¹, Radu Hristu¹, Efstathios Fiorentis¹,
Maja Radulovic², Camilla Raiborg², Harald A. Stenmark²**

[1] *Center for Microscopy-Microanalysis and Information Processing, Politehnica University of Bucharest, Bucharest, 060042 Romania*

[2] *Department of Molecular Cell Biology, Institute for Cancer Research, Oslo University Hospital, Oslo, Norway.*

E-mail: stefan.g.stanciu@upb.ro

Super-resolution microscopy techniques, capable of circumventing the resolution limit imposed by diffraction, are extremely useful for resolving important properties of eucaryotic and procaryotic cells that are not accessible to conventional microscopies¹. While the resolution advantages of some of these techniques come at the cost of high laser beam power, or very specific contrast agents², Re-scan Confocal Microscopy (RCM)³ has emerged over the past few years as a valuable tool to investigate biological specimens at sub-diffraction resolution using ultra-low beam power, and any type of fluorophores. In addition to a standard Confocal Laser Scanning Microscope (CLSM), where the beam is scanned on the sample by means of a system of mirrors, the RCM incorporates a second system of mirrors whose role is to scan the light emitted by the sample upon laser excitation on the surface of a CCD/s-CMOS image sensor. If the angular amplitude of the camera scanner (re-scanner) is double the angular amplitude of the sample scanner, a resolution advantage of $\sqrt{2}$ over a conventional CLSM is achieved. With additional deconvolution resolutions down to 120nm under 488nm excitation can be achieved. Conventional RCMs are designed for fluorescence imaging, but recent efforts showed that the Re-scan concept can also be exploited for achieving optical super-resolution based on non-linear effects not requiring contrast-agents, such as Second Harmonic Generation⁴.

In this work we discuss our results on RCM imaging of the lysosome repair process. Lysosomes are specialized organelles with many important roles, including the degradation of macromolecules, pathogen killing, and cell signaling, but their damage, which can occur due to pathogens, amphiphilic drugs, or other membrane-disrupting agents, impose serious threat to cell viability⁵. Severely damaged lysosomes are removed by lysophagy, an autophagic pathway that sequesters and degrades damaged lysosomes⁶. Lysosomes with milder damage are repaired by the endosomal sorting complex required for transport (ESCRT) machinery⁷. In the current work we place additional attention to this subject, discussing how RCMs resolution advantages are useful to investigate subtle morpho-structural aspects of cells linked to the lysosome repair process.

Acknowledgement: This work was supported by the UEFISCDI Grant RO-NO-2019-0601 MEDYCONAI.

1. Sigal, Y. M.; Zhou, R.; Zhuang, X., Visualizing and discovering cellular structures with super-resolution microscopy. *Science* **2018**, *361* (6405), 880-887.
2. Schermelleh, L.; Ferrand, A.; Huser, T.; Eggeling, C.; Sauer, M.; Biehlaier, O.; Drummen, G. P., Super-resolution microscopy demystified. *Nature cell biology* **2019**, *21* (1), 72.
3. De Luca, G. M.; Breedijk, R. M.; Brandt, R. A.; Zeelenberg, C. H.; de Jong, B. E.; Timmermans, W.; Azar, L. N.; Hoebe, R. A.; Stallinga, S.; Manders, E. M., Re-scan confocal microscopy: scanning twice for better resolution. *Biomedical optics express* **2013**, *4* (11), 2644-2656.
4. Stanciu, S. G.; Hristu, R.; Tranca, D. E.; Stanciu, G. A.; Manders, H.; Cherian, A.; Tark-Dame, M.; Manders, E. M. In *Higher-harmonic generation microscopy beyond the diffraction barrier based on re-scan strategies for optical data acquisition (HARMOPLUS)*, Proc. ATTRACT-Final Conf.—Igniting Deep Tech Revol., 2020; pp 1-5.
5. Papadopoulos, C.; Meyer, H., Detection and clearance of damaged lysosomes by the endo-lysosomal damage response and lysophagy. *Current Biology* **2017**, *27* (24), R1330-R1341.
6. Hung, Y.-H.; Chen, L. M.-W.; Yang, J.-Y.; Yang, W. Y., Spatiotemporally controlled induction of autophagy-mediated lysosome turnover. *Nature communications* **2013**, *4* (1), 1-7.
7. Radulovic, M.; Schink, K. O.; Wenzel, E. M.; Nähse, V.; Bongiovanni, A.; Lafont, F.; Stenmark, H., ESCRT-mediated lysosome repair precedes lysophagy and promotes cell survival. *The EMBO journal* **2018**, *37* (21), e99753.

LD-I-16

Raman spectroscopy of phospholipid membranes

N.V. Surovtsev¹

1- Institute of Automation and Electrometry, Russian Academy of Sciences, Novosibirsk 630090, Russia

snv@iae.nsk.su

Phospholipids are the main component of biological membranes. In water surrounding, phospholipids self-assemble into bimolecular layers of few nanometer thickness, presenting a model of biological membranes. Raman spectroscopy is a noninvasive and label-free experimental technique, which allows one to identify components of multicomponent membranes and to describe the phase state of lipid molecules in phospholipid bilayers. In this work, we present the experience of our research group in Raman spectroscopy of phospholipids. It shows examples of the Raman application to determine: the composition of membranes, the conformational state of molecules, their orientation, phase state, separation of multicomponent membranes into coexisting domains of different phases, elastic properties of membranes in the terahertz range.

The most exciting outcome of our studies relates to the importance of conformation disorder of hydrocarbon chains at temperatures, where phospholipids are still macroscopically in the ordered (gel) phase [1,2]. Sensitivity of some Raman lines to molecular ordering/disordering state was applied to the problem of the phase coexistence in multicomponent lipid bilayers [3,4]. The way for distinguishing the existence of molecular complexes and well-defined domains was suggested [4].

Low-frequency Raman spectroscopy is still an open field in the study of phospholipid bilayers. Recently, we have found that the low-frequency Raman spectrum of frozen suspensions of phospholipid vesicles demonstrates peaks in the range of 6-20 cm^{-1} , which were attributed to vibrational eigenmodes of a phospholipid bilayer (Fig. 1) [5,6]. These modes can be applied to the problem of coexisting domains of different compositions in multicomponent membranes [7,8].

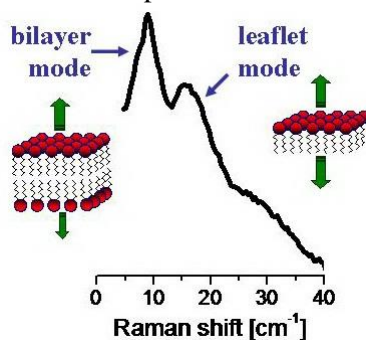


Fig. 1. Illustration of layer modes and their manifestation in the low-frequency Raman spectrum.

This work was supported by Russian Foundation (Grant No. 19-12-00127).

[1] A.A. Dmitriev and N.V. Surovtsev, Temperature-dependent hydrocarbon chain disorder in phosphatidylcholine bilayers studied by Raman spectroscopy, *J. Phys. Chem. B*, 119, 15613-15622 (2015).

[2] Yu.V. Zaytseva, S.V. Adichtchev, N.V. Surovtsev, Raman study of temperature-induced hydrocarbon chain disorder in saturated phosphatidylcholines, *Chem. Phys. Lipids*, 30, 104926 (2020).

[3] S.V. Adichtchev, K.A. Okotrub, A.M. Pugachev, I.V. Zaytseva, N.V. Surovtsev, Raman spectroscopic study of phase coexistence in binary phospholipid bilayers, *Appl. Spectrosc.*, 75, 87-93 (2021).

[4] K.A. Okotrub, I.V. Zaytseva, S.V. Adichtchev, N.V. Surovtsev, Raman spectroscopy and DSC assay of the phase coexistence in binary DMPC/cholesterol multilamellar vesicles, *BBA-Biomembranes*, 1863, 183514 (2021).

[5] N.V. Surovtsev, A.A. Dmitriev, S.A. Dzuba, Normal vibrational modes of phospholipids bilayers observed by low-frequency Raman scattering, *Phys. Rev. E*, 95, 032412 (2017).

[6] A.A. Dmitriev and N.V. Surovtsev, Vibrational eigenmodes of phospholipid layers in low-wavenumber Raman spectrum of multilamellar vesicles, *J. Raman Spectrosc.*, 50, 1691-1699 (2019).

[7] D.V. Leonov, S.V. Adichtchev, S.A. Dzuba, N.V. Surovtsev, Vibrational layer eigenmodes of binary phospholipid-cholesterol bilayers at low temperatures, *Phys. Rev. E*, 99, 022417 (2019).

[8] D.V. Leonov, S.A. Dzuba, N.V. Surovtsev, Normal vibrations of ternary DOPC/DPPC/cholesterol lipid bilayers by low-frequency Raman spectroscopy, *RSC Advances*, 9, 34451-34456 (2019).

LD-I-17

SERS-active substrates based on Au/Ag-decorated silicon nanostructures for the rapid detection of chemical and biomolecules

L.A. Osminkina^{1,2}

1- Lomonosov Moscow State University, Physics Department, Leninskie Gory 1, 119991 Moscow, Russian Federation

2- Institute for Biological Instrumentation of Russian Academy of Sciences, 142290 Pushchino, Moscow Region, Russian Federation

osminkina@physics.msu.ru

Surface-enhanced Raman scattering (SERS) has proven itself to successfully detect different biomarkers of diseases, viruses, and bacteria, etc. Due to the SERS effect, the intensity of Raman scattering of light by molecules adsorbed on nanostructured surfaces of noble metals usually increases by 6-8 orders of magnitude. The observed increase in Raman intensity can be explained by two mechanisms: electromagnetic, which is associated with localized surface plasmon resonance in nanostructures of noble metals, and chemical, caused by charge transfer between adsorbed molecules and the nanostructures. The main characteristics of a proper SERS-substrate are its homogeneity, batch-to-batch reproducibility, the stability of SERS signal intensity, and easy and cost-effective fabrication.

Silicon nanostructures such as arrays of silicon nanowires (SiNWs) and porous silicon films (PSi) are attractive objects for creating sensitive sensors due to the simplicity of their preparation methods and silicon surface tailorability. Since arrays of nanowires and porous films have a huge surface area, a high number of metallic nanoparticles (NPs) could be packed on them, which would yield a high enhancement factor when using such nanostructures as SERS-active substrates. SiNWs can be obtained by several different methods, but among the others, metal-assisted chemical etching is the simplest method that does not require expensive equipment and is attracting more and more attention in the large-scale production of SiNWs. PSi films are usually produced by electrochemical etching of crystalline silicon wafers.

In our study, the fabrication process of a SiNW matrix differently modified with Ag and Au NPs was demonstrated [1]. The process combines SiNW synthesis by the metal-assisted chemical etching with or without native Ag/Au NPs and subsequent Ag or/and Au NPs chemical deposition. This fabrication method has a short processing time, is cost-effective, and provides structural variability with high potential for SERS applications. We evaluated the SERS activity of PSi with pores ranging in size from meso to macro, the surface of which was coated with Au NPs [2]. We found that different pore diameters in the PSi layers provide different morphology of the gold coating, from an almost monolayer to 50 nm distance between nanoparticles. Methylene blue (MB) and 4-mercaptopyridine (4-MPy) were used to describe the SERS activity of obtained Au/PSi surfaces. The best Raman signal enhancement was shown when the internal diameter of torus-shaped Au NPs is around 35 nm [2]. It has been shown that molecules of pyocyanin (PYO), a specific metabolite of the bacteria *Pseudomonas aeruginosa*, can be successfully detected in artificial sputum up to 6.25 μM , which is the lower limit of the clinically significant range [1]. Moreover, the label-free rapid detection of unconjugated bilirubin up to a concentration in the clinically relevant range has been demonstrated with high reproducibility. To understand the role of plasmonic resonances in the observed SERS spectrum, we performed electromagnetic simulations of Raman scattering intensity as a function of the internal diameter. The results of these simulations are consistent with the obtained experimental data [1, 2]. These results open up the possibility of using the developed SERS-active substrates as platforms for point-of-care clinical diagnostics.

The research was funded by the Russian Science Foundation (grant number 20-12-00297).

[1] O. Žukovskaja, S. Agafilushkina, V. Sivakov, K. Weber, D. Cialla-May, L. Osminkina, J. Popp, Rapid detection of the bacterial biomarker pyocyanin in artificial sputum using a SERS-active silicon nanowire matrix covered by bimetallic noble metal nanoparticles. *Talanta*, 202, 171-177, (2019).

[2] S. N. Agafilushkina, O. Žukovskaja, S. A. Dyakov, K. Weber, V. Sivakov, J. Popp, D. Cialla-May, L.A. Osminkina Raman Signal Enhancement Tunable by Gold-Covered Porous Silicon Films with Different Morphology. *Sensors*, 20(19), 5634, (2020).

LD-I-18

Raman diagnostics of porous silicon nanoparticles biodegradation

M.B. Gongalsky¹

1- Lomonosov Moscow State University, Physics Department, Leninskie Gory 1, 119991 Moscow, Russian Federation

mgongalsky@gmail.com

Raman diagnostics is a powerful non-invasive tool for tracking of porous silicon nanoparticles (SiNPs) directly in cells. It may provide information about phase composition of SiNPs, i.e. amorphous/nanocrystalline ratio, the average size of silicon nanocrystals (nc-Si), etc. It also allows bioimaging of SiNPs inside cells.

That was used for monitoring of the SiNPs uptake and biodegradation in breast cancer cells ¹. The approach worked well for both luminescent (with small nc-Si affected by quantum confinement) and non-luminescent PSiNPs. Raman diagnostics showed complete biodegradation of SiNPs inside the living cells after 13 days of the incubation. Moreover, some intermediary states with partially biodegraded PSiNPs were characterized. The shrinking of the average nc-Si size and formation of amorphous phase have been detected.

Such a versatile tool gives opportunities to tailor the biodegradation of PSiNPs. For instance, the effect of drying and surface pretreatment on the dissolution rate of PSiNPs was demonstrated². The samples were dried with supercritical CO₂ solvent (SCD) or air (AD) and then both annealed at 600 °C for 16 hours in 1% oxygen. The obtained PSiNPs can be considered as core-shell structures with a crystalline silicon core and a SiO₂ layer on the surface. The analysis of Raman spectra allowed to estimate the sizes of the crystalline silicon cores about 4.5 nm for the initial AD-PSiNPs, and about 2 nm for the initial SCD-PSiNPs. Raman bioimaging revealed the stability of the AD-PSiNPs and the complete dissolution of the SCD-PSiNPs after 24 hours of incubation with cells. This fast biodegradation may explain the lower cytotoxicity measured for SCD-PSiNPs.

The experimental data, obtained by Raman spectroscopy, can be explained by means of a model for the biodegradation of PSiNPs³. The model is based on a diffusion equation combined with Nernst-Brunner mass transfer equation describing the dissolution of silicon and formation of silicic acid. The model can take into account more than 10 factors influencing the PSiNPs biodegradation kinetics, such as the morphology of PSi NPs, surface composition, properties of surrounding media and protective coating layer.

The research was funded by the Russian Science Foundation (grant number 19-72-10131).

- (1) Tolstik, E.; Osminkina, L. A.; Matthäus, C.; Burkhardt, M.; Tsurikov, K. E.; Natashina, U. A.; Timoshenko, V. Y.; Heintzmann, R.; Popp, J.; Sivakov, V. *Nanomedicine : nanotechnology, biology, and medicine* **2016**, *12* (7), 1931–1940.
- (2) Gongalsky, M. B.; Tsurikova, U. A.; Storey, C. J.; Evstratova, Y. V.; Kudryavtsev, A. A.; Canham, L. T.; Osminkina, L. A. *Faraday Discuss.* **2020**, *222*, 318–331.
- (3) Gongalsky, M. B.; Sviridov, A. P.; Bezsudnova, Yu. I.; Osminkina, L. A. *Colloids and Surfaces B: Biointerfaces* **2020**, *190*, 110946.

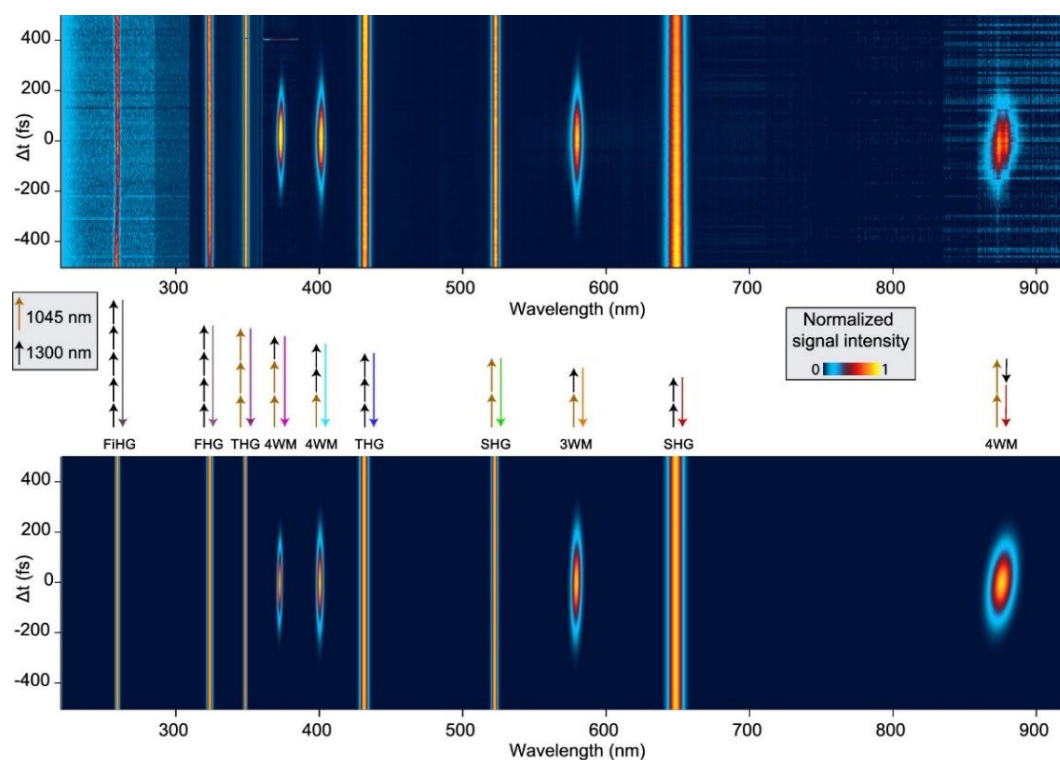
LD-I-19

Multi-order Nonlinear Mixing in Dielectric Nanoparticles for Bio-Applications

Luigi Bonacina

Department of Applied Physics, Université de Genève, 1211 Genève 4, Switzerland

Whereas most of the reports on the nonlinear properties of micro- and nanostructures address the generation of distinct signals, such as second or third harmonic, we recently demonstrated that the novel generation of dual output lasers developed for microscopy can readily increase the accessible parameter space and enable the simultaneous excitation and detection of multiple emission orders such as several harmonics and signals stemming from various sum and difference frequency mixing processes.¹ This rich response, which in our case features 10 distinct emissions and encompasses the whole spectral range from the deep ultraviolet to the short-wave infrared (SWIR), is demonstrated using various nonlinear metal-oxide nanomaterials (*Harmonic Nanoparticles*, HNPs) while being characterized and simulated temporally and spectrally.



(Top) Intensity-normalized spectrograms obtained from a KNbO_3 particle upon simultaneous 1300 and 1045 nm excitation. Direct harmonic signals (SHG, THG, FHG, FiHG) appear as continuous vertical stripes as they do not depend on the relative pulse delay Δt , contrary to signals generated by the superposition of the 1300 and 1045 nm pulses (3WM and 4WM) which display a clear Δt dependence. (Center) Photon-combinations leading to each distinct spectral element of the response. (Bottom) Numerically simulated spectrograms.¹

Notably, the multi-order response is conserved when HNPs are embedded in biological media allowing their use as nonlinear imaging probes.¹ Moreover, the efficient conversion of low-scattered SWIR light into visible light by HNPs embedded in a tissue could be exploited to develop solutions combining imaging, sensing, and photo-triggered drug release.²

References

- [1]. Campargue, G., La Volpe, L., Giardina, G., Gaulier, G., Lucarini, F., Gautschi, I., Ronan, L. D., Diviani, D., Mugnier, Y., Wolf, J.P. & Bonacina, L. (2020). Multiorder Nonlinear Mixing in Metal Oxide Nanoparticles. *Nano Letters*, 20(12), 8725-8732.
- [2]. Vuilleumier, J., Gaulier, G., De Matos, R., Ortiz, D., Menin, L., Campargue, G., Mas, C., Constant, S., Le Dantec, R., Mugnier, Y., Bonacina, L. & Gerber-Lemaire, S. (2019). Two-photon-triggered photorelease of caged compounds from multifunctional harmonic nanoparticles. *ACS Applied Materials & Interfaces*, 11(30), 27443-27452.

LD-I-20

High power CW laser heating for the study of materials at very high temperature

L. Gallais¹, G. Kermouche², M. Minissale³, Y. Pontillon⁴, M. Richou⁵, J.L. Rullier⁶

- 1- Aix Marseille Univ, CNRS, Centrale Marseille, Institut Fresnel, 13013 Marseille, France*
2- Mines Saint-Etienne, CNRS, UMR 5307 LGF, Centre SMS, F-42023 Saint-Etienne, France
3- Aix Marseille Univ, CNRS, PIIM, 13007 Marseille, France
4- CEA, DES, IRESNE, DEC, Cadarache F-13108 Saint-Paul-Lez-Durance, France
5- CEA, IRFM, F-13108 Saint-Paul-Lez-Durance, France
6- CEA CESTA, 15 Avenue des Sablières, 33114 Le Barp, France

Knowledge of material properties and their changes at high temperature, as well as the behaviour of the materials themselves, is critically important in numerous fields such as nuclear fission, fusion (plasma facing components), aerospace, defense and many industrial processes. For such studies, laser techniques are particularly suitable since they can easily drive materials to extreme temperatures with a very high amount of precision and control. They can be combined with contactless instruments (pyrometry, spectrometry, thermal imaging) to derive the thermophysical properties of materials. In this talk we will discuss our recent contributions in this field with some studies conducted on Graphite (up to 3800 K) [1], on Uranium dioxide (with generation of complex thermal gradients) [2] and Tungsten (studies of recrystallization kinetics at high temperature) [3].

- [1] L. Gallais, T. Vidal, E. Lescoute, Y. Pontillon, J. L. Rullier, 'High power continuous wave laser heating of graphite in a high temperature range up to 3800 K', *Journal of Applied Physics* 129, 043102 (2021).
 [2] T. Vidal, L. Gallais, J. Faucheux, H. Capdevila, J. Sercombe, Y. Pontillon, 'Simulation of reactivity initiated accident thermal transients on nuclear fuels with laser remote heating', *Journal of Nuclear Materials* 530, 151944 (2020).
 [3] M. Minissale, A. Durif, P. Hiret, T. Vidal, J. Faucheux, M. Lenci, M. Mondon, G. Kermouche, Y. Pontillon, C. Grisolia, M. Richou, L. Gallais, 'A high power laser facility to conduct annealing tests at high temperature', *Review of Scientific Instruments* 91, 035102 (2020).

LD-I-21

Near-field infrared nano-imaging and nano-spectroscopy of correlated quantum materials

Mengkun Liu

Stony Brook University, Department of Physics and Astronomy

Over the past decade, optical near-field techniques, especially the scattering-type scanning near-field optical microscope (s-SNOM), have undergone tremendous development. This is partly due to the ever-increasing demand for the exploration of the nano-world and partly due to the considerable progress in laser and scanning probe technologies. In this talk, I will report the recent advances in the infrared (IR) and terahertz (THz) near-field nanoscopy and spectroscopy technologies and discuss their applications for correlated quantum materials. For instance, I will present cases on current induced metal-insulator-metal stripes in Ca_2RuO_4 single crystals and moiré-type phase separations in $\text{La}_{0.67}\text{Sr}_{0.33}\text{MnO}_3$ thin films. The discovered nanoscale textures have orientations tied uniquely to the crystallographic axes of the sample or miscut steps in the substrate, implying a strong coupling of the electronic transition to lattice degrees of freedom. I will also discuss recent advances in data analysis and the cryogenic, ultrafast, and multi-modal imaging capabilities. These new developments set the stage for future spectroscopic investigations to access the low energy electron, phonon, and spin dynamics in complex quantum materials at the nanoscale.

LD-I-22

Pulsed laser fabrication of Zn and ZnO nanoparticles meant for implementation in chemical sensors

M.D. Komissarov, N.B. Leonov, T.A. Vartanyan

ITMO University, Kronverksky pr. 49, 197101 St. Petersburg, Russia

email address: tavartanyan@itmo.ru

Zinc oxide as a wide bandgap semiconductor with large exciton bounding energy has found numerous applications. It is used as an effective UV light absorber, transparent electrode in thin film solar cells, and transducer material in chemical sensors [1]. The last application is based on its intrinsic nonstoichiometry that may be affected by the gas environment. While the thin film conductivity changes in response to the different gases exposure is most explored, changes of the photoluminescence properties are also promising. Oxygen vacancies are believed to be responsible for the bright green luminescence under UV irradiation. In the presence of ambient oxygen they are healed and the luminescence intensity drops. To function as an oxygen pressure transducer zinc oxide is to be prepared in a thin film form, preferably, as nanoparticles with large surface area.

Based on our experience in physical vapor deposition of granular metal films [2,3] we adopted the following procedure. First, the granular zinc films were produced via the pulsed laser fabrication method. The metallic zinc target of 99,99% purity was irradiated by the second harmonic of Nd:YAG laser. The laser pulses with 10 ns duration follow with the repetition rate of 10 Hz. The amount of the deposited material varies in dependence of the laser pulse energies and the number of pulses.

The atomic force microscopy images show the formation of granular films of different mean thicknesses. Absorbance spectra confirm the formation of an array of densely packed flat zinc nanoparticles with the plasmon resonance that shifts from 320 to 650 nm when the mean thickness of the film changes from 5 to 12 nm and then stabilizes. Simultaneously, the surface conductivity of the granular film rapidly drops by 6 orders of magnitude. This observation attests to the arriving at the percolation threshold at this rather low amount of deposited material.

The obtained granular zinc films were transformed into zinc oxide via heating in a muffle furnace at 800°C for 3 hours. This transformation is accompanied by the plasmon bands disappearance and emerging of the exciton band at 360 nm.

Photoluminescence of zinc oxide was observed in two bands with maxima at 390 and 510 nm. The short-wavelength band corresponds to the exciton luminescence while the long-wavelength band is due to the defects. The relative intensity of the two photoluminescence bands depends on the nature of the excitation source. When the photoluminescence was excited by the 10 ns pulses of the 3-rd harmonic of the Nd:YAG laser at 355 nm the short-wavelength band dominate, while at low intensity cw excitation at somewhat shorter wavelengths both bands have comparable intensities. The reason for this difference was found to be the saturation of the long-wavelength fluorescence known as “green” luminescence of zinc oxide band and associated with defects. This saturation happens already at the fluencies as small as 2 mJ/cm². On the other hand, the short-wavelength fluorescence band associated with the exciton recombination remains unsaturated below at least 40 mJ/cm².

[1] Transparent Conductive Zinc Oxide. Basics and Applications in Thin Film Solar Cells. Ed.: K. Ellmer, A. Klein, B. Rech (Springer-Verlag Berlin Heidelberg) (2008)

[2] N.B. Leonov, I.A. Gladskikh, V.A. Polishchuk and T.A. Vartanyan, Evolution of the Optical Properties and Morphology of Thin Metal Films during Growth and Annealing, Optics and Spectroscopy, vol. 119, pp. 458-463, (2015).

[3] N.B. Leonov, V.A. Polishchuk and T.A. Vartanyan, An investigation of major factors affecting metal nanoparticle morphology in island films. In: Metal Nanoparticles: Properties, Synthesis and Applications, Ed.: Y. Saylor and V. Irby (Nova Science Publishers, Inc., New York) (2018)

LD-O-1

Optical Detection of Defects during Laser Metal Deposition: Simulations and Experiment

I.B. Gornushkin¹, G. Pignatelli¹, A. StraÙe¹

¹BAM Federal Institute for Materials Research and Testing,
Richard-Willstätter-Strasse 11, 12489 Berlin, Germany
igor.gornushkin@bam.de

Laser metal deposition is a rapidly evolving method for additive manufacturing that combines high performance and simplified production routine [1]. Quality of production depends on instrumental design and operational parameters that require constant control during the process [2]. In this work, feasibility of using optical spectroscopy as a control method is studied via modeling and experimentally. A simplified thermal model is developed based on the time-dependent diffusion-conduction heat equation and geometrical light collection into detection optics. Intense light emitted by a laser-heated spot moving across a sample surface is collected and processed to yield the temperature and other temperature-related parameters. In a presence of surface defects the temperature field is distorted in a specific manner that depends on a shape and size of the defect. Optical signals produced by such the distorted temperature fields are simulated and verified experimentally using a 3D metal printer and a sample with artificially carved defects. Three quantities are tested as possible metrics for process monitoring: temperature, integral intensity, and correlation coefficient. The shapes of the simulated signals qualitatively agree with the experimental signals; this allows a cautious inference that optical spectroscopy is capable of detecting a defect and, possibly, predicting its character, e.g. inner or protruding.

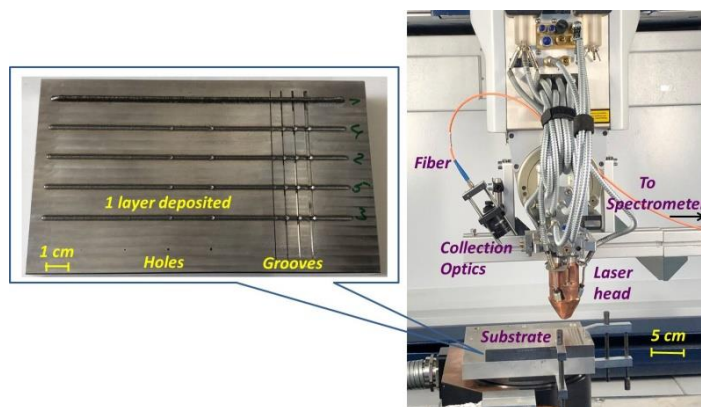


Figure 1. LMD-nozzle printer head and the optical head attached to it. Inset: the substrate with artificial defects.

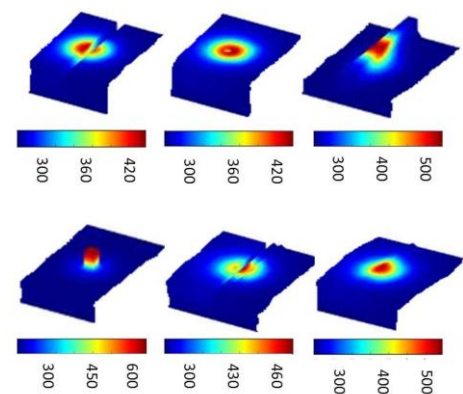


Figure 2. Temperature field around different defect types

[1] I.I. Gibson, D. Rosen, B. Stucker, Additive Manufacturing Technologies, second ed., (Springer, 2015).

[2] H.L. Wei, T. Mukherjee, W. Zhang, J.S. Zuback, G.L. Knapp, A. De, T. DebRoy, Mechanistic models for additive manufacturing of metallic components, Progress in Materials Science 116, 100703 (2021).

LD-O-2

Picosecond recording and optical features of nanostructures in AlZnO:Ag films

Sergeev M.M., Dolgoplov A.D., Gresko V.R.

ITMO University, Faculty of Nanoelectronics, Saint Petersburg, Russia

gresko.97@mail.ru

Thin sol-gel films are widely applied in the nanoelectronics, photonic crystals, and biomedical applications. This is especially true for transparent semiconductor films modified by laser emission. Therefore, the study of alterations in the optical properties of such films after laser emission becomes more and more important for the applications of such materials in the field of spectrophotometry, and especially for SERS.

In this work, nanogratings with a submicron period and a relieve depth of several tens of nm on the surface of AlZnO sol-gel films with silver nanoparticles were obtained by the method of two-beam interference processing by pulsed laser emission.

Such nanostructures can be used to enhance the luminescence signal from certain materials [1]. This study shows the effect of the resulting gratings on the luminescent properties of the dye rhodamine G6. The wavelength of the peak of the luminescence intensity of rhodamine was comparable to the period of the nanograting. The nanostructure amplified the signal of rhodamine intensity several times, while the maximum amplification occurred at a wavelength near the grating period. At the same time, both the luminescence spectra of a solution of rhodamine and rhodamine on the initial untreated AlZnO film differed from each other only slightly and had a maximum at a longer wavelength.

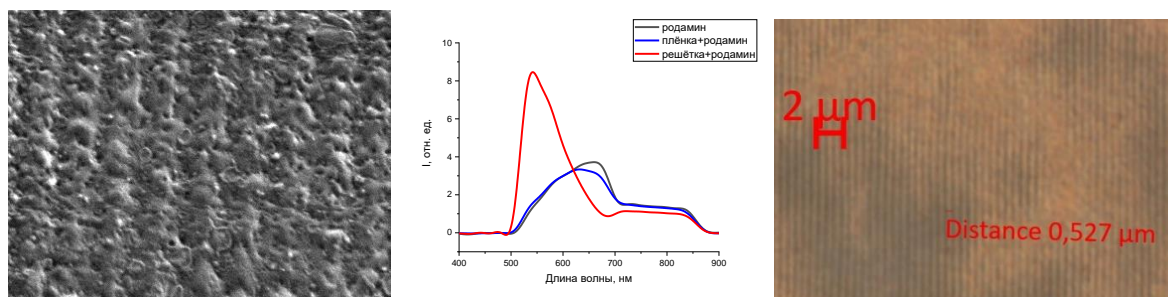


Fig.1 (a) SEM image of nanogratings (b) Dependence of the fluorescence intensity on the wavelength at normal incidence relative to the untreated surface of the AlZnO film (c) Appearance of a nanograting at high magnification in a bright field

Acknowledgments

The study is funded by the grant of Russian Science Foundation (project № 19-79-10208).

- [1] Wang J. et al. Ultrasensitive SERS detection of rhodamine 6G and p-nitrophenol based on electrochemically roughened nano-Au film //Talanta. – 2020. – Т. 210. – С. 120631..

LD-O-3

Raman spectra and a CH₂-chain length of organic molecules

V.V. Kuzmin¹, K.A. Prokhorov¹, E.A. Sagitova¹, S.M. Kuznetsov¹, M.S. Iablochnikova^{1,2},
P.V. Ivchenko³, I.E. Nifant'ev³, G.Yu. Nikolaeva¹

*1-Prokhorov General Physics Institute of the Russian Academy of Sciences,
Vavilov Str. 38, 119991 Moscow, Russia*

2-Moscow Institute of Physics and Technology,

Institutskiy Per. 9, 141700 Dolgoprudnyi, Moscow Region, Russia

*3-Department of Chemistry, M.V. Lomonosov Moscow State University,
Leninskie Gory 1-3, 119991 Moscow, Russia*

Organic matters, whose molecules contain CH₂-chains, are of great importance for petrochemical industries, pharmaceuticals, cosmetics, etc. Their physical properties, for example, a freezing point and viscosity, depend strongly on the number and length of such chains.

In our contribution, we present a comparative (theoretical and experimental) Raman study of a wide collection of such substances, namely, normal and branched alkanes (C_nH_{2n+2}), normal alkanols (C_nH_{2n+1}OH). For instance, Figure 1 shows the structural formulas and Raman spectra of some substances under study.

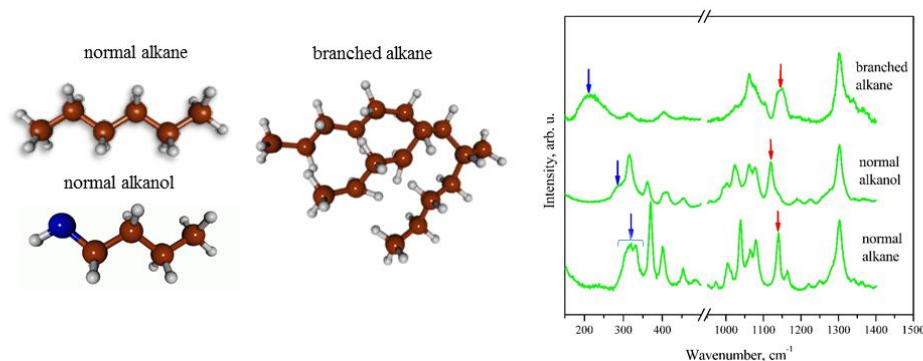


Figure 1. The structural formulas and Raman spectra of normal alkane C₆H₁₄, normal alkanol C₄H₉OH and branched alkane C₁₈H₃₈ (hydrogenated trimer of 1-hexene). The brown, blue and gray balls are C, O, and H atoms, respectively. The blue and red arrows point to the D-LAM and symmetric C-C stretching modes, respectively.

We revealed quantitative relationships between molecular characteristics and spectral features of the D-LAM and symmetric C-C stretching modes, which are active in the spectral regions 0-500 and 1100-1200 cm⁻¹, respectively. We found that the peak positions of the D-LAM in the spectra of these substances are sensitive to the total number of C atoms and the number of CH₂-chains in a molecule. The spectral characteristics (wavenumber and bands shape) of the symmetric C-C stretching mode are strongly influenced by perturbations in the chains, such as a presence of branching in molecules or substitution of terminal group, in particular, by OH group. The specific bend of molecules with a formation of two planar segments results in the splitting of the symmetric C-C stretching mode into two components with the wavenumbers, which depend on the length of these segments. Thus, Raman spectroscopy is an effective tool to determine the number and length of CH₂-chains in large variety of organic molecules, containing CH₂-chains.

This work was funded by the Russian Foundation for Basic Research (project No. 19-02-00931). We are grateful to the Joint Supercomputer Center of the RAS for the possibility of using their computational resources for our calculations.

LD-O-4

Non-Destructive Monitoring of Apples under Long-Term Storage

Ana-Maria Bratu, Cristina Popa, Mihaela Bojan, Petre Catalin Logofatu, Mioara Petrus

*National Institute for Laser, Plasma and Radiation Physics
409 Atomistilor St., PO Box MG-36, 077125 Bucharest, Romania
ROMANIA*

ana.magureanu@inflpr.ro

Fundamental requirements for extending the time that fruits can be stored and marketed is to ensure an adequate external environment and to investigate the internal environment of the commodity. Light and temperature are the main external environmental factors that can affect fruits storage. The internal environment is defined by a complex of gases and volatiles that can diffuse through fruit tissue controlling the development of the commodity. These volatiles are mostly esters, alcohols, aldehydes, ketones and ethers [1]. In apples, ethylene is present in high concentration during the development period, but decreases as the fruit matures, following a stage in which the other volatiles such as alcohols and esters increases [2]. Ethanol is naturally produced by fermentation process of fruit sugars by yeast, and its detection in an internal atmosphere of fruit can provide an additional measure of maturity [3]. Exploration of new relationships between ethylene and ethanol can be of great help in the process of plant development and in improving crop yield by delaying aging and maintaining fruit quality.

Information about external defects is important for sorting the mature and over mature fruits with the best attributes. Rapid identification of defective fruits is beneficial for reducing unnecessary storage and avoiding quality degradation.

Over the years, considerable efforts have been made to develop non-destructive sensing techniques for quality evaluation of apples, mainly spectroscopic and imaging [4,5]. Both external defects and internal physiological changes of apples are important factors in the post-harvest, sorting and storage period. Rapid identification of defective fruits is beneficial for reducing unnecessary storage and avoiding quality degradation.

This work studies the evolution in time of several varieties of apples with application in quality storage maintenance. Two different methods were used to evaluate long-stored apples for better sorting and degradation assessment. The first method was laser photoacoustic spectroscopy for the detection of ethylene and ethanol compounds from the internal atmosphere of apples. The second method was multispectral imaging that measures the image and the spectrum combined and also can be used to address features such as ripening and external defects. The experiments showed that, the ethylene value decreases and the value of ethanol increases, which sometimes we may associate with a drift of the images toward darker tones, because the apple is slowly degrading. Non-invasive, real-time inspection can reveal when the degradation process begins, improving the capability of sorting, maintaining their quality and storability.

[1] P.S. Dimick, J.C. Hoskin, T.E. Acree, Review of apple flavor—state of the art. *Crit Rev Food Sci Nutr.* 18, 387–409 (1983).

[2] N.M.M. Paillard, The flavour of apples, pears and quinces. In: Morton IE, Macleod AJ, editors. *Food Flavours, Part C. The flavour of fruits.* Amsterdam, the Netherlands: Elsevier Science; pp. 1–41(1990).

[3] M.B. Jackson, B. Herman, A. Goodenough, An examination of the importance of ethanol in causing injury to flooded olants, *Plant Cell Environ* 5, 163-172 (1982)

[4] Dumitras D.C., Dutu D.C., Matei C., Magureanu A.M., Petrus M., Popa C., Laser photoacoustic spectroscopy: Principles, instrumentation, and characterization, *J. Optoelectron. Adv. M.* 9 (13), 3655 -3701 (2007).

[5] LuR., Multispectral imaging for predicting firmness and soluble solids content of apple fruit, *Postharvest Biol. Technol.* 31(2), 147-157 (2004).

LD-O-5

Laser Induced Heating of Germanium Nanostructures

A.V.Pavlikov^{1,2}, A.M.Sharafutdinova¹, S.N.Bokova-Sirosh³, A.M.Rogov⁴, A.L.Stepanov⁴

1 - Faculty of Physics, M.V. Lomonosov Moscow State University, Leninskie Gory, Moscow 119991, Russia

2-National Research Centre “Kurchatov Institute”, Kurchatov sq., 1, Moscow, 123182, Russia

3-General Physics Institute of Russian Academy of Sciences, Moscow, 119991, Russia.

4-Zavoisky Physical-Technical Institute, FCR Kazan Scientific Center of RAS, Kazan, 420029, Russia

pavlikov@physics.msu.ru

Raman spectroscopy is a widely used method of structural diagnostics. Spontaneous Raman scattering measurements are carried out using cw lasers. Excitation of bulk materials rarely leads to their significant heating, but nanostructured materials can be locally heated up to hundreds of degrees due to the action of exciting laser radiation [1,2]. Strong heating manifests itself in an additional shift of the peak in the Raman scattering spectrum. Heating effect may be explained by low thermal conductivity of porous nanostructures. Unlike porous Si and Ge nanostructures obtained by high-temperature synthesis, Ge nanowires grown by electrochemical deposition from aqueous solutions can crystallize under the action of exciting radiation [3,4].

In this work we present Raman investigation of nanoporous Ge layers formed by implantation with Ag⁺ and Cu⁺ at energies $E = 30$ and 40 keV and doses from 9.3×10^{16} to 1.5×10^{17} ion/cm². To study the morphology of the formed implanted layers, micrographs were obtained using a high-resolution scanning electron microscope Merlin. Raman studies were carried out on Horiba LabRAM HR-800 and HORIBA LabRAM HR Evolution UV-VIS-NIR-Open micro-Raman spectrometers. Helium-neon (He-Ne) ($\lambda = 632.8$ nm), Nd:YAG ($\lambda = 532.0$ nm) and argon (Ar⁺) ($\lambda = 488.0$ nm) lasers with a maximum power of 6 mW, with a minimum spot radius of 3 μ m, were used as the exciting radiation.

It was established that implanted Ge nanostructures were amorphous. Irradiation of nanostructures by exciting lasers with an intensity exceeding threshold value leads to heating and subsequent local crystallization of the irradiated regions. The dependence of the crystallization thresholds on the conditions of ion implantation and the wavelength of the probe laser was found. Using the Stokes to anti-Stokes ratio, the local heating temperature was estimated. The results obtained will help to evaluate the thermal conductivity of the nanoporous layers. Such Ge structures can have potential application in thermoelectric elements.

[1] S. Piscanec, M. Cantoro, A. C. Ferrari, J. A. Zapien, Y. Lifshitz, S. T. Lee, S. Hofmann, J. Robertson, Raman spectroscopy of silicon nanowires, *Phys. Rev. B* 68, 241312(R) (2003)

[2] R. Jalilian, G. U. Sumanasekera, H. Chandrasekharan, M. K. Sunkara, Phonon confinement and laser heating effects in Germanium nanowires, *Phys. Rev. B*, 74, 15, 155421 (2006)

[3] S. A. Gavrilov, A. A. Dronov, I. M. Gavrilin, R. L. Volkov, N. I. Borgardt, A. Yu. Trifonov, A. V. Pavlikov, P. A. Forsh, P. K. Kashkarov Laser crystallization of germanium nanowires fabricated by electrochemical deposition. *Journal of Raman Spectroscopy* 49, 810–816 (2018).

[4] A. V. Pavlikov, P. A. Forsh, P. K. Kashkarov, S. A. Gavrilov, A. A. Dronov, I. M. Gavrilin, N. I. Borgardt, R. L. Volkov, S. N. Bokova-Sirosh, E. D. Obraztsova Investigation of the Stokes to anti-Stokes ratio for germanium nanowires obtained by electrochemical deposition. *Journal of Raman Spectroscopy* 51, 596–601 (2020).

LD-O-6

Design and fabrication of a compact multispectral laser based optical beam induced current (OBIC) microscope

Ankur Gogoi

Department of Physics, Jagannath Barooah College, Jorhat 785001, Assam

Email address: ankurgogoi@gmail.com

Recently, OBIC microscopy has become an attractive and efficient alternative to other complicated methods like atomic force microscopy (AFM), electronic beam induced current (EBIC) microscopy, *etc.*, for the failure analysis of semiconductor devices. In this contribution, we report the design and fabrication of a coherent narrow band laser based confocal OBIC microscope capable of offering non-destructive, high-resolution analysis of semiconductor media at three different wavelengths. The microscope essentially consists of a multispectral laser source, chopper, polarization optics, laser scanning module, scan and tube lens assembly, inverted microscope, semiconductor device biasing circuit, and lock-in amplifier. Preliminary results including confocal OBIC images of light emitting diodes will be presented to demonstrate the capability of the microscope.

LD-O-7

A 3-ns pulsed diode laser for a high spatial resolution lidar

S. M. Pershin¹, M.Ya. Grishin¹, V. A. Zavozin¹, V. S. Makarov², V. N. Lednev¹, A.V. Myasnikov³, A.V. Turin²

1-Prokhorov General Physics Institute of the Russian Academy of Sciences, 119991 Moscow, 38 Vavilova street, Russia

2-Space Research Institute of the Russian Academy of Sciences, Moscow, Russia

3-Sternberg Astronomical Institute Moscow State University Moscow, Russia

E-mail: pershin@kapella.gpi.ru

We report on achieving the generation of 3 ns pulses by an AlGaAs semiconductor laser (907 nm, 0.2 $\mu\text{J}/\text{pulse}$) with eye-safe energy density ($\leq 1 \mu\text{J}/\text{cm}^2$) suitable for lidar sensing. The laser consists of three stacked emitters in a plastic case. An external current pump generator was assembled on a printed circuit board along with the laser from commercially available discrete elements with a bipolar FM417 transistor as a key.

Using such a laser, a lidar based on a single photon avalanche photodiode (SPAD) was constructed. Fig.1(a) shows a lidar histogram (range distribution of backscattered photons) for measuring distance to a flat wall at ~ 33 m. In this experiment the laser emitted 50000 pulses and the range resolution was 10 cm. One can see from Fig.1(a) that the lidar histogram is asymmetric just like the laser pulse shape on the oscillogram in Fig.1(b). Such pulse shape is characteristic for diode lasers pumped by the capacitor discharge [1].

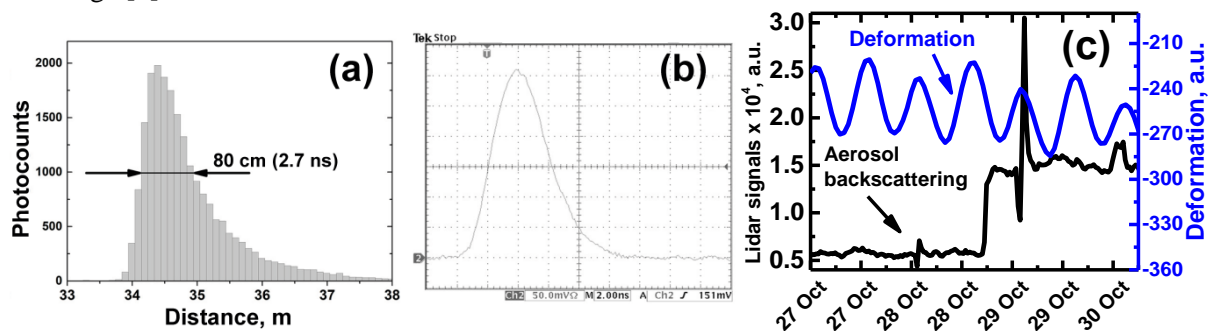


Fig.1. (a) Laser pulse in the form of lidar photocount histogram, (b) laser pulse oscillogram measured by the Aktakom ADS-2332 oscilloscope (300 MHz bandwidth), (c) comparison of magmatic aerosol lidar sensing data (lower curve) and the seasonal Earth's crust deformation measured by a laser strainmeter (upper curve) at October 27-30, 2019.

The lidar based on the described laser and a SPAD detector provided monitoring of magmatic aerosols with 10 cm spatial resolution inside a dead-end adit in the Baksan Neutrino Observatory near the Elbrus volcano ($43^{\circ}14'57.7''\text{N}$, $42^{\circ}43'19.5''\text{E}$). The lidar performed a measurement every 30 minutes by accumulating 100000 laser pulses. For the first time a 3-fold “jump” of the magmatic aerosol output has been detected (see Fig.1(c)) [2]. The nature of this “jump” remains unclear. Note that laser strainmeter with $1.6 \cdot 10^{-11}$ m sensitivity [3] have not detected any traces of the Earth's crust deformation at this time, which proves the lidar as a new, highly sensitive instrument for studying geodynamic processes.

The authors are grateful for the Russian Science Foundation for the financial support of the study (project №19-19-00712).

[1] Slipchenko S.O., Podoskin A.A., Soboleva O.S., Pikhitin N.A., Bagaev T.A., Ladugin M.A., Marmalyuk A.A., Simakov V.A., Tarasov I.S. Generation of nanosecond and subnanosecond laser pulses by AlGaAs/GaAs laser-thyristor with narrow mesa stripe contact. *Optics Express*, 24, 16500 (2016).

[2] Pershin S.M., Sobisevich A.L., Grishin M.Ya., Gravirov V.V., Zavozin V.A., Kuzminov V.V., Likhodeev D.V., Lednev V.N., Makarov V.S., Myasnikov A.V., and Fedorov A.N., Volcanic activity monitoring by unique LIDAR based on a diode laser, *Laser Phys. Lett.* 17(11), 115607 (7pp), (2020).

[3] Milyukov V.K., Myasnikov A.V., “Metrological characteristics of the Baksan laser interferometer,” *Measurement Techniques*, Instrument Society of America, vol. 48, no. 12, pp. 1183-1190, (2012).

LD-O-8

Omnidirectional dynamics of the Earth's crust seasonal deformation and the aerosol output decrease in the adit over the Elbrus volcano magmatic chamber

S. M. Pershin¹, M.Ya. Grishin¹, V. A. Zavozin¹, V. S. Makarov², V. N. Lednev¹, A.V. Myasnikov³

1-Prokhorov General Physics Institute of the Russian Academy of Sciences, 119991 Moscow, 38 Vavilova street, Russia

2-Space Research Institute of the Russian Academy of Sciences, Moscow, Russia

3-Sternberg Astronomical Institute Moscow State University Moscow, Russia

E-mail: pershin@kapella.gpi.ru

It is known [1] that seasonal Earth's crust deformations caused by temperature seasonal changes are modulated by Solar-lunar tides with diurnal and semi-diurnal waves P_1K_1 and S_1 . Recently, we have discovered that the Earth's crust autumn deformation is accompanied by a decrease in the aerosol output in the dead-end adit of the Baksan Neutrino Observatory (BNO) ($43^\circ 14' 57.7''N$, $42^\circ 43' 19.5''E$) over the Elbrus volcano magmatic chamber c. Aerosol output variations were monitored by a specially designed lidar with eye-safe laser irradiation level ($<1 \mu J/cm^2$) and a single photon avalanche photodiode as a detector. In the measurements the lidar emitted 100000 laser pulses at 10 kHz repetition rate every 30 minutes. Note that the lidar integrates the contributions of all magmatic gases and water vapor that carry aerosol in the adit volume over the whole lidar sensing path which increases the lidar sensitivity to geodynamic processes. The experimental setup and procedure are described in detail in [3].

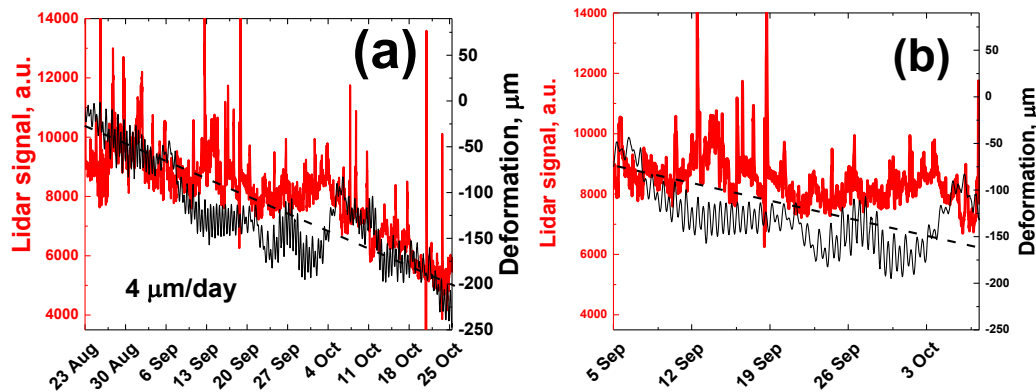


Fig.1. (a) Seasonal Earth's crust deformation (Aug-Nov 2019) measured by a 75-m laser strainmeter in BNO (black thin line) and the aerosol output (red thick line), the dashed line represents the average deformation trend; (b) a detailed picture of the Earth's crust deformation and the aerosol output in the vicinity of the fall equinox (Sep 5 – Oct 8, 2019).

The seasonal Earth's crust deformation is indicated by the strainmeter measuring arm length shortening by $\sim 4 \mu m/day$. The data analysis has revealed that the crust deformation and aerosol output in Aug-Nov 2019 are symbatic (see Fig.1(a)). Simultaneously, we have revealed that in the vicinity of the fall equinox (Sep 5 – Oct 8, 2019) both dependences omnidirectional deviate from the general trend (dashed line in Fig.1(a)) stronger than the amplitude of deformation waves caused by temperature and Solar-lunar tides (Fig.1(b)) [2] and humidity.

The authors are grateful to the Russian Science Foundation for financial support of the study (project №19-19-00712).

[1] Melchior P. J., 1983, *The Tides of the Planet Earth*, Oxford: Pergamon Press; Melchior Paul J., "The Earth Tides," Pergamon Press, Oxford, 458 pages, 1966.

[2] Milyukov V.K., Myasnikov A.V., "Metrological characteristics of the Baksan laser interferometer," *Measurement Techniques*, Instrument Society of America, vol. 48, no. 12, pp. 1183-1190, (2012).

[3] Pershin S.M., Sobisevich A.L., Grishin M.Ya., Gravirov V.V., Zavozin V.A., Kuzminov V.V., Likhodeev D.V., Lednev V.N., Makarov V.S., Myasnikov A.V., and Fedorov A.N., Volcanic activity monitoring by unique LIDAR based on a diode laser, *Laser Phys. Lett.* 17(11), 115607 (7pp), (2020).

THz SOURCES AND SPECTROSCOPY

THz-I-1

Terahertz gyrotrons and their applications: resent results

M. Glyavin

*Institute of Applied Physics RAS (IAP RAS)
603950, 46 Ulyanov str., Nizhny Novgorod, Russia
glyavin@ipfran.ru*

The last decade has contributed to the rapid progress in the gyrotron development. The paper describes the main features of high frequency gyrotrons [1,2]. The most impressive data about pulsed and CW tubes, working in the terahertz frequency range, are given. These gyrotrons operate (in some specific combinations) at very low voltage and beam current, demonstrate an extremely narrow frequency spectrum or wide frequency tuning. Although in comparison with the classical microwave tubes the gyrotrons are characterized by greater volume and weight due to the presence of bulky parts (such as superconducting magnets) they can easily be embedded in a sophisticated laboratory equipment. All these features have opened the road to many novel and prospective applications of gyrotrons.

At IAP RAS, the development of the terahertz band by the methods of vacuum electronics, as well as by using conventional gyrodevices, which employ extremely strong magnetic fields at the main cyclotron resonance and the second cyclotron harmonic, is supported by the development of gyrodevices operated at higher cyclotron harmonics (large-orbit gyrotrons (LOGs)). Pioneering work of IAP RAS demonstrated the fundamental possibility of obtaining high-power continuous-wave and pulsed radiation of the frequencies from 0.33 to 0.65 THz using gyrotrons. In recent experiments, a pulse solenoid with a magnetic field of up to 50 T generated a power of 5 - 0.5 kW at the fundamental cyclotron resonance in single pulses with a duration of 50 microseconds at record-breaking frequencies of 1 - 1.3 THz. IAP RAS developed a technology which ensures the creation of relatively simple pulse solenoids with a magnetic field of up to 30 T and a pulse repetition rate of up to 0.1 Hz. Based on such coils the gyrotron with an operating frequency of 0.67 THz and a power of 200 kW has been realized. This gyrotron can be used for recording of ionization sources from distances of several hundreds of meters. The continues wave (CW) gyrotron developed at IAP RAS jointly with GYCOM Ltd. provides CW radiation with a kW range power in the frequency range from 0.26 to 0.53 THz. The maximum power measured by a calorimeter is 1 kW at 0.26 THz and 0.24 kW at 0.53 THz. Such power is approximately five times higher than in the worldwide reported gyrotrons at the same frequency range. It is important that power values up to 10W required for spectroscopy applications can be obtained at low voltage of about 1.5 kV or low beam current of 20 mA. The phase-lock loop control of the anode voltage result in the width of the frequency spectrum from 0.5 MHz for a free-running gyrotron down to 1 Hz for the stabilized gyrotron, which corresponds to long-term stability up to $\delta f / f \sim 10^{-12}$. Recently, the phase-lock loop stabilized gyrotron was used in experiments for recording characteristic lines in pure gases and gas mixtures. It is interesting that the same scheme can be used for quick power modulation and data transmitting. High quality transmission of sound and pseudo random bit sequence (with a speed up to 1.5 Mbit/s) has been obtained. Second-harmonic CW gyrotron with improved mode selection based on double electron beam has been tested. Wide step tuning of the frequency by excitation of various modes was demonstrated in the range of 0.4-0.78 THz with a power level of about few Watts, which is useful for modern NMR/DNP spectroscopy applications. A complex cavity is under discussion for high harmonic excitation and preliminary tests confirmed operation with the frequency near 1.2 THz. The project of gyrotrons with field emission cathode are under development. Feasibility of a high-power sub-THz gyrotron with smooth wideband frequency tuning suitable for spectroscopy has been studied. Simulations and preliminary experiments demonstrated a possibility of wide-band (about 10%) fine frequency tuning. An output power of 0.5 to 1 kW can be obtained at a frequency of about 0.2 THz within a 10 GHz band, which are the parameters needed for testing of quantum electrodynamics predictions in positronium spectroscopy measurements.

[1] A.Litvak, G.Denisov, M.Glyavin. Russian gyrotrons: achievements and trends. IEEE Journal of Microwaves, 1,1, 260-268 (2021)

[2] S.Sabchevski, M.Glyavin, S.Mitsudo, Y.Tatematsu, T.Idehara. Novel and Emerging Applications of the Gyrotrons Worldwide: Current Status and Prospects. Journal of Infrared, Millimeter, and Terahertz Waves (2021) <https://doi.org/10.1007/s10762-021-00804-8>

THz-I-2

“Perfect” Vortex Beams in the THz Range: Generation and Application

**B. Knyazev^{1,2}, Yu. Choporova^{1,2}, V. Gerasimov^{1,2}, O. Kameshkov^{1,2}, A. Lemzyakov^{1,2},
N. Osintseva^{1,2}, V. Pavelyev^{1,3}, K. Tukmakov³**

1 - Novosibirsk State University, Ul. Pirogova 1, Novosibirsk, Russia, 630090

2 - Budker Institute of Nuclear Physics of SB RAS, Pr. Lavrentyeva 11, Novosibirsk, Russia, 630090

3 - Samara National Research University, Moskovskoe Shosse 34, Samara, Russia, 443086

ba_knyazev@phys.nsu.ru

In modern optics, special attention is drawn to “perfect vortex beams” (PVBs), ring beams with orbital angular momentum. These beams can be obtained by focusing Bessel beams with a lens. In the case of ideal Bessel beams, a PVB is an ideal ring. Real Bessel beams (BBs) always bear traces of their origin to one degree or another. In the terahertz range, BBs can be created using three types of diffractive phase axicons (Fig. 1, the upper row). They form practically identical Bessel beams, at least near the optical axis, as seen from the middle row in Fig. 1. However, after focusing with a lens (the bottom row in Fig. 1) the perfect beams obtained differ significantly from each other. It is seen from the results of numerical calculations [1] shown in Fig. 1.

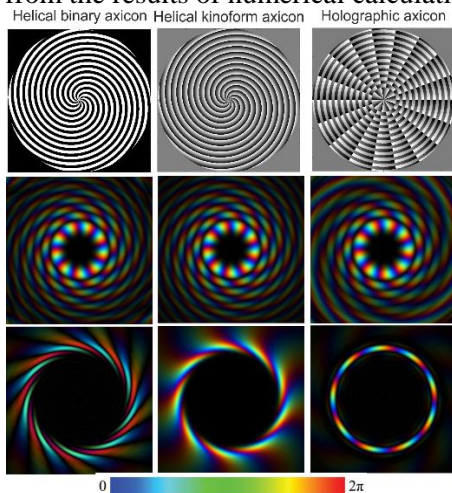


Fig. 1. Three types of phase axicons (upper row) that form Bessel beams with a topological charge $\ell = 9$ and a transverse wave number $\kappa = 3.1 \text{ MM}^{-1}$ (middle row). Bottom row: perfect beams obtained in the focal plane of the lens with $f = 100 \text{ MM}$.

It was convincingly shown in the experiments that plasmons arose at the intersections of a PB, split into spiral segments (see the lower-left frame in Fig. 1), with the edge of the cylinder and propagated to the end of the ATL along parallel disjoint trajectories, the number of which was equal to $2|\ell|$. The experimentally measured rotation angle of the plasmon trajectory on the cylindrical surface of the transmission line and the dynamics of the rotation angle of the resulting free wave, which retained the number of lobes equal to $2|\ell|$, were in good agreement with the values of these quantities calculated under the assumption of conservation of angular momentum. The results obtained can be used, for example, to create plasmonic communication lines and sensors.

This work was supported by the Russian Science Foundation, grant 19-12-00103. Experiments were carried out at the Novosibirsk free electron laser, which is a part of the Shared Research Facility “Siberian Synchrotron and Terahertz Radiation Center.”

[1] B. Knyazev, V. Cherkassky, O. Kameshkov, Perfect terahertz vortex beams formed using diffractive axicons and prospects for excitation of vortex surface plasmon polaritons, *Applied Sciences*, vol. 11, 717, (2021).

THz-I-3

Terahertz spectroscopy of nano-carbon materials

B.Gorshunov¹, S.Zhukov¹, E.Zhukova¹, M.Belyanchikov¹, A.Melentev¹, M.H.Levitt², G.Hoffman², S.Alom², G.R.Bacanu², R.J.Whitby², E.Obraztsova^{1,3}, A.Tonkikh^{1,3}, D.Kopylova⁴, D.Krasnikov⁴, Y.Gladush⁴, A.Pronin⁵, E. Uykur⁵, M.Dressel⁵, M.Sajadi⁶, A.Nasibulin⁴

¹*Moscow Institute of Physics and Technology, Moscow, Russia*

²*School of Chemistry, University of Southampton, Southampton, United Kingdom*

³*A.M Prokhorov General Physics Institute, RAS, Moscow, Russia*

⁴*Skolkovo Institute of Science and Technology, Moscow, Russia*

⁵*I.Physikalisches Institut, Universität Stuttgart, Stuttgart, Germany*

⁶*Fritz-Haber-Institut der MPG, Berlin, Germany; Department of Chemistry, University of Paderborn, Paderborn, Germany*

We will review our latest results on terahertz and infrared spectroscopy of nano-carbon materials - single-wall carbon nanotubes, and fullerenes with various ions and molecules encapsulated inside.

Measurements of spectra of transmission and reflection coefficient as well as of complex ac conductivity and dielectric permittivity of the objects are performed at frequencies from few wavenumbers up to the infrared and in the temperature interval 5 – 300 K. Fundamental mechanisms that are at the origin of single-particle and collective electronic phenomena in the studied systems are analyzed, and the prospects of their practical application in electronics and optoelectronics are discussed.

The research was supported by the Russian Science Foundation, grant №21-72-20050.

THz-I-4

High-temperature THz quantum cascade lasers: novel designs and MBE growth challenges

D. Ushakov¹, A. Afonenko¹, O.Yu. Volkov², I.N. Dyuzhikov², V.V. Pavlovskiy², A. Dolgov³,
R. Galiev³, S. Pushkarev³, D. Ponomarev³, **R. Khabibullin³**

1. Belarusian State University, Minsk, Belarus

2. Institute of Radio-Engineering and Electronics of RAS, Moscow, Russia

3. V.G. Mokerov Institute of Ultra-High Frequency Semiconductor Electronics of the Russian Academy of Sciences,
Russia,
khabibullin@isvch.ru

Over the past two decades, the operation temperature of terahertz quantum cascade lasers (THz QCLs) has continuously increased from cryogenic level to the current record value of 250 K (about -23°C) [1]. Here we review the state-of-the-art and future prospects of THz QCL designs with two-quantum wells in active module based on conventional heterojunction GaAs/AlGaAs and alternative material system HgCdTe [2]. We have analyzed the temperature dependence of the peak gain and predicted the maximum operation temperatures of the given designs.

THz QCL is one of the spectrally brightest solid-state source at THz frequencies with a potentially wide range of practical applications in high-resolution spectroscopy [3,4] and imaging systems [5]. The main barrier to the use of THz QCL “outside the laboratory” is their low operating temperatures. The limiting factors for increasing the operation temperatures of THz QCLs are associated with strong optical phonon scattering, the presence of parasitic current channels and the formation of electric field domains as was shown in [6,7]. Recently, the mode loss spectra for THz QCLs with double metal waveguide (DMW) were demonstrated in [8]. It was shown the high level of propagation loss of THz radiation in DMW, which exceeds 30 cm⁻¹ for room temperature. Thus, to improve the high-temperature performance of THz QCLs it is needed to develop new concepts of active region designs and to reduce losses in DMW.

Acknowledgments

This work was supported by the Russian Science Foundation Grant No. 21-72-30020.

References

- [1] Khalatpour A. et al. 2020 *Nat. Photonics* **15** 16.
- [2] Ushakov D.V., Afonenko A.A. et al. 2020 *Opt. Express* **28** 25371.
- [3] Hubers H.-W, H. Richter et al 2019 *J. Appl. Phys.* **125** 151401.
- [4] Volkov O., Pavlovskiy V. et al 2021 *IEEE Trans. Terahertz Sci. Technol.* **11** 330.
- [5] Sterczewski L.A., Westberg J. et al 2019 *Optica* **6** 766.
- [6] Khabibullin R.A., Shchavruk N.V. et al *Opto-Electronics Review* **27** 329.
- [7] Ushakov D.V., Afonenko A.A. et al. 2019 *Quantum Electronics* **49** 913.
- [8] Ushakov D.V., Afonenko A.A. et al. 2018 *Quantum Electronics* **48** 1005.

THz-I-5

Directional Diagram of THz radiation from DC-Biased Filament

O. Kosareva^{1,2,*}, N. Panov^{1,2}, I. Nikolaeva^{1,2}, D. Shipilo^{1,2}, D. Pushkarev², G. Rizaev², D. Mokrousova^{1,2}, A. Koribut², YA. Grudtsin^{1,2}, L. Seleznev^{1,2}, W. Liu³, A. Shkurinov^{1,4}, A. Ionin²

¹*Faculty of Physics, Lomonosov Moscow State University, Leninskie Gory, Moscow 119991, Russia*

²*P. N. Lebedev Physical Institute of the Russian Academy of Sciences, 53 Leninskiy prospect, Moscow 119991, Russia*

³*Institute of Modern Optics, Tianjin Key Laboratory of Micro-Scale Optical Information Science and Technology, Nankai University, Tianjin 300350, China*

⁴*ILIT RAS—Branch of the FSRC “Crystallography and Photonics” RAS, Svyatoozerskaya 1, 140700, Shatura, Moscow Region, Russia*

kosareva@physics.msu.ru

Terahertz generation from an air-plasma source is valuable for its broadband spectrum and scalable energy [1]. Remote generation of THz radiation is possible by frequency doubling locally and propagating the two optical beams in free space where they focus and mix at a distance to generate THz radiation. In this two-color plasma channel we have up to 50 THz spectrum with the ring-shaped directional diagram or conical emission [2]. The far-field THz beam profile in the low-frequency (< 3 THz) spectral range, which is important for explosives detection [3], has been suggested to have Gaussian shape instead of a conical one [4]. The directional diagram with on-axis maximum was observed from a DC-biased filament at 0.1 THz by Houard et al [5] and at 0.5 THz by Fukuda et al [6].

These observations raised the question if the far-field distribution of THz radiation from DC-biased filament preserves the on-axis maximum at the frequencies of ~1 THz and higher. Previous measurements showed angular distribution at a single frequency [5,6]. In our experiment THz angular distribution from a DC-biased (744 nm, 0.5 mJ, 90 fs) filament has a flat-top shape at all the selected frequencies $\nu = 0.3, 0.5, 1$ THz in the same conditions. Although a THz generation from a DC-biased filament has been studied since 2000 [7], no one has ever shown that the plasma refraction almost does not influence the THz low-frequency angular distribution. At higher frequencies the destructive interference of THz waves from the ionization front propagating with the superluminal velocity ensures the on-axis minima. Transition from the flat-top to conical angular distribution is explicitly shown in our manuscript due to 3D+time simulations based on Unidirectional Pulse Propagation Equation with unprecedentedly fine 0.01 THz resolution.

Funding. Russian Science Foundation (grant 21-49-00023), and National Natural Science Foundation of China (grant 12061131010).

[1] X. C. Zhang, A. Shkurinov, and Y. Zhang, “Extreme terahertz science,” *Nat. Photonics* **11**, 16 (2017).

[2] A. Gorodetsky, A. D. Koulouklidis, M. Massaouti, and S. Tzortzakis, “Physics of the conical broadband terahertz emission from two-color laser-induced plasma filaments,” *Phys. Rev. A* **89**, 033838 (2014).

[3] J. B. Baxter and G. W. Guglietta, “Terahertz spectroscopy,” *Anal. Chem.* **83**, 4342–4368 (2011).

[4] C. B. Sørensen, L. Guiramand, J. Degert, M. Tondusson, E. Skovsen, E. Freysz, and E. Abraham, “Conical versus gaussian terahertz emission from two-color laser-induced air plasma filaments,” *Opt. Lett.* **45**, 2132–2135 (2020).

[5] A. Houard, Y. Liu, B. Prade, V. T. Tikhonchuk, and A. Mysyrowicz, “Strong enhancement of terahertz radiation from laser filaments in air by a static electric field,” *Phys. Rev. Lett.* **100**, 255006 (2008).

[6] T. Fukuda, T. Otsuka, Y. Sentoku, H. Nagatomo, H. Sakagami, R. Kodama, and N. Yugami, “Experiments of forward THz emission from femtosecond laser created plasma with applied transverse electric field in air,” *Jpn. J. Appl. Phys.* **59**, 020902 (2020).

[7] T. Löffler, F. Jacob, and H. Roskos, “Generation of terahertz pulses by photoionization of electrically biased air,” *Appl. Phys. Lett.* **77**, 453–455 (2000).

THz-I-6

Surprising nonlinear optics of pulsed terahertz radiation

A. Tcypkin¹, A. Drozdov¹, I. Artser¹, A. Ismagilov¹, M. Melnik¹, I. Vorontsova¹, M. Zhukova¹, S. Kozlov¹

1- ITMO University, St. Petersburg, 197101, Russia
kozlov@mail.ifmo.ru

Recently, it has been theoretically predicted and experimentally confirmed that the coefficient of the nonlinear refractive index of materials in the terahertz frequency range can be several orders of magnitude higher than its value in the visible and near-IR spectral ranges both for crystals [1,2] and for liquids [3, 4]. The mechanism of this nonlinearity is low-inertia one, which means that high-speed THz photonics devices based on nonlinear effects are promising. The values of nonlinear refractive index for some materials are presented in the Table 1.

Table 1. The nonlinear refractive index coefficients in the NIR and the THz frequency range

Medium	n_2 cm ² /W in THz range	n_2 cm ² /W in NIR range
ZnSe	1×10^{-13}	3.8×10^{-14}
LiNbO ₃	7×10^{-11}	1.7×10^{-15}
Water	5×10^{-10}	1.9×10^{-16}
Ethanol	9×10^{-9}	7.7×10^{-16}

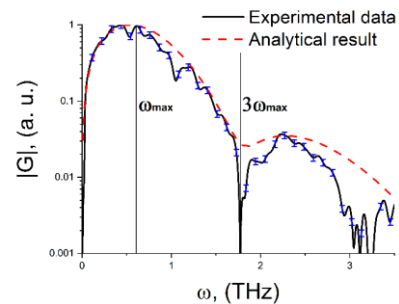


Fig. 1. Spectrum of the generated THz field. Black solid line is the experimental data, red dotted line is the analytical results, blue dashes line shows the error for experimental data

Moreover, well-known nonlinear effects in the field of pulsed THz radiation can qualitatively change their appearance. For example, the self-focusing phenomenon may not be observed even when the radiation power is significantly exceeded the critical self-focusing power [5].

Also, we discovered another amazing modification of one of the classical phenomena of nonlinear optics. The interaction of a THz pulse containing only one full oscillation of the electrical field with a medium with cubic nonlinearity can generate radiation at quadruple frequencies relative to the frequency of the power spectral density maximum, instead of radiation at triple frequency as expected. Illustration of this effect is present in the Fig.1.

It can be seen in Fig.1, that both for experimental and for theoretical results no generation of radiation at triple frequencies is observed in the spectrum of pulsed THz radiation at the output of the medium during the interaction of the generated THz field with a crystal, which also has cubic nonlinearity. Moreover, in the THz radiation spectrum instead of the triple frequency, according to the frequency of its spectral density maximum, a pronounced dip is observed. In this case, radiation of significant energy is generated at a quadruple frequency, which is not observed for similar experiments in the visible and near-IR frequency ranges. This effect is analytically proven and is determined by the asymmetry of the spectrum of such pulse.

However, some of the aspects of the measurements and calculations of z-scan curves were not completely discussed [6]. Here, we introduce some clarity to the raised issues of implementation of broadband single-cycle THz pulses for z-scan method. We are considering issues related to the spatio-spectral representation of strongly focused single-cycle THz pulse with extremely broad spectrum 0.1-2.5 THz, its nonparaxiality of propagation and influence the results measured by the z-scan technique. We also estimate the influence of ellipticity in the shape of the collimated THz beam to the beam profile close to the focus. We note that within an order of magnitude there is a very good agreement between the calculated and measured values even considering features of broadband single-cycle THz pulses.

The study is funded by RFBR project No. 19-02-00154.

- [1] K. Dolgaleva, et al., Prediction of an extremely large nonlinear refractive index for crystals at terahertz frequencies, *Physical Review A*, vol. 92, p. 023809, (2015).
- [2] M. Zhukova, et al., Estimations of Low-Inertia Cubic Nonlinearity Featured by Electro-Optical Crystals in the THz Range, *Photonics*, vol. 7, p. 98, (2020).
- [3] A. Tcypkin, et al., High Kerr nonlinearity of water in THz spectral range, *Optics express*, vol. 27, pp. 10419-10425, (2019).
- [4] A. Tcypkin, et al., Giant Third-Order Nonlinear Response of Liquids at Terahertz Frequencies, *Physical Review Applied*, vol. 15, p. 054009, (2021).
- [5] S.A. Kozlov, et al., Suppression of self-focusing for few-cycle pulses, *JOSA B*, vol. 36, pp. G68-G77, (2019).
- [6] M. Melnik, et al., Methodical inaccuracy of the Z-scan method for few-cycle terahertz pulses, *Scientific reports*, vol. 9, pp. 1-8, (2019).

THz-I-7

Methods of intense THz generation by multiterawatt, 800 nm laser pulses

M. M. Nazarov¹, P. A. Shcheglov¹, M. V. Chaschin¹, A.V.Mitrofanov^{1,3,4}, D. A. Sidorov-Biryukov^{1,2,3}, A.A. Voronin², A. M. Zheltikov^{1,2,3,5} and V. Ya. Panchenko^{1,2,4}

¹ *Kurchatov Institute National Research Center, Moscow 123182, Russia*

² *Physics Department, M.V. Lomonosov Moscow State University, Moscow 119992, Russia*

³ *Russian Quantum Center, Skolkovo, Moscow Region 143025, Russia*

⁴ *Inst. Laser and Information Technol. - Branch of FSRC "Cryst. and Photonics," RAS, Shatura, 140700 Russia*

⁵ *Department of Physics and Astronomy, Texas A&M University, College Station TX 77843, USA*

High-power terahertz (THz) sources [1-3] are in great demand as tools for the single-shot spectroscopy, advanced imaging, time-resolved studies. All these rapidly growing areas of research call for powerful and broadband, yet compact and robust sources of THz pulses. Leading this quest is the optical rectification (OR) of ultrashort laser pulses in quadratically nonlinear materials. For pump-probe experiments in strong fields with 30 fs temporal resolution, a simple method is required to obtain strong THz pulses from 0.8 μm multiTW laser systems. We demonstrated that the well-developed lithium niobate (LN) wafers have advantages in this situation, despite strong THz absorption and the absence of phase matching

THz generation in large-area LN wafers has been shown [1] to enable an OR of $\sim 2\text{-J}$, 25-fs laser pulses to 0.19-mJ THz waveforms with the coherence length for OR, $l_c \approx 50 \mu\text{m}$, is much shorter than the thickness of an LN wafer. Here, we aim at identifying the physical factors that limit the terahertz yield of an OR of ultrashort multiterawatt laser pulses in large-area thin LNs. We show that the THz yield tends to slow its growth as a function of the laser driver energy, saturate, and eventually decrease as the laser beam picks up a spatiotemporal phase due to the intensity-dependent refraction of the OR crystal. Non-phasematched generation in a thin layer provides significantly broadband and short THz pulses in comparison with other studied methods: two-color gas breakdown [3] and metal foil ablation at subrelativistic intensities [4]. As a result, in LN with 250 mJ of laser energy, we obtained a 10 μJ , single-cycle THz pulse with a broad, smooth spectrum, containing 40% of the energy at frequencies above 3 THz. That is twice more energetic THz pulse than obtained in a rare gas plasma pumped with the same laser system. This work was partially supported by RFBR grants 18-52-16024, and 18-02-40032

REFERENCES:

- [1] D. Jang, C. Kang, S.K. Lee, et.al. Optics Letters, **44**, 5634-5637, (2019)
- [2] M. Jazbinsek, U. Puc, A. Abina, A. Zidansek, Appl. Sci., **9**, 882 (2019)
- [3] M. M. Nazarov, A. V. Mitrofanov, D. A. Sidorov-Biryukov, et.al. JIMTW, 1-13.(2020).
- [4] M. M. Nazarov, P. A.Shcheglov, M. V.Chaschin, et.al. JPCS, **1692**, 012018, (2020).

THz-I-8

Terahertz emission from ionized air under single-color filamentation

**L.V. Seleznev, G.E. Rizaev, D.V. Pushkarev, A.V. Koribut, Y.A. Gerasimova,
Y.V. Grudtsyn, S.A. Savinov, Y.A. Mityagin, D.V. Mokrousova, A.A. Ionin**

P.N. Lebedev Physical Institute of RAS, 53 Leninski pr., Moscow, Russia

The presentation shows the results of an experimental study of the THz emission in the plasma of a single-color filament. The different wavelengths of filamented laser pulse (940, 740, and 370 nm) are used in the study. Particular attention is paid to the study of the frequency-angular distribution of the THz emission within 0.1 – 3 THz spectral range. It is shown that different spectral components of THz radiation have various angular distribution. It is shown that an increase in the laser beam number aperture leads to a growth in the THz emission divergence (Fig.1), especially in its low-frequency range.

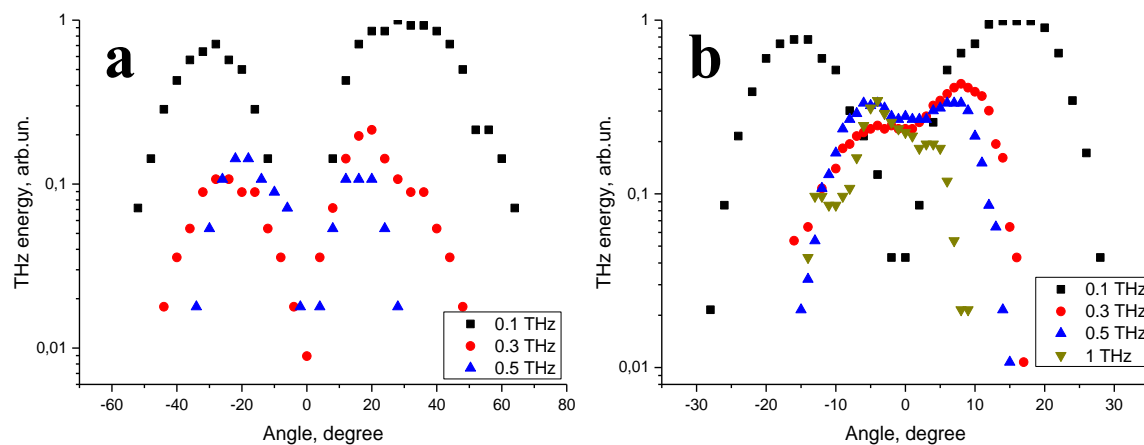


Fig.1. Angular distribution of different spectral components of THz radiation observed at various beam number aperture $2 \cdot 10^{-2}$ (a) and $5 \cdot 10^{-3}$.

The study showed a significant effect on the THz radiation characteristics of the initial wavelength of laser pulse. Transformation of frequency-angular THz emission spectrum produced by single-color (740 nm) laser filament plasma under an external electrostatic field of various strength is experimentally studied also. While there is no any static electric field, THz emission is predominantly generated in the low-frequency spectral range around 0.1 THz and propagates within a hollow cone. When the electric field is applied, the transition from the hollow cone to a filled one is observed with the field strength rise, THz emission frequency being within of 0.3 - 0.5 THz. Higher frequency emission of ~ 1 THz fills the whole cone with the emission maximum along the laser filament axis. The angular distribution for the low-frequency THz emission depends significantly on the laser pulse energy in contrast to the case of no electric field. An increase in the laser pulse energy leads to a decrease of the propagation angles for low-frequency THz emission and to disappearance of the local minimum in the angular distribution on the propagation axis.

The research is supported by RFBR grant 20-02-00114.

THz-I-9

Latest Developments in Terahertz Imaging Technologies at ETRI

D.-H. Choi, E.S. Lee, M. Kim, D.W. Park, J.-H. Shin, I.-M. Lee, K. H. Park

Terahertz Research Section, Electronics and Telecommunications Research Institute (ETRI), Daejeon 34129, Republic of Korea

choi.dh@etri.re.kr

Terahertz (THz) imaging techniques have been proven their usefulness in various fields such as medicine, pharmacy, industry, security providing unique or complementary information to that obtained from different imaging techniques [1,2].

At Electronics and Telecommunications Research Institute (ETRI), efforts have been made in THz 2D and 3D imaging technologies, especially for industry and security applications. Recently, we demonstrated a high-speed and cost-effective 2D imaging system [3]. The system utilized a telecentric f-theta lens, a brushless DC (BLDC) motor, and a stepping motor to acquire an image sized 500 x 400 pixels in about 2 s. The system is now applied to various applications including defect detection in display panels.

We also presented the THz imaging techniques to develop a high-resolution THz 3D imaging system. To increase the axial resolution of the imaging systems, a THz continuous wave (CW) system using Gouy phase shift interferometry is suggested and demonstrated [4]. Unlike the typical 3D imaging systems using CW, the system does not require a frequency sweep. Therefore, by adopting this technique the data acquisition time can be substantially reduced while obtaining sub-wavelength axial resolution. Combined with our sub-wavelength imaging system which can image human fingerprints at 518 GHz, we are expecting to realize a high-resolution THz 3D imaging system for security applications.

Lastly, we recently launched a project regarding personnel security screening technology. The project aims for developing a shoe scanner detecting concealed objects inside shoes on which the passengers stand for seconds. Details will be shown at the conference.

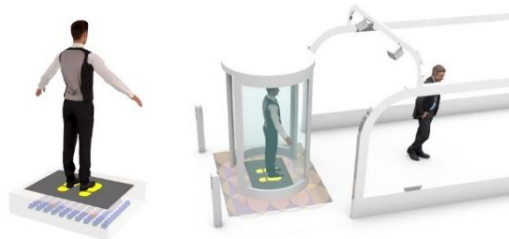


Fig. 1. Conceptual illustration of the shoe scanning system

[1] M. Tonouchi, Cutting-edge terahertz technology, Nat. Photonics vol. 1, pp. 97-105 (2007).

[2] D. M. Mittleman, Twenty years of terahertz imaging, Opt. Express vol. 26, pp. 9417-9431 (2018).

[3] E. S. Lee, M. Kim, K. Moon, I.-M. Lee, D.W. Park, J.-H. Shin, H.-S. Kim, D.-H. Choi, K.S. Choi, D.H. Lee, and K.H. Park, High-Speed and Cost-Effective Reflective Terahertz Imaging System Using a Novel 2D Beam Scanner, J. Lightwave Technol., vol. 38, pp.4237-4243 (2020).

[4] D.-H. Choi, I.-M. Lee, K. Moon, D. W. Park, E. S. Lee, and K. H. Park, Terahertz continuous wave system using phase shift interferometry for measuring the thickness of sub-100- μm -thick samples without frequency sweep, Opt. Express, vol. 27, pp. 14695-14704 (2019).

THz-I-10

Laser-driven terahertz sources and their applications

Luc Bergé

*Commissariat à l'Énergie Atomique et aux Énergies Alternatives
CEA, DAM, DIF – 91297 Arpajon - France*

Terahertz waves are highly popular because of their numerous applications, for example in security screening, medical imaging, time-domain spectroscopy and remote detection [1]. Located between microwaves and optical waves in the electromagnetic spectrum, they can be exploited in molecular spectroscopy from plasma emitters produced by femtosecond laser pulses ionizing gases such as air.

At moderate laser intensities, gas plasmas created by two- or multi-color optical pulses supply suitable emitters free of any damage. Electrons are tunnel ionized by the asymmetric light field usually composed of a fundamental wavelength and its second harmonic [2]. The resulting “photocurrent” polarized in the laser direction generates an ultrabroadband terahertz radiation, which finds direct applications in the coherent spectroscopy of complex molecules [3]. At relativistic intensities, plasma waves trigger strong longitudinal fields used, e.g., in laser-wakefield acceleration. Accelerated electrons crossing the plasma-vacuum interface then emit coherent transition radiation operating in the terahertz band, which can reach high field strengths and mJ energies [4,5,6].

This talk will review the different physical mechanisms involved in the terahertz emission by laser-plasma interaction at moderate or relativistic intensity. Results on the terahertz spectroscopy of crystal powders from atmospheric plasmas will be presented in the context of the project ALTESSE.

[1] M. Tonouchi, Nat. Photon. **1**, 9691 (2007).

[2] K.-Y. Kim, A. J. Taylor, J. H. Glowina, and G. Rodriguez, Nat. Photonics **2**, 605 (2008).

[3] L. Bergé, K. Kaltenecker, S. Engelbrecht, A. Nguyen, S. Skupin, L. Merlat, B. Fischer, B. Zhou, I. Thiele, and P. U. Jepsen, Europhys. Lett. **126**, 24001 (2019).

[4] J. Déchard, A. Debayle, X. Davoine, L. Gremillet, and L. Bergé, Phys. Rev. Lett. **120**, 144801 (2018).

[5] J. Déchard, X. Davoine, and L. Bergé, Phys. Rev. Lett. **123**, 264801 (2019).

[6] J. Déchard, X. Davoine, L. Gremillet, and L. Bergé, Phys. Plasmas **27**, 093105 (2020).

THz-I-11

High resolution spectroscopy based on frequency sweeping with using THz quantum cascade lasers

V.Vaks¹, V.A.Anferte¹, E.G.Domracheva¹, S.I.Pripolzin¹, M.B.Chernyaeva¹, A.Baranov²

1 -IPM RAS, 7, Akademicheskaya str., Afonino village, Nizhny Novgorod region, 603087 Russia

2-Institute of Electronics and Systems (IES), UMR 5214 CNRS - University of Montpellier, France

vax@ipmras.ru

Actual problems in the gas analysis are associated with developing the methods of analysis of multicomponent gas mixtures for various applications including the spectroscopy methods.

The main problem of high precise spectroscopy is development of high-stable tunable coherent radiation sources. The modern spectroscopic requirements to THz radiation sources are frequency stabilization with accuracy $\sim 10^{-8}$ - 10^{-10} from carrier frequency, Doppler resolution, high spectral purity and smooth tuning of frequency in wide frequency range.

The development of semiconductor technology will allow achieving a high level for production of the radiation sources and detectors for terahertz spectroscopy. The review of modern semiconductor radiation sources of THz ranges is presented.

The special consideration is given to possibility of using the behavior THz quantum cascade lasers (QCL) for application in spectroscopy. QCL working in continuous and pulse modes will be used for THz frequency range. The development of THz emitters based on QCL up to 3-4 THz is presented.

One of the promising methods for high resolution spectroscopy is approach on the base of fast frequency sweeping [1]. Fast frequency sweeping mode is the method of detecting the spectrum in sufficiently wide frequency range during the short time (about milliseconds) in current importance. This approach is used in high resolution gas spectroscopy in low frequency part of terahertz frequency range [2], in particular, at the analysis of multicomponent gas mixtures allowing to detect all substances, which have intensive absorption lines lying in frequency range of spectrometer and which are presented in gas mixtures at recording the spectrum. QCL working in pulse mode allows to realize the frequency sweeping of radiation. The possibility of elaboration of THz spectrometer with radiation source with fast sweeping mode based on THz QCL is investigated.

Elaboration of new semiconductor radiation sources allows developing the THz nonstationary spectroscopy for fast analysis of composition of multicomponent gas mixture, that can be important for various applications. In particularly it is important for medical diagnostics where this approach allows to detect such substances are, e.g., metabolites concerned with cancer disease for its early diagnostics.

The authors acknowledge the support from Russian Foundation for Basic Research (grant N18-52-16017).

[1] V. Khodos, D. Ryndyk, V. Vaks. Fast passage microwave molecular spectroscopy with frequency sweeping. *Eur.Phys.J.Appl.Phys.* vol. 25, pp. 203-208, (2004).

[2] V. Vaks, V. Anferte, V. Balakirev, S. Basov, E. Domracheva, A. Illyuk, P. Kupriyanov, S. Pripolzin, M. Chernyaeva. High resolution terahertz spectroscopy for analytical applications. *Phys. Usp.* vol. 63, pp. 708-720, (2020).

THz-I-12

Cavity Assisted High-Resolution THz Spectroscopy

Francis Hindle¹, Coralie Elmaleh¹, Marc Fourmentin¹, Fabien Simon², Anastasiia Pienkina¹, Robin Bocquet¹, Arnaud Cuisset¹, and Gaël Mouret¹

¹*Laboratoire de Physico-Chimie de l'Atmosphère, Université du Littoral-Côte d'Opale, 189 A Ave. Maurice Schumann 59140 Dunkerque, France*

²*SATT-Nord, 25, Avenue Charles Saint-Venant - 59800 Lille, France*

francis.hindle@univ-littoral.fr

The development of cavity-based techniques in the IR has proved to be a particularly successful approach to increase spectrometer sensitivity using a high finesse cavity. Unfortunately, the construction of similar cavities operating at THz frequencies is not possible due to the lack of high-reflectivity spherical mirrors. To overcome this limitation, we have developed a cavity using a low loss corrugated waveguide and photonic mirrors. The cavity modes have been measured around 600 GHz using a standard frequency multiplier source yielding a finesse of around 3500. Under these conditions we expect an equivalent gas interaction length of around 1 km for a table-top setup. Currently typical THz spectrometer setups use path lengths limited to around 2 m of a standard cells and up to around 100 m for a multiple pass cells.

We have constructed a cavity assisted THz spectrometer for sensitive high-resolution spectroscopy using this cavity. The mirrors are mounted on piezo-electric actuators so the overall cavity length can be finely adjusted and locked to the THz frequency of the source. The THz frequency and cavity mode are simultaneously sweep across the region of interest and a molecular signal recorded. Two different signals can be employed. The first uses a frequency modulation (FM) and is sensitive to the amplitude and cavity finesse including any molecular absorption. Alternatively, the photon residency time can also be measured after the source is removed. In this case the additional losses caused by the presence of a molecular transition can be evaluated providing a quantitative measurement of the absorption coefficient. Line strengths as weak as 10^{-27} cm⁻¹/(molecule/cm²) have been measured using this instrument.

THz-I-15

Graphene based sensor for THz imaging

S.Bodrov^{1,2}, A. Murzanev¹, Y.Sergeev^{1,2}, A.Korytin¹ and A.Stepanov¹

¹*Institute of Applied Physics, Russian Academy of Sciences, Nizhny Novgorod, 603950, Russia*

²*University of Nizhny Novgorod, Nizhny Novgorod, 603022, Russia*

step@ufp.appl.sci-nnov.ru

Graphene-based terahertz-field-induced optical luminescence is proposed as a novel technique for THz imaging. We show that optical luminescence from single layer graphene excited by terahertz pulses with electric field amplitude above 100 kV/cm can be detected by a commercial thermally cooled CCD camera. Terahertz beam transverse distributions are measured and compared with a conventional electro-optic sampling technique. The atomic thickness of a graphene detector as well as a strong nonlinear dependence of optical luminescence on THz field make the graphene-based THz imaging a useful tool for near-field mapping. Proof-of-principle experiment of the visualization of local THz-field enhancement near a metal tip of 2 μm radius curvature is performed.

THz-I-16

Terahertz spectroscopy of nanowires

V.N. Trukhin¹, I.A. Mustafin¹, A.D. Bouravleuv², G.E. Cirlin², H. Lipsanen³

1- Ioffe Institute, St.Petersburg, Russia

2- St.Petersburg Academic University, St.Petersburg, Russia

3- Department of Electronics and Nanoengineering, Aalto University, FIN-02150, Espoo, Finland

valera.truchin@mail.ioffe.ru

Despite some successes in the creation, synthesis, and application of semiconductor nanostructures such as nanowires (NW), the industry is still being in its infancy. Understanding the fundamental properties of such structures is the crucial key factor for the implementation of these systems in the field of nano-photonics and nano-optoelectronics, requiring further research.

Our international team is dedicated to the synthesis and investigation of the properties of semiconductor nanowires. Over the last years, our technology team has been able to achieve remarkable success in the development of these structures - we have succeeded in synthesizing ordered arrays of nanowires on various substrates and various A3B5 compounds, which geometrical and physical parameters are highly repeatable and stable. In this report, the main results of the investigation of these structures using time-resolved THz spectroscopy methods will be presented.

The synthesis of semiconductor NWs was carried out both by molecular-beam epitaxy and metal-organic vapour-phase epitaxy techniques. The results of studies of THz generation in GaAs-based NWs with n- and p-alloying have shown, that the mechanism of THz generation in n-type conductivity nanocrystals is due to the drift (movement of carriers in the contact electric field at the upper face of the NW and in the electric field of the n-n+ transition between the NW and the substrate) and diffusion (diffusion of carriers due to non-uniform excitation of photocarriers along the nanocrystal) currents of photoexcited charge carriers having the same direction. THz generation in p-type conductive nanocrystals is associated with drift and diffusion currents of photoexcited charge carriers moving in the opposite directions. The contribution to THz radiation generation from the drift current is stronger than the diffusion current for GaAs nanowires with catalyzed Au droplets. It has been demonstrated that THz generation in NWs is much more efficient (several-fold increase) than from the surface of a bulk semiconductor, even without taking into account the nanocrystal filling factor of the substrate surface.

For the first time it was experimentally demonstrated that the efficiency of THz generation in semiconductor NWs has a linear dependence on the NW filling factor when the NW period is larger than the wavelength of the excitation light, and does not grow to infinity when the maximum packing of nanocrystals is reached, but reaches a maximum value for the NW period of the order of the excitation light wavelength. The experimental results indicate that the near-field interaction of excited nanocrystals, when the NW array is essentially a metamaterial, leads to the attenuation of the electromagnetic field in the nanocrystal. In addition, it was shown experimentally that the efficiency of THz generation depends not only on the NW filling factor, but for a certain diameter of the nanocrystal at a given frequency of excitation light, it increases significantly. The study of the effect of polarization and angle of incidence of excitation light on the process of THz generation in periodic arrays of GaAs NWs, confirmed the essential role of resonant absorption of excitation light. The dependence of the light absorption cross section on the nanowire diameter, angle of incidence, polarization, and frequency of the excitation light obtained as a result of the simulation based on the Lorentz-Mi theory is in agreement with the experimental results. The results of studies of terahertz excitation spectra in samples with different fill factor and nanocrystal diameters further confirmed the effect of resonant excitation of the leaky modes (so-called Mie modes) in a semiconductor nanocrystal on the THz generation process. Efficient THz generation in a GaAs-based NW periodic array was demonstrated experimentally when compared with THz generation in a p-InAs semiconductor.

THz-I-19

Theory of High Harmonics Generation in Extended Gas Media by Femtosecond Laser Field Having Different Wavelengths

S. Stremoukhov

*Faculty of Physics, Lomonosov Moscow State University, Leninskie Gory, 1, build.2, 119991, Moscow, Russia
National Research Centre “Kurchatov Institute”, pl. Akademika Kurchatova, 1, Moscow, 123182 Russia*

email: sustrem@gmail.com

Scaling wavelength (λ) of the laser driver radiation towards the mid-IR range is one of the most attractive methods of enlargement of the generated in gas harmonics spectra, while its width is $\sim \lambda^2$ [1]. However, the efficiency of the generated harmonics scales as $\lambda^{-5.5}$ [2]. Here, we discuss one of the possible ways to increase the harmonics photon flux using the effects of quasi-phase matching (QPM) for high harmonics generated in periodic media [3,4].

The problem has been investigated in the frame of the interference model of extended gas [5] and the non-perturbative theory of single atom response [6]. In numerical simulations, we suppose that the perforated gas media consists of a number of gas jets having spatial sizes d divided by free spaces forming the multi gas media. It interacts with a two-color ($\omega+2\omega$) laser field consisting of two linearly polarized components with zero degree angle between their polarization directions. Laser field wavelength scales from a near IR (800 nm) to a far IR (up to 15 μm) spectral diapason.

The numerical calculations show that due to the QPM, the group of harmonics is enhanced. The influence of the gas media parameters and the laser wavelength on the position of enhanced harmonics and its value is analyzed. The simple relations between the position of the enhanced QPM harmonics, laser wavelength and gas media parameters are introduced. Boundaries of the harmonics enhancement method are discussed.

The work was partially supported by the RFBR under Projects Nos. 18-02-40014 and 19-29-12030.

- [1] T. Popmintchev, M.-C. Chen, D. Popmintchev, P. Arpin, S. Brown, S. Ališauskas, G. Andriukaitis, T. Balčiūnas, O.D. Mücke, A. Pugzlys, A. Baltuška, B. Shim, S.E. Schrauth, A. Gaeta, C. Hernández-García, L. Plaja, A. Becker, A. Jaron-Becker, M.M. Murnane, H.C. Kapteyn, Bright Coherent Ultrahigh Harmonics in the keV X-ray Regime from Mid-Infrared Femtosecond Lasers, *Science*, 336, 1287, (2012).
- [2] J. Tate, T. Augustine, H. G. Muller, P. Salières, P. Agostini, L. F. DiMauro, Scaling of Wave-Packet Dynamics in an Intense Midinfrared Field. *Physical Review Letters*, 98, 013901, (2007).
- [3] R. A. Ganeev, S. Y. Stremoukhov, A. V. Andreev, A. S. Alnaser, Application of Quasi-Phase Matching Concept for Enhancement of High-Order Harmonics of Ultrashort Laser Pulses in Plasmas, *Applied Science*, 9, 1701, (2019).
- [4] L. Hareli, G. Shoulga, A. Bahabad, Phase matching and quasi-phase matching of high-order harmonics generation – a tutorial. *Journal of Physics B: Atomic, Molecular and Optical Physics*, 53, 233001, (2020).
- [5] S. Stremoukhov, A. Andreev, Quantum-mechanical elaboration for the description of low- and high-order harmonics generated by extended gas media: prospects to the efficiency enhancement in spatially modulated media, *Laser Physics*, 28, 035403 (2018).
- [6] A. V. Andreev, S. Yu. Stremoukhov, O. A. Shoutova, Light-induced anisotropy of atomic response: prospects for emission spectrum control, *European Physical Journal D*, 66(16), (2012).

THz-I-20

Nonlinear optical phenomena with terahertz pulses

A. Shkurinov

Faculty of Physics, Lomonosov Moscow State University,

119991 Leninskie Gory 1, Moscow, Russia

ashkurinov@physics.msu.ru

The interaction of terahertz radiation with condensed media is the basis of terahertz spectroscopy. Interaction with liquids, which are the result of gas cooling, is a special area of dielectric spectroscopy in the terahertz frequency range. In your report, we will describe it with new experiments in the field of terahertz spectroscopy of liquid gases and solutions based on them. The solutions consist of a non-polar cryogenic liquid and polycrystalline molecules, which are of interest for biological applications. We analyze linear and possible nonlinear optical effects in the interaction of THz pulsed radiation with such solutions. In this paper, we consider two types of effects. The first of which is determined by the dependence of various parameters of interaction with liquids on the intensity of the incident radiation. In many respects, these are thermostimulated effects and effects determined by the equations of heat transfer. The heating of a cryogenic liquid and a solution based on it occurs in different ways under the action of a powerful terahertz pulse. At some intensities, phase transitions occur from liquid to gas phase and to supercritical liquid. These different phase states of a liquid affect their properties to be a growth agent. We will talk about this in our report. Part of our work is devoted to nonlinear optical interactions of pulsed radiation of high field strength with cryogenic solutions.

THz-I-21

Thin-film structures based on bismuth and antimony for terahertz photonics

Mikhail K. Khodzitsky^{1,2}¹ Terahertz Biomedicine Laboratory, ITMO University, Saint-Petersburg, 197101 Russia² Tydex, LLC, Saint-Petersburg, 191015 Russia

Terahertz (THz) or far infrared spectral range is promising for such applications as spectroscopy, visualization and security systems, and even for next generation wireless communications [1] due to non-ionizing nature, high selectivity of interaction with various materials and high frequency of such radiation. There is still a need for THz detectors, which would simultaneously be high-sensitive, highspeed and operate at room temperature. The problem is associated with the fact that THz photons have low energy and do not produce excess charge carriers in traditional materials. However, $\text{Bi}_{1-x}\text{Sb}_x$ films may be used to solve this problem, since they are characterized with small bandgap and thus belong to class of semimetals having good thermoelectric properties [2]. The absorption of THz photons leads to appearance of excess electron-hole pairs: the signal arising due to photo thermoelectric effect may be enhanced at the maximum thermoelectric figure of merit. The current talk is devoted to study the influence of THz radiation onto the properties of thin film $\text{Bi}_{1-x}\text{Sb}_x$ thermoelectric materials and to search for optimal conditions allowing the greatest response of detector as a result of THz radiation absorption.

ACKNOWLEDGMENTS

This research was funded by Russian Science Foundation (RSF), grant # 19-72-10141.

REFERENCES

- [1]. H.J. Song, and T. Nagatsuma, "Handbook of terahertz technologies: devices and applications," CRC press, 2015.
- [2]. M. Markov, et al., "Thermoelectric properties of semimetals," Physical Review Materials, vol. 3(9), p. 095401, 2019.
- [3]. M.K. Khodzitsky, et al., "Photothermal, Photoelectric, and Photothermoelectric Effects in Bi-Sb Thin Films in the Terahertz Frequency Range at Room Temperature," Photonics, vol. 8(3), p. 76, 2021.

THz-O-1

Sub-THz radiation of human skin under the influence of mental stress

K.A. Baksheeva¹, R.V. Ozhegov^{1,2}, G.N. Goltsman^{1,2}, N.V. Kinev³, V.P. Koshelets³, A. Kochnev⁴, N. Betzalel⁴, A. Puzenko⁴, P. Ben Ishai⁵ and Y. Feldman⁴

1 - Moscow Pedagogical State University, Moscow, 119991, Russia

2 - National Research University Higher School of Economics, Moscow, Russia

3 - Kotel'nikov Institute of Radio Engineering and Electronics of RAS, 125009, Moscow, Russia

4 - Department of Applied Physics, The Hebrew University of Jerusalem, Jerusalem, 9190401, Israel

5 - Department of Physics, Ariel University, Ariel, 40700, Israel

Main author email address: goltsman@mspu-physics.ru

In 2007, for the first time, an image of the sweat gland was obtained using optical coherence tomography [1], which showed that the apex of the sweat duct is a spiral. Later, in 2008, based on the geometric dimensions and since the channels are filled with a conductive liquid, it was suggested that the channels for sweat can function as helical antennas of the terahertz range with a low Q factor [2].

The experimental setup is based around a superconducting integrated receiver (SIR), which is being developed at the IRE RAS [3]. The SIR was used to measure the change in the brightness temperature of subject's skin under the influence of mental stress at 507 GHz. The obtained readings were compared with the readings of the traditionally used sensors of mental stress: the sensor of galvanic skin response (GSR) and heart pulse rate (PS).

The results are substantially different from the expected black body radiation signal of the skin surface. Figure 1 shows a histogram of the raw data $SIR(t)$ for 30 volunteers. The resulting distribution differs from the expected result and requires at least 5 Gaussian distributions to describe. Using a simulation model for the skin, we find that the sweat duct is a critical element. The simulated frequency spectra qualitatively match the measured emission spectra and show that our sub-THz emission is modulated by our level of mental stress. This opens avenues for the remote monitoring of the human state [4, 5].

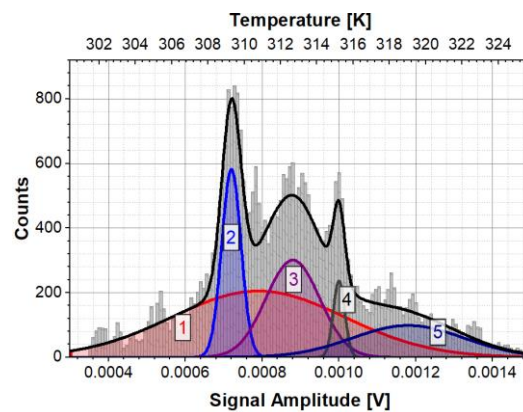


Fig.1. A histogram of raw SIR results for 30 subjects; measured at 507 GHz. The brightness temperature scale (upper axis) assumes an average room temperature of 297 K (24 °C). A minimum of 5 Gaussian distributions (labelled 1- red, 2- blue, 3- purple, 4- dark grey and 5 dark blue) are required to describe the histogram. Student t-testing reveals statistical significance only for the distributions 1,2 and 3. The broad distribution 1 is centered around the core temperature of the human body of 310 K (37 °C). The second and third Gaussians are situated 1 K lower and 2 K higher than body temperature, respectively.

[1] Lademann, J., Otberg, N., Richter, H., Meyer, L., Audring, H., Teichmann, A., Thomas, S., Knüttel, A., Sterry, W., Application of optical non-invasive methods in skin physiology: a comparison of laser scanning microscopy and optical coherent tomography with histological analysis, *Skin Res. Technol.* 13, 119–132 (2007)

[2] Yu. Feldman, A. Puzenko, P. Ben Ishai, A. Caduff and A. J. Agranat, Human skin as arrays of helical antennas in the millimeter and submillimeter wave range, *Phys. Rev. Lett.* 100, 128102-4 (2008).

[3] V. P. Koshelets and S. V. Shitov, Integrated superconducting receivers, *Supercond. Sci. Technol.*, vol. 13, pp. R53–R69, 2000.

[4] Baksheeva K., Ozhegov R., Goltsman G., Kinev N., Koshelets V., Kochnev A., Betzalel N., Puzenko A., Ben Ishai P., Feldman Y., Do humans “shine” in the sub THz?, in: 2019 44th International Conference on Infrared, Millimeter, and Terahertz Waves (IRMMW-THz). IEEE, 2019

THz-O-2

Nanosecond pulsation of THz NH₃ laser emission under optical pumping by "long" (~ 100 μs) CO₂ laser pulses

A.A. Ionin¹, I. O. Kinyaevskiy¹, Yu.M. Klimachev¹, D.I. Kormashova¹, A.A. Kotkov¹, A.A. Kozlov¹, J.-F. Lampin², Yu.A. Mityagin¹, S.A. Savinov¹, A.M. Sagitova¹, D.V. Sinitsyn¹, M.V. Ionin¹

¹*P.N. Lebedev Physical Institute of the Russian Academy of Sciences, 53, Leninskiy Prospekt, Moscow, 119991*

²*Institute of Electronics, Microelectronics and Nanotechnology, Cité Scientifique, Avenue Henri Poincaré, 59652 Villeneuve d'Ascq Cedex., Lille, France*

klimachevym@lebedev.ru

Generation of a terahertz NH₃ laser with optical pumping by "long" (~ 100 μs) pulses of an electron-beam-sustained discharge (EBSD) CO₂ laser was for the first time implemented, the NH₃ laser pulses and "long" CO₂ pump laser pulses being measured simultaneously with nanosecond resolution. We used an optical pumping scheme similar to one used in [1]. The time delay of the NH₃ lasing onset decreased, and the laser pulse duration went up with CO₂ laser pulse energy growth. Experimental results for the NH₃ laser and CO₂ laser pulses are demonstrated in Figs. 1 and 2 (ammonia pressure 4.5 mbar). The inserts in the Figures show the initial parts of the laser pulses. The temporal shape of the CO₂ laser pulses was calibrated to the measured values of the pulse energy E . The time instant $t=0$ corresponds to the beginning of the EBSD pulse, the duration of which is ~ 50 μs.

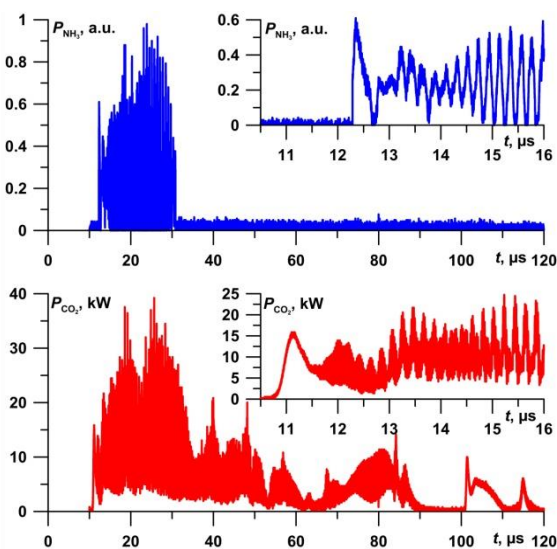


Fig. 1. Pulses of the CO₂ laser (bottom) and NH₃-laser (top) pumped by 9R(16) line. $E=0.59$ J.

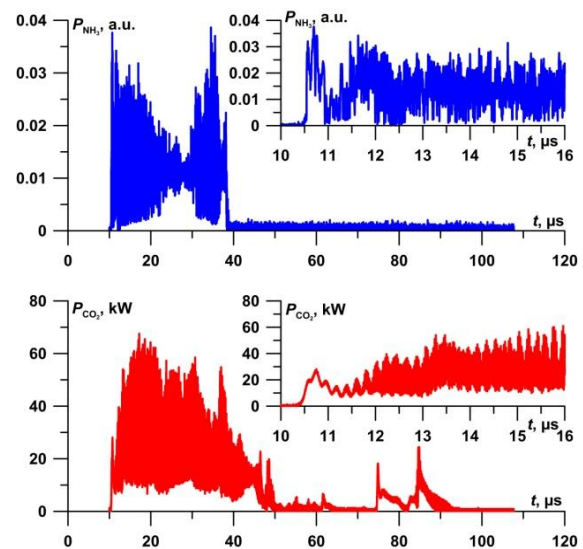


Fig. 2. Pulses of the CO₂ laser (bottom) and NH₃ laser (top) pumped by 9R(30) line. $E=0.91$ J.

The terahertz lasing was observed during the most powerful part of the CO₂ laser pulse, when the pump peak power on 9R(16) line exceeded ~15 kW, and on 9R(30) line - 25 kW. It can be seen from Fig. 1, that the NH₃ laser pulse shape follows the shape of the most powerful part of the pump pulse. In Fig. 2 two pronounced maxima in the terahertz pulse under the sufficiently stable CO₂ laser emission are observed. We assume that this fact is just a demonstration of the cascade mechanism of NH₃ lasing, which was proposed to explain the multifrequency lasing under pumping by 9R(30) CO₂ laser line. The terahertz NH₃ laser wavelengths were also measured. When the NH₃ laser was pumped by 9R(30) CO₂ laser line, the wavelengths turned out to be 67.2, 83.8, and 88.9 μm. The strongest of the observed lines was the spectral line at 83.8 μm. When the NH₃ laser was pumped by 9R(16) line of the EBSD CO₂ laser, of the all possible NH₃ lasing lines only the line with the wavelength of 90.4 μm was recorded. The dependence of the NH₃ laser energy versus pump energy for various ammonia gas pressures is also discussed.

This research was supported by the Russian Foundation for Basic Research (Project 18-52-16019).

[1] Nishi Yo., Horiuchi Ya., Wada S. et al. // Japanese J. of Applied Physics 1982. V. 21. P. 719.

THz-O-3

Detection of skin pathologies using THz spectroscopy

I. Yanina^{1,2}, V. Nikolaev^{2,4}, A. Borisov^{2,3}, A. Knyazkova^{2,3,4}, E. Buyko⁴, V. Kochubey^{1,2}, V. Ivanov⁵, Yu. Kistenev^{2,3}, V. Tuchin^{1,2,6}

¹- Saratov State University (National Research University), Research-Educational Institute of Optics and Biophotonics, 83 Astrakhanskaya str., Saratov 410012, Russia

²- Tomsk State University (National Research University), Laboratory of laser molecular imaging and machine learning, 36 Lenin's av., Tomsk 634050, Russia

³- Siberian State Medical University, Department of Physics and Mathematics, 2 Moskovskytrakt, Tomsk 634055, Russia

⁴- Russia Institute of Strength Physics and Materials Science of SB RAS, Laboratory of Molecular Imaging and Photoacoustics, 2/4Akademicheskoye., Tomsk 634055, Russia

⁵-Siberian State Medical University, Laboratory of Biological Models, 2 Moskovskytrakt, Tomsk 634055, Russia

⁶- Institute of Precision Mechanics and Control RAS, Laboratory of Laser Diagnostics of Technical and Living Systems, 24 Rabochaya, Saratov 410028, Russia

e-mail: irina-yanina@list.ru

Terahertz (THz)-based detection is non-ionizing and non-invasive, represents a very attractive tool for repeated assessments, patient monitoring, and follow-up [1,2]. Because differences between healthy and unhealthy tissues can precisely differentiate between different types of molecules, depending on water content and the difference in the properties of adipose and muscle tissue and their structure [3,4], the information obtained through THz-based scanning could have several uses in the management of patients and, more importantly, in the early detection of different pathology[5-7]. The difficulty of interpreting measurements and the transition from these measurements to *in vivo* diagnostics is caused by various reasons, for example, diffusion into a sample of saline during storage, changes in the level of hydration during the measurement, effects of scattering [8]. The purpose of this study was to detect of skin pathologies using THz spectroscopy using optical clearing method.

Studies were conducted on diabetes animal's model (the mouse and rat) *in vitro* and *in vivo*. The study of varying degrees of diabetes was considered as the main pathology. For measurements, each animal was leaned against the prism of the skin surface and several locations in the skin of each animal were analyzed. Places on the skin were chosen so that the intensity spectrum of the THz signal was the same for different points within the error. The measurements were carried out in reflection mode (prism of impaired total internal reflection-TIR from silicon). Various antireflection agents were applied to the skin of the animal at these points. Measurements are taken every 5 minutes for 60 minutes. It has been shown that glucose is promising for use as an optical clearing agent in the terahertz region. For *in vitro* measurements, skin samples of small animals stored in saline solution were used. These samples were placed on the surface of the TIR prism, and after measurement, they were placed in a cell with an optical clearing agent. Then, every 5 minutes for 60 minutes, the sample was taken out and a measurement was performed on the prism of the TIR. The findings of *in vivo* studies have been confirmed for *in vitro* studies.

The authors would like to acknowledge the support from RFBR grant No. 18-52-16025 (IYuY, VVN, VIK and VVT), and grant under the Decree of the Government of the Russian Federation No. 220 of 09 April 2010 (Agreement No. 075-15-2021-615 of 04 June 2021).

[1] S. J. Oh, J. Kang, I. Maeng, J.-S. Suh, Y.-M. Huh, S. Haam, J.-H. Son March, Nanoparticle-enabled terahertz imaging for cancer diagnosis, *Opt. Express*, vol. 17, is. 5, pp. 3469–3475 (2009).

[2] C. S. Joseph, R. Patel, V. A. Neel, R. H. Giles, A. N. Yaroslavsky, Imaging of ex vivo nonmelanoma skin cancers in the optical and terahertz spectral regions, *J. Biophoton.*, pp. 1–10 (2012).

[3] Y. He, B. S. Ung, E. P. Parrott, A. T. Ahuja, E. Pickwell-MacPherson, Freeze-thaw hysteresis effects in terahertz imaging of biomedical tissues, *Biomed. Opt. Express*, vol. 7, is. 11, pp. 4711–4717 (2016).

[4] F. Wahaja, G. Valusis, L. M. Bernardo, A. Almeida, J. A. Moreira, P. C. Lopes, J. MacUtkovic, I. Kasalynas, D. Seliuta, R. Adomavicius, R. Henrique, M. H. Lopes, Detection of colon cancer by terahertz techniques, *J. Mol. Struct.*, vol. 1006, is. 1-3, pp. 77-82 (2011).

[5] S. Fan, Y. He, B. S. Ung, E. Pickwell-MacPherson, The growth of biomedical terahertz research, *J. Phys. D.*, vol. 47, no. 37, Article ID 374009 (2014).

[6] P. C. Ashworth, E. Pickwell-MacPherson, E. Provenzano, S. E. Pinder, A. D. Purushotham, M. Pepper, V. P. Wallace, Terahertz pulsed spectroscopy of freshly excised human breast cancer, *Opt. Express*, vol. 17, is. 15, pp. 12444–12454 (2009).

[7] J. H. Son, Terahertz electromagnetic interactions with biological matter and their applications, *J. Appl. Phys.*, vol. 105, is. 10, Article ID 102033 (2009).

[8] Y. Sun, M. Y. Sy, Y.-X. Wang, J. A. T. Ahuja, Y.-T. Zhang, E. Pickwell-MacPherson, A promising diagnostic method: Terahertz pulsed imaging and spectroscopy, *World J. Radiol.*, vol. 3, is. 3, pp. 55-65 (2011).

POSTERS

LM-P-1

Luminescent Ce-based nanoparticles embedded into polycrystalline diamond matrix: synthesis and optical properties

V. Sedov¹, S. Kuznetsov¹, I. Kamenskikh², A. Martyanov¹, D. Vakalov³, V. Konov¹

¹Prokhorov General Physics Institute of the Russian Academy of Sciences, Vavilov str. 38, Moscow, Russia

²Physics Faculty of Lomonosov Moscow State University, 1-2 Leninskiye Gory GSP-1, Moscow, Russia

³North Caucasus Federal University, Kulakov Prosp. 2, Stavropol, Russia

sedovvadim@yandex.ru

Free-electron lasers allow the generation of coherent electromagnetic radiation in the X-ray range with very high peak power. Thus, there are new challenges in fabricating detectors and visualizers for the “hard” high-power radiation. Diamond is a perfect candidate for the role of X-ray transparent matrix not only due to low X-ray absorption but also due to its high thermal conductivity and chemical/radiation resistance.

Our approach is based on the integration of yttrium-aluminum or gadolinium-aluminum garnets doped with cerium (YAG:Ce and GAG:Ce, accordingly) in form of nanoparticles into robust and X-ray-transparent diamond matrix [1-4]. The solid garnet solutions were synthesized by co-precipitation from aqueous solution technique. Polycrystalline diamond films were grown in microwave plasma in the CVD reactor ARDIS-100. The thickness of composite films was in the range of 3-10 microns with a lateral size of up to 2 inches. The structure and properties of initial powders and obtained composites were studied by scanning electron microscopy, X-ray diffraction patterns, photoluminescence and X-ray luminescence.

The composite films show high-intensity X-ray luminescence with broadband peak at 550 nm ($5d \rightarrow 4f$ transition in Ce^{3+} ion), and a narrow peak of silicon-vacancy (Si-V) centers at 738 nm. The characteristic decay time was measured at $\tau_{Ce} < 50$ ns for cerium emission and at $\tau_{Si-V} \sim 1$ ns for Si-V centers.

The proposed composite material may be engineered to show XRL of desired intensity: from low intensities for high-power free-electron lasers up, which allows preserving the energy of the incident X-ray beam, to high intensities for sensitive X-ray detectors. Thus, the luminescent diamond composites suggest a new way to control X-ray visualization for fast X-ray detectors and screens.

The reported study was funded by RFBR, project №20-32-70074.

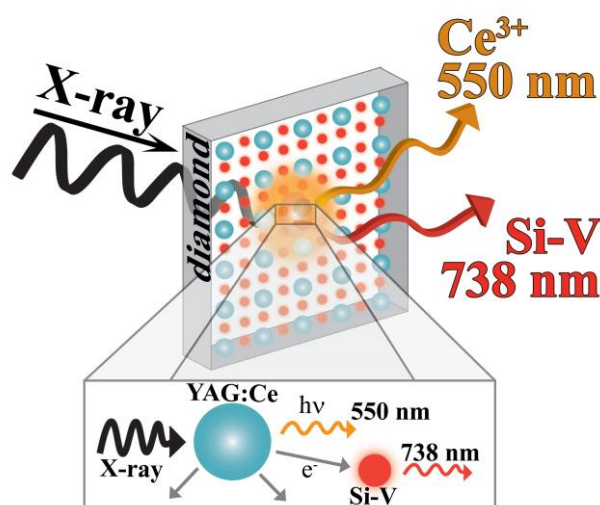


Figure 1. X-ray luminescence mechanism in diamond composites.

[1] V.S. Sedov, S.V. Kuznetsov, V.G. Ralchenko et al. *Diam. Relat. Mater.* 72, 47 (2017).

[2] V. Sedov, S. Kuznetsov, A. Martyanov et al. *ACS Appl. Nano Mater.* 3, 1324 (2020).

[3] S.V. Kuznetsov, V.S. Sedov, A.K. Martyanov et al. *Ceram. Inter.* 47, 13922 (2021).

[4] V. Sedov, S. Kuznetsov, I. Kamenskikh et al. *Carbon* 174, 52 (2021).

LM-P-2

Creation of needle-like microstructures with a high aspect ratio of geometric parameters by special laser milling

E. Surmenko, T. Sokolova, D. Bessonov, Yu. Chebotarevskiy, A. Klushev

*1- Saratov State Technical University, 77 Polytechnicheskaya st., 410054, Saratov, Russia
surmenko@yandex.ru*

The sequence of the developed technological operations of laser milling for the formation of needle and blade structures are described. Such structures act as cathode emitters.

The aspect ratio of the emitter height to the radius of curvature of the emitting surface is an important parameter affecting the field emission properties of cathodes. The higher the aspect ratio values, the higher the electric field strength values can be generated at the top of the emitter. Because the aspect ratio depends only on two parameters, then the ways of its increase lie through an increase in the height of the emitter, or through a decrease in the radius of curvature of the tip of its apex. Traditional technologies for field-emission cathodes manufacturing are deprived of such possibilities. A method has been developed for the formation of structures on the surface of materials, which makes it possible to form needle-like field-emitters with an aspect ratio of 200-1000 units by varying the height and radius of curvature of the emitter.

A distinctive feature of the proposed technological complex is the presence of original technological operations - laser milling of hemispherical surfaces and laser sharpening. Their introduction made it possible to form needle and blade emitting structures with specified parameters not only on flat, but also on spherical surfaces of processed materials.

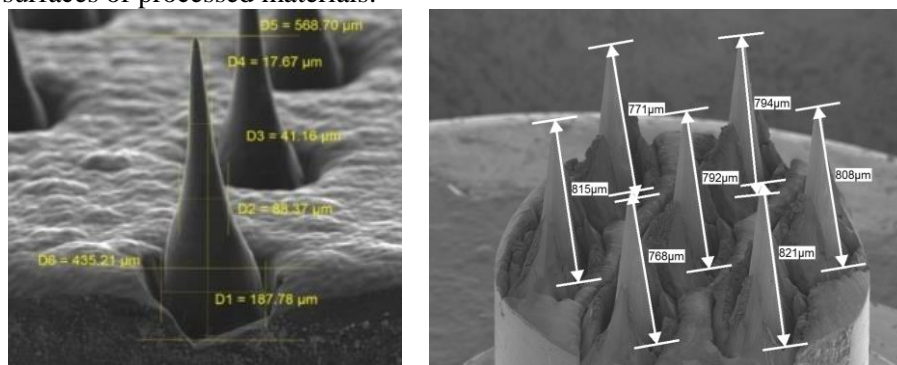


Fig.1. Needle-like structures on the surface of glass-carbon (left) and tungsten (right) plates

These structures were obtained after two-stage milling (rough and accurate) on the special programmable route. YAG-laser 1.064 μm with nano- and picosecond pulse are used (for different materials). Varying different parameters – pulse repetition rate, speed, number of passes – the structures with an aspect ratio up to 1000 were obtained.

LM-P-3

Laser fragmentation of silicon microparticles in liquids

**V. Nesterov¹, D. Shuleiko¹, A. Kolchin¹, D. Presnov¹, S. Zaboltnov¹, L. Golovan¹, P. Kashkarov¹,
E. Sergeeva^{2,1}, D. Kurakina², M. Kirillin²**

1- Lomonosov Moscow State University, Faculty of Physics, 1/2 Leninskie Gory, Moscow, 119991, Russia

2- Institute of Applied Physics RAS, 46 Uljanov street, Nizhny Novgorod, 603950, Russia

E-mail: n.slawa2011@yandex.ru

Nowadays, silicon nanoparticles (SiNPs) formed by laser technologies have potential in diagnostic and therapeutic applications in biomedicine due to their high biocompatibility and biodegradability, as well as low level toxicity [1–3].

To fabricate SiNPs we propose using the technique of laser fragmentation of silicon microparticles (1–6 μm) in water or ethanol exposed to laser pulses (1064 nm, 34 ps). The initial concentrations of the silicon micropowder and irradiation time were varied to optimize the technique. This relatively simple technology allows producing stable and chemically pure SiNPs in quantities large enough for further use in biomedical applications [3]. We have focused our attention on the study of relationships between structural properties of the fabricated nanoparticles and modes of their formation. Additionally, elastic scattering and absorption of the SiNPs suspensions were analyzed.

The analysis of scanning electron microscopy images revealed that the formed Si-NPs have a relatively smooth surface and a shape which is close to spherical. Scanning electron microscopy of the formed SiNPs and dynamic light scattering in their suspensions revealed dependences of the nanoparticles size (the mean size varied from 110 to 340 nm) on the buffer liquid used, initial concentration of silicon micropowder in suspension, and the laser pulses exposure time. The fabricated SiNPs demonstrates low agglomeration, while Raman spectra of the SiNPs evidence their high crystallinity. Spectrophotometry measurements of the SiNPs suspensions revealed that the scattering coefficient exceeds 2 mm^{-1} in the spectral range of 400 – 1000 nm, while the absorption coefficient is less by an order of magnitude in this region. The scattering spectrum demonstrates nonmonotonic behavior with a maximum in the red region, which is explained by a Mie resonance.

The obtained results show that SiNPs fabricated by laser fragmentation of silicon micropowder in a liquid have a potential for contrasting biological tissues and their phantoms in optical imaging modalities, such as optical coherence tomography or fluorescence imaging.

This work was supported by the Russian Science Foundation (project № 19-12-00192).

[1] S.V. Zaboltnov, A.V. Skobelkina, E.A. Sergeeva, et al., *Sensors*, 20, 4874, (2020).

[2] S. Besner, A.V. Kabashin, F. Winnik, et al., *Appl. Phys.*, vol. 93, 955–959, (2008).

[3] M.B. Gongalsky, L.A. Osminkina, A. Pereira, et al., *Sci. Rep.*, 6, pp. 24732, (2016).

LM-P-4

Laser direct writing technique for creation of metallic micropatterns in deep eutectic solvents

Andrey Shishov¹, Dmitry Gordeychuk¹, Lev Logunov², Aleksandra Levshakova¹, Elena Danilova¹, Maxim Panov¹, Evgeniia Khairullina¹, Ilya Tumkin^{1*}

1 - Institute of Chemistry, Saint Petersburg State University, SPbSU, 7/9 Universitetskaya nab., St. Petersburg 199034, Russia

2 - School of Physics and Engineering, ITMO University, Lomonosova, 9, Saint-Petersburg, 191002, Russia

Main author email address: i.i.tumkin@spbu.ru

The development of new technologies useful for manufacturing metallic electrically conductive structures on various dielectric substrates is necessary to create not only standard electrical circuits, but also to create flexible electronics, sensors, and other modern devices [1]. We propose to significantly improve the LCLD method [2] by using deep eutectic solvents. DESs are a mixture of the donor and acceptor of hydrogen bond, the formation of which leads to a significant decrease in the melting point of the entire system [3]. Here we studied the influence of various physical and chemical parameters on the process of laser-induced copper deposition performed from deep eutectic solvents. In our opinion, the proposed approach is rather promising for fabrication of various conductive structures based on copper and other metals. We prepared DESs based on choline chloride, glycerol, urea, ethylene glycol and five acids (citric, tartaric, malonic, oxalic and succinic).

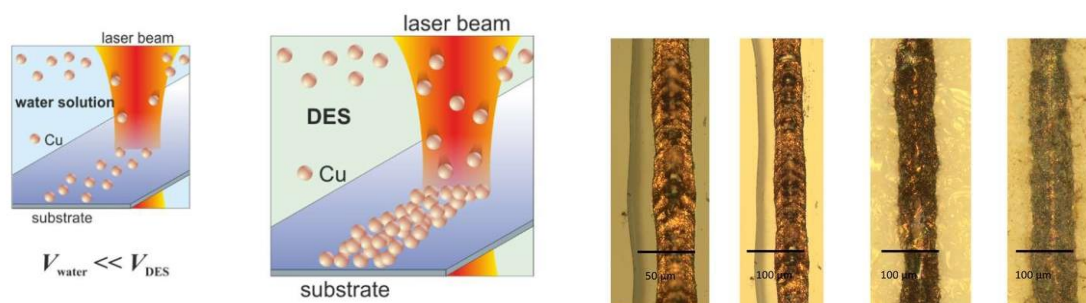


Fig 1. Dependence of the width and morphology of the copper line on the irradiation power and laser scanning speed.

We determined the optimal laser power (1000-1500 mW) and scanning speed (1-20 $\mu\text{m min}^{-1}$), which are necessary to produce conductive copper microstructures. We also studied the influence of the chemical nature of DES components on the copper deposition process. It was shown that one two of the main parameters affecting the efficiency and reproducibility of the discussed approach is are the reducing ability of the acid used and the adhesion of DES toward the substrate surface.

Acknowledgements

I.I.T., M.S.P., L.S.L. and E.M.K., acknowledge the financial support by RFBR, project number 20-33-70277. This research was partially supported by Fellowship of President of Russia MK-1521.2020.3. The authors express their gratitude to the SPbSU Nanotechnology Interdisciplinary Centre, Centre for Optical and Laser Materials Research, Centre for X-ray Diffraction Studies and Nanophotonics Centre.

[1] J. Zhang, J. Feng, L. Jia, H. Zhang, G. Zhang, S. Sun, T. Zhou, Laser-Induced Selective Metallization on Polymer Substrates Using Organocopper for Portable Electronics, *ACS Appl. Mater. Interfaces*. 11 (2019) 13714–13723.

[2] M. Panov, I. Tumkin, A. Smikhovskaia, E. Khairullina, D. Gordeychuk, V. Kochemirovsky, High rate in situ laser-induced synthesis of copper nanostructures performed from solutions containing potassium bromate and ethanol, *Microelectron. Eng.* 157 (2016) 13–18.

[3] E. L. Smith, A. P. Abbott and K. S. Ryder, *Chemical Reviews*, 2014, 114, 11060-11082.

LS-P-5

Q-switched two-micron lasing on ZrO₂-Y₂O₃-Ho₂O₃ crystals

S.A. Artemov¹, E.A. Artemov², E.E. Lomonova², P.A. Ryabochkina¹, A.N. Chabushkin³

1 - N.P. Ogarev Mordovian State University, ul. Bol'shevistskaya 68, 430005 Saransk, Russia;

2 - LLC 'International Center of Quantum Optics and Quantum Technologies', ul. Novaya 100, 143025 Skolkovo, Moscow region, Russia;

3 - Prokhorov General Physics Institute, Russian Academy of Sciences, ul. Vavilova 38, 119991 Moscow, Russia

Sergey560113@gmail.com

We investigated the energy and time characteristics of Q-switched pulsed two-micron lasing at the $^5I_7 \rightarrow ^5I_8$ transition of Ho³⁺ ions in ZrO₂-Y₂O₃-Ho₂O₃ crystals under resonance pumping to the 5I_7 level of these ions by a CW solid-state laser based on the LiYF₄:Tm crystal.

The laser cavity 80 mm long was formed by a flat input mirror (T=93% at a pump wavelength of 1910 nm and T=0.1% at a lasing wavelength of 2120 nm) and a spherical output mirror (with a radius of curvature of 150 mm and a T=6% at a generation wavelength). To ensure the laser operation in the Q-switched mode, an acousto-optic modulator (AOM) was placed in front of the output spherical mirror. The active elements 3x3x21 mm in size were cut from a ZrO₂-13.4mol.% Y₂O₃-0.6mol.% Ho₂O₃ crystal grown by directional crystallization of the melt in a cold container at a rate of 4 mm/h. The faces of active elements were subjected to mechanochemical polishing for 10 min.

Fig. 1 shows the spectrum of lasing on the $^5I_7 \rightarrow ^5I_8$ transition of Ho³⁺ ions, obtained in the Q-switched mode with a pulse duration of 117 ns at a pulse repetition rate of 1 kHz. The oscillogram of the shortest pulse and a typical pulse train at a repetition rate of 1 kHz are shown in Fig. 2.

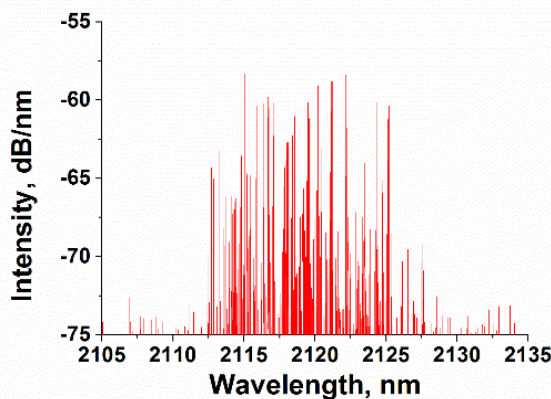


Fig. 1. The spectrum of lasing on the $^5I_7 \rightarrow ^5I_8$ transition of Ho³⁺ ions, obtained in the Q-switched mode

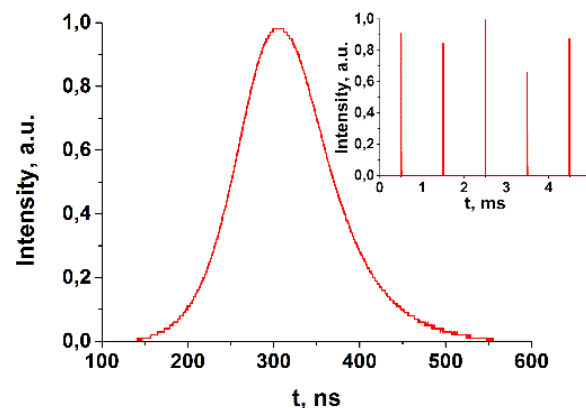


Fig. 2. The oscillogram of the shortest pulse 117 ns and a typical pulse train at a repetition rate of 1 kHz

This work was supported by the Russian Foundation for Basic Research (Grant No. 18-29-20039).

LS-P-6

Refractive index of silica for temperatures far beyond the glass transition, measured using intrinsic thermal radiation

G. Bufetova¹, A. Kosolapov², V. Tsvetkov¹, I. Bufetov²

1. Prokhorov General Physics Institute of the Russian Academy of Sciences, Vavilov Str., 38, 119991, Moscow, Russia

2. Prokhorov General Physics Institute of the Russian Academy of Sciences, Dianov Fiber Optics Research Center, Vavilov Str., 38, 119333, Moscow, Russia

bufetova@lsk.gpi.ru

In the manufacturing process of interference elements based on glass fibers, a local heating of fiber sections can be used, e.g., in recording of long-period gratings in hollow-core fibers [1]. This process requires temperatures well above the glass transition temperature (for pure silica $T_g \approx 1200$ C). To control the grating parameters during recording, you need to know the variation of the glass refractive index (RI) caused by heating. The available in literature data for glass RI are usually limited to the temperature not higher than 800°C [2]. Moreover, the comparison of the glass RI values obtained for temperatures above and below T_g can provide an additional information on the glass structure in these conditions.

This talk presents the results of measuring the RI and the absorption coefficient of silica glass at $T = 1870^\circ\text{C}$ in the visible range by analyzing the intensity distribution of the intrinsic thermal radiation of the sample for S- and P-polarizations [3]. The intrinsic thermal radiation of a silica sample is used as a probe radiation. Due to the cylindrical symmetry of the sample, the profile of a polarized radiation intensity distribution along the sample diameter in the image plane corresponds to the intensity angular diagram for polarized radiation. A cylindrical sample ($d = 10\text{mm}$) was rotated around the axis and heated in a burner flame of an MCVD lathe (Fig.1a). The sample image for each polarization was formed by a telescopic optical system (Fig.1b). The profiles of intensity distribution for both polarizations and their difference enables to determine the absorption coefficient of the sample material and the RI of it (Fig. 1c).

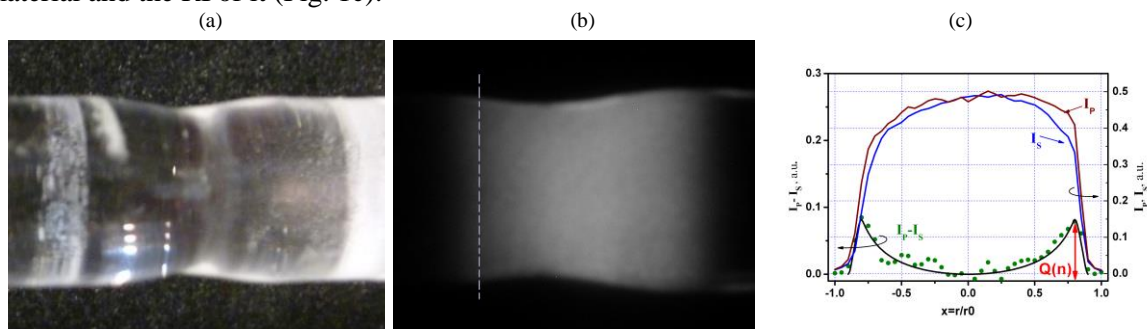


Fig 1. a) - General view of the sample at room temperature; b) Picture of the heated region of the sample; polarized radiation intensities were determined along the direction marked by the dashed line; c) The measured intensities I_P and I_S of the thermal radiation for two polarizations (dashed lines) and their difference $I_P - I_S$ (circles) along the sample diameter. Calculated (line) values of $I_P - I_S$ for $n = 1.40$ against x - coordinate, $r_0 = 4.5$ mm.

The maximum difference Q (Fig 1c) in the intensities of polarized radiation is almost proportional to RI. The comparison of the calculated and experimental results gives the value of the absorption coefficient of silica glass at $T = 1870^\circ\text{C}$ to be $\approx (0.6-0.8) \text{ cm}^{-1}$ and the RI to be $n = 1.40 \pm 0.01$. Earlier it was shown that at $T_1 = 828^\circ\text{C}$ in the visible range $n > 1.47$ and $dn/dT > 0$ [2]. Our results imply that at high temperatures the refractive index is lower than at $T_1 = 828^\circ\text{C}$. Therefore, there exists an interval in the range (T_1, T) where the derivative dn/dT is negative. This work was carried out with the financial support of the Ministry of Education and Science in the form of grant No. 075-15-2020-912 for the creation and development of a world-class research center «Photonics»

References

- [1] A. Iadicicco, R. Ranjan, S. Campopiano, "Fabrication and Characterization of Long-Period Gratings in Hollow Core Fibers by Electric Arc Discharge", IEEE Sensors Journal, **15**, 5 (2015).
- [2] J. H. Wray and John T. Neu. "Refractive Index of Several Glasses as a Function of Wavelength and Temperature," JOSA, **59**, 6 (1969).
- [3] G. A. Bufetova, V. V. Kashin, S. Ya. Rusanov, V. F. Seregin, and V. B. Tsvetkov. "Measurement of the refractive index of an Er^{3+} :YAG crystal melt," J. Appl. Phys. **127**, 035104 (2020).

LS-P-7

(Ca_{1-x}Sr_x)₃(VO₄)₂ solid solutions - the new crystalline materials for ultrafast Raman lasers

I. S. Voronina, E. E. Dunaeva, V. V. Voronov, V. E. Shukshin, S. N. Smetanin, L. I. Ivleva

*Prokhorov General Physics Institute of the Russian Academy of Sciences,
Vavilov str.38, Moscow 119991, Russia*
edunaeva@lst.gpi.ru

Interest in the search and creation of optical crystals with broad Raman scattering (RS) lines arose due to their high potential for use as active media of stimulated Raman scattering (SRS) lasers with the shortest radiation pulses. Recently, it was shown that it is possible to control the quadratic nonlinear optical activity and ferroelectric properties of a material by changing the structure of composites Ca_{10.5-x}Pb_x(VO₄)₇ [1, 2] and Ca_{9.5-1.5x}Bi_xCd(VO₄)₇ [3].

Orthovanadate crystals of the heavy alkali-earth cations (Me = Sr²⁺, Ba²⁺, Pb²⁺) possess the palmierite structure. Interest in use the Sr²⁺ cation is due to the fact that the properties of Sr²⁺ (ion size and mass) are closest to those of Ca²⁺. Usage of Ca₃(VO₄)₂ – Sr₃(VO₄)₂ solid solution with disordered whitlockite structure can provide the formation of the widest homogeneously broadened Raman lines to solve the problem of obtaining SRS radiation pulses shorter than a picosecond.

The (Ca_{1-x}Sr_x)₃(VO₄)₂ (x=0.3; 0.6; 0.9; 1.2; 1.35) crystals were grown by Czochralski method from the platinum crucible in the air in the [100] direction. The starting material was mixed carefully from previously sintered calcium and strontium orthovanadates, Sr₃(VO₄)₂ content in the melt varied from 10 to 45 mol.%. The grown crystals were optically homogeneous, free of cracks and inclusions up to 40 mol.% of Sr₃(VO₄)₂. At 45 mol.% of Sr₃(VO₄)₂ some scattering centers were observed even at low bulk crystallization rate, what indicates the limit of whitlockite phase formation.

Ferroelectric domain structure and dislocations density were investigated for the crystals of different composition by the selective chemical etching. The etching patterns indicate that the shape and size of the domains practically don't change with increasing strontium content in the crystal structure. A slight change in the shape of the domains and an increase in their size is characteristic only for solid solutions with a high strontium content. The dislocation density in all the crystals was not higher than 10³/mm². It was estimated that the *a* and *c* parameters of the trigonal lattice of the (Ca_{1-x}Sr_x)₃(VO₄)₂ solid solution increase with increasing the Sr₃(VO₄)₂ content in the composition. The excitation of spontaneous Raman scattering in the samples was carried out at a wavelength of 532 nm (the second harmonic of the YAG:Nd³⁺ laser).

Data of x-ray diffraction analysis and spontaneous Raman spectroscopy indicate that single-phase crystalline solid solutions with a gradually changing structure are formed in the series (Ca_{1-x}Sr_x)₃(VO₄)₂ with *x* = 0.3; 0.6; 0.9; 1.2; 1.35.

1. Frank M., Smetanin S. N., Jelínek M., Vyhlídal D., Shukshin V. E., Zverev P. G., Kubeček V. 860 fs GdVO₄ Raman laser at 1228 nm pumped by 36 ps, 1063 nm laser. *Laser Phys. Lett.* 16 (8), 085401 (2019).
2. Frank M., Smetanin S.N., Jelínek M., Vyhlídal D., Shukshin V.E., Ivleva L.I., Dunaeva E.E., Voronina I.S., Zverev P.G., Kubeček V. Stimulated Raman scattering in alkali-earth tungstate and molybdate crystals at both stretching and bending Raman modes under synchronous picosecond pumping with multiple pulse shortening down to 1 ps. *Crystals*, 9, 167 (2019).
3. Zverev P. G., Karasik A. Ya., Basiev T. T., Ivleva L. I., and Osiko V. V. Stimulated Raman scattering of picosecond pulses in SrMoO₄ and Ca₃(VO₄)₂ crystals. *Quantum Electron.* 33 (4), 331-334 (2003).

LS-P-8

Investigation of Q-switch mode-locking lasing regime in Yb:YAG disk laser with SWCNT.

D. Guryev¹, D. Nikolaev¹, N. Arutyunyan¹, E. Obraztsova¹, V. Tsvetkov¹

1 - Prokhorov General Physics Institute of the Russian Academy of Sciences

e-mail address: guryevden@gmail.ru

Compact ultrashort pulsed lasers are interesting for diverse application areas. Particularly, lasers based on Yb³⁺-doped crystals possess advantages over those in other materials [1]. There are a number of publications devoted to waveguide Yb-lasers, operating in Q-switch or ultrashort pulses lasing mode with saturable absorbers [2]. However, the waveguide fabrication is a complex and expensive procedure. So a competitive idea with the use of disk lasers is interesting also. Disk lasers are widely used for creation of high-power laser systems with high quality of output radiation. Small thickness of disk active medium allows to avoid influence of thermo-optical effects. In addition, the small thickness of an active element allows to make the cavity length rather small that the fundamental frequency pulse repetition rate is at the GHz level.

Application of a waveguide result in self-starting lasing in a mode-lock regime in most case. The question is what will be with disk active medium and carbon nanotubes as saturable absorber.

In present publication we demonstrate Yb:YAG disk laser with single wall carbon nanotubes (SWCNT) as saturable absorber and investigate its operation with different cavity length – 6 cm (2.5 GHz), 90 cm (166 MHz).

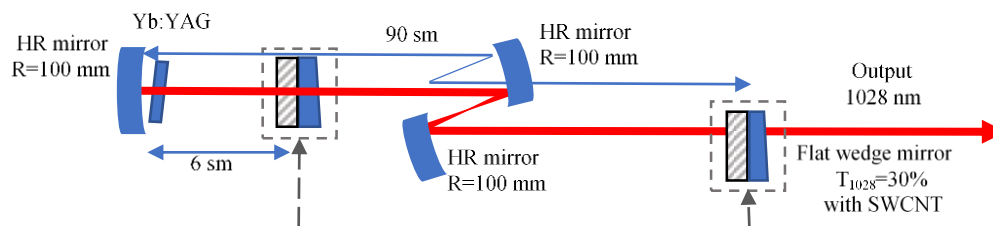


Fig. 1. The schematic configuration of the passively Q-switched mode-locked Yb:YAG laser with the SWCNT-SA. Dashed line shows positions of output coupler in cavities of different length.

The active disk thickness was 0.77 mm. The pumping was realized at 940 nm with the pigtailed laser diode. The pumping emission was focused in active disk through concave HR mirror. The output coupler was plane and wedge-shaped with reflection coefficient $R=70\%$ at the lasing wavelength. We used SWCNT being prepared by CoMoCat method as the saturable absorber. SWCNT was incorporated in a polymer film and positioned on the plane reflection surface of the output coupler.

In both cases (with both cavity length) the Q-switch mode-lock (QSML) lasing was observed. In the 90 cm cavity, the duration of the Q-switch envelope was 1 - 5 microsecond, depending on the pump power. Maximum average power – 140 mW at 8 W of absorbed pump power. The Q-switch mode-locked pulses followed at a frequency of 166 MHz. In the 6 cm cavity, the duration of the Q-switch envelope was 100 ns. Maximum average power – 90 mW at 8 W of absorbed pump power. The Q-switch mode-locked pulses followed at a frequency of 2.5 GHz.

It is possible that the self-starting mode-locking in waveguide lasers is determined both the saturable absorber and nonlinear effects in a waveguide. So, the main question is how to organize the self-starting operation of disk laser.

Acknowledgments: The reported study was funded by RFBR, project number 18-29-19113.

[1] Sun Young Choi, Thomas Calmano, Fabian Rotermund, Christian Kränkel, 2-GHz carbon nanotube mode-locked Yb:YAG channel waveguide laser, *Optics Express* 26, 5140 (2018)

[2] Ji Eun Bae, Sun Young Choi, Christian Kränkel, Kore Hasse and Fabian Rotermund, Evanescent-field Q-switched Yb:YAG Channel Waveguide Lasers with Single- and Double-pass Pumping, *Current Optics and Photonics* 5, 180 (2021)

LS-P-9

Influence of ionizing irradiations on the optical characteristics of the Gadolinium-Aluminum-Gallium-garnet single crystals

N. Kozlova¹, O. Buzanov², E. Zabelina¹, P. Lagov^{1,3}, V. Kasimova, Y. Pavlov³, V. Stolbunov⁴

¹National University of Science and Technology MISiS, Moscow, Russia

²JSC "Fomos-Materials" Co., Moscow, Russia

³A.N. Frumkin Institute of Physical Chemistry and Electrochemistry Russian Academy of Sciences (IPCE RAS), Moscow, Russia

⁴Institute of Theoretical and Experimental Physics (ITEP), Moscow, Russia

E-mail: kozlova_nina@mail.ru

Modern requirements for the devices used in fields of high-energy radiation technologies (nuclear medicine, atomic physics, and space research) determine new the requirements for the sensors and detectors and their working elements. Thus, the devices of nuclear and space technology operate in harsh conditions under intense electromagnetic radiation. The working element of the high-energy radiation detector is scintillation material. One of the promising and studied scintillation materials is garnets due to the wide possibilities of isomorphic substitution of cations and the introduction of alloying additives. It is this feature of garnets doped with rare-earth elements that allows us to control the properties and determine new areas of their application in the future [1-3].

New cerium-doped scintillation garnets $Gd_3Al_2Ga_3O_{12}:Ce$ (GAGG:Ce) first synthesized in 2011 [4] are currently considered for applications in the various fields: nuclear medicine, high energy physics, space research, security systems, radiological exploration, lighting. However, their fundamental properties are not sufficiently studied; in particular, the process of defect formation in these crystals remains unclear. Getting insight to the defects structure and its formation in multicomponent oxide single-crystal dielectric materials is nontrivial task. The study of the irradiation effects on ion structures is a productive method for investigation of the origin of the defect structure and mechanisms of its formation.

Here, we present first results of our studies of GGAG group crystals optical properties under electron and proton irradiations carried out in order to clarify the origin of the defect formation.

All investigated samples were cut from crystals grown in JSC "Fomos-Materials" Co. using Czochralski method in iridium crucibles.

Electron irradiation was performed at the Center of Physical Measurements Investigations of IPCE RAS using the linear accelerator (energy 6 MeV, doses up to 2500 MRad).

Proton irradiation was performed on linear accelerator I-2 at the Center of Collective Use "Kamiks" of ITEP (energy 20 MeV, doses up to 630 MRad).

The **optical properties** of the crystals were measured in the certified Cary-5000 spectrophotometer "Agilent Technologies" with an automatic universal measuring accessory UMA in the accredited testing laboratory "Single Crystals and Stock on their base" of NUST MISiS. The spectral dependences of the transmission coefficients $T(\lambda)$ at the normal incidence of light of natural polarization and the reflection coefficients $R(\lambda)$ are measured at different angles of incidence of p -polarized light.

[1] P. Lecoq Development of new scintillators for medical applications, Nuclear Inst. and Methods in Physics Research A, 2016, V. 809, pp. 130–139.

[2] P. Dorenbos Electronic structure and optical properties of the lanthanide activated $RE_3(Al_{1-x}Ga_x)_5O_{12}$ (RE= Gd, Y, Lu) garnet compounds, Journal of Luminescence, 2013, V. 134, pp 310-318.

[3] K. Kamada, T. Yanagida, J. Pejchal, M. Nikl, T. Endo, K. Tsutumi, Y. Fujimoto, A. Fukabori, A. Yoshikawa Scintillator-oriented combinatorial search in Ce-doped (Y, Gd)₃(Ga, Al)₅O₁₂ multicomponent garnet compounds, Journal of Physics D: Applied Physics, 2011, V. 44, №. 50, pp. 505104.

[4] Kamada K., Yanagida T., Endo T., Tsutumi K., Usuki Y., Nikl M., Fujimoto Yu., Yoshikawa A. // IEEE NSS/MIC, 2011., pp. 1927-1929.

LS-P-10

Synthesis, Microstructure and Spectroscopic Properties of Erbium-Doped $(\text{Sc}_x\text{Y}_{1-x})_2\text{O}_3$ Transparent Ceramics

Roman Maksimov^{1,2,*}, Liza Basyrova³, Vladislav Shitov¹, Danil Vasin¹, Jean-Louis Doualan³, Patrice Camy³, and Pavel Loiko³

1–Institute of Electrophysics UrB RAS, Amundsen St. 106, 620016 Ekaterinburg, Russia

2–Ural Federal University named after the first President of Russia B.N. Yeltsin, Mira St. 19, 620002, Ekaterinburg, Russia

3–Centre de Recherche sur les Ions, les Matériaux et la Photonique (CIMAP), UMR 6252 CEA-CNRS-ENSICAEN, Université de Caen Normandie, 6 Boulevard Maréchal Juin, 14050 Caen Cedex 4, France

*romanmaksimov@el.ru

During the past decade, high-power and ultrafast mid-IR laser sources have attracted considerable attention owing to their broad range of applications such as molecular spectroscopy, advanced material processing, atmospheric sensing, laser surgery and biondiagnostics [1]. Solid-state lasers based on erbium ions (Er^{3+}) operating on the $^4\text{I}_{11/2} \rightarrow ^4\text{I}_{13/2}$ transition generate mid-IR emission near 2.8 μm . Among the laser host materials for Er^{3+} doping, cubic sesquioxides A_2O_3 (where $\text{A} = \text{Y}, \text{Lu}, \text{Sc}$ or their combination) in the form of single-crystals or transparent ceramics appear to be very promising [2]. Compositionally “mixed” sesquioxides such as $(\text{Sc}_x\text{Y}_{1-x})_2\text{O}_3$ are expected to ensure inhomogeneous spectral broadening leading to smooth and broad gain profiles for Er^{3+} ions. The latter is advantageous for broadband wavelength tuning, as well as generation of ultrashort pulses in the 2.8 μm spectral range.

In this work, we have fabricated a series of “mixed” (solid-solution) sesquioxide transparent ceramics with a general formula of $\text{Er}_{0.14}(\text{Sc}_x\text{Y}_{1-x})_{1.86}\text{O}_3$ ($x = 0-0.5$) using sesquioxide nanopowders synthesized by laser ablation [3]. Various characterization techniques including ICP MS, TEM, BET, XRD and dilatometric analysis were used to reveal the impact of the Sc content on the chemical composition, morphology, average particle size, crystal structure and sintering behavior of the obtained nanopowders. The fabrication process of ceramic samples is schematically shown in Fig. 1. The synthesized nanopowders with various Sc/Y ratios were uniaxially pressed into cylindrical compacts and then sintered at 1650–1800 °C under vacuum followed by calcination in air to eliminate oxygen vacancies.

The fabricated ceramics are of single-phase nature (cubic class, C-type or bixbyite structure). The microstructure of ceramics, the grain size distribution and the content of scattering centers were studied. The absorption and emission cross-section spectra of Er^{3+} ions were determined. The luminescence lifetimes of the $^4\text{I}_{11/2}$ and $^4\text{I}_{13/2}$ Er^{3+} states were measured. The effect of Sc content on the microstructure and spectroscopic properties of ceramics was investigated.

The developed $\text{Er}:(\text{Sc},\text{Y})_2\text{O}_3$ transparent ceramics are promising as gain media of continuous-wave and mode-locked mid-IR lasers.

The reported study was funded by RFBR (Russia) according to the research project No. 21-53-15014 and CNRS (France) according to the project IEA No. 00432.

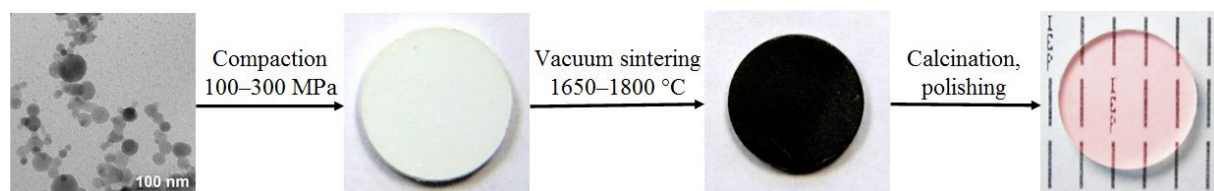


Fig. 1. Schematic diagram showing the fabrication process of Er^{3+} -doped $(\text{Sc}_x\text{Y}_{1-x})_2\text{O}_3$ transparent ceramics.

[1] J. Ma, Z. Qin, G. Xie, L. Qian, D. Tang, Review of mid-infrared mode-locked laser sources in the 2.0 μm –3.5 μm spectral region, *Appl. Phys. Rev.*, vol. 6, pp. 021317-29 (2019).

[2] T. Li, K. Beil, C. Kränkel, G. Huber, Efficient high-power continuous wave $\text{Er}:\text{Lu}_2\text{O}_3$ laser at 2.85 μm , *Opt. Lett.*, vol. 37, pp. 2568-2570 (2012).

[3] V.V. Osipov, V.V. Platonov, V.V. Lisenkov, A.V. Podkin, E.E. Zakharova, Production of nanopowders of oxides by means of fiber and pulse-periodical CO_2 lasers, *Phys. Status Solidi C*, vol. 10, pp. 926-932 (2013).

LS-P-11

The Spectral Properties of Nd-disk Laser with Degenerate Cavity Configuration.

D.A.Nikolaev¹, V.B.Tsvetkov¹.

1. Prokhorov General Physics Institute, Russian Academy of Sciences, 38 Vavilov Str., 119991 Moscow, Russian Federation

nikolaev@lsk.gpi.ru

The goal of the presentation is the demonstration of the possibility of CW TEM₀₀ Nd:YVO₄ disk laser with degenerate cavity configuration [1-3] to produce a narrowband emission. Any other mode selection technique was not used. A one- two- or three- point pumping of active disk (AD) was used.

The optical scheme of the laser with degenerate cavity configuration and intracavity beam path is shown on figure 1. The use of off-axis beams and a standing wave in the cavity was the basic demand to the optical schematic. The cavity with the length of 50 mm was formed by a flat HR mirror deposited on the back surface of the active disk, and concave spherical mirror M1 (r=200 mm). Output coupler was formed also in spherical mirror. As an AD the Nd:YVO₄ crystal 20×20×0.5 mm³ in sizes and Nd³⁺-ions concentration of 2.5×10²⁰ cm⁻³ was used.

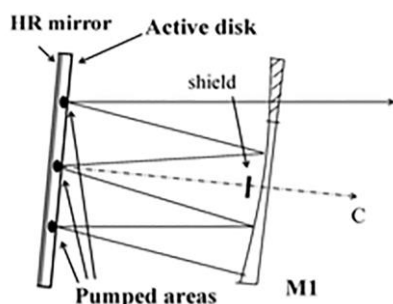


Fig.1. Degenerate laser cavity schematic.

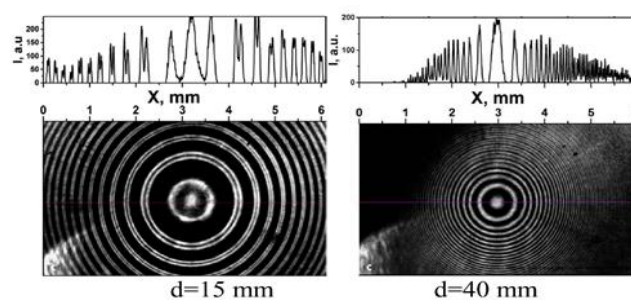


Fig.2. Fabry-Perot interference patterns of the laser emission.

Dichroic AR coating with high transmission both at pumping and lasing wavelength was deposited on the AD forward surface. Mirror M1 had reflection coefficient $R=95\%$ in a small part of the surface and $R\geq 99.8\%$ was organized in other part of a mirror. This small part of the mirror served as an output coupler for the laser. We used one, two or three pumping points produced by focusing of the emission of three 808-nm diode modules. The pumping points possessed the sizes of about 170 μm . It corresponded to TEM₀₀ intracavity beam waist. Distances between pumping points were made 5.7 mm. Total pumping power absorbed in AD varied in a range to 15.6 W.

Spectral, power and spatial parameters of the laser were studied. At research of spectral parameters there were used glass ($n=1.51$) cylindrical Fabry-Perot interferometers (IFP) with reflection coefficient of mirrors $R=85\%$ and bases of 1.18 mm, 3.3 mm, 15 mm and 40 mm. The maximum of optical system resolution was $\sim 6 \times 10^{-3} \text{ cm}^{-1}$ ($\sim 180 \text{ MHz}$).

Results of researches have shown that in all range of pumping power the beam divergence was $2.3 \pm 0.23 \text{ mrad}$ (FWHM) that corresponded to the calculated value 2.4 mrad for TEM₀₀ lasing. The spectral characteristics of a lasing also did not depend on a pumping power and number of pumping spots. In all cases, the lasing spectrum contained two lines with approximately equal intensity with widths (FWHM) of $\leq 6 \times 10^{-3} \text{ cm}^{-1}$ ($\leq 180 \text{ MHz}$) and distance between them of $5 \times 10^{-2} \text{ cm}^{-1}$ (5 GHz).

In figure 2 it is shown interference patterns of a laser radiation for case IFP with base of 15 and 40 mm. The maximum output power of the laser was 3.2 W.

To explain the nature of the spectrally selective properties of the degenerate resonator, the additional studies were carried out with using the pulsed pumping. The results of it demonstrated that selection of longitudinal modes it is provided at the expense of a several cavity shoulders with different length.

[1] D. Herriott, H. Kogelnik and R. Kompfner, Off-Axis Paths in Spherical Mirror Interferometers, Applied Optics, vol.3, 523-526, (1964).

[2] I. A. Ramsay, J. J. Degna, A ray analysis of optical resonators formed by two spherical mirrors, Applied Optics, vol.9, 385-398, (1970).

[3] A. M. Bul'kanov, D. A. Nikolaev, A. I. Shamatova, I. A. Shcherbakov, V. B. Tsvetkov, Single-mode Nd:GGG laser with three-beam diode pumping and a degenerate cavity, Quantum Electronics, vol.48 (5), 468-471, (2018).

LS-P-12

Double-range RF Discharge Slab CO Laser

A.A. Ionin, A.Yu. Kozlov, A.A. Kotkov, Yu.M. Klimachev, O.A. Rulev, D.V. Sinitsyn

P.N. Lebedev Physical Institute of Russian Academy of Sciences, 53 Leninskiy prosp., 119991 Moscow, Russia

email: rulevoa@lebedev.ru

Carbon monoxide laser can operate on transitions of fundamental vibrational band in spectral range of $\lambda \sim 4.9\text{-}7.5\ \mu\text{m}$ [1] and on transitions of first vibrational overtone band of CO molecule ($\lambda \sim 2.5\text{-}4.2\ \mu\text{m}$) [2]. The laser has high efficiency and its wide spectral range makes it possible to use this laser for spectroscopy. The overtone CO laser emission overlaps the atmospheric transparency window. Moreover, this laser is a more suitable source of radiation for cutting glass and ceramics than a widely used CO₂ laser [3]. In the Gas Lasers Lab of the Center for Laser and Nonlinear Optical Technologies, two RF discharge slab CO laser facilities with cryogenically cooled electrodes operating without forced replacement of the active gas mixture were previously developed [4-8]. But average laser power of these lasers was not high enough for some applications, such as cutting glass, ceramics, or polymer materials. Higher laser power was required. Therefore, as extension of the previous experiments, we developed a new facility with an increased surface area and the length of its electrodes.

The laser chamber was designed as a cylinder with internal volume of $\sim 28\ \text{l}$ and was designed similar to the laser chamber described in [6]. The electrode system consisted of two hollow Au-coated copper electrodes of 470 mm length and 25 mm height. Discharge gap was 3-5 mm at different experiments. RF power supply with carrier frequency of 40 MHz and maximal output RF power up to 2 kW was operated in repetitively pulsed mode with low repetition rate of 100 Hz - 2 kHz.

To obtain lasing in free running mode on fundamental vibrational band of CO molecule, the hybrid positive branch unstable-waveguide 500 mm long internal cavity with Au-coated Cu mirrors with curvatures of 3600 and -2600 mm was used. The maximal averaged laser power of $\sim 38\ \text{W}$ was obtained under active medium pressure of 51 mbar, pulse repetition rate of 400 Hz, and pump pulse duration of 0.625 ms. A typical spectrum of the laser emission consisted of ~ 20 spectral lines in the wavelength range from 5.07 to 5.62 μm .

To carry out lasing on transitions of first overtone vibrational band of CO molecule in free-running mode, 500 mm long stable resonator formed by dichroic mirrors with high reflection in the spectral range corresponding to transitions of overtone band and low (<20%) reflection in the spectral range of 5.0-6.0 μm was used. The maximal averaged laser power was $\sim 5.7\ \text{W}$ at active medium pressure of 25 mbar and the same pump conditions. Typical laser spectrum consisted of ~ 50 lines at the spectral range from 2.6 to 3.05 μm .

To obtain lasing in Q-switching mode on transitions of CO molecule fundamental band, 2 m long stable double-pass V-type laser cavity with 50% reflection of output coupler was used. Q-switching was performed by a rotating mirror. Maximal peak power of laser radiation in these experiments was $\sim 4.5\ \text{kW}$ at pulse duration of $\sim 1.3\ \mu\text{s}$ (FWHM) and RF pump pulse repetition rate of 145 Hz. The laser spectrum in this case consisted of ~ 100 spectral lines in the wavelength range of 4.95 – 7.0 μm .

- [1] A.A. Ionin "Electric Discharge CO Lasers" in [Gas Lasers], M. Endo and R.F. Walter eds, CRC Press - Taylor and Francis Group, Boca Raton, 201-237, 2007.
- [2] A.A. Ionin, A.K. Kurnosov, A.P. Napartovich, L.V. Seleznev, "Lasers on Overtone Transitions of Carbon Monoxide Molecule" // *Laser Physics*, **20** (1), p.144, 2010.
- [3] Ce Shi, M. Ermold, G. Oulundsen, and L. Newman "CO₂ and CO laser comparison of glass and ceramic processing", *Proc. SPIE* **10911**, p.109110M, 2019.
- [4] A.A. Ionin, A.Yu. Kozlov, L.V. Seleznev, D.V. Sinitsyn, "RF discharge slab CO laser operating in both fundamental and first-overtone bands", *Optics Communications*, **282**, p.629, 2009.
- [5] A.A. Ionin, A.Yu. Kozlov, L.V. Seleznev, D.V. Sinitsyn, "Slab overtone CO laser operating in the 2.5 - 4.0 micron spectral range", *IEEE Journal of Quantum Electronics*, **45**, (3), p.215, 2009.
- [6] A.A. Ionin, A.Yu. Kozlov, O.A. Rulev, L.V. Seleznev, D.V. Sinitsyn, "Repetitively Pulsed Cryogenically Cooled Quasi Sealed-Off Slab RF Discharge First-Overtone CO Laser" *Applied Physics B: Lasers and Optics*, **122**:183, 2016.
- [7] A.A. Ionin, Yu.V. Kochetkov, A.Yu. Kozlov, et al., "Q-switched slab RF discharge CO laser", *Laser Phys. Lett.*, 2017, **14**, 055001.
- [8] I.A. Chebotarev, A.A. Ionin, I.O. Kinyaevskiy, et al., "Frequency-selective Q-switched repetitively pulsed slab RF-discharge carbon monoxide laser", // *Optics & Laser Technology*, **131**, 2020, 106431.

LS-P-13

Laser device designed for treatment of capillary skin angiodyplasia and telangiectasia

O. Tikhonevich¹, G. Kuzmin¹, A. Sirotkin¹, N. Gorbatova², D. Safin², M. Remennikova^{3,4}, D. Seleznev⁴

1 - Prokhorov General Physics Institute of the Russian Academy of Sciences, 38 Vavilov st., Moscow, 119991, Russian Federation

2 - Research Institute of Emergency Pediatric Surgery and Traumatology, 22 Bolshaya Polyanka st., Moscow, 119180, Russian Federation

3 - Perm Federal Research Center UB RAS, 13a Lenina, Perm, 614990, Russia Federation

4 - Perm Scientific Production Instrument-Making Company, 106 25 October, Perm, 614990, Russia Federation

Main author email address: tichon@kapella.gpi.ru

The experimental sample of a solid-state laser device based on semiconductor diodes operating at a radiation wavelength of 520 ± 5 nm in the green spectral range, near the absorption peak of hemoglobin and oxyhemoglobin, was developed at the Prokhorov General Physics Institute of the Russian Academy of Sciences [1-3]. The prototype manufactured at the Perm Federal Research Center of the Ural Branch of the Russian Academy of Sciences (Fig. 1).



Fig. 1. Prototype laser device

Table 1 Technical and operational characteristics of the device

Parameter	Value
Wavelength, nm	520 ± 5
Average power, W	3
Pulse duration	from 50 μ s to 50 ms
Pulse repetition rate	from 10 kHz to 10 Hz
Control with software	touch screen, pedal
Power supply	220V / 50Hz
Light delivery	flexible light guide 400, 600 μ m, length 2 m

[1] Sirotkin A.A., Kuzmin G. P. , Gorbatova N. E. , Yushina T. E., Dorofeev A. G. , Brynsev, A.V., Zolotov S.A., Tikhonevich O.V., Drozdov D. S. Optimization of selective photodestruction by laser radiation of the yellow-green range of capillary angiodyplasia of the skin. 2018 International Conference Laser Optics (ICLO). St Petersburg, RUSSIA., JUN 04–08, 2018 p. 602 <https://doi.org/10.1109/lo.2018.8435420>

[2] O. V. Tikhonevich, A. A. Sirotkin, N. E. Gorbatova, G. P. Kuzmin, M. V. Remennikova and D. A. Seleznev, Development of a laser medical device for the selective removal of pathological vascular, 2020 International Conference Laser Optics (ICLO 2020), Proceedings of a meeting held 2-6 November 2020, Saint Petersburg, Russia. p.396, IEEE, Mar 2021 <https://doi.org/10.1109/ICLO48556.2020.9285442>

[3] Gorbatova, N., Gasanova, E., Zolotov, S. et al. Experimental confirmation of the promising selective use of “green” laser radiation for photothermolysis of hemoglobin-containing tissues. Lasers Med Sci (2021). <https://doi.org/10.1007/s10103-020-03220-x>

LS-P-14

Fabrication of laser $\text{Ca}_3(\text{VO}_4)_2:\text{Mn}$ crystals by the method of impurity diffusion from a solid source

I.S. Voronina, E.E. Dunaeva, A.G. Papashvili, L.D. Iskhakova, M.E. Doroshenko, L.I. Ivleva

*Prokhorov General Physics Institute of the Russian Academy of Sciences,
Vavilov str.38, Moscow 119991, Russia
irina.voronina.78@list.ru*

Single crystals with disordered structure are widely investigated due to their potential use as a host media for diode-pumped lasers. Inhomogeneous broadening of the spectral lines of these materials provides the good matching between the active element absorption spectrum and the emission lines of laser diodes. Among them, calcium orthovanadate ($\text{Ca}_3(\text{VO}_4)_2$, CVO) with disordered whitlockite structure has effective ferroelectric and nonlinear properties, high laser damage threshold and can be used as a multifunctional laser material.

Laser generation in near-IR spectral range was obtained previously in a group of alkali-earth vanadates doped with Mn^{5+} ions [1]. For the first time $\text{Ca}_3(\text{VO}_4)_2:\text{Mn}$ crystals were grown by Czochralski method [2]. It was shown that Mn ions substitute both Ca^{2+} (as Mn^{2+} , and Mn^{3+}) and V^{5+} (as Mn^{5+}) in the medium.

In the work $\text{Ca}_3(\text{VO}_4)_2:\text{Mn}$ crystals were obtained by the high-temperature solid state diffusion method. The samples (thickness plates of 3 mm) were cut from optically homogeneous nominally pure CVO crystals grown by Czochralski method. Manganese oxide Mn_2O_3 was used as the diffuzant. The annealing regimes were as follows: annealing temperature 1050 - 1300°C; annealing duration – 24 and 48 h; sample orientation [100] and [001]. Diffusion process was carried out in the “open zone” (the sample on the Mn_2O_3 surface, the air atmosphere), and diffusion process - in the “closed zone” (the sample is immersed in Mn_2O_3 powder). It was shown that annealing in the closed zone allows to obtain homogeneously doped CVO crystals with ultimate solubility of Mn ions. In the case of open-zone annealing the Mn concentration profile (Fig.1) can be described by the second Fick’s law. The diffusion coefficients for different annealing temperatures and crystal orientations were calculated. The activation energy for diffusion process was also estimated. Chemical composition of the annealed crystals was investigated by energy-dispersive X-ray spectroscopy (EDXS) method.

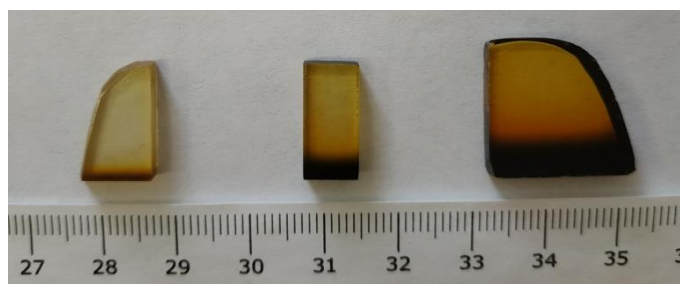


Fig.1. CVO:Mn crystals after diffusion doping at different temperatures.

The optical homogeneity of diffusion doped crystals was investigated by conoscopic method and laser beam diffraction. Ferroelectric domain structure and dislocations were revealed by selective chemical etching. The absorption and luminescence spectra showed the presence of the specific lines for Mn^{2+} , Mn^{3+} and Mn^{5+} . It was estimated that the Mn^{5+} concentration is higher for diffusion doped CVO in comparison with CZ-grown crystals. Due to this redistribution of dopant ions, the diffusion-doped CVO:Mn crystals can be of great interest for developing lasers based on Mn^{5+} ions. It was demonstrated that high-temperature solid-state diffusion method is simple enough and effective technique to obtain disordered oxide crystals doped with transition elements having small ionic radii.

- [1] L.D. Merkle, H.R. Verdun, B. McIntosh, Spectroscopy and Laser Operation of Mn^{5+} -Doped Vanadates, OSA Proceedings on Advanced Solid-State Lasers, v.15, pp.310-314 (1993), A.A. Pintro and Tso Yee Fan (eds.), <https://doi.org/10.1364/ASSL.1993.TL6>.
[2] I.S. Voronina, V.V. Voronov, E.E. Dunaeva, L.D. Iskhakova, A.G. Papashvili, M.E. Doroshenko, L.I. Ivleva, Growth and properties of manganese doped $\text{Ca}_3(\text{VO}_4)_2$ single crystals, J. Crystal Growth, v. 555, 125965 (2021) <https://doi.org/10.1016/j.jcrysgro.2020.125965>.

B-P-15

Mutual influence of intense LED light and cold signaling through the CRISPR/Cas9-edited *HOS1* gene

V.P. Bulgakov¹, G.N. Veremeichik¹, T.Y. Gorpenchenko¹, Y.A. Yugay¹, T.V. Avramenko¹, Y.N. Shkryl¹, E.P. Subbotin², Y.N. Kulchin²

¹ Federal Scientific Center of the East Asia Terrestrial Biodiversity (Institute of Biology and Soil Science), Far Eastern Branch of the Russian Academy of Sciences, 159 Stoletija Str., Vladivostok, 690022, Russia

² Institute of Automation and Control Processes Far Eastern Branch of the Russian Academy of Sciences (IACP FEB RAS), Far Eastern Branch of the Russian Academy of Sciences, 5 Radio str., Vladivostok, 690041, Russia

V.P. Bulgakov: bulgakov@biosoil.ru

E3 ubiquitin-protein ligase HOS1 is a key integrator of temperature information and developmental processes. However, HOS1 connection with the central integrator of the light signaling system, transcription factor HY5 is unknown. HY5 acts downstream of the light receptor network and directly affects transcription of numerous light-induced genes. Here we studied the intersection of intense LED lighting and cold acclimation signaling pathways by using *hos1*^{Cas9} *Arabidopsis* plants, in which the *HOS1* gene was subjected to genome editing via the CRISPR/Cas9 technology. The *hos1*^{Cas9} plants were highly resistant to cold stress. When *hos1*^{Cas9} plants were exposed to cold stress combined with intense LED lighting (HL, 1200 $\mu\text{mol m}^{-2} \text{s}^{-1}$), the light signaling system underwent significant changes due to increased expression of the *HY5* gene. The *hos1* mutation changed the balance between reactive oxygen species (ROS) production and ROS decomposition in cells via modulation of gene activity. Single-cell confocal imaging showed that levels of ROS were decreased in *hos1*^{Cas9} mutant plants under combined action of cold and HL. Co-regulation of cold-induced and HL-induced ROS appears to be accomplished by the HOS1 —| ICE1 —| ABI5 → *RbohD* and HOS1 —| PIF4(HY5) → *ABI5* → *RbohD* signaling modules. These data show that the search for the optimal combination of strong LED illumination and resistance to temperature stress during plant cultivation should be continued by regulating the expression of the *HOS1* and *HY5* genes.

B-P-16

Laser based oblique incidence reflectometry for meat quality assessment

Ankur Gogoi

Department of Physics, Jagannath Barooah College, Jorhat 785001, Assam

Email address: ankurgogoi@gmail.com

Recent years showed considerable interest in monitoring meat quality due to increased recognition of the potential risk of encountering a biological, chemical, or physical agent in the food due to adulteration and spoilage with potential adverse health effects [1]. In this contribution, we report the design and fabrication of a laser based optical metrology system (Fig. 1) based on oblique incidence reflectometry (OIR) to measure the absorption and reduced scattering coefficients (μ_a and μ'_s , respectively) of biological tissues. Notably, these scattering parameters carry a sufficient amount of information to discriminate between healthy and rotten tissues, thereby providing a pathway to comprehensive meat quality monitoring. Preliminary results containing the measured scattering properties as a function of time dependent degree of spoilage of different food products will be presented. The results will be useful in the development of portable devices for rapid and non-invasive meat quality assessment.

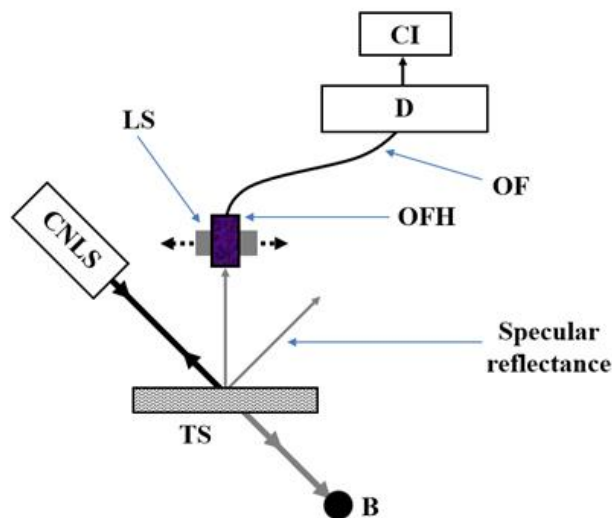


Fig. 1. Schematic of the proposed optical design for the laboratory setup. CNLS: Coherent narrowband light source; TS: tissue sample; OF: optical fiber; OFH: mechanical mount for the optical fiber which is capable of moving along a translational stage; LS: motorized linear translation stage; B: beam trap; D: photodetector; CI: computer interface.

- [1] Gamal ElMasry, Douglas F. Barbin, Da-Wen Sun, Paul Allen, Meat quality evaluation by hyperspectral imaging technique: an overview, *Critical reviews in food science and nutrition* vol. 52, no. 8, 689-711, (2012).

B-P-17

A study of activated macrophages in the accumulation of different photosensitizers and the PDT effect on their metabolic changes

Klementeva M.V.^{1,2}, Sadykova E.Z.¹, Skobeltsin A.S.^{1,2}, Romanishkin I.D.², Pominova D.V.^{1,2}, Loschenov V.B.^{1,2}, Ryabova A.V.^{1,2}

1- National Research Nuclear University, MEPhI (Moscow Engineering Physics Institute), Moscow, Russia

2- Prokhorov General Physics Institute, Russian Academy of Sciences, Vavilov Str., 38, Moscow, 119991, Russia

klementevamv@yandex.ru

Introduction Antitumor immunity induced by photodynamic therapy (PDT) plays an essential role in the outcome of treatment, and it depends on the degree of inflammation. In this regard, understanding how immune cells such as macrophages, which are caused by inflammation, interact with different photosensitizer (PS) is great of interest. Here, we investigated accumulation of various PS, such as 5-aminolevulinic acid (5-ALA) induced protoporphyrin IX (PpIX), Photosens, Chlorin e6 and methylene blue (MB) in LPS-induced macrophages. Also, we examined the effects of PDT mediated by MB to detect phenotypic changes in M0, M1 and M2 macrophages.

Experiments The LPS-induced macrophages were derived from THP-1 monocytes cell line by addition 1 µg/ml of LPS from *Escherichia coli* O55:B5 [1]. The cells were incubated with PS at next doses: 5-ALA – 20 mg/kg, Photosens – 5 mg/kg, Chlorin e6 – 10 mg/kg and MB – 6 mg/kg. PS accumulation was estimated using a confocal microscopy (LSM-710, Carl Zeiss, Germany). M0 polarized macrophages were derived from THP-1 monocytes using PMA (Phorbol 12-myristate 13-acetate, 20nM). To obtain M2 polarization M0 macrophages were incubated with IL-13 20 ng/ml. To obtain M1 polarization M0 macrophages were incubated with IFN-gamma (20ng/ml) and LPS (100ng/ml) [2]. For PDT cells were irradiated with a laser 675 nm at doses 5 J/cm² and 50 J/cm². Changes in cell viability were analyzed with using Annexin V and propidium iodide staining. For macrophages phenotype changes staining CD206/CD86 was applied. Also, for all experiments fluorescence lifetime data was received using FLIM (Becker&Hickl, Germany, with 2P excitation at 770 nm).

Results Significant differences in dye accumulation between LPS-activated and non-activated monocytes were demonstrated for PpIX. The intensity of the PpIX was higher in LPS-activated cells, while MB and Chlorine e6 showed higher values for cells without activation. A high dose of PDT led to a depolarization of all macrophages to the M2 type. For low-dose (5 J/cm²) PDT M0 macrophages turned to M1 phenotype, in other cases, the M2 type predominated slightly. For M1 macrophages, the apoptotic type of cell death prevails during PDT treatment with a dose of 5 J/cm². For a dose of 50 J/cm², necrosis predominates in all macrophage types.

Conclusion Low dose PDT can change macrophages polarization. Found, that 5-ALA induced PpIX accumulations in macrophages is the most sensitive to their polarization.

This work was supported by RFBR, № 20-02-00928.

[1] Liu X. et al. LPS-induced proinflammatory cytokine expression in human airway epithelial cells and macrophages via NF-κB, STAT3 or AP-1 activation //Molecular medicine reports. – 2018. – T. 17. – №. 4. – C. 5484-5491.

[2] Zhu Z. et al. Photodynamic activity of Temoporfin nanoparticles induces a shift to the M1-like phenotype in M2-polarized macrophages //Journal of Photochemistry and Photobiology B: Biology. – 2018. – T. 185. – C. 215-222.

B-P-18

Refractive properties of glycated albumin and hemoglobin in a wide range of wavelengths and temperatures

Ekaterina N.Lazareva^{1,2}, Andrey Y. Zyubin³, Ilya G. Samusev³, Valery V. Tuchin^{1,2,4}

¹Saratov State University, Saratov, 410012, Russia

²Tomsk State University, Tomsk, 634050, Russia

³Immanuel Kant Baltic Federal University, 236041, Kaliningrad, Russia

⁴Laboratory of Laser Diagnostics of Technical and Living Systems, Institute of Precision Mechanics and Control RAS, Saratov, Russia
lazarevaen@list.ru

Most modern diagnostic methods for detecting diabetes mellitus and controlling the degree of its compensation are associated with the determination of fasting blood glucose. Whereas blood, plasma, or serum glucose measurements are short-term and reflect diabetic status over a 24-hour period, glycated protein levels are long-term glycemic indicators. The main glycated blood proteins are glycated hemoglobin HbA1c and glycated albumin. The HbA1c test measures the average blood glucose level over the past 2-3 months in relation to the concentration of hemoglobin (Hb) molecules that have a glucose molecule attached to them [1, 2]. Glycated albumin has been proposed as an additional marker for the control of glycemic status in people with type II diabetes [3]. In vivo, the proportion of glycated albumin in healthy people ranges from 1% to 10% [4], and in the case of diabetes mellitus, this proportion can increase two to three times [5].

Optical research methods occupy a special place and are widely used in the field of medical diagnostics and therapy [6]. Many of the studies demonstrate the possibility of using optical methods for the determination of glycated proteins [7]. In most cases, the application of optical methods requires complex calculations and requires accurate information about optical parameters, such as refractive index, absorption coefficient, scattering coefficient, and others, under various environmental conditions.

This study presents data on the measurement of the refractive index of glycated hemoglobin and glycated albumin in the spectral range of 480-1550 nm at room, physiological and high temperatures. The graphs of dispersion and temperature dependences and comparison with data for non-glycated forms of hemoglobin and albumin are presented.

Basing on the results obtained, we found an increase of the modulus of temperature increment for the glycated form of hemoglobin by an average of $(0.34 \pm 0.02) \times 10^{-4} \text{C}^{-1}$ for the wavelengths 546, 589, and 644 nm. The total derivative of the RI with respect to temperature is related to the effect of thermal expansion and the temperature dependence of the molecular polarizability. In this case, the total polarizability is considered equal to sum of the polarizability of each of molecules. Thus, the molecular complex of hemoglobin with glucose has a larger molecular polarizability and RI depends on the content of charged amino acids in the molecule. The dependence of the RI of dry erythrocytes from diabetic patients on pH (pH = 2-13) and, consequently, on the charge of the protein R-group was shown by Mazarevica et al. by using polarization-sensitive interference microscopy for the wavelength 550 nm[8].

The reported study was funded by RFBR, project number 20-32-90058 and a grant under the Decree of the Government of the Russian Federation No. 220 of 09 April 2010 (Agreement No. 075-15-2021-615 of 04 June 2021).

[1] E.J. Gallacher, D. Le Roith, Z. Bloomgarden, "Review of hemoglobin A1c in the management of diabetes," *Journal of Diabetes*, 1, p. 9-17 (2009)

[2] C. Weykamp, "HbA1c: A Review of Analytical and Clinical Aspects," *Ann Lab Med.*, 33(6), p. 393-400 (2013)

[3] Ph. Rondeau, E. Bourdon, "The glycation of albumin: Structural and functional impacts," *Biochimie*, vol. 93 (2011)

[4] H.V. Roohk, A.R. Zaidi, "A review of glycated albumin as an intermediate glycation index for controlling diabetes," *J. Diabet. Sci. Technol.*, vol. 2 (2008)

[5] E. Bourdon, N. Loreau, D. Blache, "Glucose and free radicals impair the antioxidant properties of serum albumin," *FASEB J.*, vol. 13 (1999)

[6] V. V. Tuchin, *Tissue Optics: Light Scattering Methods and Instruments for Medical Diagnostics*, 3rd ed., PM 254, p. 988, SPIE Press, Bellingham, Washington (2015)

[7] O.A. Smolyanskaya et al., "Multimodal Optical Diagnostics of Glycated Biological Tissues," *Biochemistry (Moscow)*, vol. 84 (1), p. 124-143 (2019)

B-P-19

Effect of photoactivatable iron oxide nanoparticles on the autofluorescence lifetime of polarized macrophages

E.Z. Sadykova¹, I.D. Romanishkin², D.V. Pominova^{1,2}, A.V. Ryabova^{1,2}

1- National Research Nuclear University, MEPhI (Moscow Engineering Physics Institute), Moscow, Russia
2- Prokhorov General Physics Institute of the Russian Academy of Sciences, Vavilov Str., 38, Moscow, 119991, Russia

Email: sadykova.leonora@gmail.com

Introduction The effect of iron oxide particles on the metabolism of immune cells, especially macrophages, is of considerable interest in the field of oncology. Combined Fenton reaction and photodynamic therapy (PDT) of malignant neoplasms by photoactivatable iron oxide nanoparticles seems to be an effective method of theranostics [1, 2].

Experiments Photoactivatable iron oxide nanoparticles (IONPs) were obtained from iron oxide γ -Fe₂O₃ (NanoArc, USA), size 20-40 nm, coated with a photosensitizer (PS) of aluminum phthalocyanine (IONPs@PS). Various populations of macrophage cells, derived from THP-1 human monocytic cell line, including tumor-associated macrophages, using time-resolved fluorescence spectroscopy were investigated. After incubation with IONPs, IONPs@PS, PS metabolic changes in THP-1 cells were observed using a laser scanning confocal microscope (Carl Zeiss LSM 710 NLO, Carl Zeiss, Germany). Cell autofluorescence lifetime data were obtained using FLIM (Becker & Hickl, Germany) at 2P excitation at 770 nm by Chameleon Ultra II Laser, Coherent, USA).

Results A very short lifetime of fluorescence from magnetic particles was found in the region of 0.1-0.2 ns. The autofluorescence lifetime was used as a marker of changes in the metabolic state of cells. As a result, the lifetime of metabolic conferment NADH autofluorescence increased from 1.8-2 ns (lifetime in THP-1 control cells) to 2.0-2.3 ns. The fluorescence lifetime of the aluminum phthalocyanine was recorded in the range from 2.3 ns to 4.7 ns.

Conclusion Photoactivated IONPs@PS changed the autofluorescence lifetime of cells. Specifically, the autofluorescence lifetime of protein-bound NADH is increased.

The study was funded by a grant from the Russian Foundation for Basic Research № 21-52-12030.

[1] Penon, O. et al. Iron oxide nanoparticles functionalized with novel hydrophobic and hydrophilic porphyrins as potential agents for photodynamic therapy, *Journal of Colloid and Interface Science*, vol.462, pp. 154–165, (2016).

[2] H. Hou, X. Huang, G. Wei, F. Xu, Y. Wang, S. Zhou. Fenton Reaction-Assisted Photodynamic Therapy for Cancer with Multifunctional Magnetic Nanoparticles. // *ACS Appl. Mater. Interfaces* 2019, 11, 33, 29579–29592

B-P-20

Promising target areas for selective laser photothermolysis in treatment of capillary skin angiodysplasia and telangiectasia

O. Tikhonevich¹, G. Kuzmin¹, A. Sirotkin¹, N. Gorbatova²

1 - Prokhorov General Physics Institute of the Russian Academy of Sciences, 38 Vavilov st., Moscow, 119991, Russian Federation

2 - Research Institute of Emergency Pediatric Surgery and Traumatology, 22 Bolshaya Polyanka st., Moscow, 119180, Russian Federation

Main author email address: tichon@kapella.gpi.ru

Selective laser photodestruction of the yellow-green range is widely used in treatment capillary skin angiodysplasia and telangiectasia. The most commonly used for this purpose are pulsed dye laser and the second harmonic of the Nd:YAG laser. However, many experts note an unsatisfactory clinical and esthetic result of treatment due to photodestruction of not only capillary structures containing hemoglobin but also unpredictable thermal damage to the skin [1].

Hemoglobin and oxyhemoglobin chromophores are equally present in capillary and precapillary blood in normal conditions and in pathological vascular structures of various forms and localizations of the skin with different depths relative to the surface of epithelium. Laser radiation that is equally absorbed in the hemoglobin and oxyhemoglobin chromophores acts more effectively on the mixture of chromophores. Close absorption coefficients provide a more even heating of the irradiated area. There are five points of intersection of the absorption curves of hemoglobin and oxyhemoglobin in the yellow-green area. Laser radiation at a wavelength of 525 nm has approximately an equal absorption coefficient for hemoglobin and oxyhemoglobin, which gives a good result [2-5], but there are points of intersection of absorption curves with a large absorption coefficient.

A higher absorption coefficient will allow the use of lasers with a lower intensity, which will make it possible to carry out photodestruction of pathological surface capillary structures and more deeply located unwanted vascular elements of the skin, without damaging the basal epithelial growth zone.

[1] Chang CJ, Hsiao YC, Mihm MC Jr et al (2008) Pilot study examining the combined use of pulsed dye laser and topical Imiquimod versus laser alone for treatment of port wine stain birthmarks. *Lasers Surg Med* 40(9):605–610. <https://doi.org/10.1002/lsm.20716>

[2] Sirotkin A.A., Kuzmin G. P. , Gorbatova N. E. , Yushina T. E., Dorofeev A. G. , Brynsev, A.V., Zolotov S.A., Tikhonevich O.V., Drozdov D. S. Optimization of selective photodestruction by laser radiation of the yellow-green range of capillary angiodysplasia of the skin. 2018 International Conference Laser Optics (ICLO). St Petersburg, RUSSIA., JUN 04–08, 2018 p. 602 <https://doi.org/10.1109/lo.2018.8435420>

[3] Gorbatova, N.E., Dorofeev, A.G., Drozdov, D.S., Zolotov, S.A., Kuzmin, G.P., Sirotkin, A.A., Tikhonevich, O.V. Laser medical device for the treatment of vascular pathologies of the skin Proceedings X International Conference of Young Scientists and Specialists "OPTICA-2017", pp. 229-230.

[4] O. V. Tikhonevich, A. A. Sirotkin, N. E. Gorbatova, G. P. Kuzmin, M. V. Remennikova and D. A. Seleznev, Development of a laser medical device for the selective removal of pathological vascular. 2020 International Conference Laser Optics (ICLO 2020), Proceedings of a meeting held 2-6 November 2020, Saint Petersburg, Russia. p.396, IEEE, Mar 2021 <https://doi.org/10.1109/ICLO48556.2020.9285442>

[5] Gorbatova, N., Gasanova, E., Zolotov, S. et al. Experimental confirmation of the promising selective use of "green" laser radiation for photothermolysis of hemoglobin-containing tissues. *Lasers Med Sci* (2021). <https://doi.org/10.1007/s10103-020-03220-x>